The Dissertation Committee for Hongbo Lu Certifies that this is the approved version of the following dissertation:

Global and Local Controls on Depositional Cyclicity: Canterbury Basin, New Zealand

Committee:

William L. Fisher, Co-Supervisor

Craig S. Fulthorpe, Co-Supervisor

William E. Galloway

William P. Mann

Ronald J. Steel

Hongliu Zeng

Global and Local Controls on Depositional Cyclicity: Canterbury Basin, New Zealand

by

Hongbo Lu, B.S.; M.S.

Dissertation

Present to the Faculty of the Graduate School of

The University of Texas at Austin

in Partial Fulfillment

of the Requirements

for the Degree of

Doctor of Philosophy

The University of Texas at Austin

May, 2004

Dedication

To my middle school mentor, Mr. Cun Shixi,

who had a profound influence on my choice of career.

Acknowledgements

First and foremost, I would like to thank my wonderful wife Chunlou, who has been a constant source of support and encouragement as I pursued my degree. I am especially grateful to my research advisor, Craig Fulthorpe, and my faculty supervisor, William Fisher, both of whom have been instrumental in the success of my research through their generous contributions of time and ideas. I earnestly thank them for allowing me to pursue my ideas freely and for providing outstanding critiques of my work. Much appreciation goes to my permanent committee members, Bill Galloway and Paul Mann for their valuable direction. Also, without information from Bill Galloway, the opportunity to pursue this project would not have been available. I also appreciate the efforts of my other dissertation committee members, Hongliu Zeng and Ronald Steel, as well as Mark Cloos and Scott Tinker, who served on my qualifying committee.

The project was mainly supported by National Science Foundation awards to Drs. C. Fulthorpe, P. Mann, and C. Frohlich. I am also grateful to the Institute for Geophysics Fellowship Committee for giving me Ewing/Worzel Fellowships and Student Training Funds. I also received funds from the Department of Geological Sciences of the Jackson School of Geosciences, The University of Texas at Austin for participating in meetings and conferences. The generous funding I received enabled me to concentrate fully on my research.

My experience has been enriched by association with numerous talented researchers and students at UT who have contributed to my work in a variety of ways. Jamie Austin, John Goff, Cliff Frohlich, Sean Gulick, Paul Stoffa, Laurie Duncan, Rob Rogers, Sylvia Nordfjord, Alejandro Escalona, Xinxia Wu, and many others have both increased the quality of my research through their input and ideas, and made life as a graduate student much more enjoyable through their friendship. Drs. Donna Cathro, Bob Burger, and Qunling Liu deserve a special mention here. Their contributions to my work, as well as the value I place on their friendship, cannot be overstated. Similarly, I am particularly indebted to Lisa Gahagan and Dr. Tip Meckel for their irreplaceable assistance.

My project has also been greatly improved by the interaction with scientists outside UT. I would like to especially recognize Bob Carter, Lionel Carter, Lincoln Pratson, Alexandra Isern, Dorrik Stow, Michelle Kominz, Timothy Horscroft, Peter Copeland, and Cary Cosper for their contributions to my publications. My life was made much easier due to the efforts of the excellent staff at the Institute for Geophysics, and in particular I would like to thank Steffen Saustrup, Mark Weiderspahn, and Kevin Johnson for their computer support, and Judy Sansom and Nancy Hard for helping me to deal with financial and routine issues.

Finally, I will never be able to adequately express my appreciation for encouragement and assistance given to me by Roland Goldring, a representative English gentleman, and an outstanding professor in ichnology. Without his help, my achievement would not have been possible.

Global and Local Controls on Depositional Cyclicity: Canterbury Basin, New Zealand

Publication No._____

Hongbo Lu, Ph.D.

The University of Texas at Austin, 2004

Supervisors: William Fisher, Craig S. Fulthorpe

The eastern margin of the South Island of New Zealand is part of a continental fragment that rifted from Marie Byrd Land in Antarctica beginning at about 80 Ma. High rates of sediment supply since the middle Miocene have resulted in the preservation of a high-frequency, seismically resolvable record of depositional cyclicity in the offshore Canterbury basin. In addition, along-strike currents have influenced deposition, modifying sequence architecture while forming large sediment drifts. High-resolution multichannel seismic (MCS) data provide insights into the interplay of global (eustastic) and local controls (tectonics and current activity) responsible for continental margin depositional cyclicity and sequence architecture.

At least eleven large, elongate sediment drifts are identified within the Neogene shelf-slope sediment prism. The drifts were deposited in water depths of 300-750 m and developed in response to a northward flowing current. Their subsequent evolution is influenced by sediment supply, relative sea-level change, and seafloor morphology. Unconformities created by paleoslope erosion at the

landward edges of drift moats differ from sequence boundaries by being strongly diachronous.

Nineteen regional sequence-bounding unconformities are interpreted. Correlation with oxygen isotopic records suggests that eustasy controls the timing of sequence boundaries. In contrast, sequence thickness, shelf edge stacking patterns, internal seismic facies, and slope inclination, are strongly influenced by local processes, principally the along-strike currents responsible for drift development. Sequences with conventional clinoform geometries along strike from active drifts suggest that currents might influence clinoform formation even in locations lacking seismic evidence of current reworking.

Reconstruction of Australian-Pacific relative plate motion reveals divergence in the central Southern Alps prior to ~20.1 Ma, followed by increasing average rates of convergence, with a marked increase after ~6 Ma. Sedimentation rates, calculated from sequence volumes, correlate well with convergence rates since ~11.5 Ma, indicating that tectonism has been the dominant control on sediment supply. In particular, high rates of sediment supply since 6 Ma, may reflect previously recognized increased plate convergence and Southern Alps uplift. In contrast, high sedimentation rate from ~15-11.5 Ma correlates with low convergence rates and is therefore probably a response to global climatic forcing and eustasy.

Table of Contents

List of Tables

List of Figures

Chapter 1: Introduction

1.1 Origin of Problems and Study Purposes

In spite of intense research, many aspects of the geology of continental margins remain poorly understood. Seafloor and sub-seafloor morphologies are complex and, until recently, were difficult to map accurately (Galloway and Hobday, 1996). Slope depositional and erosional features occur at a great range of scales; even the largest outcrops are inadequate for revealing slope facies architecture. Furthermore, continental margins are influenced by a combination of numerous terrestrial and oceanic processes, making interpretation of architectures difficult. Such investigation is worth the effort, however, because of the long record of processes operating on continental margins that is preserved in the strata formed at the seabed. The history of many of the events influencing the Earth (both on land and in the ocean) can be unraveled by carefully documenting and accurately interpreting sedimentary strata on continental margins (Nittrouer and Kravitz, 1996). Only recently have new technologies (e.g., side-scan sonar, bathymetric swath mapping, high-resolution multichannel seismic (MCS) data) and interpretation tools, such as high-resolution sequence stratigraphic models, allowed us to interpret the history of processes responsible for forming continental margins.

In recent years stratigraphic research guided by sequence models (Figure 1.1) has fundamentally improved our understanding of stratigraphic processes and controls on basin architecture. However, sequence stratigraphy has encountered problems in its application and further development. The two most critical problems are:

The basic sequence models developed by the Exxon group (Vail, 1987; Vail et al., 1977, 1984, 1991) are intended for a specific type of tectonic setting, extensional continental margins, and were developed primarily from northern hemisphere basins containing siliciclastic sediments and assuming little or no along-strike sediment transport. The models must be tested in different types of setting, including more tectonically active basins and nonmarine basins.

Haq et al. (1987, 1988) assumed that stratigraphic architecture is controlled primarily by eustasy. They produced global cycle charts and inferred that marine sequences should correlate between basins worldwide. This is controversial for three reasons: 1) Unconformities bounding sequences can also be generated by local processes such as vertical tectonism, and erosion by marine currents (e.g, Galloway, 1989a,b; Christie-Blick, 1991). 2) Such local processes, also including rate of sediment supply, can influence sequence geometry and timing, and critics of the global curve assert that such local effects preclude global correlation because they can cause sequence boundary formation to lead or lag the time of maximal rate of eustatic fall (Christie-Blick, 1991; Fulthorpe, 1991). Even eustatic sequences, therefore, may not be synchronous. 3) Currently available

chronostratigraphic techniques (biostratigraphy, radiometric dating, magneto-stratigraphy, and chemostratigraphy) are inherently imprecise. Various authors have estimated the dating precision over different intervals of geological time and have assessed the incremental improvements in the global time scale that have been built from local and regional correlation programs (e.g., Harland et al., 1990; Miller, 1990; Aubry, 1991; Jones at al. 1994 a,b). Kidd and Hailwood (1993) estimated the resolution for various time slices back to the Triassic and claimed that the high-order sequences in the global cycle chart (those with periods of 10^6 years or less) have durations shorter than the range of error involved in their dating and correlation, except for late Cenozoic glacioeustatic cycles. Many researchers, therefore, have criticized eustatic cycle charts (Christie-Blick et al., 1990; Christie-Blick, 1991; Carter et al., 1991; Dickinson, 1993).

Two challenges – an improved interpretation and prediction of the high-resolution sedimentary record preserved on shelves and slopes, and an evaluation of the role of eustasy in controlling relative sea level, and hence stratigraphic architecture – are the subjects of ongoing investigation and have been recognized as important problems by numerous advisory groups (e.g., Conference on Scientific Ocean Drilling (COSOD) I and II, 1981, 1987; Joint Oceanographic Institutions/ U. S. Science Advisory Committee (JOI/USSAC) Workshop "Role of ODP Drilling in the Investigation of Global Changes in Sea Level" (Watkins et al., 1990).

The strategy proposed by COSOD II (1987) involves three independent methods: the atoll, isotopic, and passive margin approaches. They seek to investigate: 1) timing, magnitude, and rate of eustatic change; 2) stratigraphic responses to sea-level oscillation; and 3) mechanisms for causing eustatic change, in three main time slices: the Neogene "Icehouse", Paleogene "Doubthouse" and Cretaceous "Hothouse". The offshore Canterbury basin is an excellent location for applying the passive margin approach in the "Icehouse" time period. High rates of sediment supply since the middle Miocene and perhaps earlier, associated with activity along the nearby Alpine Fault plate boundary, have resulted in the preservation of an unusually high-frequency (0.5–1 my. periodicity), seismically resolvable record of depositional cyclicity. In addition, along-strike currents have influenced deposition in parts of the basin, modifying sequence architecture while forming large sediment drifts within the prograding Neogene section**.** The basin is also the target of an existing Ocean Drilling Program drilling proposal and the sediments are correlative with these drilled of New Jersey (Legs 150 and 174A, Austin et al., 1998), Bahamas (Leg 166, Eberli et al., 1996)**.**

Supported by the National Science Foundation (NSF), the University of Texas Institute for Geophysics (UTIG) collected high-resolution MCS data in the offshore Canterbury basin. These data allow us to improve on interpretations of the sedimentary record preserved beneath the shelf and slope that are based on existing lower-resolution commercial MCS data. The ultimate goal is to understand the interplay of global (eustastic) and local controls (tectonics, sediment

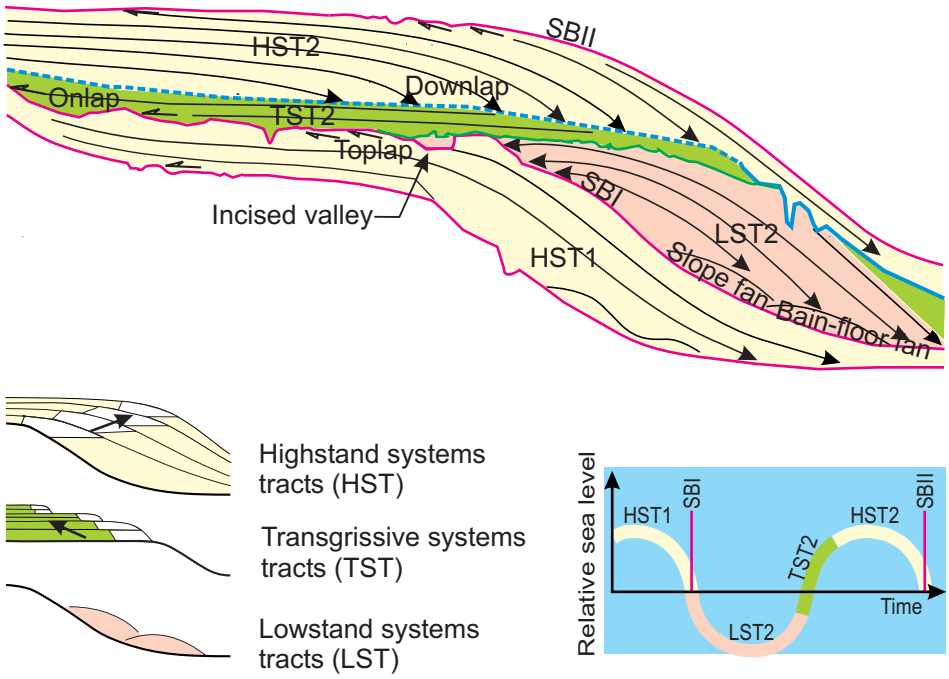

Figure 1.1. Idealized dip stratigraphic cross-section for the Exxon model in a shelf break setting showing stratal surfaces and system tracts. The basic element of sequence stratigraphy is the unconformity-bounded sequence, which represents sedimentation within a complete relative sea-level cycle. Ideally, a sequence consists of lowstand (LST), transgressive (TST) and highstand (HST) systems tracts, that are genetically related depositional units formed during different phases of a sea-level cycle. (Modified from Galloway, 1989a; Galloway and Hobday, 1996).

supply rate, and current activity) responsible for continental margin depositional cyclicity and sequence architecture. The target strata are middle Miocene to Recent.

1.2 Overview of Dissertation

The study is organized as follows: Chapter 2 describes the complex geological history in the Canterbury basin as currently understood, and also describes the data and methodology used to image shelf and slope sequences in the offshore basin. Chapters 3, 4, and 5 are stand-alone studies, summarized below, evaluating specific aspects of the middle Miocene to Recent depositional history of the basin. Each of these chapters has been, or will be, submitted for publication (Lu et al., 2003; Lu and Fulthorpe, in press). Chapter 6 presents conclusions arising from the composite seismic analysis and tectonic reconstruction and discusses ended potential future work in the Canterbury basin.

Chapter 3 describes sediment drifts formed on paleoslopes by along-slope submarine currents. This chapter focuses on three-dimensional sediment drift architecture and internal seismic facies and the influence of sediment supply and sea-level change on drift geometries. Chapter 4 constitutes the main body of this dissertation. Based on an interpreted sequence stratigraphic framework, this chapter discusses the relative roles of global (eustasy) and local forcing (current active and sediment drift) on sequence timing and architecture. The late Pliocene termination of drift deposition is analyzed based on the evolving relationship

between along-slope and downslope sedimentary processes. Chapter 5 uses tectonic reconstructions and sequence volume calculations to describe the link between plate boundary tectonism at the Alpine Fault and sediment supply to the offshore basin. As a whole, chapters 2-6 infer the processes, varying in both space and time, which have influenced formation and preservation of seismically observed sequences and sediment drifts across this passive margin. Sediment drift and sequence stratigraphic models, specific to the unique setting of the Canterbury basin, are proposed and sedimentary paleoenvironments and depositional processes implied. These hypotheses will ultimately be tested by: 1) proposed two-dimensional subsidence analyses and forward stratigraphic modeling and 2) proposed scientific drilling by the Integrated Ocean Drilling Program (IODP).

Chapter 2: Geological Setting and Methodology

2.1 LOCATION

The Canterbury basin occupies the central part of the eastern South Island of New Zealand and the adjacent offshore area (Figure 2.1). The onshore part of the basin extends from the foothills of the Southern Alps across the Canterbury Plains to the coast, an area of >12,000 km^2. Offshore, it extends across the adjacent shelf to the continental slope. Though most of the offshore area of ~30,000 km^2 lies under less than 250 m of water, the largest sub-basin partly underlies the slope where water depths can exceed 1000 m. Northeast of the Canterbury basin, the Chatham Rise is a submarine plateau that extends for 1,100 km to Chatham Island. Most of the rise is shallower than 1000 m with the crest averaging ~400 m water depth. Eastward, sediment from the Canterbury basin is transported into the Bounty Trough. Southward, the basin is contiguous with the larger Great South basin between Campbell Plateau and South Island (Killops et al., 1997; Sutherland and Browne, 2003)

2.2 GEOLOGICAL SETTING

2.2.1 Tectonic Setting

The eastern margin of the South Island of New Zealand (Figure 2.1) is part of a continental fragment, including the Campbell Plateau, Chatham Rise, and

Bounty Trough, that rifted from Marie Byrd Land in Antarctica beginning at about 80 Ma (Molnar et al., 1975; Weissel et al., 1977; Carter et al., 1991; Lawver and Gahagan, 1994; Weaver et al., 1994). The Canterbury basin is located at the landward edge of the continental fragment Localized igneous centers of late Eocene to Oligocene and Miocene ages are present (Milne, 1975; Coombs et al., 1986). The Canterbury Bight is bounded by the Miocene volcanic centers of the Banks Peninsula (5.8-12 Ma) to the northeast and the Otago Peninsula (9.6-12.9 Ma) to the southwest (Watters, 1978; Barley, 1987; Sewell and Lewis, 1988). Neogene sediments thin toward these features and also onshore, where, at the basin's western edge, they become involved in subsidiary faulting and folding associated with the development of the Southern Alps.

The Alpine Fault plate boundary separates the Pacific and Australian plates and has been the focus of intensive research directed at understanding its origin (Adams, 1979; Kamp, 1987a,b; Tippett and Kamp, 1993a, 1995; Koons, 1994, Koons and Henderson, 1995; Chamberlain et al., 1995; Bourne et al., 1998; Koons et al., 1998; Beavan, et al., 1999; Batt et al., 2000) and its influence on the development of adjacent basins (Carter and Norris, 1976; Carter, 1988a,b; Fulthorpe, 1991; Chamberlain et al., 1995). Kamp (1987b) indicated that the Alpine Fault formed as a shear zone; dextral strike-slip motion has led to 500 km displacement since the earliest Miocene (23 Ma). Uplift of the Southern Alps began at ~8-5 Ma (Tippett and Kamp, 1993b; Batt et al., 2000) or ~10-8 Ma (Carter and Norris, 1976; Norris et al., 1978; Adams, 1979) indicating a

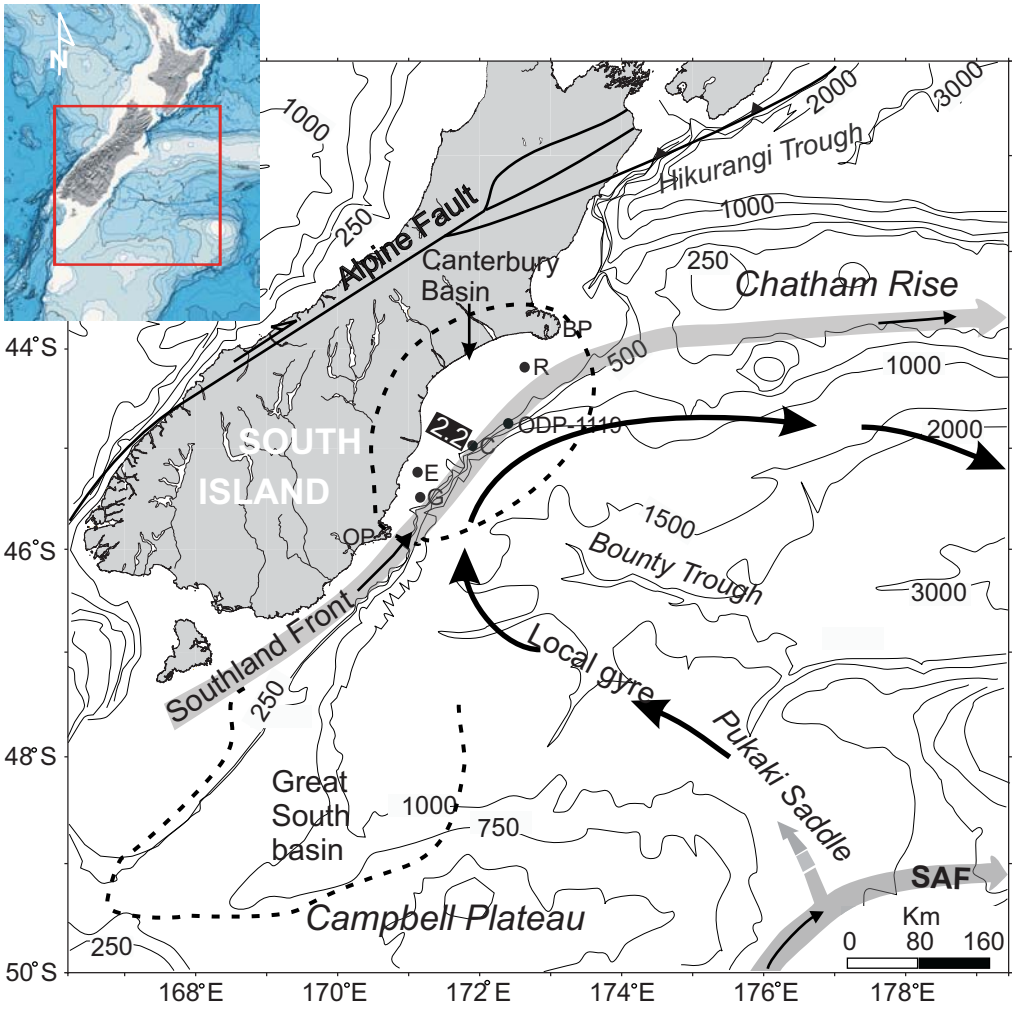

Figure 2.1. Location map showing the South Island of New Zealand. The Canterbury Basin underlies the present-day onshore Canterbury Plains and offshore continental shelf. It is bounded by the Miocene volcanic centers of the Banks Peninsula (BP; 7.5 -12 Ma) to the northeast and the Otago Peninsula (OP; 9.6-12.9 Ma) to the southwest (Watters, 1978), and faces the Bounty Trough to the southeast. The Alpine Fault is the dextral strike-slip boundary between the Australasian and Pacific plates. Locations of the modern Southland Front, Subantarctic Front (SAF), and a local gyre associated with SAF are shown (Chiswell, 1996; Davis, 1998; Shipboard Scientific Party, 1999; Carter and Wilkin, 1999; Morris et al., 2001). Also shown are the four exploration wells in the offshore basin (Resolution, R; Clipper, C (Figure 2.2); Endeavour, E; and Galleon, G) and ODP Site 1119. Bathymetric contours are in meters.

component of convergence along the fault. Transpression led to an increase in the rate of sediment supply to the offshore Canterbury Basin, though terrigenous sediment had begun accumulating offshore by perhaps as early as 15 Ma, based on seismic interpretation and ties to offshore exploration wells (Fulthorpe and Carter, 1991).

In spite of the proximity of the Alpine Fault, the central part of the offshore Canterbury basin is undisturbed by plate-boundary tectonism. For example, folding and faulting are absent within the survey area (the only faulting occurs near shore, mainly associated with local igneous intrusions; Milne, 1975; Coombs et al., 1986). The amount of rock uplift over the last 8 Ma decreases almost exponentially away from the Alpine fault to zero near the present shoreline (Tippett and Kamp, 1993b). Deep-penetration (16 s) profiles of the South Island Geophysical Transect (Davey et al., 1998; Stern et al., 2001) also indicate that uplift is peripheral to the survey area where strata are undeformed as far back as the Eocene (Godfrey et al., 2001). Furthermore, geodetic studies (Walcott, 1979; Pearson et al., 1995) are consistent with the entire Pacific-Australian plate motion (DeMets et al, 1990, 1994) being taken up on onland. Finally, backstripping suggests little Neogene vertical tectonism in the central part of the offshore basin until ~8-5 Ma, when subsidence rates increased (Figure 2.2, Kominz unpublished data; Browne and Field, 1988). This increase in subsidence rates may be caused by flexure associated with increased plate convergence during this period.

2.2.2 Sedimentation

Rifting, followed by development of the transgressive Alpine Fault plate boundary, generated a large-scale (80 m.y.) transgressive-regressive cycle (Figure 2.3). The Onekakara, Kekenodon, and Otakou groups (Carter and Carter 1982) were deposited during the regional transgressive, highstand, and regressive phases of this cycle, respectively. Marine transgression accompanied post-rift, thermal subsidence during the Late Cretaceous and Paleogene. Basal Onekakara Group sedimentary rocks comprise alluvial-fluvial sandstone and conglomerate. These basal sediments are overlain by interbedded coal measures and sandstone with occasional marine mudstone, with shallow marine siltstone and mudstone at the top of the group. Reduced terrigenous influx during maximum transgression in the Eocene to Oligocene (~30 Ma) led to the deposition of two basin-wide, pelagic to hemipelagic, bioclastic limestone units, the Amuri and Weka Pass Formations (Carter, 1988a). The limestone units drape the broad, near-horizontal platform formed by the top of the Cretaceous to Paleogene, transgressive, siliciclastic rocks. The Amuri and Weka Pass Formations are separated by the Marshall Paraconformity (33 Ma, Kennett and der Borch, 1986; 29-32 Ma, Fulthorpe et al., 1996), a regional unconformity at the base of the Kekenodon Group. The thin, glauconitic Concord Formation, a basal facies of the Weka Pass Formation, immediately overlies the Marshall Paraconformity (Carter, 1985) (Figure 2.3). The subsequent regressive phase occurred in response to increasing rates of sediment supply that began with the mid-Cenozoic development of strike-slip

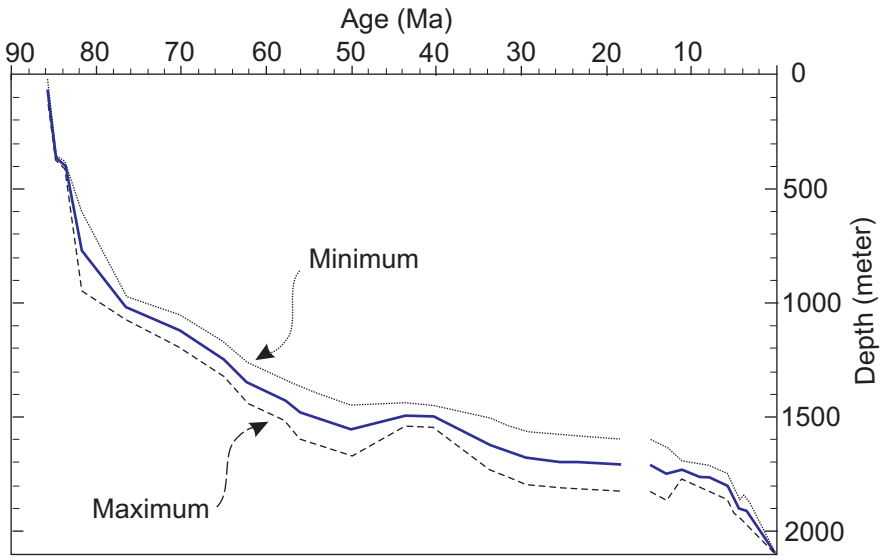

Figure 2.2. Tectonic subsidence curve (minimum, mean, and maximum) for the Clipper exploration well (see Figure 2.1 for location). Most tectonic subsidence occurred during the early late Cretaceous, with mild uplift during the latest Cretaceous. Little tectonic subsidence occurred between 30 Ma and ~8 Ma. The increase in tectonic subsidence beginning at ~8 Ma is probably associated with increasing convergence at the Alpine Fault. Curve provided by M. Kominz (unpublished data, 2003)

motion on the Alpine Fault and grew as the amount of convergence at the plate boundary increased. This sediment influx was deposited as the progradational Otakou Group (Figure 2.3). Offshore oil exploration wells Clipper (Hawkes and Mound, 1984), Galleon (Wilson, 1985), and Endeavour (Wilding and Sweetman, 1971) reveal the strata of the Otakou Group to be predominantly terrigenous silt, variably argillaceous, with intermittent intervals of fine to very fine-grained sand and mud. A 60-m-thick, very fine-grained, quartz sandstone overlies the limestone and forms the base of the Otakou Group at Clipper (Hawkes and Mound, 1984). At Resolution, the lithology is predominantly silty mudstone (Milne, 1975). Shell debris and glauconite also occur, and the unit becomes increasingly calcareous toward its base. Large, elongate sediment drifts developed within the Otakou group from the middle Miocene to early Pliocene and form a significant part of the prograding shelf sediment prism (Fulthorpe and Carter, 1991; Lu et al., 2003, Lu and Fulthorpe, in press).

The high rate of Neogene sediment accumulation and tectonically stable setting combine to make the offshore Canterbury basin an attractive location for studying the origins of high-frequency stratigraphic sequences (Loutit and Kennett, 1981; Carter, 1985, 1988a,b; Browne and Field, 1988; Fulthorpe and Carter, 1989; Carter et al., 1991; Fulthorpe, 1991; Lewis, 1992; Abbott and Carter, 1994; Fulthorpe et al., 1996; Adrian, 1997). An estimated 9.1 cm/k.y. of sediment (uncorrected for compaction) has accumulated since the Oligocene at Clipper exploration well (Fulthorpe and Carter, 1989). The thickest sedimentary

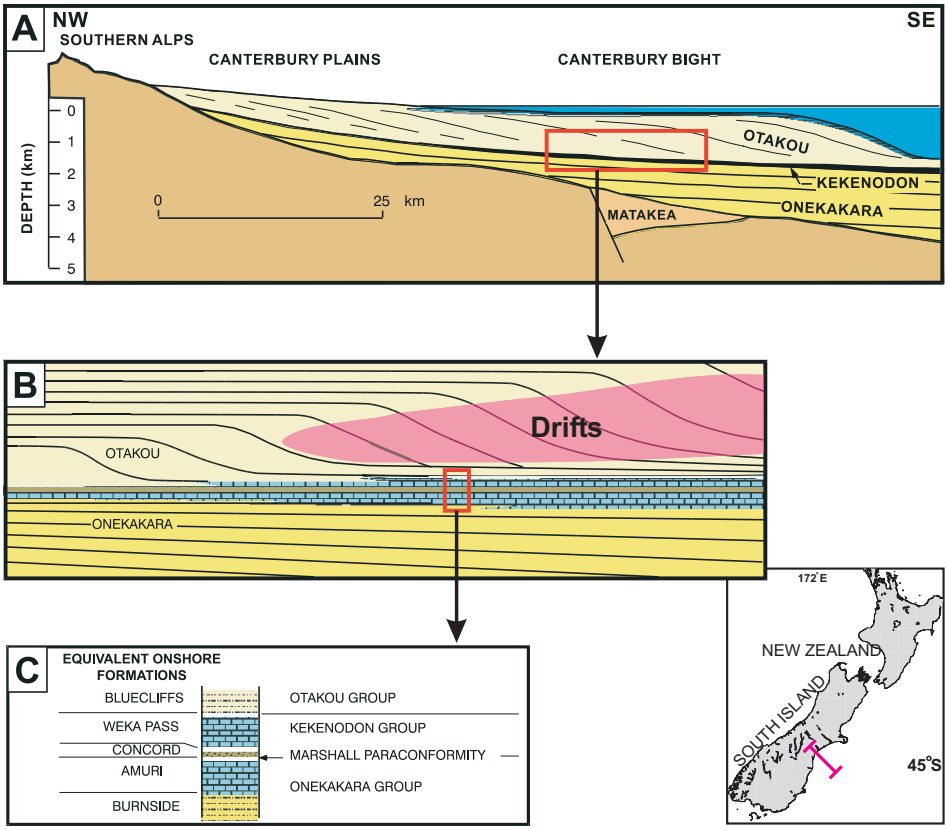

Figure 2.3. Schematic stratigraphy of the Canterbury Basin at three different scales. (A) Large-scale, post-rift stratigraphy. Onekakara, Kekenodon and Otakou groups were deposited during regional transgressive, highstand and regressive phases, respectively. (B) Seismic-scale stratigraphy. The sediment drifts occur within the Otakou Group. The limestones are shown as distal facies of the uppermost transgressive Onekakara Group and lowermost regressive Otakou Group. (C) Outcrop-scale stratigraphy across the Marshall Paraconformity. (Modified from Fulthorpe et al., 1996.)

section, 6.5 km including basal rift fill, lies near Clipper, approximately midway between the Banks and Otago Peninsulas, near the present-day shelf edge (Browne and Field, 1988).

2.2.3 Modern Offshore Sedimentation and Hydrographic Regime

Large, modern, coarse-grained, braided rivers (from north to south, the Rakaia, Rangitata, Pareora, and Waitaki; Figure 2.1), sourced in the Southern Alps, have shed significant volumes of sediment (50,000 km^3), onto the margin during the last 5 Ma (Herzer, 1981; Browne and Naish, 2003). Alongshore transport moves 400,000-700,000 m^3/yr of pebbles, cobbles, and sand northward toward Banks Peninsula (Kirk and Tierney, 1978). The modern shelf break is ~90 km offshore at 144-153 m water depth. Modern slope inclination decreases from >5° to ~2° from south to north in the Canterbury Bight and the shelf break is ~1000 m above the slope toe. Near 45°S, the shelf edge is incised by Waitaki Canyon, which leads downslope to the Bounty Channel.

Differences in both temperature and salinity between inshore and offshore waters are sufficiently large to form a sharply delineated front, the Southland Front, continuous with the Subtropical Convergence (Figure 2.1; Chiswell, 1996; Shipboard Scientific Party, 1999; Morris et al., 2001). The northward-flowing Southland Current lies inboard of the Southland Front (Burling, 1961; Chiswell, 1996; Morris et al., 2001). The current is bounded to the east, across the

Southland Front, by low-salinity subantarctic water, associated with the Subantarctic Front (SAF; Figure 2.1; Davis, 1998; Morris et al., 2001). SAF forms the leading edge of the Antarctic Circumpolar Current and extends northeastwards along the eastern edge of Campbell Plateau. A small, shallow branch leaks northwards through Pukaki Saddle, recirculating clockwise around the head of Bounty Trough as a local gyre (Figure 2.1; Bryden and Heath, 1985; Orsi et al., 1995; Carter and Wilkin, 1999). Together, the combination of this local gyre and the Southland Current influences the margin to a depth of ~900 m (Burling, 1961; Chiswell, 1996; Morris et al., 2001). Maximum surface current speed within the Southland Current is ~13 cm/s, with an average of ~6 cm/s (Carter and Herzer, 1979; Shipboard Scientific Party, 1999). Greater current speeds (>30 cm/s) are possible where the current is reinforced by tidal flow and storm waves and where seafloor topography constricts and focuses the flow (Shipboard Scientific Party, 1999). The Southland Current is strengthened under stronger westerly wind systems (Thiede, 1979; Stewart and Neall, 1984) and/or higher temperature gradients when increased cold water from south of the SAF is introduced via the Pukaki Saddle during glacial times (Barnes, 1992; L. Carter, personal communication, 2002). A precursor of this current system contributed to construction of the Neogene sediment drifts.

2.3 DATA AND METHODOLOGY

2.3.1 Multichannel Seismic (MCS) Reflection Data and Well Data

The primary data comprise 2-D high-resolution MCS profiles collected during a 21-day cruise from 9-29 January 2000 (R/V *Maurice Ewing* cruise EW00-01). The survey grid lies approximately midway between the Banks and Otago Peninsulas on the present-day middle to outer shelf and slope, above the late Miocene to Recent depocenter and over the area where the largest sediment drifts developed (Figure 2.4). The seismic source consisted of two GI air guns (45/45 $in.^3$) and the streamer was deployed with 12.5 m groups in 96 and 120-channel configurations (Table 2.1). A total of 57 profiles (~3750 line-km) were collected, covering ~4840 km^2. Line spacings are 0.7-3.0 km in the dip direction and 2.0-5.5 km in the strike direction. Penetration, 1.7-2.0 s below seafloor, is sufficient to image the entire Oligocene to Recent section. Data processing used Focus software (see Table 2.2 for processing sequence) and the data were loaded into the GeoQuest interpretation system.

High resolution was achieved by using reliable high-frequency sources (maximum frequency: 500 Hz), small sample interval (1 ms) and high fold (48-60). Vertical resolution (~5m for two-way travel times <1 second) is up to 4-5 times better than that of existing commercial MCS data (see Figure 2.5) However, seafloor and peg leg multiples are pronounced beneath the shelf. In order to deal with this problem, pre-stack deconvolution and FK-filtering, were applied to

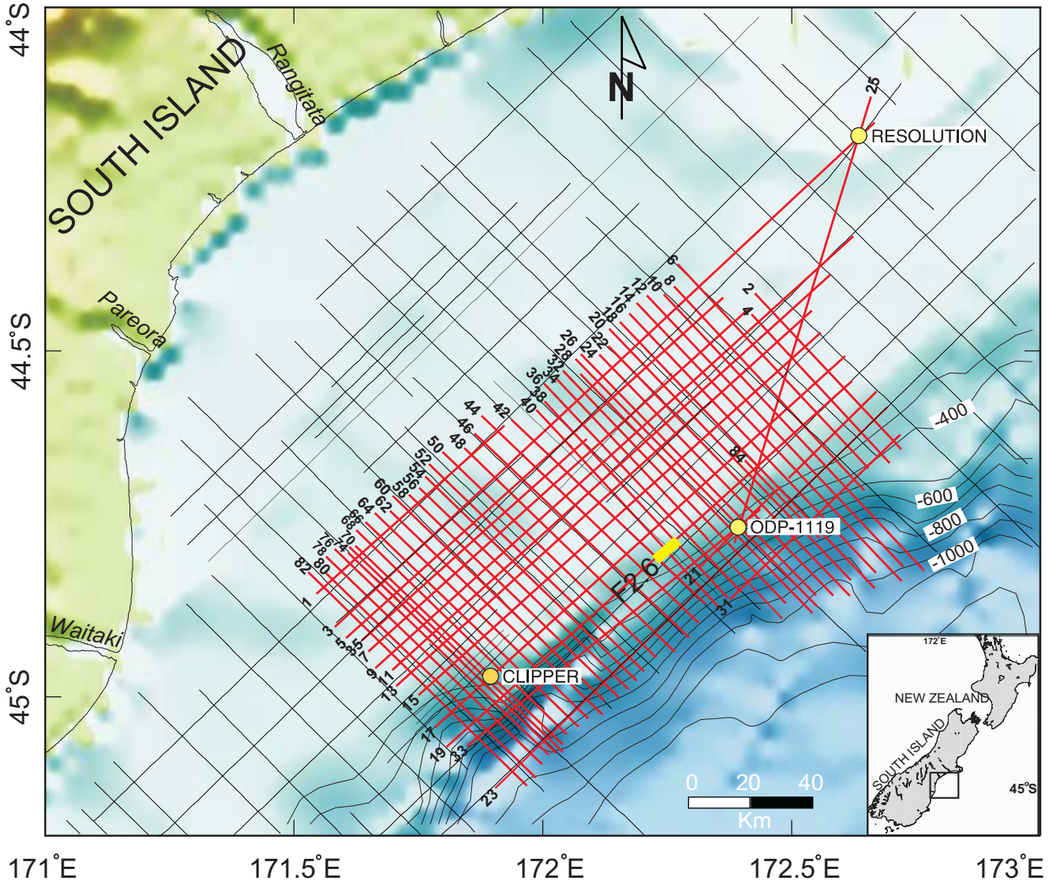

Figure 2.4. EW00-01 high-resolution MCS grid (red straight lines). Odd-numbered profiles are strike profiles, and even-numbered profiles are dip profiles. Black straight lines represent the low-resolution CB82 commercial MCS grid. Also shown are exploration wells Clipper and Resolution and ODP Site 1119. Three main rivers, Rangatata, Pareora, and Waitaki discharge into the offshore basin. Locations of Figures 2.6 is indicated by F2.6. Bathymetric contours are in meters.

Table 2.1. Acquisition parameters of new grid (EW00-01 cruise)

Total channels	96 *, 120
Shot point spacing	~12.5 m or (5 s per shot); Source: two 45/45 cu.in. GI guns
Nyquist frequency	500 Hz (vertical resolution <5m within upper 0.5 s)
Environment	Mid-outer shelf, slope. Water depth: 40-1100m
Group interval	12.5 m
Sample interval	1 ms
Record length	3000 ms
Near channel offset	26.25 m
Far channel offset	1500 m
CDP spacing	6.25 m
Maximum Foldage	48*, 60
Filed work area	4840 km^2
Total strike profiles	16
Total dip profiles	41
Total line length	~ 3500 km
* The profile was initially configured with 96 channels (lines 2, 4, 8, 23, 82, 80,78, and 74). The remaining profiles were shot with 120 channels.	

Table 2.2. Data processing Sequence and Focus Functions

Data processing	Focus Function
Read and reformat field data from tape	[GIN, IN, DSKRD]
Recover amplitude loss due to geometric spreading and frequency attenuation	[GAIN] 200 μs
Remove frequency-differentiable noise	[FILTER] 5-10-200-230
Remove bad traces	[EDIT] Delete channel 19
PREPROCESSING END	
Set up Database	[PROFILE]
CDP gather sorting	[SORT]
Reshape source, smooth frequency spectrum, collapse multiples	[DECONV] [FKFILTER]
Correct for normal moveout (offset)	[NMO]
Remove post-critical and stretched or distorted energy	[MUTE]
Lateral balance	[BALANCE]
Sum CDP gather into a trace: improves S/N, attenuates multiples	[STACK]
F/K Migration: “moves” energy to correct position, collapses diffraction	[F/KMIG]
Save result	[DSKWRT]
Improve display	[FILTER, AGC]
Plot	[DECPLOT]

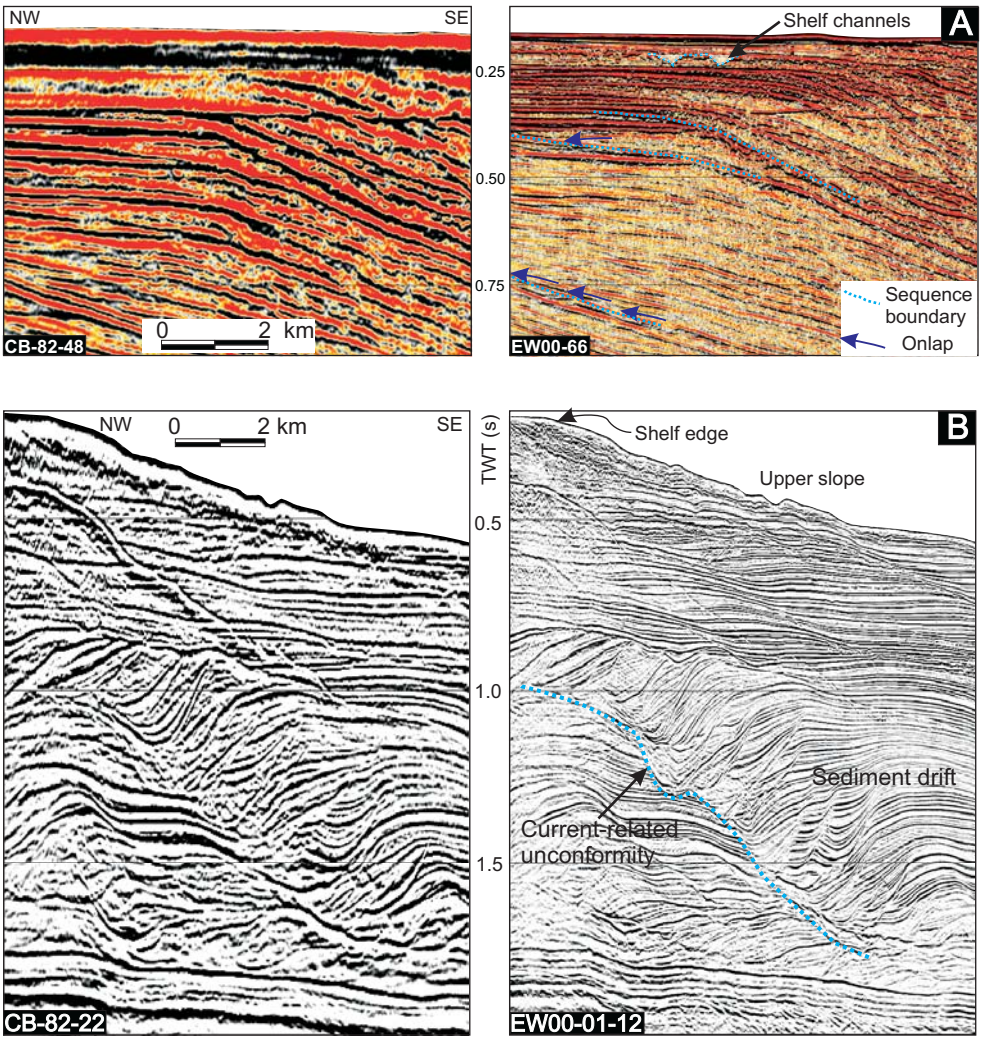

Figure 2.5. Comparison of resolution of CB82 commercial MCS data (left) and EW00-01 survey (right). (A) Mid-outer shelf showing onlap, truncation and erosional channels that can be identified by using the EW00-01 profile. (B) Sediment drift beneath the slope. Vertical resolution of the EW00-01 data is about 4 times better than that of the CB82 profile.

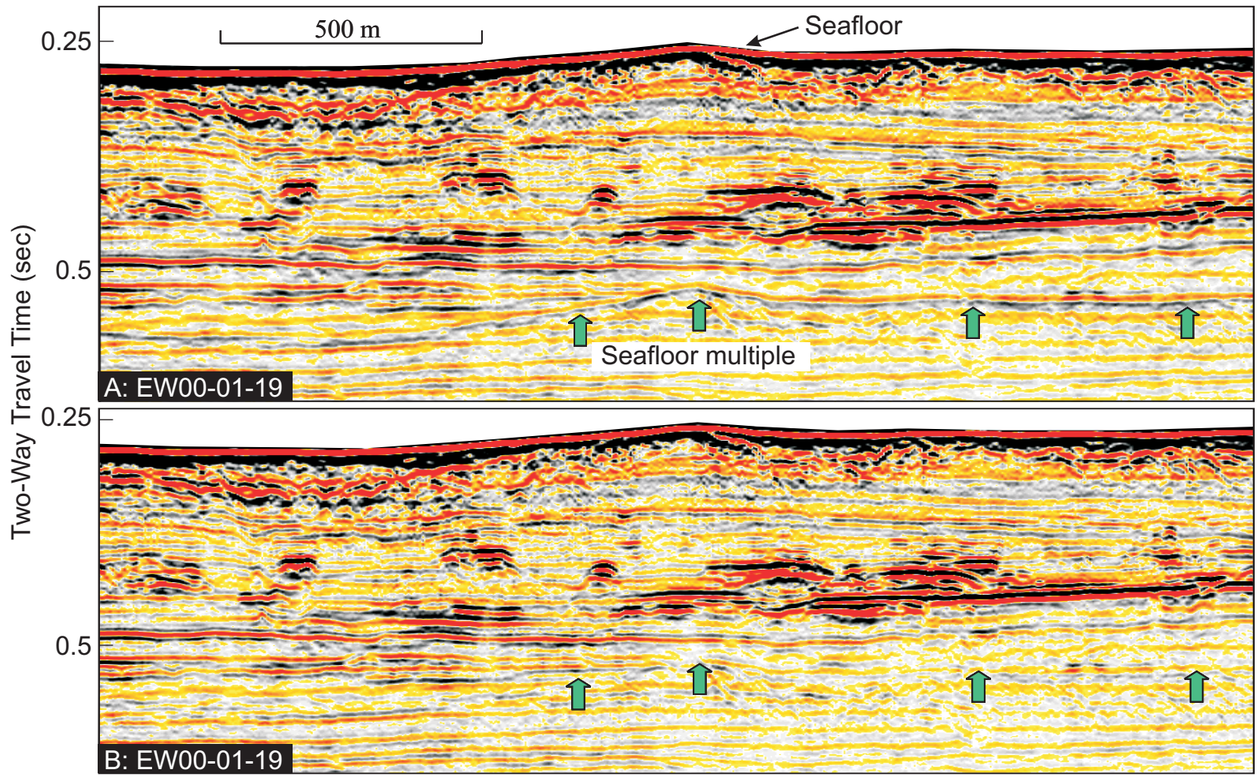

Figure 2.6. Seafloor multiple suppression. Multiple is indicated by green arrows. (A) Before pre-stack deconvolution and fk-filter.(B) After pre-stack deconvolution and fk-filter, seafloor multiple has been apparently depressed. See Figure 2.4 for profile location.

some critical sections yielding some improvements in quality (see Figure 2.6). A more areally extensive, but lower resolution (20 m vertically) commercial MCS grid (CB82 profiles), collected in 1982 for a petroleum exploration consortium (B.P. Shell Todd), was also used to extend interpretations beyond the EW00-01 grid. The CB82 data were particularly useful for ties to exploration wells, determining sediment drift distribution and locating clinoform breakpoints, onlap and canyons associated with the oldest sequences. The grid consists of 81 profiles, representing ~6000 line-km (Figure 2.4). Record length is 5 seconds; sample rate is 4 ms. Digital copies of all stacked profiles were loaded into the GeoQuest system. Paper copies of migrated profiles were also available and twenty of the digital profiles were migrated as part of this project.

Four petroleum exploration wells, Endeavour (Wilding and Sweetman, 1971), Resolution (Milne et al., 1975), Clipper (Hawkes and Mound, 1984), Galleon (Wilson, 1985), and ODP site (1119) have been drilled within Canterbury Bight (Figure 2.1). Clipper, Resolution and ODP Site 1119 lie within the EW00-01 grid. Endeavour was tied to the grid using CB82 data. Information from these wells, including electric logs, lithologic, geochemical, and paleontologic data, as well as hard copies of each well completion report, are available at UTIG. Summary information for each of the wells, including MCS profiles and well locations, is given in Table 2.3.

2.3.2 Seismic Interpretation and Analysis

2.3.2.1 Construction of sequence stratigraphic framework

A primary goal is to interpret and map the sedimentary sequences in the research area. Numerous surfaces of sequence stratigraphic significance, defined by onlap, downlap and toplap terminations (see Figure. 2.5A), are clearly recognizable on the seismic profiles. However, submarine currents have modified sequence geometries and form current-related erosional unconformities (Figure 2.5B), which can be superficially similar to sequence boundaries, but are instead strongly diachronous. Interpretation made use of the following observations: 1) Landward and basinward shifts of paleoshelf edges indicate the increase and decrease of accommodation space. 2) Seismic reflection stacking patterns, including progradation, retrogradation and aggradation, are controlled by the interplay of sediment supply and accommodation space. Usually, highstand systems tracts (HST) are dominated by aggradational and progradational stacking patterns (parasequence sets), lowstand systems tracts (LST) by aggradational and slowly retrogradational patterns, and transgressive systems tracts (TST) by retrogradational stacking patterns (Van Wagoner et al., 1988; Posamentier and Vail, 1988; Vail et al., 1991). 3) Incised valleys, truncation and onlap on the inner shelf generally indicate sequence boundaries. 4) Forced regressive system tracts

Table 2.3. Summary of wells within 2D volume

Well	Drilling date, location	Crossing seismic profiles	Drilling depth	Objective and comments
Endeavour	(1971) 44º 11.3' S 171º 7.5' E	CB82-17 CB82-80a	8731 ft	Test for possible hydrocarbon accumulations in an anticlinal structure. Result: all prospective zones water bearing. Used to date the oldest sequence boundaries (U1-U2).
Resolution	(1975) 44º 11.3' S 172º 38.2' E	EW00-01 (3, 25)	1953.0 m	Test the hydrocarbon potential of basal Tertiary/Upper Cretaceous sandstones in a closed anticlinal high. Result: all potential reservoir intervals were fresh water-bearing. Good source for calibrating the upper sequence boundaries (U9-U19).
Clipper	(1984) 44º 58.2' S 171º 53.8' E	EW00-01 (74, 17) CB82-54	4617.0 m	Test potential Cretaceous reservoirs with structural closure beneath the Blue seismic horizon. The hydrocarbon accumulation was uncommercial. Four gas/condensate-bearing sandstone encountered near 4300 m in depth. Most important well for age control in this project.
Galleon	(1985) 45º 29.3' S 171º 9.8' E	CB82-43 CB82-88	3078 m	Evaluate the occurrence of hydrocarbon within the Late Cretaceous coal measures within a dipclosed future. Result: Plugged and abandoned gas condensate discovery. Not used in this project.
ODP-1119	(1998) 44º 45.3' S 171º 23.6' E	EW00-01 (28, 33, 25, 21a)	484.80 m	Site 119 was drilled to sample upper slope sediments and underlying sediment drifts. Provides best age control for uppermost sequence boundaries (U11-U19).

(FRS), inserted between HST and LST, are "smoothed-topped and attached forced regressive deposits forming on a gently inclined shelf" (Posamentier and Morris, 2000). They are thought to be controlled by asymmetric glacioeustatic cycles, driven by eccentricity, during the last 0.8-0.9 Ma and are inferred to form during periods of decreasing accommodation caused by high-amplitude relative sea-level falls (Plint and Nummedal, 2000; Posamentier and Morris, 2000; Hernandez-Molina et al., 2000; Chiocci, 2000; Trincardi and Correggiari, 2000; and Kolla et al., 2000). Recognition of such geometries is indicative of eustatic control.

2.3.2.2 Mapping 3-D sediment drift morphologies

Because of the low resolution and large line spacings of the commercial CB82 MCS profiles, the sediment drift model of Fulthorpe and Carter (1991) is only 2-D. The more dense, and higher-resolution, EW00-01 grid allows documentation of 3-D drift morphologies and construction of a 3-D model of drift evolution. Conventional, clinoform sequence boundaries can be traced laterally and/or downslope to, and through, sediment drifts. By determining the relationship between current erosional surfaces and sequence boundaries, the drifts can be placed within a sequence stratigraphic context.

2.3.2.3 Isochron maps, sequence volumes and sedimentation rates

Travel time (isochron) maps are useful for understanding the 3-D distribution of sediment and are constructed using GeoQuest software. Map units

are milliseconds of two-way travel time. Similarly, isochron maps of sediment drifts reveal 3-D drift geometries and distribution.

To allow direct comparison between isochron maps of sequences representing differing time intervals, additional maps are created by converting time thickness to sediment volume and using age control to determine sediment accumulation rates. The volume of each sequence is calculated using a velocity model (Figure 2.7), derived from seismic stacking velocities and calibrated by check-shot velocities from Clipper exploration well and the sonic log from ODP Site 1119. The procedure used to calculate sequence volumes is illustrated by Figure 2.8. The effects of compaction are accounted for by determining the volume of solid grains within each sequence (sequence grain volume) using porosity data from boreholes following the method of Liu and Galloway (1997). This methodology is discussed in more detail in Chapter 5. Such compaction-corrected volumes and resultant sedimentation more correctly reflect the history of sediment supply to the offshore basin.

2.3.2.4 Documentation of local versus global controls on depositional cyclicity

Documentation of 3-D along-strike variability in sequence geometries is a key to documenting local versus eustatic control. Sequences are three-dimensional sediment bodies whose character can change along-strike in response to varying local conditions (e.g., Fulthorpe and Austin, 1998). Mapping the distribution of

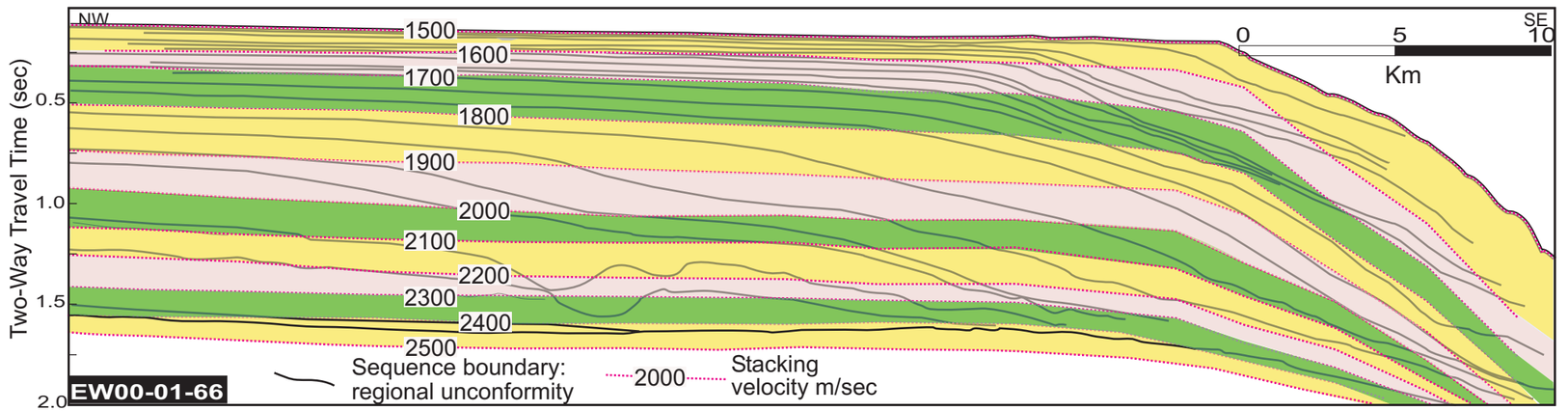

Figure 2.7. Velocity model for calculations of sequence volumes and accumulation rates. This model is constructed from seismic stacking velocities and calibrated by check-shot survey velocities from Clipper exploration well and the sonic log from ODP Site 1119. Velocities are mainly controlled by burial depth. Therefore they do not follow the interpreted sequence boundaries. Velocity at each sequence depocenter is used as the average velocity for the entire sequence

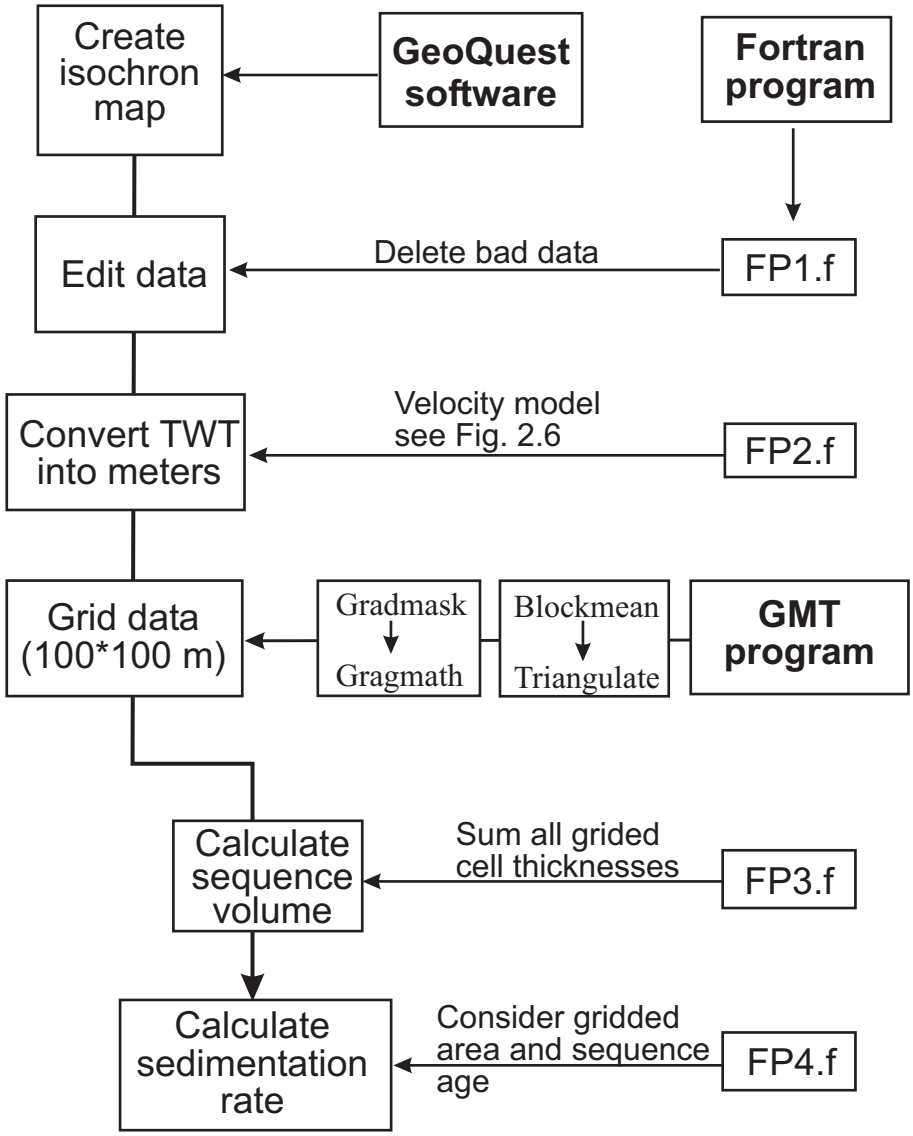

Figure 2.8. Flow chart of procedure to calculate sequence volume and sedimentation rate using GeoGuest, GMT, and Fortran software.

sedimentary sequences reveals spatial and temporal changes in sequence geometry. Migration of depocenters can indicate variations in sediment supply and sediment transport processes, including currents: erosion and deposition by contour-following currents are dominant processes in the Canterbury basin. The influence of global controls is evaluated by correlating sequences with the global sea-level curve of Haq et al. (1988), oxygen isotopic data (e.g. Billups and Shrag, 2002) and other climatic records.

2.3.2.5 Plate boundary reconstruction

The influence of local tectonism on sediment supply is evaluated by reconstructing relative plate motions at the Australia-Pacific plate boundary, marked by the Alpine Fault. Plate positions at times 33.54 Ma (chron 13o), 26.55 Ma (8o), 20.13 Ma (6o), 11.53 Ma (5o), 6.04 Ma (3Ay), 2.58 Ma (2Ay) are reconstructed, and relative plate motions (normal and parallel to the plate boundary) calculated at eleven positions along the Alpine Fault. Variations in convergence rates are then correlated with rates of sediment accumulation derived from sequence volume calculations. The methodology is described in greater detail in Chapter 5.

2.3.2.6 Ties to boreholes

Ages of seismic sequences are constrained by ties to commercial wells and ODP Site 1119. Synthetic seismograms are used to relate depth-referenced well

data to time-referenced seismic profiles (Telford et al., 1976). Ideally, synthetic seismograms are generated using both sonic and density logs. Because logging runs are not continuous to the surface, the sonic log is calibrated to the seismic datum (sea level) using a 1D check shot velocity survey from the Clipper exploration well

Synthetic seismograms are created using GeoQuest software (Figure 2.9). A suitable wavelet is convolved with acoustic impedance calculated from the sonic. Wavelets are extracted from seismic data adjacent well site. A statistical extraction function in GeoQuest produces a zero-phase wavelet with an average frequency derived from a specified seismic window; the autocorrection of all selected seismic traces is transformed into the frequency domain. The spectra are then averaged and transformed back to the time domain as a zero phase wavelet. This study uses a minimum phase wavelet instead of zero phase wavelet, which was generated from traces 4896 – 4916 on profile EW00-01-70, near Clipper well, using a window from 1550- 2002 ms. Principal frequency content ranges from 40-125 Hz with a peak at 75 Hz.

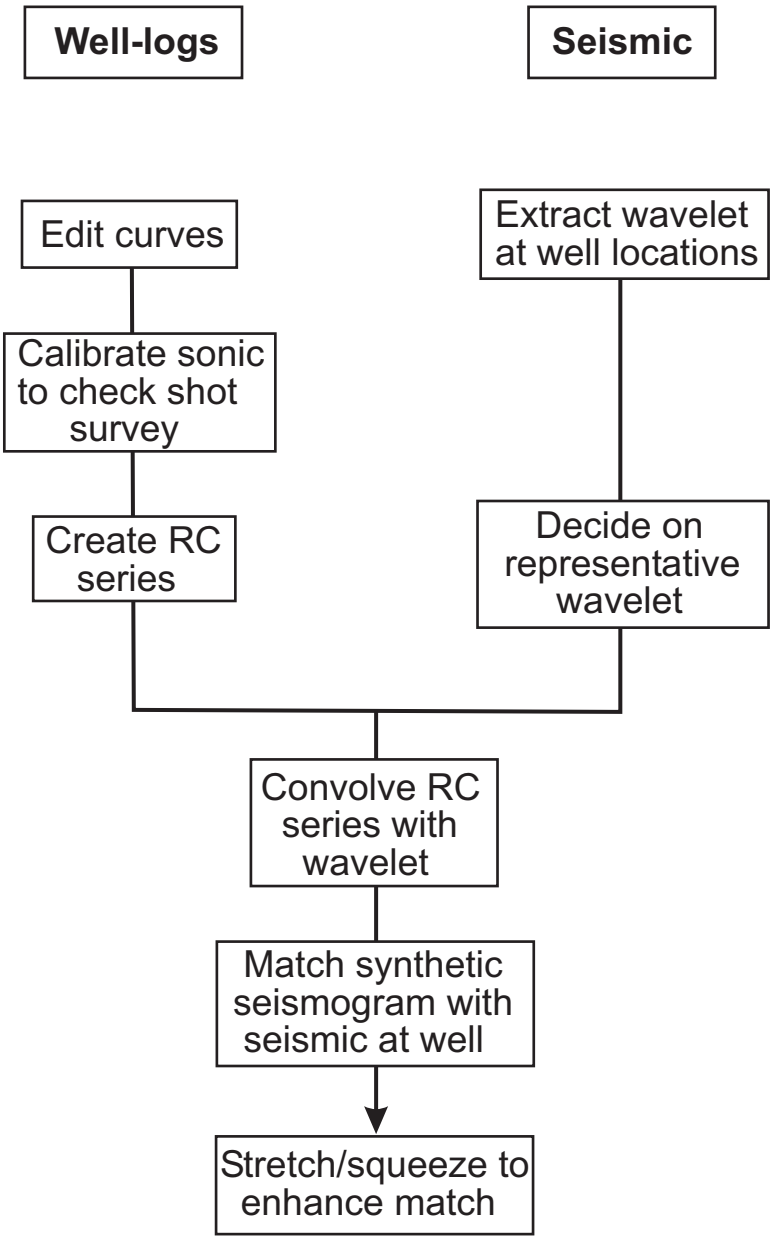

Figure 2.9. Flow chart of generalized procedure to create synthetic seismograms to tie seismic data to exploration well. RC: reflection coefficient (from Cathro, 2002).

Chapter 3: Three-dimensional architecture of shelf-building sediment drifts in the offshore Canterbury basin, New Zealand†

3.1 ABSTRACT

A grid of high-resolution, multichannel seismic profiles from the offshore Canterbury basin, New Zealand, reveal that at least eleven large (up to 1000 m thick, >50 km long, along-strike, and 20 km wide, down dip) elongate sediment drifts developed within the middle Miocene to Recent shelf-slope sediment prism. The drifts overlie a condensed section of late Eocene to late Oligocene limestone and cover an area of ~5000 km^2. The drifts were deposited in water depths of 300-750 m, probably by a northward-flowing contour current, and aggraded to shelf depths. The drifts exhibit mounded morphologies with channel-like moats along their landward flanks. Erosion of the landward flanks creates prominent unconformities; these unconformities are diachronous and, therefore, not sequence boundaries. The internal architecture of the drifts defines two end members of elongate drift, which I describe as simple and complex. Early (middle Miocene) simple drifts are small (<400 m thick, 10 to 28 km long and several km wide) and concentrated in the southern part of the survey area. Drift thickness increased as the shelf aggraded and the locus of drift development migrated

† Published in Marine Geology vol. 193 (2003), p. 19-47, with co-authors C.S. Fulthorpe, and P. Mann.

northeastward through time. Late (late Miocene to Recent) simple drifts are, therefore, larger (up to 1000 m thick, >50 km long and up to 20 km wide) and occur in the northeastern part of the survey area. These late, simple elongate drifts are subdivided into three parts (base, core, and crest) based on seismic facies. These facies form in response to progressive confinement of current flow within the moat. Complex drifts may be multi-crested or multistage. Multi-crested drifts form in response to rapid lateral shifts in position of the moat, perhaps associated with relative sea-level change, modulated by paleoslope inclination and orientation. Such drifts, together with the observation that several drifts were often active simultaneously, indicate that flow patterns were complex and involved multiple pathways. Multistage drifts comprise superimposed subdrifts whose retrogradational and progradational stacking patterns indicate fluctuations in the rate of sediment supply. Complex drift formation may require intermediate shelf relief: high enough to sustain drift development during changes in sea level and rate of sediment supply, but low enough so that such changes are still able to influence moat position. In addition, coeval climatic cooling may amplify changes in sea level, current intensity and sediment supply, thereby contributing to complex drift formation.

3.2 INTRODUCTION

Sediment drifts, or contourites, have been defined as "sediments in relatively deep water, deposited or significantly reworked by a stable geostrophic

current" (Faugeres and Stow, 1993). The effects of contour-following, deep geostrophic currents are particularly marked on continental slopes and rises and on basin plains adjacent to continental margins. In such locations, the change in seafloor gradient may locally intensify and focus currents. Sediment drifts commonly form positive topographic relief on the seabed and may be accompanied by associated sediment wave fields. Where bottom currents are particularly strong, they may cause erosion of the seabed and formation of channels, moats and furrows, resulting in complex physiography (Stoker et al., 1998).

Although sediment drifts were first described in deep-water settings swept by major current systems, they are now recognized to occur in three main settings: 1) **deep-water drifts** occur in water depths in excess of 2000 m beneath semi-permanent bottom currents (Tucholke and Mountain, 1979; McCave and Tucholke, 1986); 2) **mid-water drifts**, occur in intermediate water depths (300-2000 m) on continental slopes, as well as in mid-depth seaways and on sills (McCave and Tucholke, 1986; Fulthorpe and Carter, 1991; Armishaw et al., 2000); and 3) **outer shelf/upper slope drifts** form in relatively shallow water (50-300 m), but away from the influence of coastal or inner-shelf processes (Stow et al., 1998). Common sediment drift morphologies include paired or single, flow-parallel, longitudinal mounds and accretionary drifts that grow where currents flow along the lower slope (McCave and Tucholke, 1986; Faugeres et al., 1999). Recent work has shown that drifts can develop normal to the strike of the margin

as a result of upwelling (Serrane et al., 1999). Sediment drifts accumulations can be recognized by: 1) accretionary bedding architecture, which can be seismically imaged, 2) streamlined, flow-elongate geometry, and 3) along-slope facies trends (Galloway and Hobday, 1996).

Numerous seismically defined, channel-like features occur within the Neogene prograding sediment prism in the offshore Canterbury basin on the eastern margin of the South Island of New Zealand. The features lie near the seaward ends of paleo-foresets and were therefore initially interpreted by Carter and Carter (1987) as slope and toe-of-slope canyons. These authors assumed that these canyons were oriented normal to the strike of the coastline and shelf edge and acted as conduits for the transport of sediment from the shelf into deep water. However, subsequent recognition that the features are oriented along strike, sub-parallel to the paleomargin, and are associated with mounded seismic geometries, similar to those of North Atlantic drifts (Tucholke and Mountain, 1979; McCave and Tucholke, 1986; Stoker et al., 1998; Serrane and Abeigne, 1999), led to the reinterpretation as off-shelf sediment drifts initiated at the toes of paleoslopes (Fulthorpe and Carter, 1991). The Canterbury basin drifts are unusual in that they are up to 1000 m thick and aggraded to shelf depths (~200 m or less). Fulthorpe and Carter (1991) proposed that the shelf edge prograded by accretion of successive sediment drifts. This work also implied that the current-eroded surface formed along the paleoslope (i.e., the landward wall of the moat), might be a sequence boundary analogous to those of Vail (1987); Vail et al. (1977, 1984,

1991); Posamentier and Vail (1988). However, this model was based on low-resolution (frequencies ~15-50 Hz, vertical resolution ~20 m), widely spaced (>3 km between dip profiles and > 7 km between strike profiles) commercial multichannel seismic (MCS) profiles. As a result, previous studies provide only a two-dimensional perspective on drift development; the along-strike terminations of the drifts and the details of their accretion to the paleoshelf were not imaged.

New, high-resolution (frequencies up to 300 Hz) MCS profiles from the Canterbury basin (Figure 3.1) reveal the three-dimensional (3-D) geometries of these drifts for the first time. Some of the drifts intersect the paleoslope at an acute angle and their evolution appears to involve processes related to both along-strike current flow and downslope sediment transport. Several drifts were active simultaneously, indicating multiple current pathways. Some drifts have complex internal architecture created by local fluctuations in the position of the current core and/or changes in the rate of sediment supply. Furthermore, the enhanced vertical resolution (~5 m in the upper 1 s) allows reinterpretation of the significance of drift-bounding unconformities as diachronous surfaces distinct from sequence boundaries.

3.3 RESULTS

3.3.1 Sediment drift geometries and classification

I interpreted the channel-like features and associated mounded geometries within the Otakou Group, near the seaward ends of some paleo-foresets, as sediment drifts (Figures 3.1 and 3.2) because these features: 1) are subparallel to the paleo-shelf edge and present coastline; 2) show consistent (northwestward) onlap on dip profiles and southwestward onlap on strike profiles indicate that the sediment bodies in all cases migrated landward; 3) associated mounded morphologies are similar to those of migrating sediment drifts described in the North Atlantic (Tucholke and Mountain, 1979; McCave and Tucholke, 1986). ODP Site 1119 (Leg 181) was drilled above one of the largest, mounded drifts. Limited penetration prevented sampling of the large drift, but current deposition of the overlying sediment was confirmed (Shipboard Scientific Party, 1999). The drifts are inferred to have been deposited by a northeastward-flowing current analogous to the modern Southland Current (Carter and Herzer, 1979; Chiswell, 1996). Southland Current is intensified adjacent to the eastern continental slope of the South Island by the Coriolis deflection (Figure 2.1; Fulthorpe and Carter, 1991). Additionally, Southland Current has stronger density gradient/flow speed in winter because of stronger temperature contrasts across the Southland Front. The Southland Current can affect most of the slope to a water depth of ~800 m (Burling, 1961; Chiswell, 1996; Morris et al., 2001).

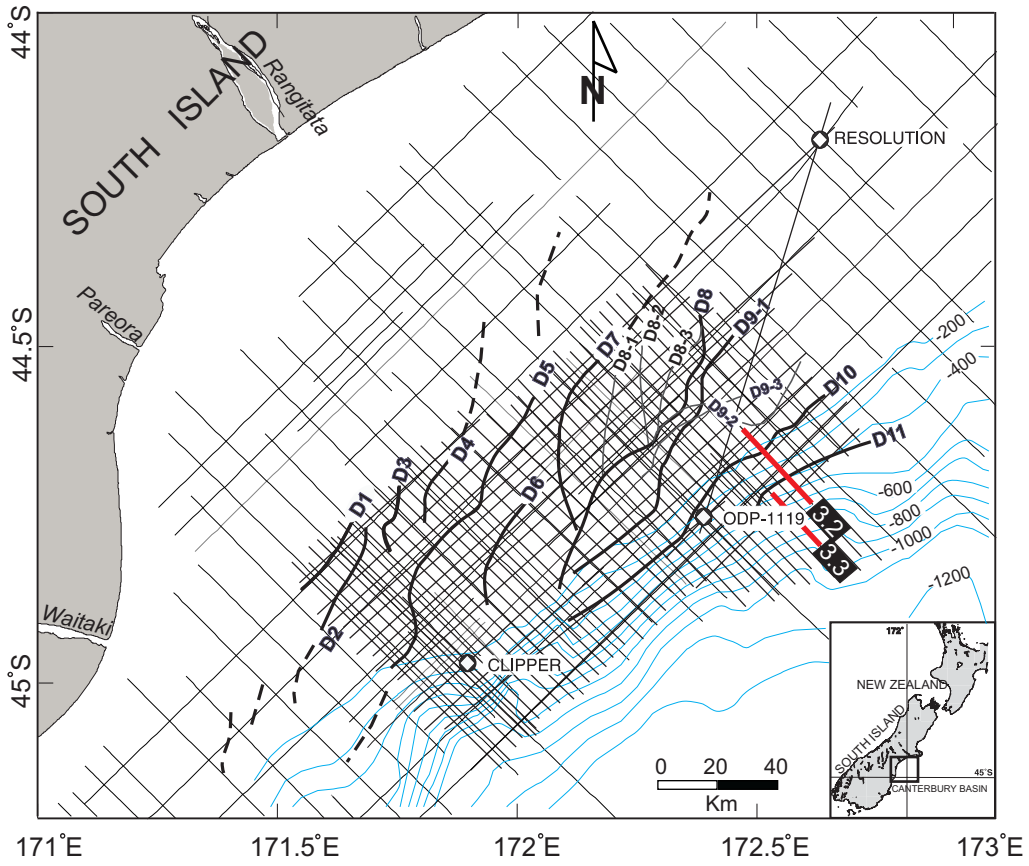

Figure 3.1. EW00-01 high-resolution MCS grid (thick straight lines), low-resolution CB-82 commercial MCS grid (thin straight lines), exploration wells Clipper and Resolution, and ODP Site 1119. Also shown is the distribution of seismically resolvable sediment drifts (D1 to D11; curved lines mark the crests of the drift mounds). D1-D6 and D10-D11 are simple elongate drifts, which comprise single drift mounds and associated moats. D7-D9 are complex drifts. The south end of D7 is truncated by D8. D8 has three subcrests (D8-1, -2, -3) and is a multi-crested complex drift. D7 may be an early phase of D8. D9 is multistage drift with superimposed sub-drifts D9-1, D9-2, and D9-3. Dashed lines represent drifts identified on CB-82 profiles outside the EW00-01 grid. Locations of Figures 3.2 and 3.3 are indicated by red lines. Bathymetric contours are in meters (blue curves).

Based on the classification of Stoker et al. (1998) for Late Eocene/Oligocene to Holocene sediment drifts of northwest Britain, two types of current deposits occur within the offshore Canterbury basin: elongate drifts and sediment waves. The elongate drifts are the largest features and dominate the stratigraphy in parts of the Otakou Group. They comprise mounded main bodies with prominent moats along their landward flanks (Figure 3.2). The Canterbury basin elongate drifts are unusual in their proximity to paleoshelf edges and their upward growth into shelf water depths (~200 m or less). Sediment waves are less important volumetrically and occur mainly at relatively shallow burial depths (<500 m beneath the sea floor) in the northern part of the survey area (Figure 3.3). Sediment waves are also locally preserved basinward of elongate drifts. The high density of EW00-01 seismic coverage was designed to provide information on 3-D stratigraphic geometries in general, and the 3-D morphologies of the sediment drifts in particular, in order to improve on the earlier 2-D model of drift morphology and development (Fulthorpe and Carter, 1991). The EW00-01 profiles reveal that the internal geometries of the drifts are far more complex than previously thought.

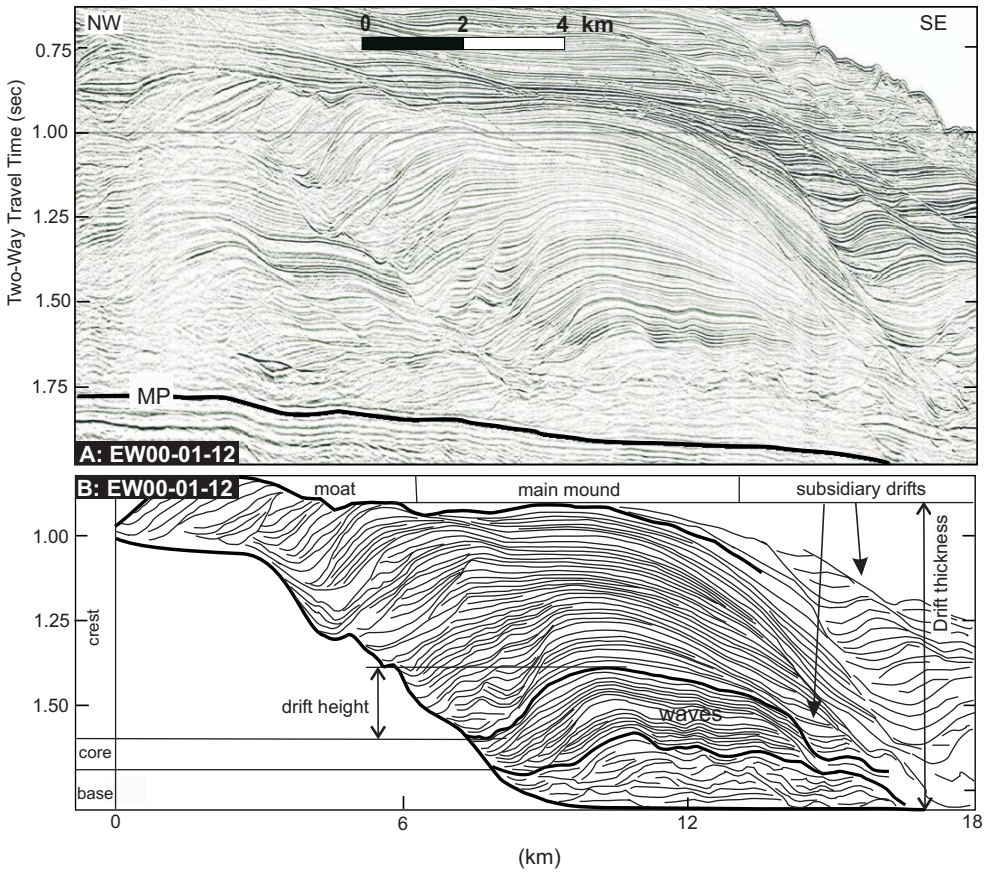

Figure 3.2. (A) Dip profile EW00-01-12 showing the main features of a large, late simple elongate drift in the north-eastern Canterbury Bight (late Miocene - Pliocene age). (B) Interpreted internal structure. The drift deposit is 18 km wide and 1000 m thick. Laterally, it can be divided into three sub-components: moat, mound, and subsidiary drifts (which may include waves). Vertically, the drift base, core (multiple small drifts or waves) and crest (main drift mound) represent three phases of drift development. Drift thickness is the total preserved accumulation from drift base to crest. Drift height is the vertical distance from moat thalweg to adjacent crest along a single reflection and is one measure of active drift height. MP: Marshall Paraconformity.

3.3.1.1 Elongate Drifts

Eleven distinct elongate drifts (D1 to D11) are mapped within the offshore basin (Figure 3.1). Internal reflections within elongate drifts downlap basinward and onlap the paleoslope (Figure 3.2). Within the main body of each drift, reflection amplitudes tend to increase vertically from the base to the central part of the deposit, followed by a decrease toward the top of the drift (Figure 3.2). Elongate drifts can be divided into two categories, simple and complex, based on their internal architecture and morphology. I describe the drifts using three representative examples (D5, D8 and D10), shown on Figure 3.4.

Simple Elongate Drifts: Simple drifts can be subdivided into early (D1-D6) and late (D10-D11) types, based on their distribution and size. Most of early simple drifts occur beneath horizon U4 and are of middle Miocene age (Figure 3.5). They evolved in the southwestern part of the EW00-01 survey area and, internally, comprise simple, asymmetric (on dip profiles) mounds. The height of the slope increased through time, from ~300 m (Fulthorpe and Carter, 1991) in the early-middle Miocene to about 900 m at present, as the shelf prograded and aggraded. Early simple drifts are therefore relatively small, <400 m thick, averaging 80-100 m, 10 to 28 km long (along- strike) and several km wide (down-dip) (Figure 3.5). Thicknesses cited refer to the thickness of the entire, preserved drift deposit and are not corrected for compaction. The height of the drift mound at any instant in time during its active phase was less than its preserved thickness.

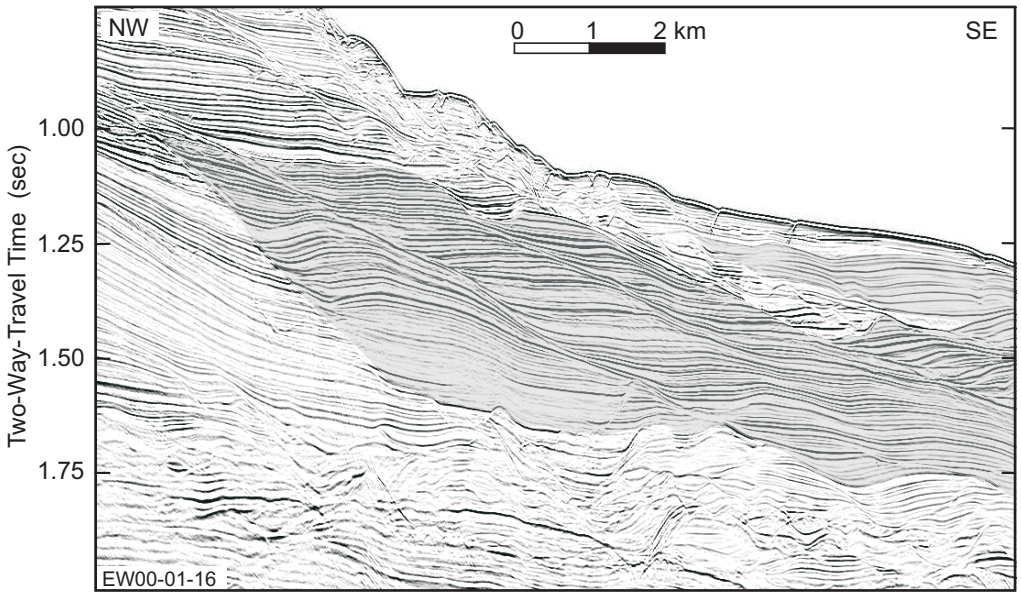

Figure 3.3. Dip profile EW00-01-16 showing sediment waves (shaded area). Wavelength is about 2 km and amplitude averages 50 m. Generally, amplitudes increase upward from the base to the middle part of the wave, then decrease to the top. See Fig. 3.1 for profile location.

The vertical distance between moat thalweg and coeval drift crest is one measure of this active drift height (Figure 3.2). Early simple drifts are the most deeply buried (>1300 m) of the drifts and have therefore experienced the most post-depositional compaction. Their apparently simple geometries could therefore be partly a consequence of compaction deformation and degraded seismic resolution with depth.

D5 (Figures 3.4 and 3.5; Table 3.1) is an example of a typical simple drift. D5 has two preserved thickness maxima along strike. The intervening thickness minimum is caused by erosion associated with overlying drift D6 (Figure 3.5A), although the eroded seaward flank of the D5 mound is overlain by drift D7 farther north (Figure 3.1). Width and thickness of D5 are greatest in the center and decrease to the north and south. At its southern end, the crest of its mound is eroded and only part of the moat remains (Figure 3.5C). Burial depth also increases southward.

Late simple drifts (D10-D11; Figure 3.1) are late Miocene to Recent in age and occur above horizon U5 (Figure 3.6). They are the largest drifts, up to 1000 m thick, >55 km long, and 20 km wide. The zone of drift development migrated northward and eastward; these largest and most recent drifts therefore underlie the northeastern part of the EW00-01 grid. They are characterized by well-developed moats, and drift mounds (Figures 3.2 and 3.6A). The drift mound is semi-symmetric to symmetric. Because of their size and shallow burial depths,

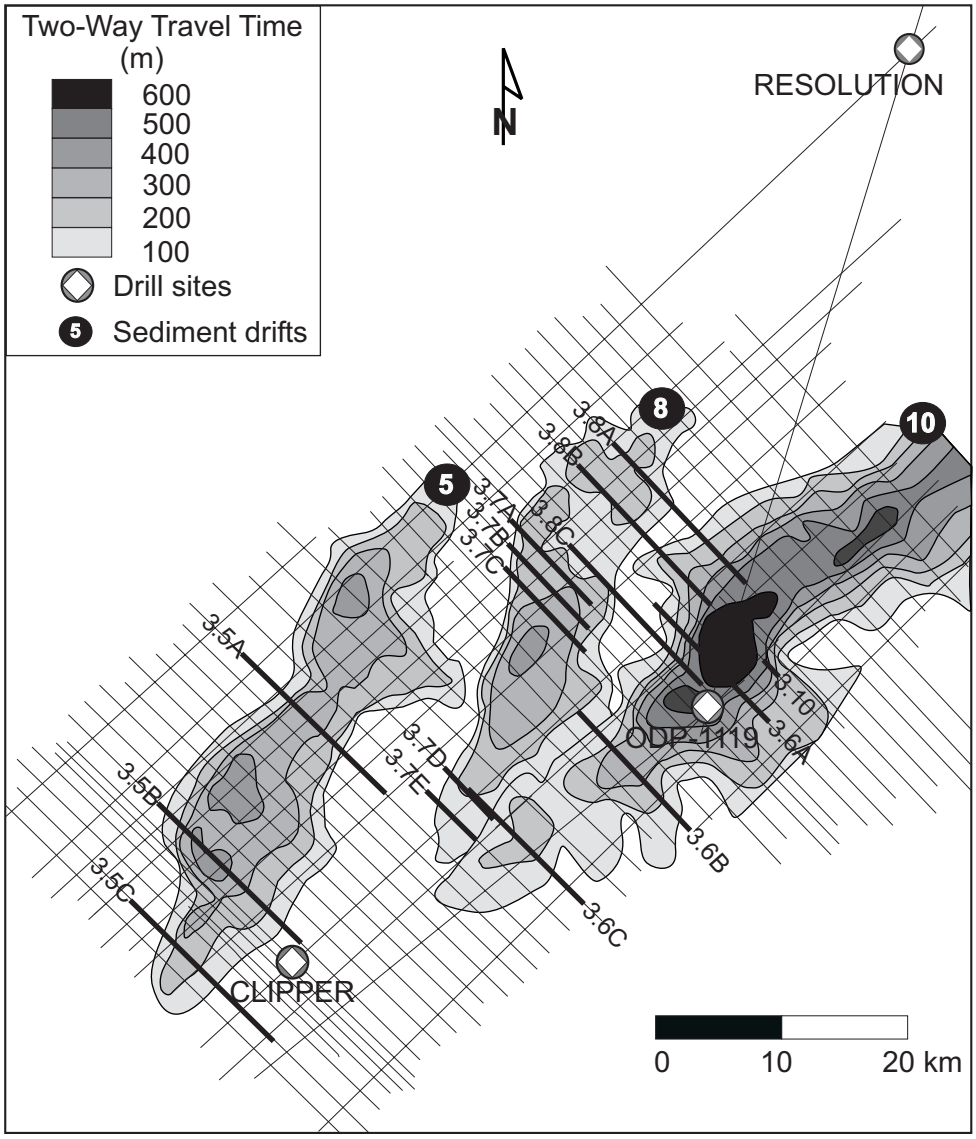

Figure 3.4. Isochron map (in msec two-way travel time) showing sediment drifts 5, 8,and 10. Drifts trend to be thick in the middle and thin along strike. Drift thickness, length, and width all increase northeastward across the basin and drift orientation becomes progressively more easterly. See text for discussion. Locations of profiles used in subsequent figures (bold lines) are shown.

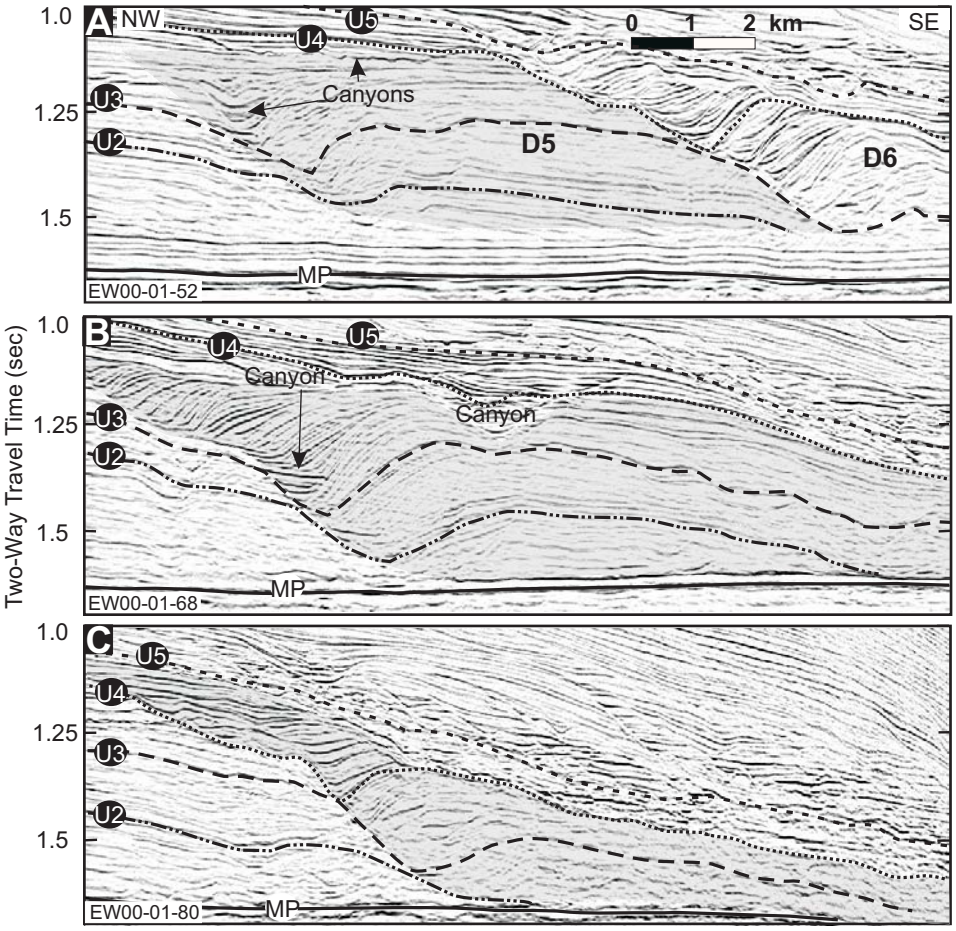

Figure 3.5. (A) Dip profile EW00-01-52 through the central part of early simple drift D5 (shaded). The basinward part of the drift mound has been eroded by drift D6. The top of the moat contains canyon-type fill. The drift is overlain by a broad canyon with a fill of high-amplitude horizontal reflections. (B) Dip profile EW00-01-68 through the south central region of D5. The mound is about 500 m thick and its crest is incised by a canyon. (C) Dip profile EW00-01-80 through the southern end of D5. Here the drift has thinned to less than 200 m. Chronostratigraphic horizons U2-U5 are shown on all profiles. See Figure 3.4 for profile locations.

late drifts are well imaged seismically and display the most complex internal structures. Vertically, late simple drifts exhibit three component seismic facies, a base, a core, and a crest (Figure 3.2), which may represent three different phases of drift development. The base facies is characterized by chaotic reflections indicating erosional scour and filling. Reflections within the overlying core are undulatory, with small (10-30 m high, 500-1000 m wide) waves/drift mounds separated by narrow (10-40 m wide) troughs/channels (also see Figure 3.6A). The moat develops adjacent to the paleoslope as the largest of these channels. Erosion of the paleoslope is common. Multiple small mounds /and waves coalesce to form the crest phase. Formation of the drift base and the original moat may relate to slide/slump deposits at the toe of slope and a depression (canyon) between the lower slope and the topographic high (slide) as observed by Rona (1969, 1970). The drift is fully mature with a well-developed moat displaying landward-dipping and aggrading, high-amplitude reflections and, usually, a single drift mound with mainly continuous reflections.

The drift D10 (Figures 3.1, 3.2, 3.4, 3.6; Table 3.1) is representative of late simple drifts. The maximum thickness of ~1000 m (averaging ~800 m) occurs near ODP Site 1119 in the central part of the drift, which thins southward along strike (Figures 3.4 and 3.6). The mapped part of D10 is 55 km long, but its northern end lies outside the EW00-01 survey area, so this thickness is a minimum estimate. The chaotic reflections of the base facies, the undulatory core

Table 3.1. Characteristics of Drifts D5, D8, and D10

Drift name	D5	D8	D10
Azimuth of crest axis	26°	20°	40°
Length along strike (km)	47	40	>55
Width (dip direction) (km)	12-17	10-15	16-21
Av. preserved Thickness (m)*	500	500	800
Maximum height (m)**	200	150	250
Comments	Early simple elongate drift	Complex drift: Multiple crests (3) in north converge southward to form a single crest.	Young large simple elongate mounded drift.

* Thickness is defined as the total thickness of preserved drift deposit.

** Height is the vertical distance from moat thalweg to the adjacent crest along a single seismic reflection. It is a measure of the active height of the drift.

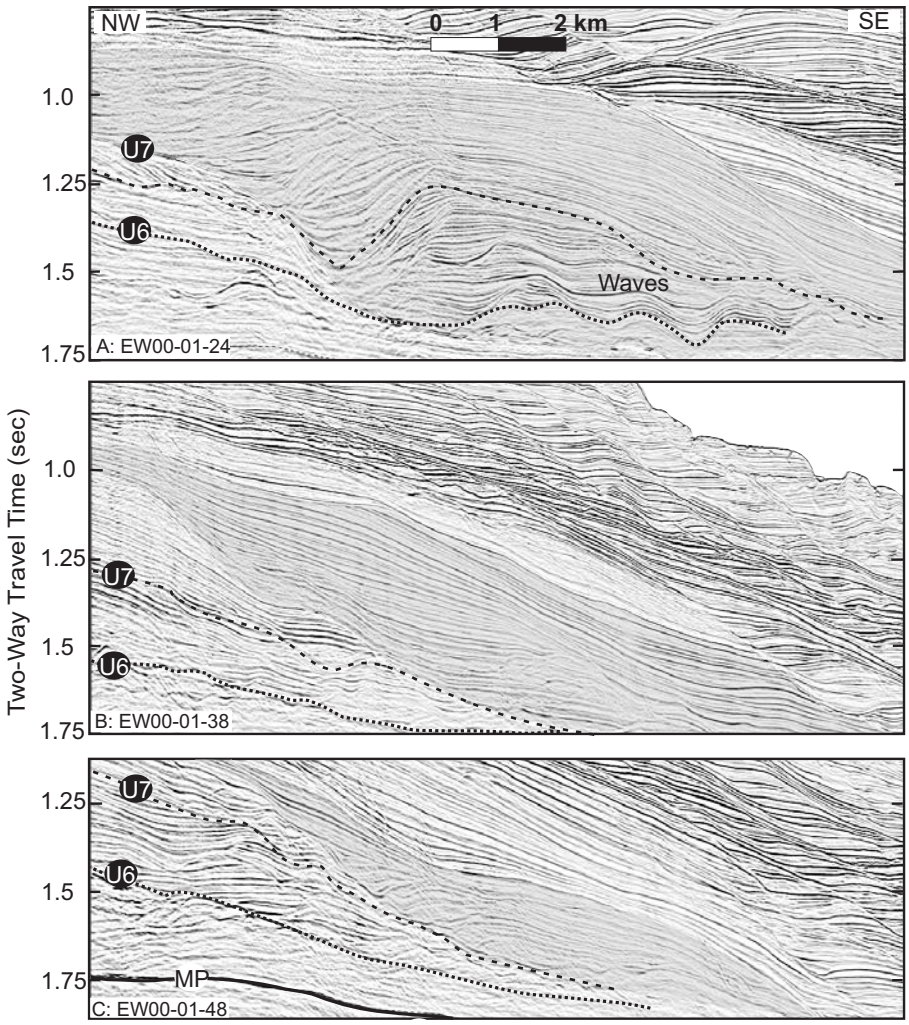

Figure 3.6. (A) Dip profile EW00-01-24 through the central zone of drift D10. Here D10 comprises a well-developed moat and a >800 m thick mound. Waves or small drifts occur within the base and core facies of the mound. (B) Dip profile Ew00-01-38 through D10 farther south. The drift thins southward and the moat and mound become less pronounced. (C) Dip profile EW00-01-48 close to the southern end of D10. Chronostratigraphic horizons U6 and U7 are shown on all profiles. See Figure 3.4 for profile locations.

facies, and the well-defined mounded crest are best developed in the thick central part of the drift (Figures 3.2 and 3.6A). Unlike drifts D5 and D8, which are eroded at their southern ends (Figures 3.5C, 3.7D and 3.7E), the drift geometries of D10 grade southward into more conventional clinoform progradational geometries (Figure 3.6B).

Complex Drifts: Complex drifts (D7-D9, Figure 3.1) developed during the middle to late Miocene, between the periods of early and late simple drift deposition. Complex drifts are therefore of intermediate thickness (>550 m for drift D8 and >650 m for the central zone of drift D9) and length (40-60 km). Along strike, these drifts are thickest in the center and thin northward and southward. The preserved deposit of complex drifts may be dominated by either moat or crest. Complex drift D8 (Figures 3.1, 7.4, 3.7; Table 3.1) is a multi-crested, or multi-mounded drift: near its northern end, it has three subcrests (Figure 3.4), which converge southward and ultimately merge to form a single, narrower drift mound. The average thickness of Drift D8 is 250-550 m. Its maximum thickness (> 550 m) occurs near the intersection of the first two crests (Figure 3.7C).

Complex drift D9 is a multistage deposit. It comprises a base drift, D9-1, upon which two smaller drifts, D9-2, and -3 (20-33 km long, <170 m thick; Figures 3.1 and 3.8), are vertically superimposed. Near its southern end, it resembles a large, simple elongate drift. Here, the moats of D9-1, -2, and D9-3 display a retrogradational stacking pattern, migrating northwestward (landward),

while remaining in close lateral proximity (Figure 3.8C). To the north, D9-1, -2, and -3 are separated by surfaces of erosional truncation and are more easily distinguished (Figure 3.8A, B). In addition, the vertical stacking pattern of D9-1, -2 and -3 has changed from retrogradational to progradational and the lateral separation of successive moats increases. In this northern zone, D9-1 displays the characteristics of a multi-crested drift (Figure 3.8A, B). Table 3.2 summarizes the characteristics of multi-crested, multistage, subsidiary drifts, and sediment waves as used in this paper.

Distinguishing the complex drifts from simple elongate drifts is not always straightforward and depends on both seismic resolution and degree of drift preservation. A single complex drift can be composed of several different drift types. For example, the south part of complex drift D8 (Figure 3.7C, D, E) is composed of a simple elongate drift that progressionally changes to a multi-crested drift to north (Figure 3.7A, B).

3.3.1.2 Subsidiary drifts

The basinward flanks of drifts are commonly truncated by current erosion associated with overlying drifts (Figures 3.5, 3.7, and 3.8). Alternatively drifts may be overlain by conventional progradational seismic geometries (Figures 3.2 and 3.6). In some cases, subsidiary drifts are perched on the basinward flanks of elongate drift mounds (Figures 3.2 and 3.8A). Subsidiary drifts are relatively

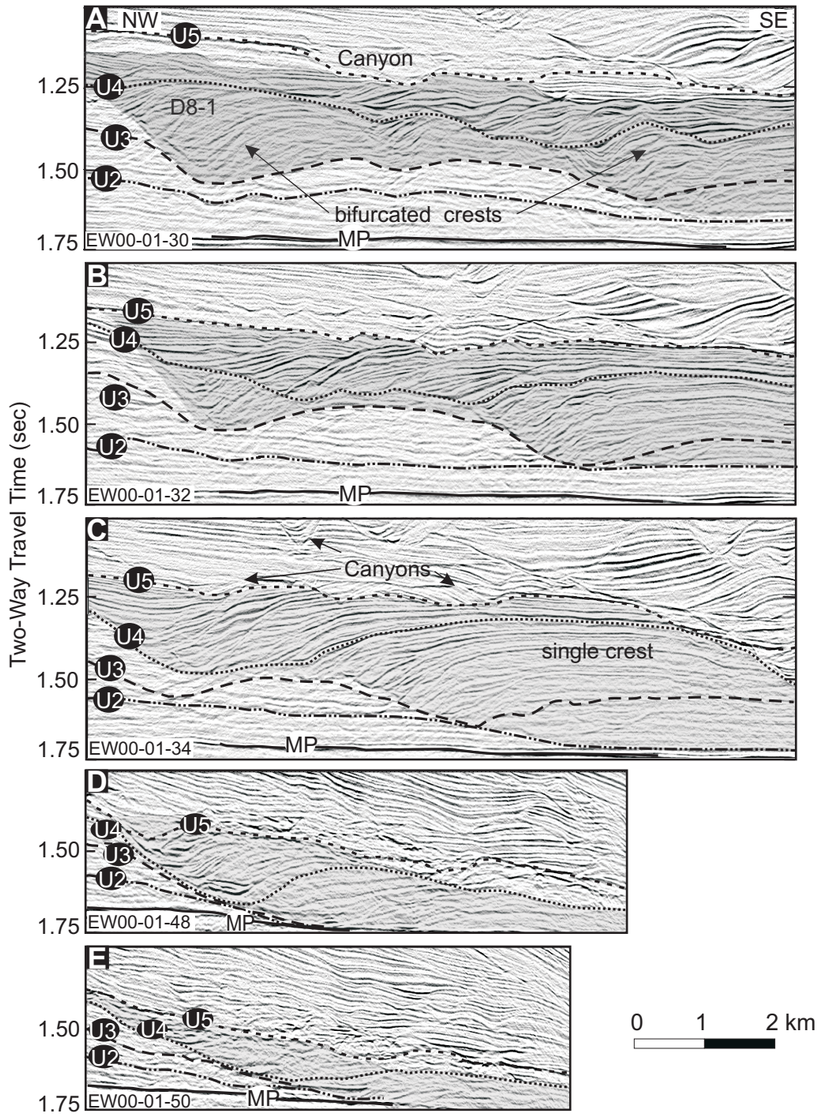

Figure 3.7. Geometry of multi-crested drift D8. (A) Dip profile Ew00-01-30 showing lateral separation of moats and a canyon that developed above the drift. (B) and (C)show the progressive southward merging of the sub-crests into a single mound. (D) Seismic profile EW00-01-48 near the southwest end of D8. The preserved drift is thin and the moat forms a large part of the deposit. (E) Seismic profile EW00-01-50 at the southwest end of D8. The drift has thinned markedly and is characterized by discontinuous and chaotic reflections. Chronostrati-graphic horizons U2-U5 are shown in all profiles. See Figure 3.4 for profile locations.

small (<100 m high from moat thalweg to adjacent crest, averaging 20-65 m, <10 km long, 20-250 m wide). Subsidiary drifts are mounded, resemble small versions of their parent elongate drifts, and develop throughout the period of elongate drift formation. The landward boundaries of subsidiary drifts pinch out against, or merge with, the parent drift mound.

3.3.1.3 Sediment waves

Sediment waves constitute only a minor component of the Otakou Group. They are common in the section post-dating the period of large, elongate drift formation and occur near paleoslope toes (Figure 3.3; Table 3.2). Sediment waves also occur at the bases of late large elongate drifts (Figures 3.1 and 3.6A). Wave amplitudes vary from ~30-90 m, with an average of 50 m, and wavelengths range from 800 to 3000 m, with an average of ~2000 m. Typical seismic facies include a basal zone of moderate amplitude reflections, interbedded with transparent layers, grading upward to a zone of high-amplitude continuous sinusoidal reflections. Moats are absent and reflection truncation is therefore rare. The landward limbs of buried waves merge with the paleoslope (Figure 3.3).

Most waves that developed beneath the slope have asymmetric profiles (Figure 3.3), whereas those basinward of the slope toe are symmetrical. The asymmetry of slope waves is the result of asymmetric transportation/deposition characteristics of the currents moving along slope. Asymmetry of slope waves may be partly a result of velocity pull-down caused by downslope increase in

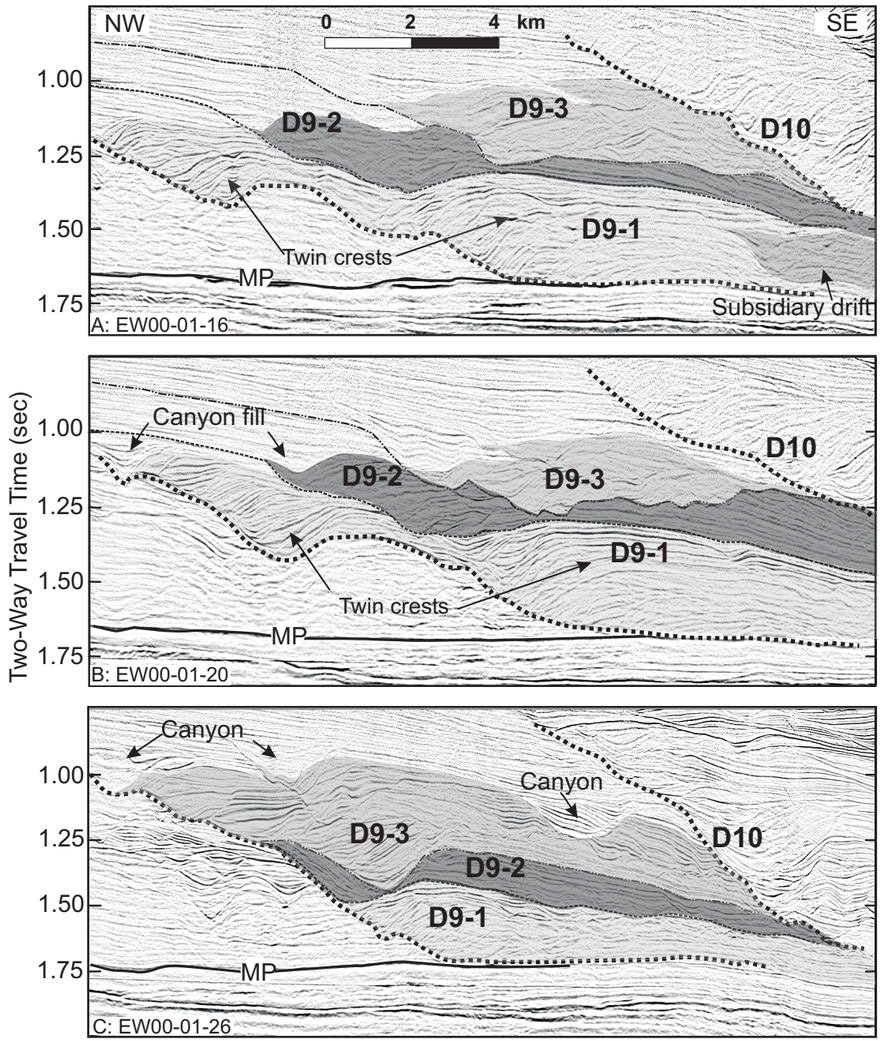

Figure 3.8. Multi-stage complex drift D9. Thick dashed lines are upper and lower boundaries of D9. D9 is composed of three successive sub-drifts (D9-1, -2, -3), which are vertically superimposed. (A) Dip profile EW 00-01-16. In the north, the moats of D9-1, -2 and -3 are separated laterally and the drifts display a progradational stacking pattern. (B) (dip profile Ew00-01-20) and (C) (dip profile EW00-01-26) are progressively more southward slices through D9. Sub-drift moats are more closely superimposed toward the south. The sub-drifts display a change from a progradational to a retrogradational stacking pattern from northeast to southwest (A to C). Other points to note are: 1) D9-3 is composed of two even smaller drifts (A, B); 2) the final phase of moat development involves canyon fill, characterized by horizontal or draped V-shaped reflections within moats (B, C), in contrast to the landward progradation typical of moat fill. Basinward prograding canyon fill occurs on the top of D9-3 (C); 3) D9-1 is a multi-crested drift in the north (A, B) where, in addition, a subsidiary drift developed basinward of the main crest (A). See Figure 3.4 for profile locations.

water depth across the modern slope. The regularity of wave shapes and their well-defined internal structure of continuous parallel reflections suggest that sediment waves are primarily depositional bedforms. Their geometries are similar to those of sediment waves adjacent to the Bounty Channel at the distal end of the eastern South Island sedimentary system (Carter et al., 1990).

3.3.2 Chronostratigraphic Significance and Three-dimensional Evolution of Sediment Drifts

The earliest drifts in the southern part of the survey area are overlain by conventional, clinoform sequences, with sequence boundaries defined mainly by seismic onlap and truncation (Fulthorpe and Carter, 1989). The geometries of these sequences are typical of those inferred to have been formed by eustasy (e.g., Vail 1987; Vail et al. 1977, 1984). The sediment drifts are also bounded by erosional surfaces and Fulthorpe and Carter (1991) speculated that the drifts might form a type of sequence that is globally synchronous. Sequence stratigraphic interpretation of the EW00-01 data, however, indicate that the bounding surfaces of sediment drifts are not sequence boundaries.

Nineteen chronostratigraphic horizons (U1-U19) are shown within the Miocene-Recent section (see surfaces U2-U7 on Figures 3.5, 3.6, 3.7, and 3.9; see Chapter 4 for detail characteristics and age controls of these horizons).

Surfaces U2-U6 provide a chronostratigraphic framework against which the evolution of the sediment drifts can be evaluated. Structure maps of these

Table 3.2 Drift terminology

Simple drift	Elongate drift with one dominant crest and moat. D5 (Figure 3.5) and D10 (Figure 3.6) are typical simple drifts.
Multi-crested drift	Elongate drift with several crests. They indicate a complex pattern of current flow and rapid lateral migration of the moat. D8 is typical multi-crested drift (Figure 3.8).
Multi-stage drift	Comprises component drifts developed sequentially and superimposed vertically. Drifts D9 (Fig. 3.9) and D11 are examples.
Subsidiary drift	Small drift that develops on the basinward flank of the parent drift (see Figures 3.2 and 3.9-U1, U2). All of the drifts (D1-D11) feature subsidiary drifts.
Sediment wave	Asymmetric (on slope) or symmetric (slope toe and basin) wave-like shape without erosional moat (Figure 3.3). Its formation relates to transportation and deposition of submarine sheet-like unconfined currents.

surfaces (Figure 3.9) provide further insight into the three-dimensional geometries and evolution of the drifts.

Deposition of drifts D5, D7 and D8 began before time U2. D5 and D7 are the two dominant active drifts at U2 and U3 times (Figures 3.5 and 3.9-U2, -U3). They became inactive after U3 time. Drift D8 has a relatively long duration and was prominent at U3 times, terminating just after U5 (Figure 3.9-U3, -U4, -U5). D9 was dominant at U5 and U6 time, while drift D10 was initiated after U5 time and dominant after U6 time. Early simple drifts and the complex drifts (D1-D9) dominated before, and late drifts (D10-D11) after U5 time (Figure 3.9).

More than one drift was therefore active simultaneously. For example, drifts D5 and D7 are dominant at U2 and U3 times; drifts D5, D6, D7, and D8 are active at U3 time (Figure 3.9). Furthermore, the seismic profiles (Figures 3.5 - 3.7) show that drift-bounding unconformities cut the chronostratigraphic surfaces, which can be traced through the cores of some drifts. The drift-bounding surfaces are therefore diachronous and the drifts are not analogous to sequences, which is an anticipated consequence of drift deposition (Christie-Blick et al., 1990).

In addition to the main moats, subsidiary, transverse moats developed on the crest of drift D5 (Figure 3.9-U2). They may be the result of leakage, across the top of drift D5, of part of the flow through the main moat. Elongate drifts are neither parallel, nor perpendicular, to paleoshelf edges (Figure 3.9). The angles between drift crests and paleoshelf edges range from several degrees to ~15°. Late simple drifts tend to be more nearly parallel to paleoshelf edges than the early

simple drifts (Figure 3.9). Paleoshelf edge orientation became progressively more easterly, changing from ~29^{o} (U4) to ~36^{o} (U6). As a result, from drifts D5 to D10 the azimuths of drift crest axes increased from ~21° (average of drifts D5, D6, D8) to 34° (average of drifts D9, D10). During this period, a pronounced increase in slope inclination occurred in the southwestern part of the survey grid (Figure 3.9). This ultimately created the modern slope configuration with slope inclination in the northern part of the grid of only 2.2^{o}, in contrast to 5^{o} in the south. The shallow inclinations beneath the northern slope reflect high accumulation rates associated with presence of the large late sediment drifts. To the south, the slope is more erosive, with canyons incising the modern seafloor just south of the EW00-01 grid (Carter and Carter, 1987; Carter et al., 1996). These canyons may be a main source for the drifts during lowstands when the canyons are most active.

Figure 3.9 also shows how the drifts evolved in three dimensions. For each drift, the moat and active drift mound migrated westward (landward). Along strike, drifts can grow toward both ends after initiation (D8), with increasing tendency to grow toward the southwestern end as the drift develops. Development of each drift ceased with filling of its moat throughout its entire length.

Finally, the structure maps provide an indirect method of estimating the water depths in which drifts developed. The travel time to the paleoseafloor at the southern (deepest) end of each moat is a measure of the depth to the area near the

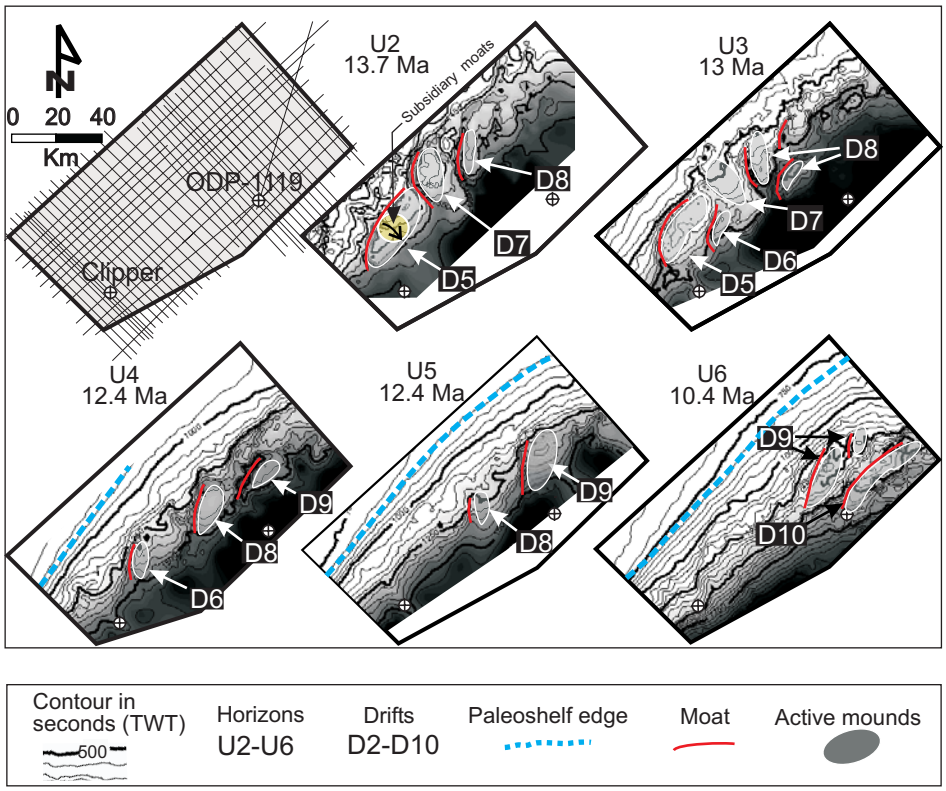

Figure 3.9 Structure maps of horizons (U2- U6). Each map covers the same area (see top left). Drifts are highlighted by shading and main moats are indicated by thin continuous lines. Subsidiary moats cross D5 (yellow circled arrows) and may represent paths of escape for parts of the flow as the moat filled. Thick dotted lines show approximate paleoshelf edges, whose orientations change from 29° (NE) to 36° from U4to U6 time. The angles between drifts and paleoshelf edges range from several to 15 degrees. Paleoslope inclinations are relatively lower at U2 to U3 time and increase from U4 to U6 time in south area; inclinations at U6 time are low in the north, as they are today, reflecting the presence of the large late drifts beneath the northern slope. See text for more discussion.

paleoslope toe where each drift initiates. The difference in traveltime between this point and the slope break at the landward side of the moat is a measure of the relief of the prograding sediment prism, adjacent to which the drift forms. This relief is, 300 to 500 ms for early drifts (D5-D8; Figure 3.9-U2, -U3) and 550 to 650 ms for late drifts (D9, D10; Figure 3.9-U4, -U5, -U6). Traveltime depth conversion and decompaction (method of Falvey and Deighton, 1982) yields relief of ~300 to ~500 m. I further assume that the slope break is identical with the paleoshelf edge. Water depths at paleoshelf edges are unknown, but probably fell within the range from 0 m to ~150 m (the latter being the water depth at the modern shelf edge). The water depths in which the drifts developed, therefore, probably ranged from ~300 to ~750 m. Although based on several assumptions, these inferred water depths, and the architectures of the Canterbury basin drifts, are similar to those associated with drifts in the Corsica Channel (300-600 m; Marani et al., 1993). Such water depths are smaller than the final thicknesses of the drift deposits (up to 1000 m, without decompaction) because the drift continued to develop during the period covered by two or more time horizons while accommodation space increased, mainly as a result of sediment loading.

3.3.3 Role of Downslope Processes

The significance of along-strike current deposition and erosion is dominant in the Canterbury basin but the effects of downslope processes on the margin are also apparent. For example, large canyons incise the modern slope

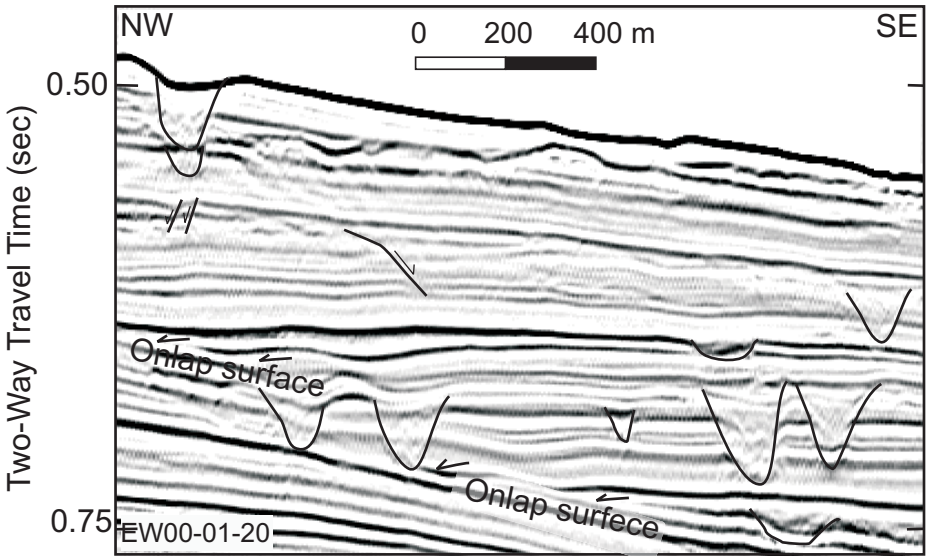

Figure 3.10. Buried V- and U-shaped gullies beneath the modern slope. The canyons are 150 m wide, and ~100 m deep. Some of them incise an onlap surface. See Figure 3.4 for profile location.

south of the EW00-01 survey area (Figure 2.1) and there is seismic evidence of buried canyons and channels.

Channels incise some buried paleoslopes in the study area (Figure 3.10). These V- or U-shaped gullies (definition of gully see Stow and Mayall, 2000), characterized by transparent and chaotic reflection fill, are too small (20-150 m width, <120 m height) to correlate between adjacent profiles (line spacings are 0.7 to 3 km). I therefore estimate gully lengths to be of the order of 1-3 km. Gullies ~100 m deep incise an onlap surface (Figure 3.10), suggesting that they are a response to a sea-level fall.

Larger V-shaped canyons (0.5->4 km width, 100-300 m height; definition of canyon see Gallowy and Hobday, 1996) incise the tops of some buried early and complex drifts (Figures 3.5B, 3.7A, C, and 3.8C). I distinguish these canyons from current-related moats because the canyon fill comprises symmetrical V-shaped, horizontal or progradational reflection geometries, in contrast to the retrogradational geometries characteristic of moats. Canyons also exhibit erosional truncation of underlying reflections on both sides. In addition, canyons are commonly offset basinward from the location of the associated moat. The change of depositional regime from retrogradational to progradational indicated by some of these drift-top canyons suggests that the incised surface can also be a maximum flooding surface, with canyon formation resulting from sediment starvation as sources are displaced landward during transgression (Galloway, 1998).

There is also evidence for canyon-related processes within some drift moats. The northern parts of the moats of drifts D5 (Figure 3.5A, B) and D7 periodically display erosion of both landward and basinward banks as those drifts approach the end of their active phases. Furthermore, the moat fill comprises symmetrical or horizontal reflections in contrast to the more typical landward migrating or chaotic fill. These characteristics suggest that some moats acted as conduits for downslope sediment transport, particularly when individual drifts approach maturity and the current within the moat wanes.

3.4 DISCUSSION

3.4.1 Hydrographic Regime

The differences in both temperature and salinity between inshore and offshore waters are sufficiently large to form a sharply delineated front, the Southland Front, continuous with the Subtropical Convergence at Present-day (Figure 2.1; Chiswell, 1996; Shipboard Scientific Party, 1999; Morris et al., 2001). The presence of drifts in the Canterbury basin suggests that the Miocene-Pliocene hydraulic regime was at least as active as the modern Southland Current. The locus of drift development migrated northeastward with time (Figures 3.1 and 3.9). Drifts migration, coupled with the increasing size of the drifts, influenced the orientation of the South Island continental margin and the inclination of its slope (decreasing to northeast). This northeastward drift migration may constitute the

best evidence for current flows to the north during the drift period, as it does today. I therefore assume, as did Fulthorpe and Carter (1991), that the paleoflow was also northward enabling Coriolis deflection (to the left in the Southern Hemisphere) to cause topographic enhancement of current velocities along paleoslopes. Current strength at water depths equivalent to the paleoslope toe (400->600 m) may have been enhanced by flow analogous to that of the modern Subantarctic Front.

3.4.2 Drift Evolution in Three-dimensions

The 2-D model of drift evolution proposed by Fulthorpe and Carter (1991) involved initiation of each elongate drift near the toe of the paleoslope with formation of strike-parallel moat between drift crest and paleoslope. As the drift crest aggraded, the elevation of the moat thalweg also increased and the thalweg migrated landward up the paleoslope. Aggradation of the drift to shelf level and filling of the moat completes the accretion of the drift to the shelf/slope sediment prism.

This simple model must be modified to incorporate the 3-D complexity revealed by the EW00-01 data (Figure 3.11). Drifts A, B, and C (Figure 3.11) illustrate the development of a typical succession of simple elongate drifts. Drift A is in an early stage of development and Drift B is more mature. Drifts grow both northward and southward along strike during these stages. However, the northern end of mature drift B has a higher elevation than its southern end. This

suggests enhanced deposition at the downcurrent end of the system, but may also reflect a higher base elevation: the drifts are oriented with their northern ends angled inboard and therefore lying higher on the paleoslope. Drift C is in its waning stage, its northern end having accreted to the slope. Along-strike growth can only be southward.

The three phases recognized in late simple drifts are probably related to the changes in the hydrographic regime accompanying drift evolution. The chaotic seismic facies of the drift base either lacks individual channels or contains numerous small channels and intervening mounds (Figures 3.2 and 3.6A). The current is therefore largely unconfined, although erosion of the palaeoslope toe occurs even at this early stage. In the drift core, seafloor morphology is more undulatory and irregular, with multiple small, mounded drifts or waves, separated by channels/troughs. The largest channel (moat) is located at the toe of the paleoslope, where erosion was by then intense (Figures 3.2 and 3.6A). Moat development accompanied non-deposition and erosion resulting from topographic intensification of the current adjacent to the paleoslope by Coriolis deflection. Deposition of the adjacent drift mound indicates reduced velocities immediately basinward. Aggradation of the drift mound leads to confinement of the current within the moat. In the drift crest phase, the small drifts have coalesced to form a single large drift mound with a well-defined moat at its landward edge forming an erosional, along-slope channel/moat. Sediment accumulation rates are lower on

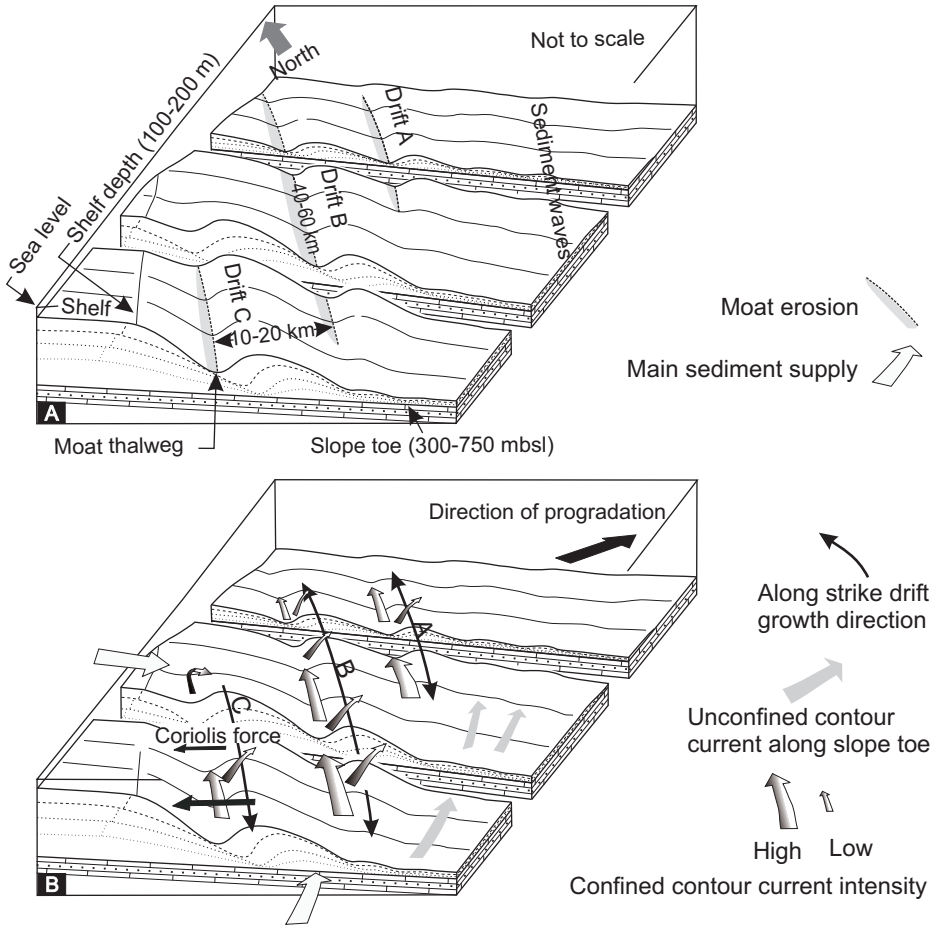

Figure 3.11. Three dimensional (3-D) schematic representation of the development of the Canterbury Basin sediment drifts. (A) 3-D drift morphology showing the geometrical relationships between moats, elongate drift mounds and sediment waves. The maximum depth of drift initiation is 300-750 meters below seal level (mbsl). Erosion typically occurred at the landward sides of moats (shaded). Drifts A, B, and C are simultaneously active. (B) Current pathways during drift development. Coriolis deflection tends to focus the current adjacent to the paleoslope. Drift A is in an early stage of development, while Drift B is more mature. Coriolis deflection enhances erosion of the landward walls of moats. Part of the current flows basinward across drift crests, sometimes through subsidiary moats. Drifts grow both northward and southward along strike in their early stages (Drifts A and B). Drifts generally achieve their maximum active height during the mature stage (Drift B). Drift C is in the waning stage of drift development. Southward growth becomes dominant as the northern end of the moat fills and the drift accretes to the paleoslope. Vertically exaggerated and not to scale.

basinward flanks drift mounds, where subsidiary drifts or sediment waves may form under the influence of the weaker flow velocities there.

As drifts aggrade to shelf water depths (e.g., Drift C, Figure 3.11), the influence of waves and tides increases. Downslope sediment transport processes also become more significant, resulting in canyon formation. This occurs in parallel with filling of the northern end of the moat, which restricts flow along the moat.

The simultaneous existence of several drifts in different stages of development attests to the complexity of current pathways. Coriolis deflection tends to focus the current adjacent to the paleoslope. However, the water mass is clearly in movement across a broad swath encompassing several drifts and also a distal sediment wave field (Figures 3.9 and 3.11). The most landward drift (D5, Figure 3.9-U2; see also Drift C, Figure 3.11) is the most mature. The northern end of its moat has filled, closing the direct current pathway. Progressive filling of the main moat causes an increasing proportion of the flow to leak across the drift crest. This can lead to formation of subsidiary moats transverse to the drift (Figure 3.9-U2).

Multi-crested complex drifts indicate that fluid pathways can also move laterally during growth of a single drift. Formation of multi-crested drifts (northern parts of D8 and D9-1; Figures 3.1, 3.7 and 3.8) appears to be related to rapid lateral shifts of the primary moat during formation of a single drift. This could be related to migration of the core of the current accompanying fluctuations

in sea level, as has been inferred to be responsible for migration of the Gulf Stream (Pinet and Normark, 1985). Comparison of Figures 3.7C and B indicates that the basinward subcrest formed first, and that the moat subsequently moved landward at around U3 time. After U4 time, the active moat jumped seaward before recommencing its landward migration. However, this only occurred in the northern parts of D8 and D9-1 (Figures 3.1, 3.7, and 3.8). The along-strike (southward) merging of subcrests indicates that migration of flow pathways is not uniform along strike and may be influenced by paleoslope orientation and gradient. The southern of D8 is indeed a simple drift, while its middle and northern is multi-crested drift, suggesting the controls of sea floor morphology and sediment supply on development of sediment drifts, the existing of current is not the necessary to form drifts.

The second type of complex drift, the multistage drift, is formed from vertically superposed subdrifts (D9; Figure 3.8). This implies fluctuations in current intensity, possibly coupled with changes in sediment supply. Changes in sediment accumulation rate along strike are indicated by the south-to-north change from retrogradational to progradational superposition of the component drifts.

Elongate drifts are not forming at present, though sediment waves occur on the modern seafloor, east of the South Island (Shipboard Scientific Party, 1999). This may be linked to the reduction in sediment supply to the slope

associated with present highstand conditions. In addition, changes in the hydraulic regime cannot be discounted.

3.4.3 Controls on Drift Development and Evolution

Shelf relief, and the water depths in which drifts initiated (~300 to~750 m), increased through time while the drifts progressed from simple (D1-D6) to complex (D7-D9) and back to simple (D10-D11). For all types, drift thickness differs from shelf relief. Instantaneous shelf relief and water depth are smaller than final drift thicknesses (up to 1000 m, without decompaction for D10 and D11) because each drift develops over an extended period of time, accompanied by increasing accommodation. However, drift thickness and evolution are related to shelf relief. Small, simple drifts (D1-D4) formed when shelf relief was low. In this setting, a relatively small change in sediment supply or relative sea level may result in abandonment and filling of the main moat and termination of the drift. High shelf relief favors formation of large drifts (D10-D11). Once the drift base has formed, small changes in sediment supply or sea level are less likely to affect moat development. Complex drifts D8 and D9 are transitional types. Moderate shelf relief may allow changes in external forcing to cause moat bifurcation (D8) or moat migration (D9) without terminating the drift. Climatic events could also influence the development of complex drifts. Drifts D8 and D9 are cut by unconformities U2-U6 and were therefore active from ~14 - 9 Ma. This period encompasses two major cooling events (at 12.5-11.5 Ma and 11-9 Ma) identified

in the southwest Pacific using the benthic foraminiferal oxygen isotope record (Kennett and der Borch, 1986). Therefore, the origin of complex drifts D8 and D9 may be linked to enhanced changes in sea level, current strength and sediment supply caused by these climatic changes.

Drift development involves both downslope and alongslope processes. However, two results indicate that downslope processes are associated with reduced drift development: 1) canyons incise the tops of some drifts (Figures 3.5B, 3.7A, C, and 3.8C); 2) moats act as conduits for downslope sediment transport only at the ends of their active phases. However, the relationship between downslope (canyon) and alongslope (drift) processes is not necessarily entirely negative. For example, glaciations at 12.5-11.5 Ma and 11-9 Ma would produce both eustatic lowstands, often associated with canyon incision, as well as enhanced current velocities, which favor drift development.

3.5 CONCLUSIONS

The Neogene shelf/slope prism in the Canterbury basin was formed by a combination of conventional clinoform progradation and the accretion of large, elongate sediment drifts. The drifts are inferred to have been formed by a northward flowing current analogous to the present Southland Current. Eleven drifts (D1-11) have been recognized and mapped within the early Miocene to Recent shelf sediment prism. Drift deposition was initiated in the southwestern part of the EW00-01 seismic grid and the locus of drift activity migrated

northeastward. Most drifts are classified as simple drifts, with a well-defined moat, sub-parallel to paleoshelves, and a large drift mound in basinward of the moat. The youngest and largest of these simple drifts occurs in the northwestern part of the EW00-01 survey area. Their internal seismic facies (base, core and crest) reflect increasing confinement and intensification of the current, initially by Coriolis deflection and later by physical confinement within the moat as the adjacent drift aggrades.

The succession of simple drifts is broken by a period of complex drift deposition. Drifts D8, and the lowermost part of D9 have multiple, laterally displaced crests, indicating rapid lateral shifts by the core of the current, possibly in response to relative sea-level change, modulated by paleoslope inclination and orientation. The identification of such multicrested drifts, together with the observation that more than one drift was commonly active simultaneously, show that flow pathways were more complex than previously recognized. In addition to flow through moats, there is also flow across the crests of the drifts, which can create subsidiary transverse moats.

Drift D9 contains multiple vertically superimposed phases, whose progradational and retrogradational stacking patterns may result from variations in the rate of sediment supply. The presence of canyons, both independent of, and associated with drifts, indicates that downslope sediment transport accompanied drift development, but its significance is obscured by that of along-strike current

deposition and erosion. Moats can act as canyons when current strength decreases as the moat fills.

The period of complex drift deposition occurred when shelf relief was intermediate. Shelf relief may have been sufficient for the drifts to sustain changes in sea level and sediment supply without the drift being terminated, but low enough so that the changes influenced moat development by causing bifurcation or migration. In addition, climatic cooling at this time may have enhanced changes in sea level, current intensity and sediment supply, thereby contributing to complex drift formation.

The new data also provide the first evidence that the unconformities created by paleoslope erosion at the landward edges of moats can be diachronous. Seismic correlation around the grid confirms that some sediment beneath the unconformities is younger than the oldest sediments overlying the unconformities. Defining the precise relationship between these unconformities and coeval conventional clinoform sequence boundaries along strike is a focus of future work.

Chapter 4: Controls on sequence stratigraphy of a middle-Miocene to Recent, current-swept, passive margin: Offshore Canterbury basin, New Zealand‡

4.1 ABSTRACT

The offshore Canterbury basin exemplifies sequence development on a prograding passive margin strongly influenced by submarine currents. Nineteen middle Miocene to Recent, regional, sequence-bounding unconformities are interpreted using high-resolution multichannel seismic data. The sequences can be grouped into larger units, based on seismic geometry and facies, which reflect different combinations of controls on sequence architecture.

Correlation with oxygen isotopic records suggests that eustasy controls the timing of sequence boundaries. The number of sequences is similar to that of coeval cycles on a temperature-adjusted, Miocene and early Pliocene $\delta^{18}O$ record. The late Pliocene to Pleistocene sequence record is of lower frequency than the isotopic record of this period, either because of the limitations of seismic resolution or removal of sequence boundaries by erosion associated with high-amplitude eustasy. However, the last two sequence boundaries correlate well with the last two 100 k.y. isotopic cycles.

---

‡ In press in GSA Bulletin, with co-author C.S. Fulthorpe.

In contrast, sequence architecture is strongly influenced by local processes. Along-strike currents create large, elongate sediment drifts that control sequence thickness; current erosion in drift moats forms diachrononous unconformities. Drifts focus deposition on the slope, reducing the rate of basinward advance of the shelf edge, but increasing that of the slope toe, thereby reducing slope inclination. Replacement of along-strike processes by downslope processes increases rates of shelf-edge progradation and the slope steepens as the reduced accommodation space over the expanded slope is filled. Clinoform geometries along strike from active drifts suggest that currents might influence clinoform formation even in locations lacking seismic evidence of current reworking.

4.2 INTRODUCTION

Depositional and erosional features on continental margins occur at a wide range of scales and are influenced by numerous terrestrial and oceanic processes, whose effects on sedimentary facies and geometries can be difficult to decipher. The effort to do so is worthwhile, because of the long history of processes recorded in continental margin stratigraphy. New technologies, e.g., side-scan sonar, multibeam bathymetry, and high-resolution seismic data, are providing new insights into the formation of continental margin sedimentary strata (Nittrouer and Kravitz, 1996; Nittrouer, 1999). In addition, stratigraphic research guided by high-resolution sequence stratigraphic models has fundamentally improved our

understanding of the controls on basin architecture (e.g., Duncan et al., 2000; Burger et al., 2002).

Sequence stratigraphy has, however, always been controversial. The assumption that sequences are controlled primarily by eustasy, and can be correlated globally (Haq et al., 1987), remains a focus of controversy because unconformities similar to those bounding sequences can also be generated by local processes, such as vertical tectonism, and erosion by submarine currents (e.g., Christie-Blick, 1991; Galloway, 1989a). Furthermore, rates of subsidence and sediment supply can also influence sequence geometry and timing by causing sequence-boundary formation to lead or lag the time of maximum rate of eustatic fall (Christie-Blick, 1991). Even eustatic sequences, therefore, need not be synchronous. A final barrier to global correlation is the imprecision of available chronostratigraphic techniques, e.g., biostratigraphy, radiometric dating, magnetostratigraphy, and chemostratigraphy (Christie-Blick et al., 1990; Christie-Blick 1991; Carter et al., 1991; Dickinson, 1993; Miall and Miall, 2001). Kidd and Hailwood (1993) estimated age resolution for various time slices since the Triassic and claimed that, except for late Cenozoic glacioeustatic cycles (Plio-Pleistocene to Present), sequences with periods $\leq 10^6$ years have durations shorter than the error in their dating and correlation.

Two distinct challenges are subjects of ongoing investigation: 1) high-resolution interpretation and prediction of the sedimentary record preserved on shelves and slopes, and 2) evaluation of the role of eustasy in controlling

sequence timing and architecture. Most recent high-resolution sequence stratigraphic analyses have focused on Pleistocene to Recent strata (Anderson et al 1996; Abbott, 1997; Chiocci et al., 1997; Naish and Kamp, 1997; Carter et al., 1998; Saito et al., 1998; Rodero et al., 1999; Duncan et al., 2000), and most such analyses concentrate on the influence of eustasy, tectonism and sediment supply on sequence development. Sediment drifts deposited by contour-following currents have been studied worldwide (Heezen and Rawson, 1977**;** Tucholke and Mountain, 1979; Locker and Laine, 1992; Hollister, 1993; Rebesco and Stow, 2001; Michels et al., 2001; Laberg et al., 2001; Lucchi et al., 2002; Franz and Tiedemann, 2002; Masson et al., 2002; Hernandez-Molina et al., 2003). However, the sequence stratigraphic significance of sediment drifts is poorly defined (e.g., Fulthorpe and Carter, 1991; Locker and Laine, 1992; Seranne and Abeigne, 1999; Llave, et al., 2001; Lu et al., 2003).

The offshore Canterbury basin (Figure 4.1) provides the opportunity to investigate sequence development in a passive margin setting strongly influenced by along-strike currents (Loutit and Kennett, 1981; Carter, 1985, 1988a,b; Browne and Field, 1988; Fulthorpe and Carter, 1989; Carter et al., 1991; Fulthorpe, 1991; Fulthorpe and Carter, 1991; Lewis, 1992; Abbott and Carter, 1994; Fulthorpe et al., 1996; Adrian, 1997; Lu et al., 2003). The focus is the Neogene "Icehouse" time period (Watkins and Mountain, 1990; Miller, et al., 1991). High rates of sediment supply since the middle Miocene, and perhaps earlier, associated with uplift along the nearby Alpine Fault plate boundary, have

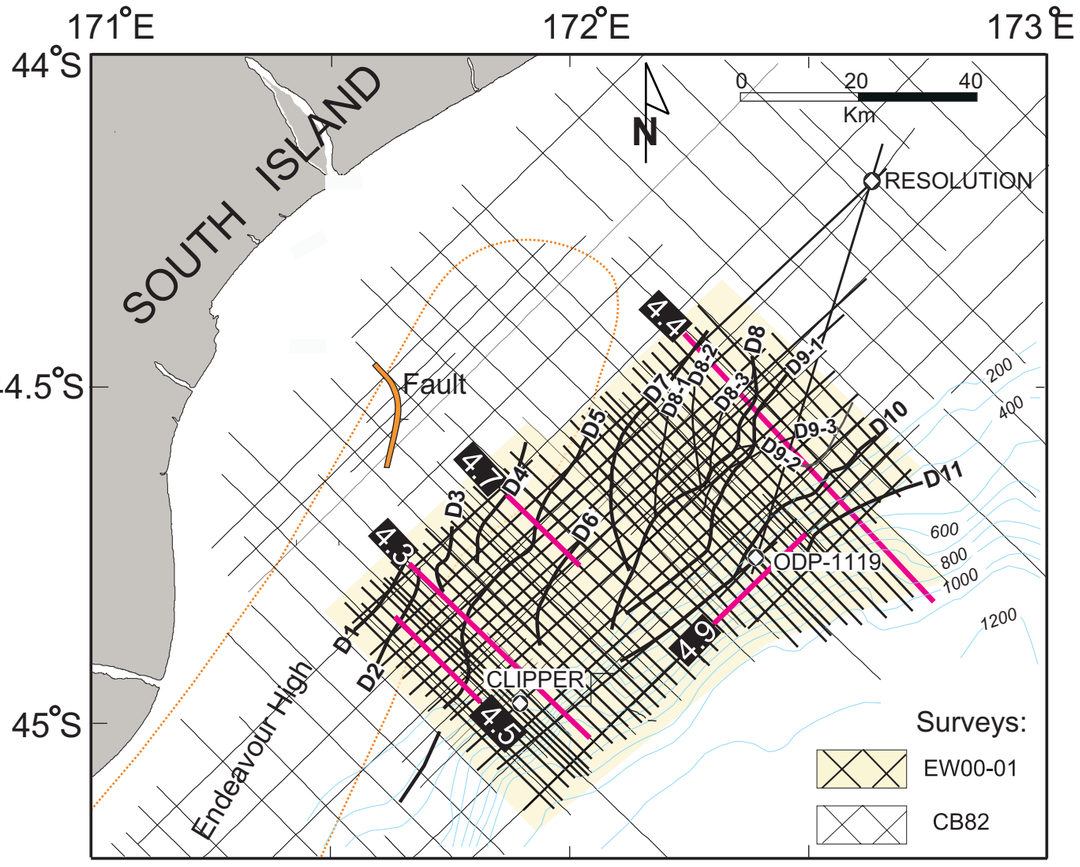

Figure 4.1. EW00-01 high-resolution MCS grid (shaded area, thick straight lines), CB82 commercial MCS grid (thin straight lines), exploration wells Clipper and Resolution, and ODP Site 1119. Also shown is the distribution of seismically resolvable sediment drifts (D1 to D11; curved lines mark the crests of the drift mounds; Lu et al., 2003). D1-D6 and D10-D11 are simple elongate drifts. D7-D9 are complex drifts. D8 has three subcrests (D8-1, D8-2, D8-3) and is a multi-crested complex drift. D9 is multistage drift with superimposed sub-drifts D9-1, D9-2, and D9-3. Endeavour High (Field and Browne, 1993) and a Pliocene-Recent north -south trending fault are delineated. Locations of Figures 4.3, 4.4, 4.5, 4.7, and 4.9 are shown by red lines. Bathymetric contours are in meters.

resulted in the preservation of an unusually high-frequency (~0.1–1.4 m.y. periods), seismically resolvable record of depositional cyclicity. In addition, along-strike currents have influenced deposition in parts of the basin, modifying sequence architecture while forming large sediment drifts within the prograding Neogene section (Otakou Group; Fulthorpe and Carter, 1991). The drifts are oriented along strike, sub-parallel to paleomargins, and each comprises a moat with an adjacent, basinward mound (Fulthorpe and Carter, 1991; Lu et al., 2003, Figure 4.1). The drifts are unusual compared to other drifts on basin margins in that they are up to 1000 m thick and aggraded almost to shelf water depths.

Middle to late Miocene sequence boundaries have been previously interpreted using widely spaced (>3 km between dip profiles and > 7 km between strike profiles), low seismic resolution (~15-50 Hz, vertical resolution ~20 m), commercial multichannel seismic (MCS) data (CB82 profiles; Figure 4.1; Fulthorpe and Carter, 1989). Upper Quaternary sequence stratigraphy has also been evaluated, using ultra-high-resolution 3.5 kHz profiles (Herzer, 1981; Barnes, 1995; Browne and Naish, 2003), but most of the Plio-Pleistocene section has received no attention. High-resolution MCS data collected in January 2000 (cruise EW00-01; Figure 4.1) provide enhanced resolution (30 to 140 Hz; vertical resolution ~5 m within the upper 0.5 s.) of the shelf sediment prism and allow a revised sequence stratigraphic interpretation of almost the entire middle Miocene to Recent section. Nineteen regional sequence-bounding unconformities and fourteen local unconformities are identified. Sequence geometries and

unconformity morphologies reflect competing influences of eustasy, contour currents, rate of sediment supply, and seafloor morphology. This interval can be subdivided into three sections, based on seismic geometries and facies, which reflect different combinations of controls on sequence architecture. Correlation with regional and global oxygen isotopic records and the Haq et al. (1987) eustatic curve suggests a strong component of eustatic control.

4.3 RESULTS

4.3.1 Seismic Stratigraphic Framework

4.3.1.1 Sequence framework

The nineteen middle Miocene to Recent regional unconformities (U1-U19) define basin-wide (~5000-8000 km^2), regional sequences, S1-S19 (sequence numbers are those of the underlying regional unconformity, Figure 4.2; Table 4.1). Unconformities U1-U19 can be subdivided into three units based on seismic facies, unconformity geometry, and sequence architecture (Figures 4.3 and 4.4). U1-U3 represent basin-wide events, but much of their sequence stratigraphic significance remains uncertain because their paleoshelves are not present within either the EW00-01 or CB82 survey areas. The presence of clinoform breakpoints and paleoshelves at regional unconformities, beginning with U4, provides more direct evidence of changing depositional regime, e.g., shelf onlap, shelf channel incisions, truncation of underlying reflections near paleoshelf edges, and changes

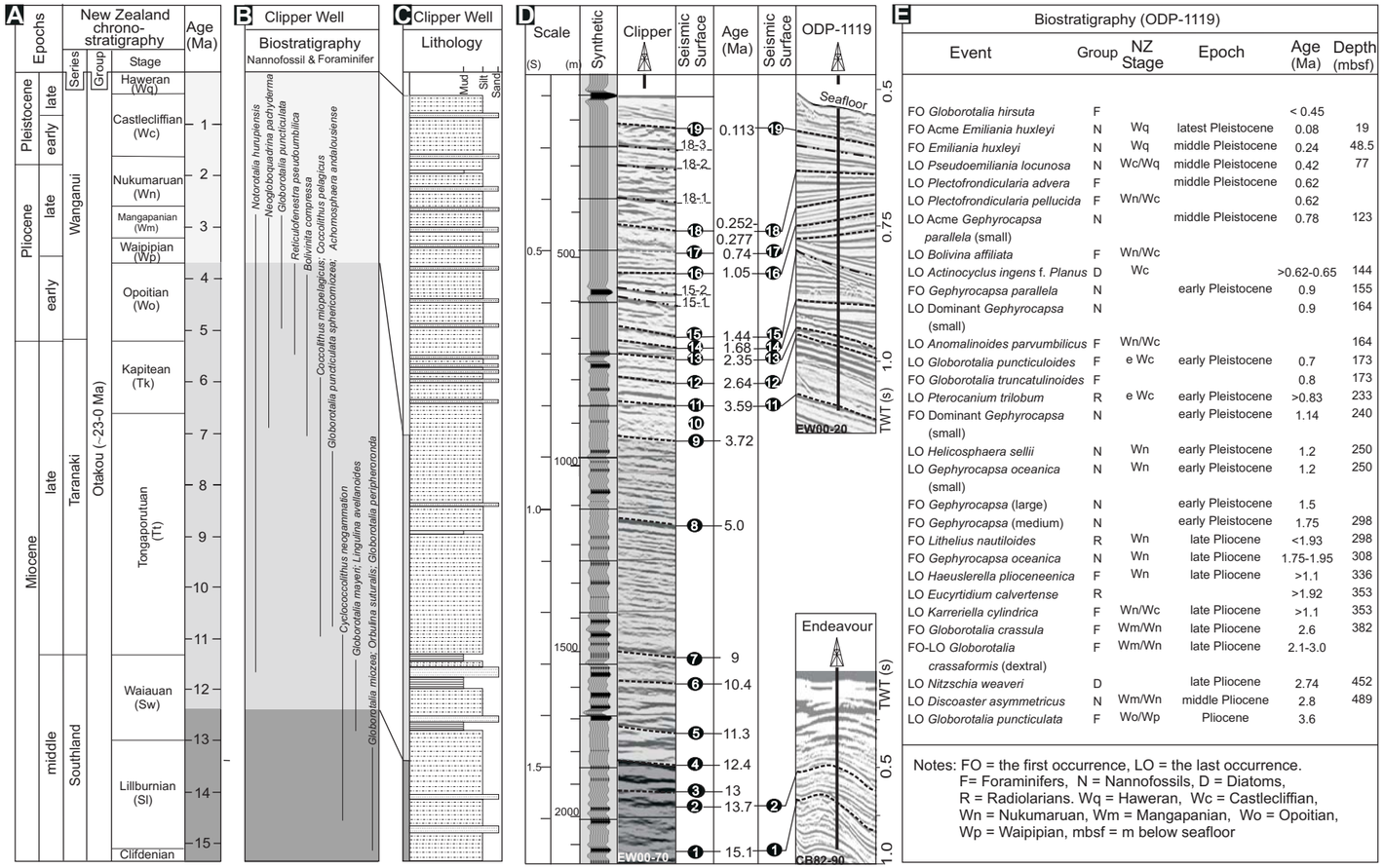

Event	Group	NZ Stage	Epoch	Age (Ma)	Depth (mbsf)
FO *Globorotalia hirsuta*	F			< 0.45	
FO Acme *Emiliania huxleyi*	N	Wq	latest Pleistocene	0.08	19
FO *Emiliania huxleyi*	N	Wq	middle Pleistocene	0.24	48.5
LO *Pseudoemiliania locunosa*	N	Wc/Wq	middle Pleistocene	0.42	77
LO *Plectofrondicularia advera*	F		middle Pleistocene	0.62	
LO *Plectofrondicularia pellucida*	F	Wn/Wc		0.62	
LO Acme *Gephyrocapsa parallela* (small)	N		middle Pleistocene	0.78	123
LO *Bolivina affiliata*	F	Wn/Wc			
LO *Actinocyclus ingens* f. *Planus*	D	Wc		>0.62-0.65	144
FO *Gephyrocapsa parallela*	N		early Pleistocene	0.9	155
LO Dominant *Gephyrocapsa* (small)	N			0.9	164
LO *Anomalinoides parvumbilicus*	F	Wn/Wc			164
LO *Globorotalia puncticuloides*	F	e Wc	early Pleistocene	0.7	173
FO *Globorotalia truncatulinoides*	F			0.8	173
LO *Pterocanium trilobum*	R	e Wc	early Pleistocene	>0.83	233
FO Dominant *Gephyrocapsa* (small)	N		early Pleistocene	1.14	240
LO *Helicosphaera sellii*	N	Wn	early Pleistocene	1.2	250
LO *Gephyrocapsa oceanica* (small)	N	Wn	early Pleistocene	1.2	250
FO *Gephyrocapsa* (large)	N		early Pleistocene	1.5	
FO *Gephyrocapsa* (medium)	N		early Pleistocene	1.75	298
FO *Lithelius nautiloides*	R	Wn	late Pliocene	<1.93	298
FO *Gephyrocapsa oceanica*	N	Wn	late Pliocene	1.75-1.95	308
LO *Haeuslerella plioceneenica*	F	Wn	late Pliocene	>1.1	336
LO *Eucyrtidium calvertense*	R			>1.92	353
LO *Karreriella cylindrica*	F	Wn/Wc	late Pliocene	>1.1	353
FO *Globorotalia crassula*	F	Wm/Wn	late Pliocene	2.6	382
FO-LO *Globorotalia crassaformis* (dextral)	F	Wm/Wn	late Pliocene	2.1-3.0	
LO *Nitzschia weaveri*	D		late Pliocene	2.74	452
LO *Discoaster asymmetricus*	N	Wm/Wn	middle Pliocene	2.8	489
LO *Globorotalia puncticulata*	F	Wo/Wp	Pliocene	3.6	

Notes: FO = the first occurrence, LO = the last occurrence.
F= Foraminifers, N = Nannofossils, D = Diatoms,
R = Radiolarians. Wq = Haweran, Wc = Castlecliffian,
Wn = Nukumaruan, Wm = Mangapanian, Wo = Opoitian,
Wp = Waipipian, mbsf = m below seafloor

Figure 4.2. (A) Canterbury Basin stratigraphy (Hornibrook, 1992). (B) Biostratigraphy (nanofossil and foraminefer) from Clipper well (Crux et al., 1984). (C) Lithology from Clipper well (Hawkes and Mound, 1984). (D) Ages of regional unconformities U1-U10 are derived mainly from the Clipper and, for U1 and U2, Endeavour exploration wells (Hawkes and Mound, 1984; Wilding and Sweetman, 1971). Ages of U11-U19 are from ODP Site 1119 (Shipboard Scientific Party, 1999; R.M. Carter et al., 2004). Local unconformities 15-1, 15-2, 18-1, 18-2, and 18-3 are also indicated. Traveltime/depth conversion used synthetic seismograms derived from digital sonic and density logs for Clipper and Site 1119. Seismic profile segments shown are EW00-01-70 at Clipper, EW00-01-20 at ODP-1119, and CB-82-90 at Endeavour. (E) Biostratigraphic events (foraminifer, calcareous nannofossil, diatom, and radiolarian) and absolute ages from Site 1119 (Shipboard Scientific Party, 1999).

Table 4.1. Middle Miocene-Present sequences of Canterbury basin and comparison with climatic events of the southwest Pacific region

Seismic surface	Age estimate (Ma)	Sequence	Period (Ma)	Order*	Southwest Pacific Cenozoic climatic events (Kennett and von der Borch,1986)
		S19	0.113	5	Intensified glacial-interglacial fluctuations linked to expansion of Northern Hemisphere ice sheets
U19	0.113	S18	0.139 - 0.164	5	
U18	0.252-0.277	S17	0.463	4	
U17	0.74	S16	0.31	4	
U16	1.05	S15	0.39	4	Late Pliocene cooling: beginning of major Northern Hemisphere ice accumulation (2.6-2.4 Ma)
U15	1.44	S14	0.24	4	
U14	1.68	S13	0.67	3	
U13	2.35	S12	0.29	4	
U12	2.64	S11	0.95	3	Middle Pliocene cooling due to increased Antarctic glaciation (3.6-3.4 Ma)
U11	3.59	S10	0.06	6	
U10	3.65	S9	0.07	6	
U9	3.72	S8	1.28	3	Warming (5-4 Ma)
U8	5	S7	4	3	Terminal Miocene cooling (6.3-5 Ma). Late Miocene warming (9-6.5 Ma).
U7	9	S6	1.4	3	First late Miocene cooling period (11-9 Ma)
U6	10.4	S5	0.9	3	
U5	11.3	S4	1.1	3	Latest middle Miocene cooling period (12.5-11.5 Ma)
U4	12.4	S3	0.6	3	
U3	13	S2	0.7	3	Middle Miocene cooling period: major ice-volume increase in East Antarctica (14.5-13 Ma)
U2	13.7	S1	>1.4	3	
U1	>15.1				

* The definitions of sequence orders are same as those of Duval et al. (1998) and Fulthorpe (1991): >50 Ma (1st order), 3-50 Ma (2nd order), 0.5-3 Ma (3rd order), 0.1-0.5 Ma (4th order), ~0.1 Ma (5th order), and ~0.04 Ma (6th order).

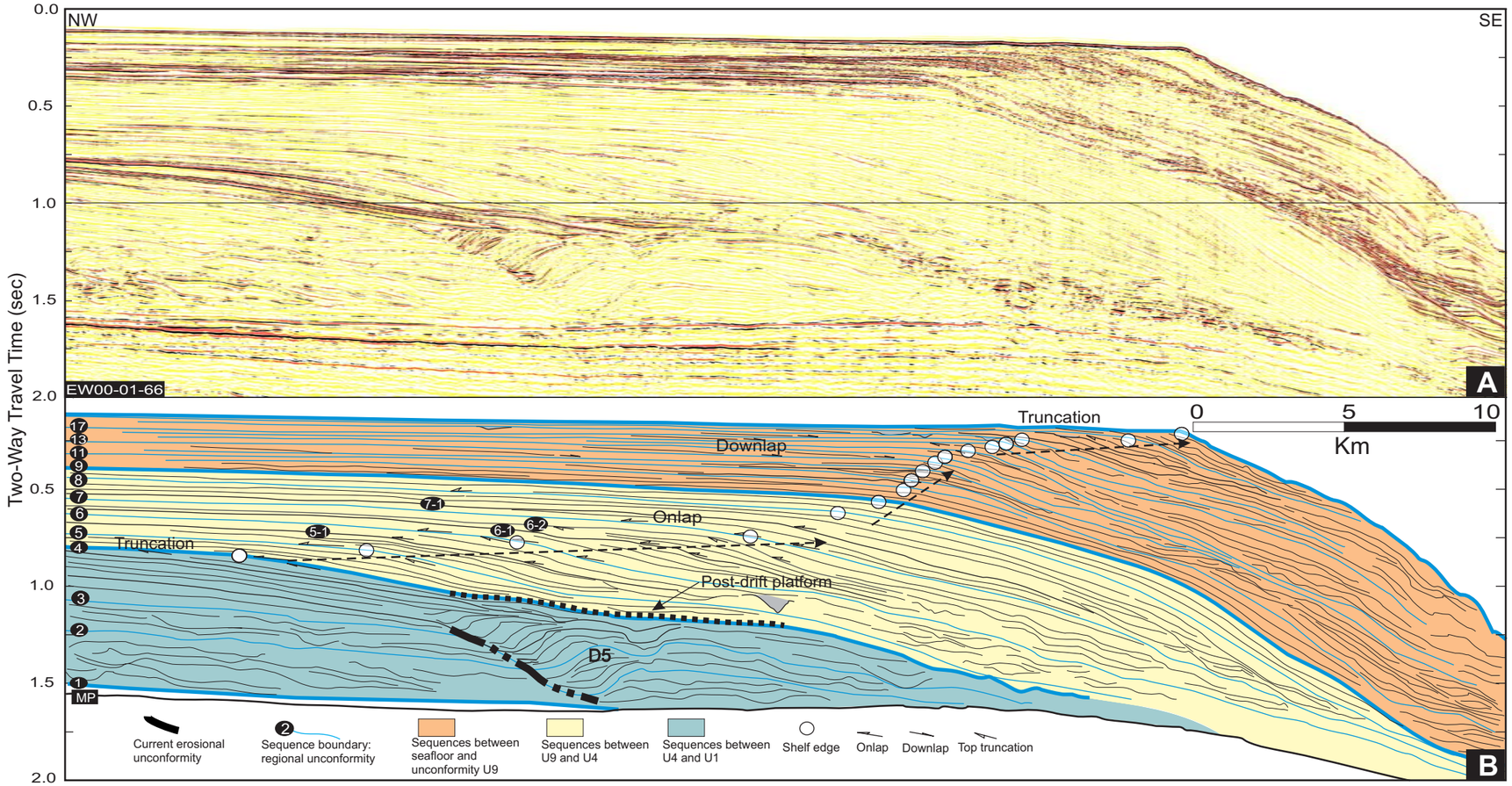

Figure 4.3. (A) Uninterpreted MCS dip profile EW00-01-66 from southern part of the survey grid (see Figure 4.1 for location). (B) Interpretation showing sequence boundaries and selected locations of seismic terminations. The amount of progradation decreases from U8-U12, increasing again from U13-U19. Unconformities U4-U8 are onlapped and truncate underlying reflections; In contract, U10-U19 are downlapped on paleoshelves, but also truncate underlying reflections. Sediment drift development in this area had largely ceased by U4. Only drift D5 is present; it is capped by a post-drift slope platform at U4. Prograding clinoforms dominate later sequences and the slope steepens (3-5°). Erosional unconformities at the landward edges of drift moats are diachronous and intersected by multiple sequence boundaries.

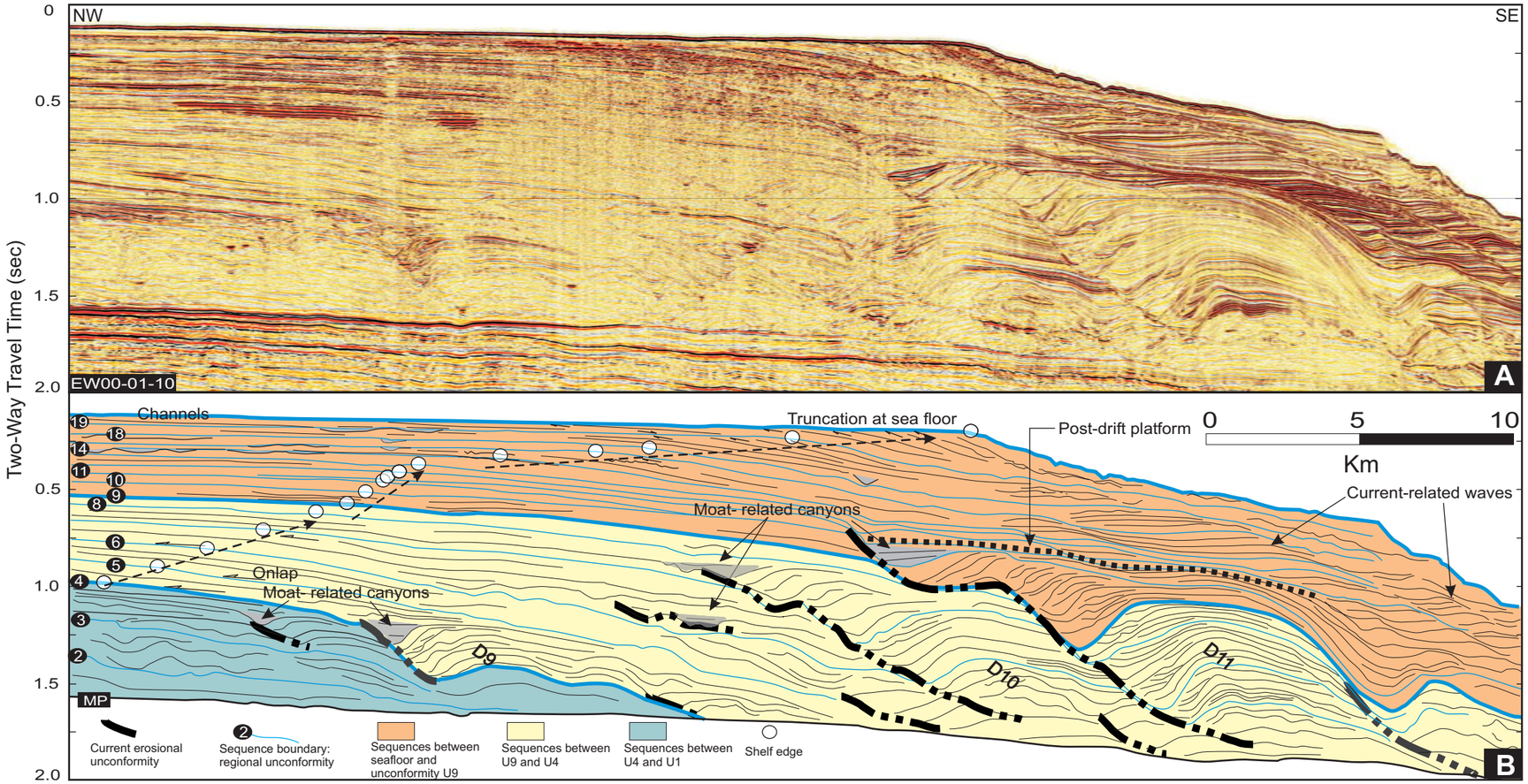

Figure 4.4 (A) Uninterpreted dip profile EW00-01-10 in the northern part of the survey grid (see Figure 4.1 for location). (B) Interpreted profile. Mounded sediment drifts, with landward moats, occur higher in the section than in the south (Figure 4.3) and are both larger and more numerous (D9-D11 are shown). Fill of some moats during their waning stages is symmetrical, in contrast to the dominant northwestward-migrating fill, indicating that they act as canyons near the end of their active phase. Slope gradients of U4-U8 are more gentle (<3°) than in the south and paleoshelf edges less well defined. Shelf edge progradation is slower than in the south, but sediment drift development causes thickening of sequences between U4 and U9 on paleoslopes. Consequently, slope toes prograde more rapidly than in the south. Shelf-edge progradation is more pronounced after termination of drift deposition at U13 and slope inclination begins to increase with the transition to clinoform progradation, which is, however, less advanced than in the south. A paleoslope platform existed above the last elongate drift (D11), creating a concave slope profile, in contrast to the convex profile during this period farther south (Figure 4.3).

in sequence internal reflection patterns. Based on such evidence, together with the presence of occasional upper-slope canyons (at U4 and U9–U19), U4-U19 are defined as sequence boundaries. Fourteen areally restricted, local unconformities also occur, mainly preserved at their paleoshelves. Local unconformities terminate landward either by onlap against the underlying regional unconformity (U5-1, U6-1, 2, U7-1) or truncation by the overlying regional unconformity (local unconformities between U15 and U19). Basinward, they can be truncated by the overlying regional unconformity (U3-1, 2; U5-1, U13-1), dowlap against the underlying regional unconformity (U6-1, U12-1), or pass through sediment drifts, thereby becoming difficult to trace on the slope.

Three buried structures lie within the area covered by the CB82 survey, but outside the EW00-01 grid (Figure 4.1). 1) Uplift of southwest-to-northeast-oriented Endeavour High was initiated during the late Oligocene and terminated in the early Miocene (Field and Browne, 1993). 2) A more localized paleohigh, in the vicinity of Resolution exploration well, was caused by intrusions associated with Banks Peninsula volcanism (12-5.8 Ma, Sewell and Lewis, 1988). 3) A Pliocene-Recent, near-vertical, north-south trending fault, ~15 km in length, with rupture at or near the sea floor, occurs northwest of the EW00-01 grid (Figure 4.1). Vertical displacement is up to 250 m, downthrown to the east, and decreases southward. All three structures bound the basin depocenter, which lies in the area covered by the EW00-01 survey and is undeformed.

4.3.1.2 Age controls of sequence boundary

Clipper exploration well and ODP Site 1119 lie within the EW00-01 grid (Figure 4.1). The ages of regional unconformity surfaces U3 to U10 are constrained by foraminifereral and nannofossil biostratigraphies from Clipper (Crux et al., 1984; Figure 4.2). Ages of U11 to U19 are mainly derived from ODP Site 1119 biostratigraphy (foraminiferal, nannofossil, diatom, and radiolarian; Shipboard Scientific Party, 1999; Carter et al., 2004; Figure 4.2). Synthetic seismograms for Clipper and Site 1119, derived from digital sonic and density logs, aided traveltime/depth conversion. Endeavour (Wilding and Sweetman, 1971) and Resolution (Milne, 1975) exploration wells were tied to the EW00-01 survey using CB82 profiles to define and calibrate the lowermost unconformities U1, U2, and U3.

Ages of late Pliocene to Recent unconformities U11-U19 are most reliable since they derive from Site 1119, which cored a near-complete section of late Pliocene and Pleistocene sediments; only one downlap unconformity (U18 at 87 mbsf) has a significant hiatus (~25 k.y.). U19 (48 mbsf) corresponds to the stage 5/6 boundary (~113 ka) and the age of the deepest sediment recovered is ~3.6 Ma (Carter et al., 2004). Furthermore, ages within the upper ~100 m below sea floor at Site 1119 have been refined using radiocarbon dates and by matching the Site 1119 gamma-ray log with the Vostok ice core record (Carter et al., 2004). Ages of Miocene unconformities are less well constrained, with the possible exceptions of

U3 (13 Ma), U5 (11.3 Ma), and U8 (5 Ma), which are coincident with New Zealand chronostratigraphic stage or series boundaries.

4.3.1.3 Middle miocene unconformities U1-U4 (>15 -12.4 Ma)

Unconformities U1-U4 bound sequences comprising high-amplitude, continuous reflections on the upper-middle slope (Figure 4.5). Onlap against U1, U2, and U3 is present only on CB82 profiles outside the EW00-01 grid. Onlap is particularly pronounced at U1 on Endeavour High. U1 downlaps onto a reflection interpreted as the Marshall Paraconformity (Figure 4.3). U1 also marks the initiation of seismically resolvable elongate sediment drifts. Drifts D1-D8 were all initiated near U1 time in the southwestern part of the EW00-01 grid (Figure 4.6). U2 can be traced into the northern part of the EW00-01 grid where it passes through drifts D1-D3 in their waning stages, and through D5-D8 as mature drifts. U2 is onlapped and, in turn, onlaps U1. U3 is a downlap surface over the high at Resolution and possibly farther south. In contrast, U3 is onlapped over Endeavour High. U3 marks the termination of elongate drifts D1-D4 in southern part of the EW00-01 survey and also terminates some poorly defined drifts, lacking moats and mounds, farther north. U3 is mappable across both EW00-01 and CB82 surveys. U1-U3 lack clinoform breakpoints, throughout the available seismic coverage. All imaged onlap is, therefore, against paleoslopes. However, two local unconformities (U3-1 and U3-2), which occur between U3 and U4, display breakpoints in the northeastern corner of the EW00-01 grid. Unconformity U4 is

the oldest regional unconformity with a distinct breakpoint (Figures 4.3-4.5). Its paleoshelf is onlapped, with truncation or toplap occurring below the paleoshelf near the breakpoint. Large U-shaped, upper-slope canyons (several hundreds to1000 m wide, >100 m deep) incise U4 on Endeavour High and V-shape slope canyons (40-80 m deep, <100 m wide) occur on the high near Resolution. These features suggest that U4 is the product of a significant relative sea-level fall accompanied by erosion. U4 terminates the development of D5 and coincides with the waning stages of D6-D8 and initiation of D9 (Figure 4.6). Termination of D5 led to formation of a post-drift slope platform above U4 in the southern part of EW00-01 survey (Figure 4.3).

4.3.1.4 Upper middle Miocene to lower Pliocene unconformities U5-U8 (11.3 - 5 Ma)

Unconformities U5-U8 are continuous reflections with distinct breakpoints and bound sequences whose internal reflections are sigmoid and of lower amplitude than those below U5 (Figures 4.3-4.5). Paleoshelves of U5-U8 are onlapped by overlying reflections, with truncation or toplap beneath their outer paleoshelves near breakpoints. Such reflection terminations are particularly pronounced at U5 and U7. Paleoshelf onlap is less common against U8. U5-U8 cannot be traced far south of the EW00-01 grid, toward Endeavour High, because an intervening canyon truncates these surfaces.

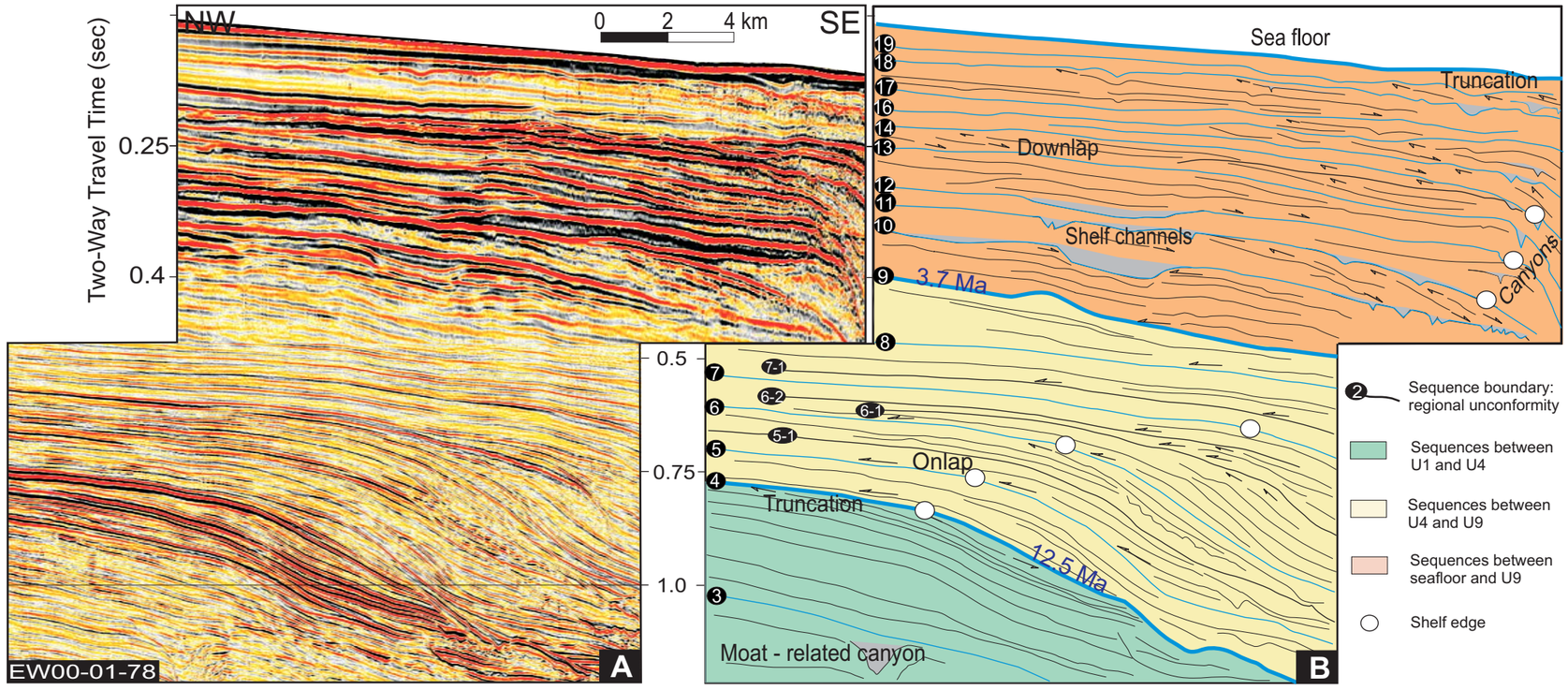

Figure 4.5. (A) Uninterpreted dip profile EW00-01-78 in the southern part of the survey grid (see Figure 4.1 for location). (B) Interpretation showing characteristics of regional unconformities. Note, the upper and lower panels in both A and B are continuous and have the same horizontal scales, but vertical scales differ in order to highlight the geometries of the thin upper sequences. Distinctive clinoform breakpoints (paleoshelf edges) have occurred since U4. U4-U8 are onlapped and truncate underlying reflections. U9-U19 truncate underlying reflections, but are downlapped by overlying reflections. Channels incise paleoshelves of U10 to U19 and canyons develop near paleoshelf edges on the upper slope.

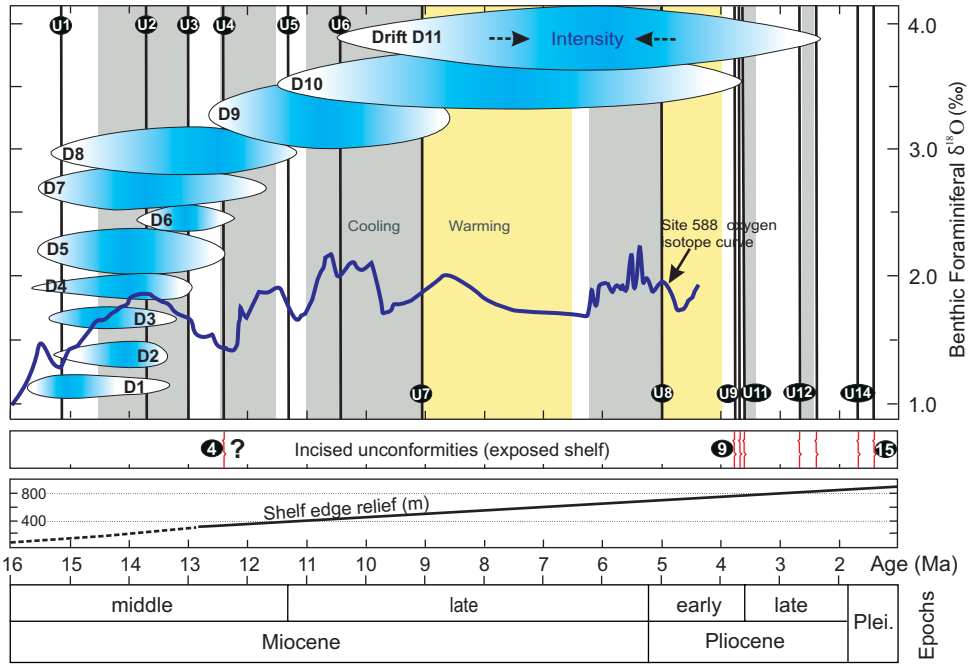

Figure 4.6. Correlation of unconformities U1-U14 with periods of activity of sediment drifts and an oxygen isotopic record from DSDP Site 588 in the southwest Pacific, between Australia and New Zealand (Kennett and von der Borch, 1986). The relative size of the ellipse representing each drift is an approximate measure of drift volume. Drifts D1-D4 are of short duration (~3 m.y.), while D10-D11 are both larger and longer lived (~7 m.y.). Gray and yellow shading represent cool and warm periods, respectively, as defined by Kennett and von der Borch (1986; see also Table 4.1).

Paleoslopes of U5-U8 pass through a zone of large elongate drifts in the northeastern part of the EW00-01 survey (Figure 4.4), but are unaffected by drift development in the south, where geometries are clinoformal (Figure 4.3). Paleoslope inclinations in the south are ~4º. In central to northern areas, D9-D11 are the dominant drifts (Figures 4.4 and 4.6) and paleoslopes relatively gentle (~2º-3º). A total of four local unconformities (U5-1, U6-1, U6-2, and U7-1; Figure 4.3) occur within the U5-U8 interval interval. These onlap the paleoshelves of the underlying regional unconformities (U5, U6, and U7) and are either truncated basinward by the overlying regional unconformity, or intersect drifts, which prevents their being traced basinward of their middle-upper paleoslopes. The local unconformities are less apparent in central and northern areas, where active drifts D8-D11 disrupt sequence architecture.

A distinctive characteristic of U5-U8 is the lack of channel and canyon incision of paleoshelves and slopes, which are mainly smooth surfaces. However, a broad (2-4 km wide in the dip direction) erosional platform extends for 15 km along the shelf edge of local unconformity U6-1 in the central and southern parts of the EW00-01 survey (Figure 4.3). Small channels, interpreted as upper slope canyons, occur within this zone. In addition, a canyon occurs between U5 and U6 on the middle slope (Figure 4.3).

4.3.1.5 Late Pliocene to Recent unconformities U9-U19 (3.7-0 Ma)

The trend of decreasing paleoshelf onlap, begun at U8, continues with U9. Instead, downlap onto paleoshelves becomes increasingly common at U10 and overlying unconformities (Figures 4.3-4.5). Unconformities within this group are identified as sequence boundaries based on paleoshelf channel incision, indicating subaerial erosion, together with truncation of underlying reflections beneath outer paleoshelves and erosional truncation beneath paleoslopes (Figure 4.7). U10-U19 are continuous, high-amplitude reflections. Reflections within sequences are oblique and downlap onto underlying sequence boundaries, indicating that most sediment accumulated during periods of falling relative sea-level. U12-1, U13, and U14 are underlain by attached shelf-perched wedges near their breakpoints (Figure 4.7, shaded areas), suggestive of forced regressive deposits (placing the forced regressive deposits beneath the associated sequence boundary follows the practice of Plint and Nummedal, 2000). Continuity of internal reflections decreases above U9; sequences contain mixed high-amplitude and chaotic reflections. Nine local unconformities occur within this interval. Each is truncated landward by its overlying regional unconformity; most are preserved only on the outer shelf and upper slope. Like the regional unconformities, the local unconformities are defined by downlap above and truncation below. They define sequences that thin southward and eventually pinch out south of the Clipper well.

Unconformity U10 can be traced across its entire paleoshelf, but its slope is truncated by U11. The paleoshelf of U10 is incised by wide U-shaped channels

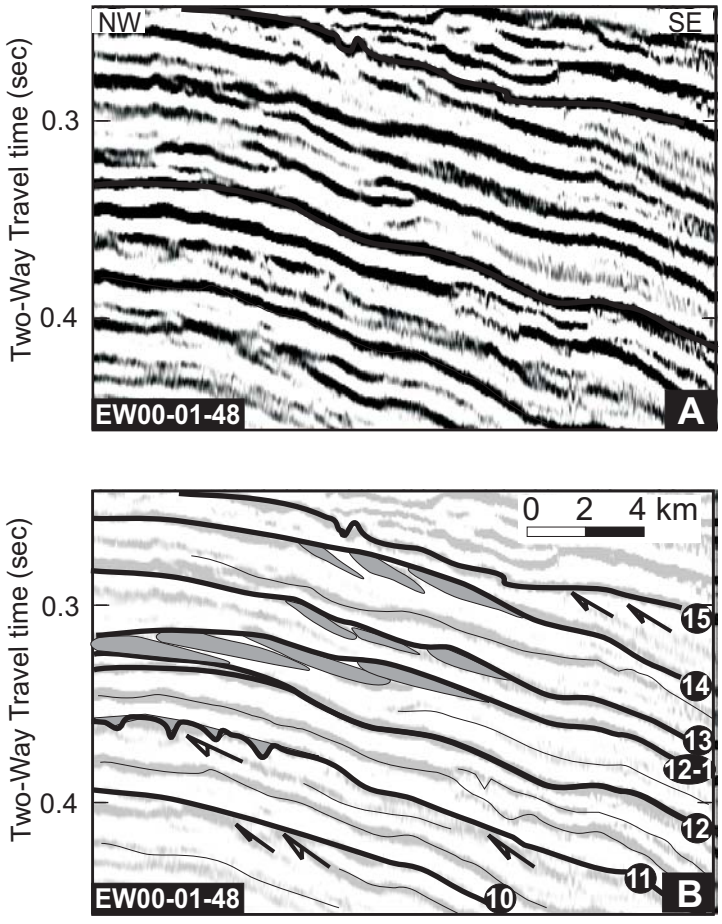

Figure 4.7. (A) Uninterpreted dip profile EW00-01-48 (see Figure 4.1 for location). (B) Interpretation showing sequence boundaries. Stratal architectures of S12-S14 suggest forced regressive deposits (Posamentier and Morris, 2000). Forced regressive deposits composed of prograding shelf-edge deltas or shelf-perched wedges (shaded areas) formed during sea-level falls. Forced regressive deposits are shown underlying associated sequence boundaries following the definition of Plint and Nummedal (2000). Truncation (arrows) beneath sequence boundaries (U10, U11 and U15) and V-shaped incised valleys are also shown.

(200 m wide, 20-50 m deep, Figure 4.5) in the south and by smaller (tens of meters wide and deep) V-shaped channels in the north. U9-U12 pass through drift D11 in the north, but are unaffected by drift development in the south. U13 (~2.4 Ma) marks the termination of all elongate drift activity within the EW00-01 area (Figure 4.6). A second post-drift platform formed above D11 at about this time (Figure 4.4).

4.3.2 Sequence Stacking Patterns and Seismic Facies

Lacking breakpoints, sequence stacking relationships of S1-S3 are unclear. Above U4, however, stacking patterns can vary vertically through the section and also along strike. Furthermore, paleoshelf edges and paleoslope toes can display differing patterns of horizontal migration. In the southern part of the EW00-01 survey area, paleoshelf edges of U4-U8 are strongly progradational. Formation of a paleoslope platform above extinct drifts D1-D6 limits accommodation space and favors this local progradational pulse (Figure 4.3). Paleoshelf-edge migration becomes increasingly aggradational from U8 to U13 (Figure 4.3). Above U13, paleoshelf-edge aggradation decreases and progradation increases. Paleoslopes steepen from U4 to U13 (from ~2 to ~4°), following termination of drift development in this area, because clinoform breakpoints are prograding faster than paleoslope toes. In the north, however (Figure 4.4), U4-U13 display more uniform breakpoint progradation, but at rates intermediate between those of U4-U8 and U8-U13 in the south. Sediment drifts D8-D11 remain active in this area,

focusing deposition on paleoslopes. This has the effect of reducing paleoshelf-edge progradation relative to that in the south, but markedly increasing paleoslope-toe advance (Figure 4.4). U14-Seafloor stacking patterns are dominated by rapid shelf-edge progradation in both north and south. Local variations in sequence stacking pattern are reflected on structure maps, which display along-strike changes in orientations and relative rates of progradation of both paleoshelf-edges and paleoslope-toes (Figure 4.8).

Internal reflections change from sigmoid, in sequences S4 to S8, to oblique or mixed oblique/sigmoid in sequences above U9 (Figure 4.3). However, conventional seismic facies apply only in areas lacking sediment drift development. For example, in the south, where elongate drifts are absent (D5 and D6 are in their waning stages during this period), S4-S8 are dominated by sigmoid reflections (Figure 4.3). In contrast, drift development of D9-D11 in the north during this period leads to seismic facies dominated by mounded drift crests with erosional moats.

Transparent and chaotic slope facies, possibly mass flows or slumps, become more common on paleoslopes from U9-U19 (Figure 4.9). Two growth faults occur on the seaward flank of D10 (Figure 4.9). Absence of an associated moat distinguishes growth faults from current-eroded, drift-bounding unconformities (compare Figures 4.9 and 4.4). Stratigraphic thickness is greater on the basinward side in both cases.

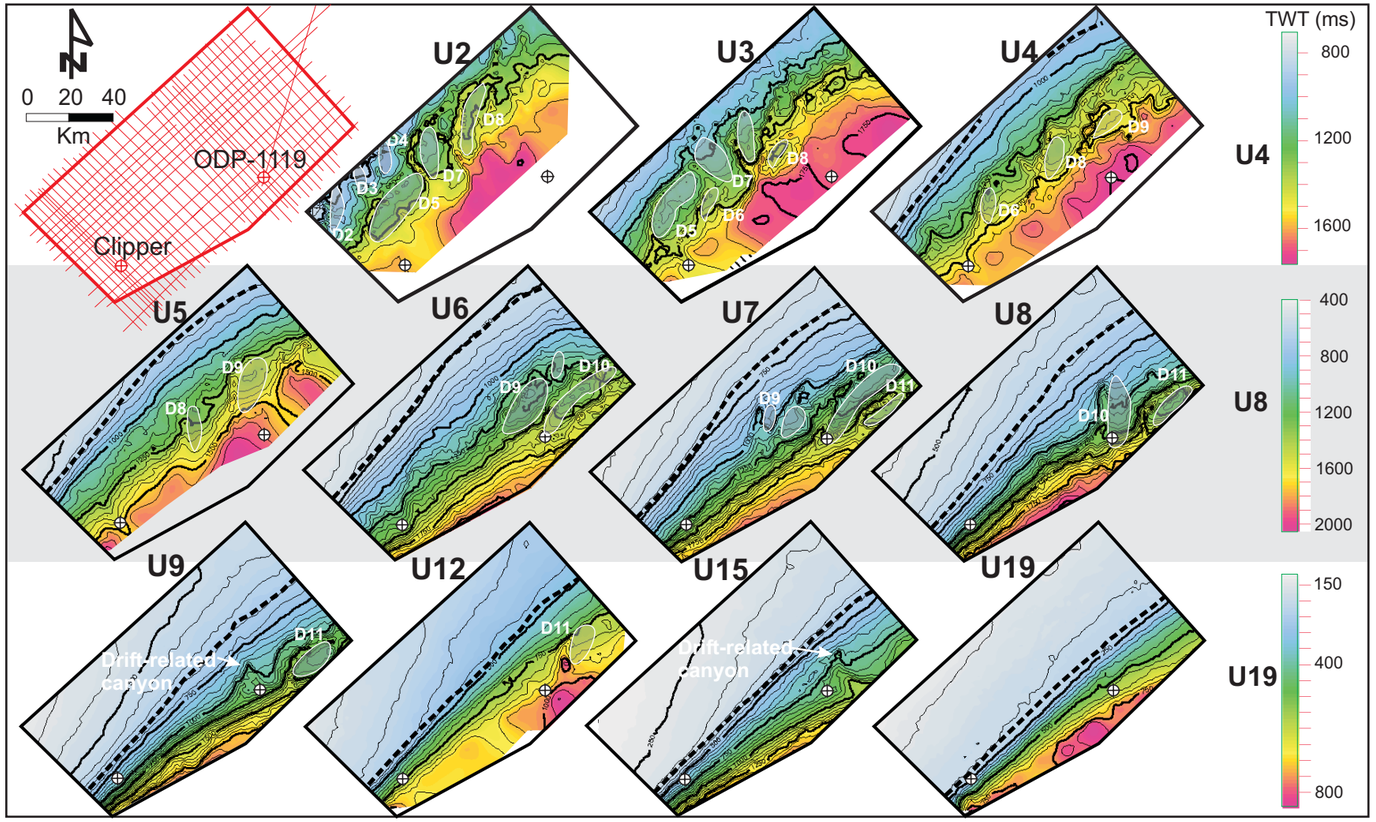

Figure 4.8. Structure maps of selected sequence boundaries. Colored scales schematically represent two-way travel time of interpreted horizons, which is deepen to southeast (basinward). Each map covers the same area (see first panel). Locations of Clipper exploration well and ODP Site 1119 are shown on each map. The presence or absence of sediment drifts is the principal factor influencing slope morphology. Drifts developed first in the south-central part of the EW00-01 grid and the locus of drift activity migrated northward. Each drift was initially sub-parallel to the clinoform breakpoint (paleoshelf edge, thick dashed line), but drift orientation became more perpendicular to the paleoshelf edge in the waning stage, e.g., D10 and D11 on U6-U9 structure maps. All elongate drifts had terminated by U13, although sediment waves continued to occur. Sequence boundaries prior to U4 do not have paleoshelf edges within the survey grid. From U4-U8, paleoshelf edges prograded more rapidly in the south than in the north, where elongate drifts D8-D11 remained active. Drift development restricted progradation of the shelf break by shifting the center of deposition to the slope. As a result the toe of slope continued to migrate basinward (see Figure 4. 4). Shelf-edge progradation seems to be favored by downslope, versus along-strike, processes. Slope gradients were fairly uniform on U4 and U5, when drift activity was reduced (D6, D7, and D8 were waning and U9 was just beginning to be formed). Generally, however, the focusing of deposition on the slope by drifts causes reduced slope gradients relative to areas subject to conventional clinoform development (e.g., contrast northern and southern slope gradients on U7-U9). The northern slope continued to have reduced gradient as a result of the underlying drifts, though a trend of increasing gradient began after the termination of drift deposition (see Figure 4. 4).

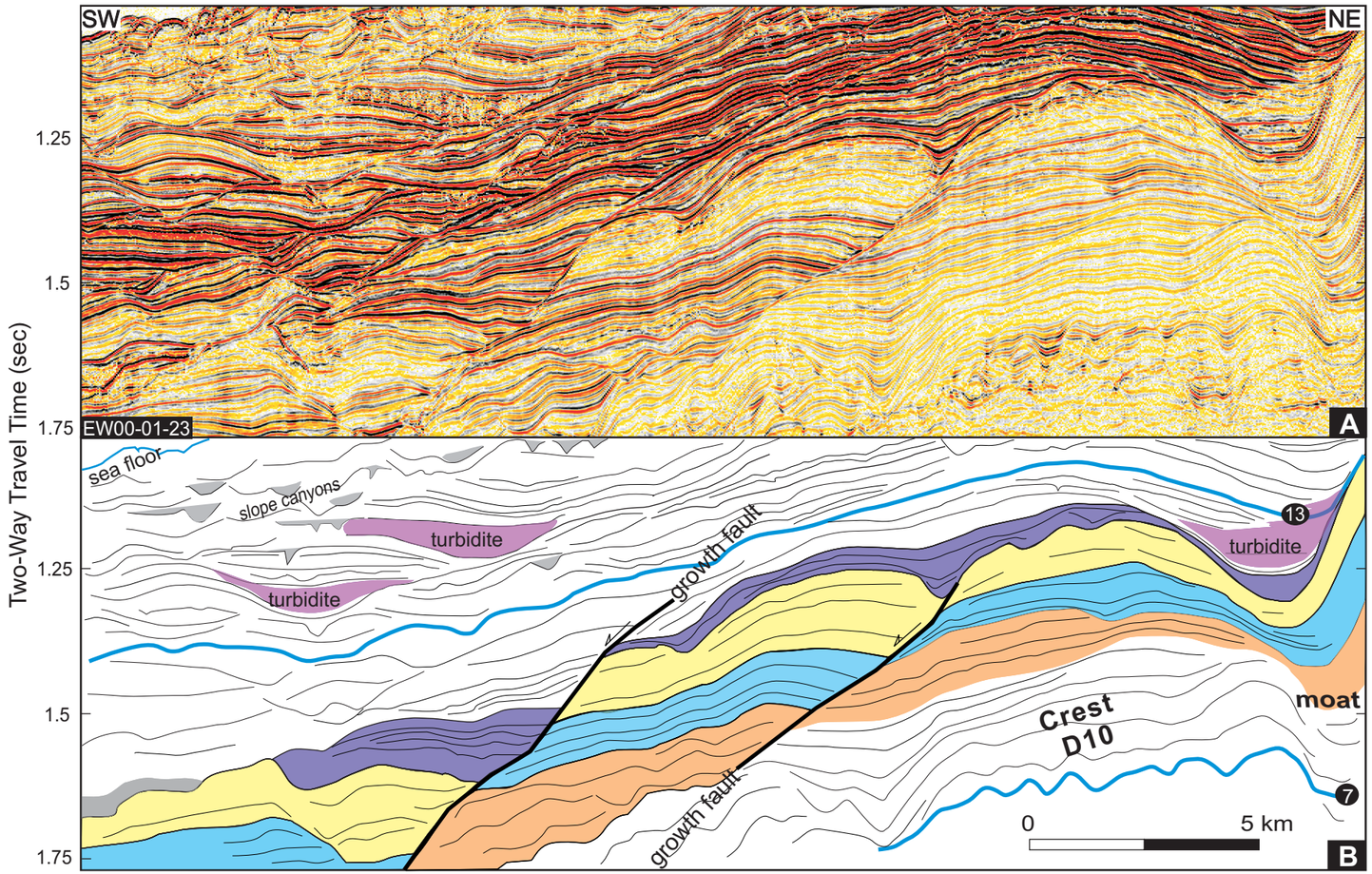

Figure 4.9. (A) Uninterpreted strike profile EW00-01-23 (see Figure 4.1 for location). (B) Interpreted profile. Numbers indicate regional unconformities. Transparent and chaotic facies are common on the slope. Development of canyons and gravity deposits above U13 illustrates the increasing dominance of downslope transportation and deposition following the termination of elongate drift development. Also shown are two faults on the seaward flank of drift D10. Shaded layers illustrate fault throw. Thicker hanging-wall deposits, relative to those of the footwall, suggest that the faults are growth faults, indicating high sedimentation rates on the drift crest (Davis, 1984). These faults are distinguished from current-eroded moat-flank unconformities by the absence of moats and well defined erosional features along the fault plane. Cessation of elongate drift development was accompanied by decreasing sedimentation rate on the drift crest, which terminated fault development. During the waning stage of D10, current flow in the main moat decreases and leakage across the crest increased; relatively strong currents may sweep the crest (Lu et al., 2003). Focusing of such currents adjacent to the fault plane, above the downthrown block, may be responsible for forming the channel above the right-hand fault.

4.3.3 3-D Stratigraphic Architecture

The Neogene shelf/slope prism in the Canterbury basin was formed by a combination of conventional clinoform progradation and the accretion of large, elongate sediment drifts (Fulthorpe and Carter, 1991; Shipboard Scientific Party, 1999; Lu et al., 2003), which exert a profound influence on slope morphology (Figures 4.8 and 4.10). Drifts D1, 2, 3, and D4 initiate just before U1 and terminate around U3 (Figures 4.1, 4.6, and 4.8). D5, D7, and D8 also initiate near U1, but they terminate later: D5 immediately after U4, and D7 between U4 and U5. D8 has a relatively long duration, terminating just after U5 (Figures 4.6 and 4.8). D4, D5, and D7 all reach maturity at U2. D8 is active throughout much of the same period as D7 but reaches maturity later, between U2 and U4.

The U4 slope gradient is uniform along strike and the locus of drift activity is transitioning northward (Figure 4.8). D5 and D6 remain active, though in their waning stages (Lu et al., 2003). D9 initiates at U4 and is most active at U6, ceasing at ~U7 (Figures 4.6 and 4.8). Drift development is also limited at U5: the early drifts in the south are inactive and the later drifts have not yet reached maturity (Figure 4.6). D10 initiates after U5 and is dominant at U7-U8, waning at U8 and ceases to be active by U11. Cessation of drift activity can result in formation of a sub-horizontal slope platform overlying extinct drifts. For example, a platform formed at U4 in the south, above inactive drifts D1-D6 (Figure 4.3), restricting slope accommodation space and contributing both to rapid local progradation of overlying sequences S4-S6 and resultant thickening over the

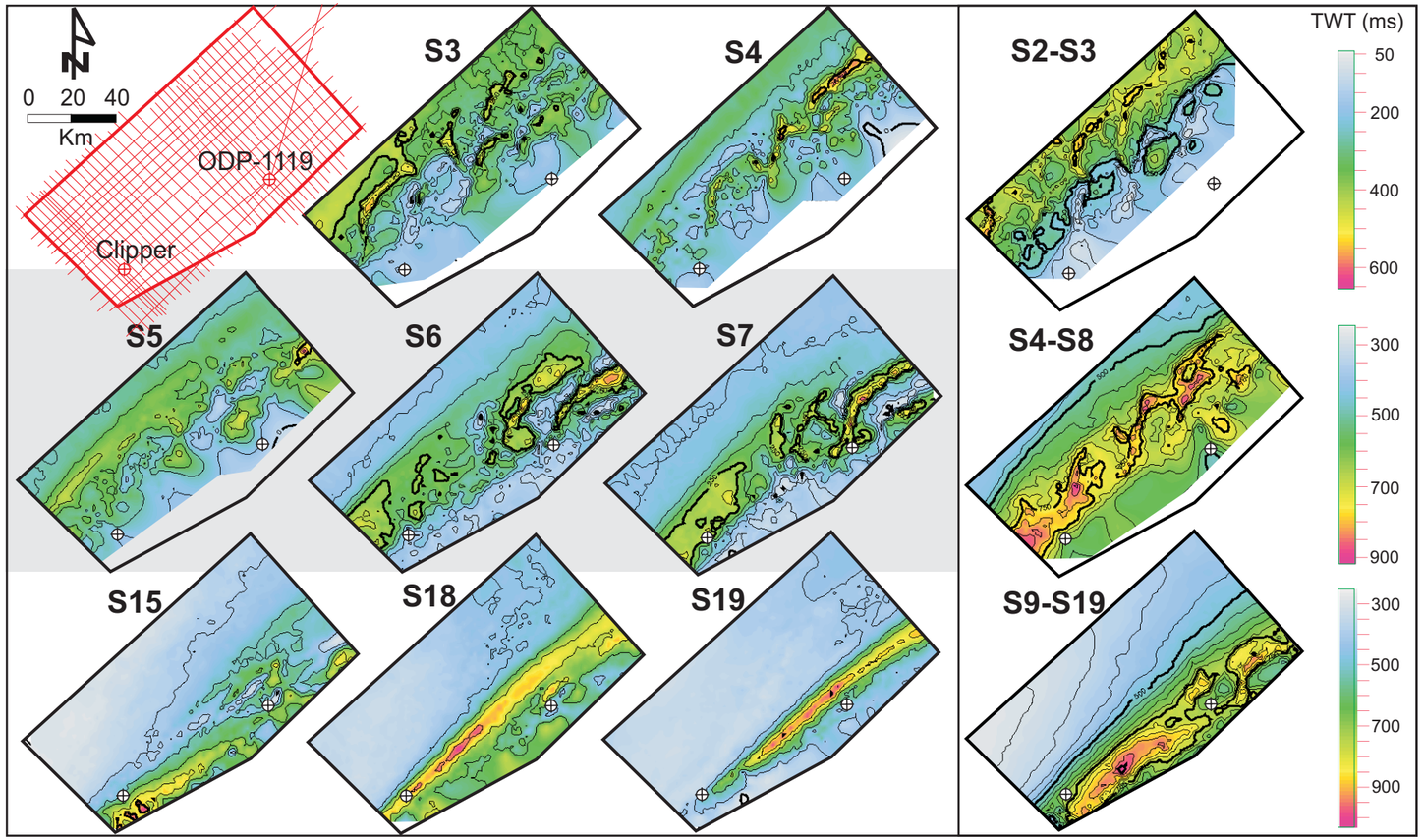

Figure 4.10. Isochron maps of selected individual sequences (left) and groups of sequences (right, in box). Maps cover the same area as those of Figure 4.8. Locations of Clipper exploration well and ODP Site 1119 are shown on each map. Darker shading represents greater sediment thickness. During periods of drift development, sequence thickness is strongly influenced by the locations of drift crests (thick) and moats (thin) (e.g., S3, S4; S2-S3 group). In the absence of elongate drifts, depocenters of the younger sequences are elongate along strike, parallel to paleoshelf edges (e.g., S14, S15, S18, S19; S9-S19 group). The middle sequences, S5, S6, S7 and the S4-S8 group, are transitional, with isochrons most influenced by drift development in the north.

southern slope shown on S4-S7 isochron maps (Figure 4.10). Owing to truncation by overlying drifts and U6, U5 cannot be traced to the slope toe. D11 initiates at U6, matures between U7 and U9 and ends by U13 (Figures 4.6 and 4.8). A second slope platform in the central to northern part of the EW00-01 survey area formed at U11 above D11 as it was waning and other elongate drift activity had ceased (Figure 4.4). This platform, narrowing to the southwest, existed until U16.

Orientations of individual elongate drifts change as they progress through early, mature, and waning stages (Lu et al., 2003). D10 and D11 illustrate this most clearly (Figure 4.8). In their early stages, crests and moats are almost parallel to paleoshelf edges. However, the angle between drift axis and paleoshelf edge increases through time until moats are almost normal to paleoshelf edges and can act as canyons. Canyons incising U9 and U15 formed during the waning stages of D10 and D11, respectively (Figure 4.8).

When drifts are active, slope gradients are low and change little through time, e.g., prior to U5 in the south and between U5 and U9 in the north (Figures 4.3, 4.4, 4.6, and 4.8). However, slope gradient increases when drift activity ceases and downslope processes become dominant. Slope gradient increases after U5 in the south, with termination of D1-D6, and in the north after U13, when D10-D11 terminated (Figures 4.3, 4.4, 4.6, and 4.8).

Representative isochron maps from each of the three principal seismic units (S2-S3, S4-S8, and S9-S19) illustrate changes in sequence thickness (Figure 4.10). A complex pattern of drifts influenced the thickness of the S2-S3 interval

(Figure 4.10); active moats are marked by thinning while adjacent basinward thickening represents drift mounds (D5-D8). This non-uniform pattern of deposition results from complex current pathways (Lu et al., 2003). With only D9 mature, thickness of S5 is relatively uniform (Figure 4.10). However, maturation of D10 and D11 in the north controls thickness distributions within S6-S8 (Figure 4.10). Meanwhile, formation of the post-drift, middle-upper slope platform on U4 in the south results in an elongate zone, of uniform thickness along strike, basinward of paleoshelf edges (Figure 4.10). D11 began waning after U9 and the subsequent absence of drifts resulted in a more uniform sediment distribution (Figure 4.10: S14-S19). The total thickness isochron map from S9 to S19 (Figure 4.10) shows an elongated, upper-slope depocenter parallel to the shelf edge; isolated thinning around ODP Site 1119 represents a vestige of D11. Such elongate, strike-oriented sediment thickness maxima suggest a linear sediment source. However, the common occurrence of slope canyons from U9-U19 (Figures 4.4 and 4.5), and of shelf channels of probable fluvial origin (Figure 4.5) supports the existence of point sources. Along-strike sediment redistribution by currents may be responsible for muting the influence of such point sources at depocenter scale, while allowing localized canyon development. At this late stage (U13-U19) of basin development, sediment waves replace elongate drifts as the dominant current-related depositional features (Figures 4.4 and 4.9).

4.4 DISCUSSION

4.4.1 Role of Global Forcing

The most common proxy record of global sea-level change is that derived from the oxygen isotopic composition ($\delta^{18}O$) of foraminiferal calcite obtained from deep-sea cores. The $\delta^{18}O$ signal is currently the best parameter available for estimating the magnitude and rate of global sea-level change and provides the best evidence for the extent of eustatic control of sequence formation (Kennett and von der Borch, 1986; Chappell and Shackleton, 1986; Williams, 1988; Williams et al., 1988; Zachos et al., 2001). Deep-sea $\delta^{18}O$ records provide a proxy for ice volume and sea-level for the Oligocene to Recent period dominated by glacioeustasy (Raymo and Ruddiman, 1992). However, $\delta^{18}O$ in marine sediment is dependent on several variables, primarily water temperature, postdepositional diagenesis, and the $^{18}O/^{16}O$ ratio of sea water ($\delta^{18}Osw$), in turn a function of the amount of sea water removed from the oceanic reservoir, and deposited in ice sheets, and local salinity (Lear, et al, 2000; Visser et al., 2003). Oxygen isotope records lend themselves to identification of climatic trends (Figure 4.6; Table 4.1; Kennett and von der Borch, 1986; Zachos et al., 2001), but correlation of sequence boundaries with individual isotopic cycles is commonly difficult, because of contrasting cycle frequencies and limited age control, though there are exceptions (e.g., Miller and Mountain, 1996).

The temperature dependence of the Mg/Ca ratio of planktonic foraminifers can be used in parallel with $\delta^{18}O$ to isolate $\delta^{18}Osw$, providing an improved proxy for eustasy (Lear et al., 2000; Billups and Schrag, 2002; Visser et al., 2003). For example, the $\delta^{18}Osw$ record of Billups and Schrag (2002) agrees better with the Haq et al. (1987) eustatic curve than does the unmodified $\delta^{18}O$ record (Figure 4.11). Individual Miocene through Pleistocene third-order sequence boundaries TB2.4 through TB3.9 of Haq et al. (1987) correspond approximately to increases in $\delta^{18}Osw$ (Figure 4.11E, G). These results are also in good agreement with those of Miller and Mountain (1996), who correlated Oligocene to Miocene New Jersey margin sequence boundaries with times of increasing foraminiferal $\delta^{18}O$ values, consistent with the formation of sequence boundaries during glacioeustatic falls (Figure 4.11D, E). The pronounced $\delta^{18}Osw$ trends at ~12-11 Ma and ~10-8.5 Ma are not apparent on the uncorrected benthic foraminiferal $\delta^{18}O$ curve. However, both have equivalents in the Canterbury basin seismic record (U5 and U7) and on the Haq et al. (1987) curve (TB3.1 and TB3.2; Figure 4.11E, F and G). These comparisons illustrate how the corrected $\delta^{18}Osw$ record reconciles the geochemical and sequence stratigraphic approaches to sea-level change (Billups and Schrag, 2002). The $\delta^{18}Osw$ record contains at least sixteen cycles since 15 Ma (Billups and Schrag, 2002), the period during which nineteen regional Canterbury basin sequences formed (Figure 4.11E, F). However, the temporal resolution of the $\delta^{18}Osw$ record is 100-200 kyr (Billups and Schrag, 2002). Some

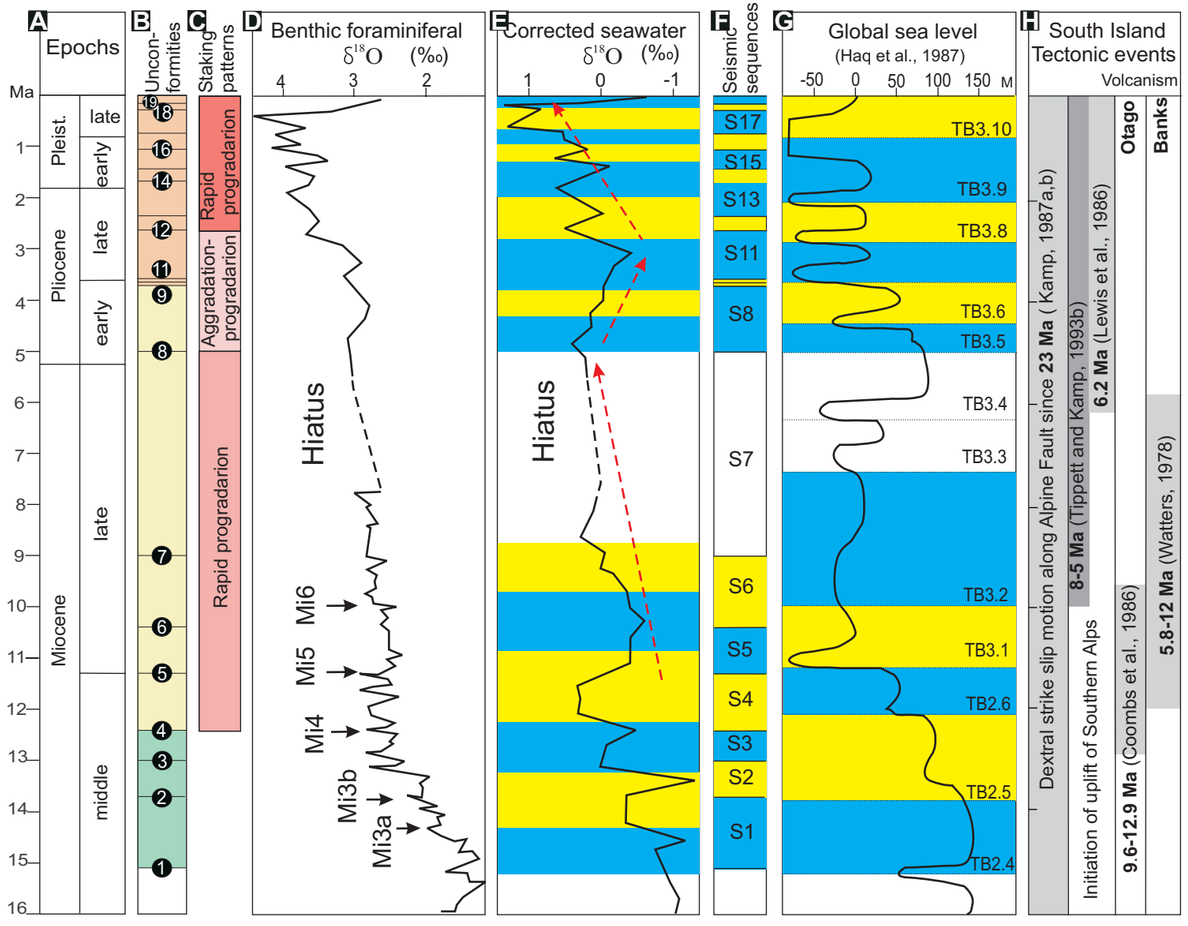

Figure 4.11. Seismic sequence boundaries (column B) and sequences (F) correlated with the oxygen isotopic record from ODP Site 747 in the Indian ocean, southwest of Australia (Billups and Schrag, 2002): an unmodified benthic foraminiferal 18O record (D) and the same record corrected using Mg/Ca thermometry (E) to remove the temperature effect and yield the 18O of sea water (18Osw). This signal is predominantly an indicator of ice volume and therefore an enhanced proxy for global sea level. The 18Osw record correlates better both with individual seismic sequences and longer term progradational and aggradational trends, as well as with the Haq et al. (1987) eustatic curve (G; recalibrated to the timescale of Berggren et al, 1995). Cooling events Mi2, Mi3a, Mi3b, Mi4, and Mi5, derived from oxygen isotope record from DSDP Site 608 and ODP Sites 703 and 704 (Miller and Mountain, 1996) are also shown (D), as is a summary of South Island tectonic and volcanic events (H).

seismic sequences (e.g., S9, S10, S18, and S19) with comparable or higher frequencies would not be resolved by the δ^{18}Osw data. This brings the total numbers of cycles in the δ^{18}Osw (16) and seismic records (15) into better agreement. I compare only cycle numbers and frequency. The available age control is insufficient to permit precise correlation of individual cycles. Sequence stacking patterns are also reflected in the δ^{18}Osw record. In the southern part of the EW00-01 survey area, where drifts have least effect on sequence architecture, paleoshelf edges of U4-U8 are strongly progradational, becoming increasingly aggradational from U8 to U13 and progradational above U13 (Figure 4.3). These trends are present within the δ^{18}Osw record, but are not apparent in the uncorrected, benthic foraminiferal δ^{18}O record (compare Figure 11C, D, E). They are also similar to some aspects of the global sequence stratigraphic trends recognized by Bartek et al. (1991), particularly late middle Miocene and late Miocene progradation and early Pliocene aggradation.

Late Pliocene to Pleistocene isotopic records have much higher resolution (Figure 4.12; Nelson et al., 1986; Joyce et al., 1990; Mederios et al., 2000) than the Miocene record. The last ~0.7 Ma, at least, was dominated by 100 k.y eccentricity cycles (such cycles may have been dominant to 0.8-0.9 Ma; Williams, 1988; Chiocci, 2000; Hernandez-Molina, et al., 2000). Prior to that, 40 k.y. obliquity cycles were dominant (from ~0.7-1.0 Ma) and 20 k.y. precessional cycles dominated from 1.0-1.8 Ma (Williams, 1988).

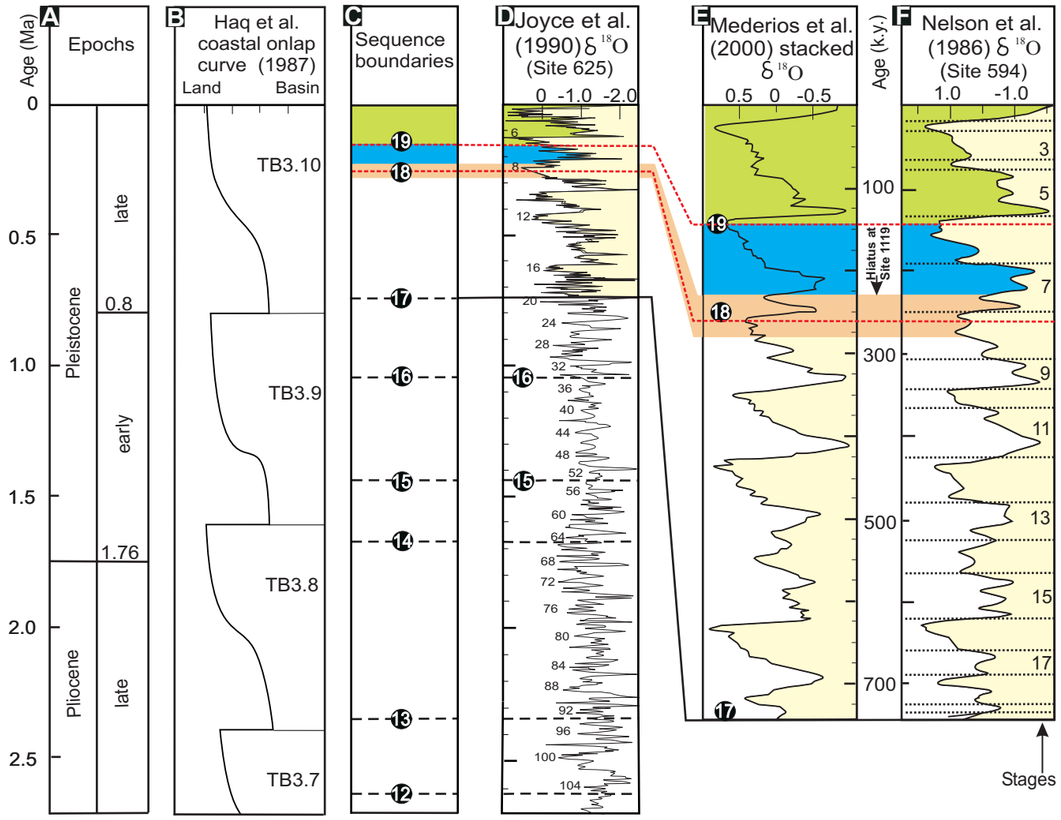

Figure 4.12. Timing of late Pliocene to Pleistocene unconformities (U12-U19, C) and comparison with oxygen isotope curves of Joyce et al. (1990), from planktonic foraminifera (D), Mederios et al. (2000), from benthic foraminifera (E), and Nelson et al. (1986) from both planktonic and benthic foraminifera (F), together with the coastal onlap curve of Haq et al. (1987; B). U18 and U19 correlate with isotope stage boundaries 7/8 and 5/6, respectively. U18 is a downlap unconformity and represents a hiatus of ~25 k.y (shaded; Carter et al., 2004). In general, however, there are many more oxygen isotopic cycles than sequence boundaries. The sequence record has been filtered by a combination of limited seismic resolution and removal of sequence boundaries by shelf erosion.

Sequences S12 to S16 encompass multiple precessional cycles (Figure 4.12). Two local unconformities are identified within S15, which define three fifth-order sequences with durations of ~0.130 m.y. The duration of fourth-order sequence S17 (~0.45 m.y.) indicates that it comprises up to five 100 k.y. eccentricity cycles, which are not identified seismically. U18 (0.252-0.277 Ma) is the only seismic unconformity identified as a hiatus in cores from Site 1119 and corresponds to the stage 7/8 boundary (Carter et al., 2004). There are at least three local unconformities (U18-1, U18-2, U18-3; Figure 4.2D) between U18 and U19 within stages 6 and 7. Therefore the fifth-order sequence S18 (U18-U19) may comprise four sixth-order sequences. The last unconformity below the sea floor (U19, 0.113 Ma) corresponds to the penultimate glacial maximum (Herzer, 1981) or stage 5/6 boundary (Shackleton and Opdyke, 1973; Nelson et al., 1986; Williams et al., 1988; Joyce et al., 1990).

Sequences S14-S17 do not, therefore, correlate well with oxygen isotope stage boundaries and individual Milankovitch-scale cycles. Most sequences are third- and fourth-order, but fifth-, and sixth-order sequences also occur (Table 4.1). U18 and U19, however, correlate with isotope stage boundaries 7/8 and 5/6, respectively. It is unlikely that earlier lack of direct correlation indicates diminished influence of eustasy on sequence development. Eustatic amplitudes during the last 0.8-0.9 Ma were >100 m (Williams, 1988; Hernandez-Molina, et al., 2000), in comparison to Neogene (Miocene and early Pliocene) amplitudes of 50-100 m (Williams, 1988). The high amplitudes of recent eustatic changes,

coupled with limited accommodation space, led to extensive shelf erosion. This may have removed the paleoshelves of some sequences preventing the identification of sequence boundaries by reflection truncation. Disruption of paleoslopes by currents further contributes to the difficulty of sequence identification.

Available age control precludes cycle-by-cycle correlation. However, the match between numbers of sequences and oxygen isotope cycles, in the Miocene and Pliocene (Figure 4.11) and also in the latest Pleistocene (Figure 4.12), together with trends in sequence stacking patterns, favors a strong component of eustatic control of the formation of U1-U19.

4.4.2 Sequence Architecture

S4-S8 contain sigmoid reflections with landward shelf onlap and downlap basinward of paleoslopes, except where interrupted by sediment drifts (Figures 4.3-4.5), geometries typical of highstand systems tracts (Van Wagoner et al., 1988, Plint and Nummedal, 2000). In contrast, S9-S19 contain mainly oblique reflections, truncated landward by overlying sequence boundaries. These sequence boundaries are commonly incised by shelf channels and slope canyons. Reflections downlap on the shelf and converge, or are truncated by overlying sequence boundaries, basinward (Figures 4.3-4.5). Forced regressive deposits are interpreted to occur beneath U12-1, U13, and U14 (Figure 4.7) and are inferred to form during periods of decreasing accommodation caused by high-amplitude

relative sea-level falls (Plint and Nummedal, 2000; Posamentier and Morris, 2000; Hernandez-Molina et al., 2000; Chiocci, 2000; Trincardi and Correggiari, 2000; and Kolla et al., 2000). This hypothesis is consistent with interpretations of overlying Quaternary deposits, comprising basinward thickening and downstepping units (up to 40 m thick) of high-amplitude offlaping reflections, as coarse-grained forced-regressive systems tracts (Browne and Naish, 2003).

Analyses of Quaternary continental-margin sequences (Hernandez-Molina et al., 2000; Chiocci, 2000; Trincardi and Correggiari, 2000; Kolla et al., 2000) suggest that forced regressive systems tracts are linked to asymmetric sea-level changes during the last 0.8-0.9 Ma. Using late Pleistocene $\delta^{18}O$ records, Broecker and van Donk (1970), Berger and Labeyrie (1986), and Williams (1988) reported a rapid transition from glacial lowstand to interglacial highstand, with sea-level rising at 10-15 m/1000 yr. In contrast, the subsequent return to full glacial lowered sea levels may take an order of magnitude longer (rates of 1 to 1.5 m/1000 yr). This late Pleistocene asymmetry suggests that ice sheets decay more rapidly than they accrete on time scales of 100 ky or less and reduces the volumetric significance of transgressive and highstand systems tracts. The slow sea-level falls maximize accommodation space during regression and favor development of oblique reflections and forced-regressive systems tracts. Driscoll and Karner (1999) reported that the formation of forced-regressive systems tracts requires high sediment supply during the relative sea-level fall. This requirement is consistent with tectonic reconsctructions and sedimention rate calculations for

middle Miocene-Recent sequences that suggest the high sediment supply about 6 Ma and may further amplified by montane glacier influence since late Pliocene (see Chapter 5 for detail). Most of sequences S9-S19 may contain forced regressive systems tracts, implying that asymmetric sea-level cycles existed as early as 3.7 Ma (S9-S19, late Pliocene to Present). However, such asymmetry is not apparent on isotope curves correlative with S9-S16 (Figures 4.11 and 4.12D; Joyce et al., 1990). Erosion during rising sea level may have contributed to the limited deposition of transgressive and lowstand systems tracts; sequence boundaries may therefore coincide with ravinement surfaces (e.g., Barnes, 1995; Burger et al., 2002).

4.4.3 Sediment Drifts and Sequence Stratigraphy

Eleven drifts (D1-D11) are recognized and mapped within the middle Miocene to Recent shelf sediment prism (Figures 4.1, 4.3, 4.4 and 4.6; Lu et al., 2003). The drifts were initiated in water depths of 300-750 m, but aggraded to near shelf depthts. They are inferred to have been formed by a northward flowing current analogous to the present Southland Current and grew to large sizes: up to 1000 m thick and 20 km wide in the dip direction and >60 km long in the strike direction. Drift deposition was initiated in the southwestern part of the EW00-01 seismic grid and the locus of drift activity migrated northeastward from D1 to D11. Most drifts are “simple”, comprising a single moat and mound, but “complex”, multicrested and multistage drifts also occur (Figure 4.1; Lu et al.,

2003). The observation that more than one drift was commonly active simultaneously, and that one drift is multicrested drift, both show that flow pathways were complex. The most recent drifts (D10 and D11) have the largest volumes and were active for the longest periods (~7 m.y.; Figure 4.6).

Sequence boundaries can be traced through the sediment drifts allowing them to be placed within a sequence stratigraphic framework (Figures 4.3, 4.4, and 4.6). Such seismic correlation confirms that some sediment beneath the unconformities created by paleoslope erosion at the landward edges of moats (Figures 4.3 and 4.4) is younger than the oldest sediment overlying the unconformities. Such unconformities are therefore diachronous (Lu et al., 2003). This, together with their generally limited areally distributions (Figure 4.13G), indicates that moat unconformities are not sequence boundaries. Indeed, all eleven elongate drifts are intersected by more than one sequence boundary (Figures 4.3, 4.4, and 4.6); each drift, therefore, was active through multiple cycles of base-level change. "Simple" drifts, therefore, may differ from "complex" drifts only in that their component drifts are superposed without lateral displacement of either moat or crest.

The influence of along-strike transport and deposition is particularly pronounced on this margin. Elsewhere, clinoform progradation is more common and hence more widely investigated (Bartek et al., 1991, 1996, 1997; Sorensen et al. 1997; Fulthorpe and Austin, 1998; Burger et al., 2001, 2002; Cathro and

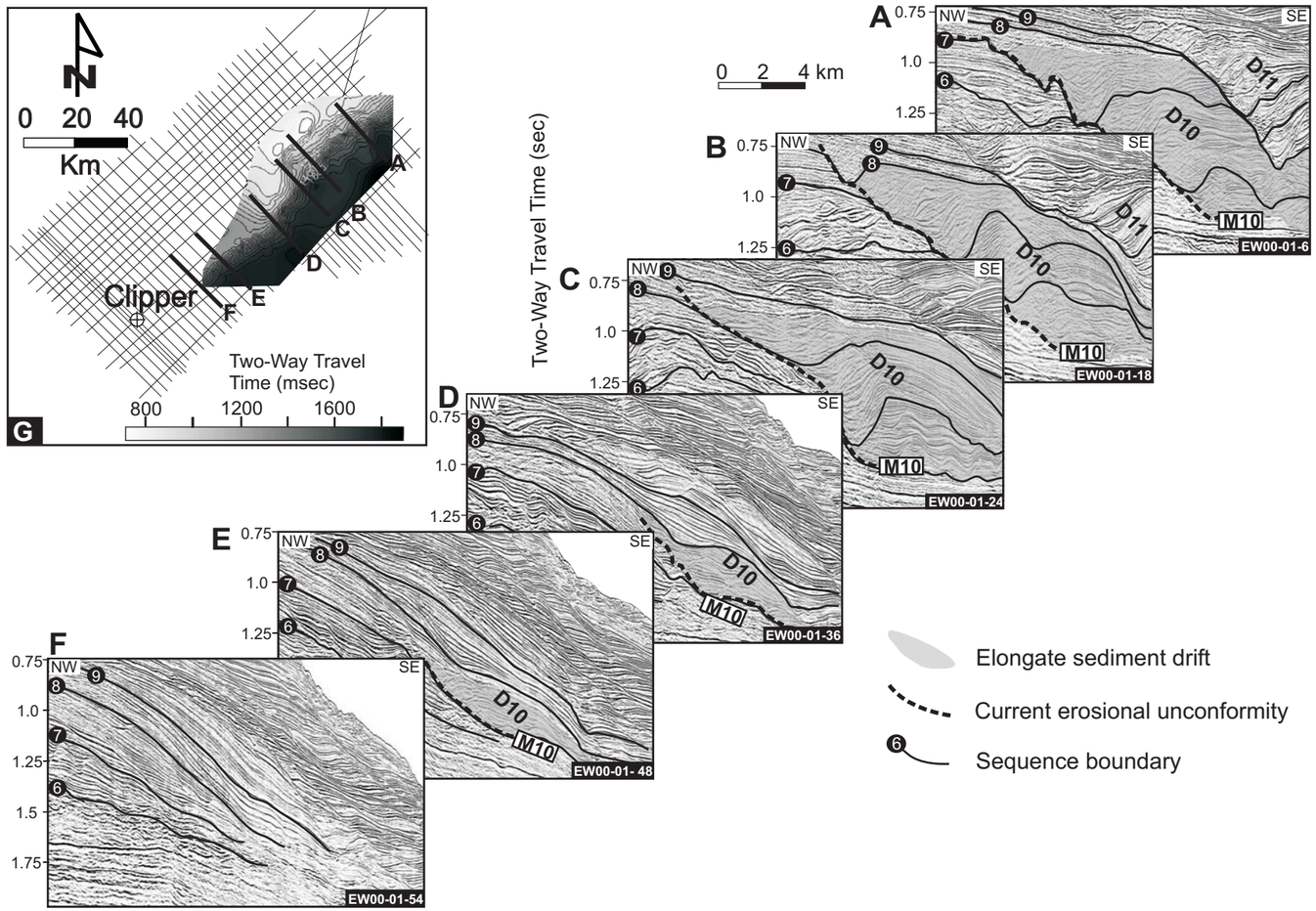

Figure 4.13. Series of dip profiles illustrating the along-strike transition between strongly current-influenced deposition to the north (drift D10, overlain by D11) and coeval development of more conventional clinoforms to the south. D10 is fully developed in the central to northern parts of the survey area (A-C) and its moat erosional unconformity (M10) cuts downward to U6. Farther south along strike, landward erosion in the moat is reduced and that part of M10 preserved between U7 and U8 is poorly defined (D). Still farther south, the portion of M10 above U8 has disappeared, while a broad erosional unconformity, inferred to have been formed by unconfined current erosion, coincides with U7. Prograding clinoforms, with minimal drift disruption, dominate between U8 and U9 (E). Finally, on the southernmost profile, mounded drifts are absent, the only evidence of current activity being some sediment waves above U7 (F). G shows the locations of profiles A-E and a structure map of M10. The landward edge of M10 is most shallowly buried (~800 msec in two-way travel time) in the center (along-strike) of the drift (near sections B and C) and deepens both northward and southward, indicating that the middle portion of drift has longest duration. Even though D10 is one of the largest drifts, its moat erosional unconformity covers an area of <1000 km2, limiting its value for seismic correlation.

Austin, 2001). The Canterbury basin, however, provides coeval examples of clinoform progradation and drift accretion, together with transitional geometries. Figure 4.13 shows dip profiles from north to south during the development of simple elongate drift D10. The drift (~800 m high and >20 km wide, down dip) is fully developed in the central to northern parts of the survey area (Figures 4.13A-C) and its moat erosional unconformity (M10) cuts downward to U6. Farther south along strike, landward erosion in the moat is reduced; that part of M10 preserved above U8 has disappeared (Figure 4.13D). Still farther south, M10 does not reach to U8. Instead, a broad erosional unconformity, inferred to have been mainly formed by unconfined current erosion, coincides with U7. Prograding clinoforms, with minimal drift disruption, dominate between U8 and U9 (Figure 4.13E). Finally, on the southernmost profile, mounded drift and current-eroded unconformity are absent. The only evidence of current activity is some sediment waves above U7 (Figure 4.13F).

Therefore, the distribution of Canterbury basin drifts is variable both spatially and temporally, in spite of the documented presence of currents since the Oligocene (Fulthorpe, et al., 1996). Hence, a current alone is not sufficient to generate sediment drifts. Furthermore, the relative absence of seismic evidence for current activity in Figure 4.13F, in spite of the presence of a current strong enough to produce a large elongate drift nearby, suggests that along-strike transport could play a role in forming clinoform morphologies generally, even where geometries diagnostic of current reworking are lacking.

4.4.4 Controls on Drift Development and Evolution

The formation and intensity of contour currents are generally related to temperature and salinity differences, the rotation of the earth (Coriolis force), and seafloor topography (Heezen and Rawson, 1977; Locker and Laine, 1992; Laine et al., 1994; Viana et al., 1998). In addition, formation of sediment drifts requires a supply of sediment (Gao et al., 1998; Laberg et al., 2001). Climate and sea-level change are also important controls on drift formation. Development of drifts may be inhibited during highstands, when clastic material is trapped on the shelf (Faugeres and Stow, 1993; Dowling and McCave, 1993; McGinnis et al., 1997), and hence favored at lowstand (Pratson and Laine, 1989; Faugeres and Stow, 1993). In addition, current velocity, strength, and depth of influence may be enhanced during eustatic lowstands (Kennett and von der Borch, 1986; Lewis et al., 1986). However, studies of carbon and oxygen isotopes (Duplessy et al., 1988), micro-grain-size data (Dowling and McCave, 1993), and seismic interpretation (McGinnis et al., 1997) indicate that glacial-interglacial transitions may be the times of the strongest bottom circulation activity (Faugeres et al., 1999).

The largest Canterbury basin drifts span multiple sequences, so that they do not respond to individual eustatic cycles (Figure 4.6). However, they may develop preferentially during longer-term periods of lowered sea level. For example, most of the drifts (D1-D9) were active during middle-late Miocene, southwest Pacific cooling episodes of Kennett and von der Borch (1986; Figure

4.6; Table 4.1). The two remaining drifts (D10-D11) continued to be active during warming periods (9-6.5 Ma), perhaps because of the high rate of sediment supply associated with uplift at the Alpine Fault beginning at ~8-5 Ma (Tippett and Kamp, 1993b; Batt et al., 2000) and also their large size. Shelf edge relief had increased from several hundred meters to ~1000 m by this time (Lu et al., 2003), allowing the drifts to reach a comparable thickness. In filling the available accommodation, they were active for longer periods than earlier drifts (Figure 4.6). Their size may have contributed to their independence of sea-level change and resulting stability. Changes of sea level are small relative to drift height and less likely to influence the position of the moat of such large drifts. However, simple drifts D1-D4 formed when shelf relief was low. A relatively small change in sediment supply or relative sea level may result in abandonment and filling of the main moat and termination of the drift. Intermediate shelf relief may favor formation of complex drifts by allowing changes in sea level and sediment supply to cause moat bifurcation (D8) or moat migration (D9) without terminating the drift (Figures 4.1 and 4.8).

Seafloor topography is another important influence on drift formation. Drift growth is favored at sharp changes in slope inclination and such changes may be essential in order to build characterisitic drift geometries (Michels et al., 2001). However, the drifts themselves strongly influence slope gradient. Canterbury basin drifts developed on slopes with gradients ranging from 1˚ to 4˚. Slope gradient increases nonuniformly through time. There is little change in

slope gradient in the south during drift development (before U5). Similarly, slope gradient was unchanged in the north while drifts (D9-D11) were developing there. However, increases in slope gradient occur when drift development ceases and downslope processes assume dominance. Elongate drift development restricts the basinward movement of the shelf edge because Coriolis deflection (leftward in the Southern Hemisphere) concentrates erosion in the moat, at the landward edge of the drift (Viana et al., 1998), while deposition is focused in the drift mound on the lower-middle slope and slope toe. This limits slope gradient and promotes basinward movement of the slope toe. This occurred in the north from U7 to U13. Pertinently, by simulating across- and along-margin sediment transport and deposition, Driscoll and Karner (1999) reported that strong along shelf diffusion caused by shore parallel currents, diminishes the dip of clinoform. In contrast, the southern area was dominated by downslope processes at this time and slope gradient was steeper. A platform can form on the upper slope above extinct or waning drifts (Figures 4.3 and 4.4). When drift development ceases, downslope processes quickly fill this limited accommodation space allowing rapid shelf-edge progradation and slope steepening. In both southern and northern parts of the survey area, along-slope processes were superceded by downslope processes (Figure 4.9), and this transition occurred earliest in the south.

Termination of elongate drift development by U13 (~ 2.4 Ma) may have been caused by significant changes in the frequency and amplitude of sea level change represented by $\delta^{18}O$ records since 1.8 Ma (Shackleton and Opdyke, 1976;

Prell, 1982) High- amplitude sea-level changes (>100 m from at least 0.8-0.9 Ma to Present; Williams, 1988; Hernandez-Molina, et al., 2000), which favor shelf-edge exposure and formation of slope canyons, resulting in the dominance of downslope processes on the slope, may be the most important element that terminates the drift development. Therefore, although the current still exists after U13 time, the only current-related deposits are waves and randomly distributed erosional features on the middle-upper slope. The shelf edge was also exposed at U4 and drift activity was approaching a relatively minimum at this time (Figures 4.6 and 4.8), supporting the link between shelf exposure and enhancement of downslope processes at the expense of along-strike processes. Stable geostrophic circulation, enhanced during glacial periods, is an essential requirement for elongate drift formation. However, sediment supply, sea-level amplitudes and seafloor morphology, e.g., slope gradient and eastward deflection of the current by Chatham Rise (Figure 2.1), are contributing factors and interact to create drifts of a range of scales and architectural complexity.

4.4.5 Reconstruction of Shelf-Slope Stratigraphic Systems

Sequences S4-S8, with distinctive shelf edges (especially in the south), onlap and truncation at sequence boundaries, and sigmoid internal reflection geometries, are inferred to comprise mainly transgressive and highstand systems tracts across the middle-outer shelf and slope (Figure 4.14A). Shelf channel incisions are mostly absent and shelf edges were not exposed during sea-level

lowstands (except possibly U4, near Endeavour High and the high at Resolution). The shelf edge was therefore distant from points of sediment discharge at the coastline. Sediment was redistributed by waves and along-strike currents. Drifts developing during this period were increasing in size and duration and the locus of drift deposition was moving northward. Downslope processes were dominant in the southern part of the survey area. Shelf edges prograded rapidly across a slope platform, filling accommodation space above extinct drifts D1-D6, and slope gradient increased. In the absence of disruption by sediment drifts, several local unconformities (U5-1, U6-1, 2, U7-1; Figs. 4.3 and 4.5) can be identified. In contrast, in the central to northern parts of the EW00-01 survey, along-strike processes were dominant, and the slope gradient was low because of the concentration of deposition in drifts on the middle to lower slope. Current activity disturbed the sequence architecture by creating mounded morphologies and disrupting reflection terminations even on the outer shelf. Onlap and truncation are therefore rare and local sequence unconformities cannot be identified (Figure 4.4).

Controls on formation of S9-S19 may have included asymmetrical sea-level cycles, with relatively higher amplitudes, and along-strike currents. Paleoshelves were subaerially exposed during sea-level lowstands and outer shelves are eroded by channels, with canyons forming on upper slopes (Figure 4.14B). Outer-shelf and upper-slope regions of sequences can comprise forced regressive systems tracts (Plint and Nummedal, 2000). Sequence boundaries were

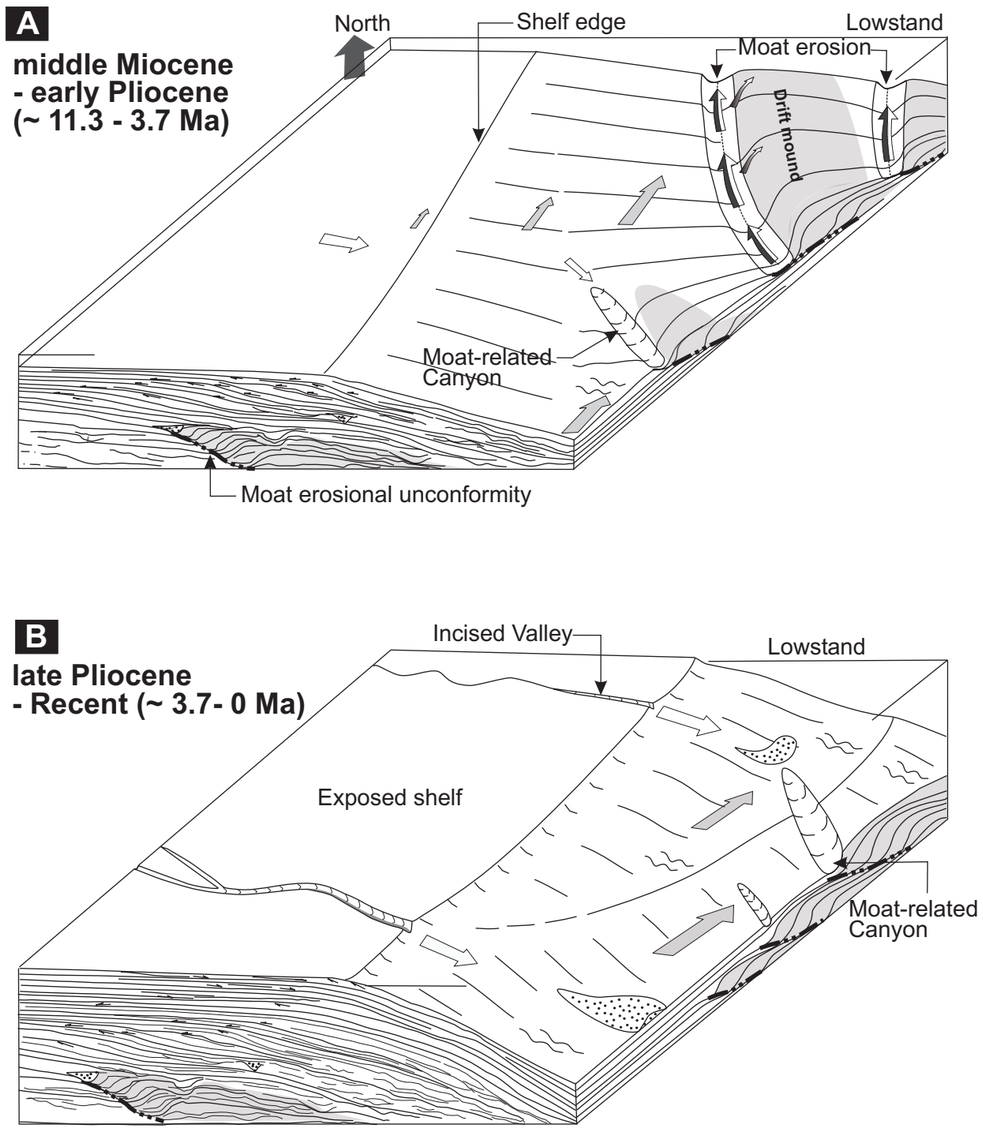

Figure 4.14. Schematic diagrams representing sedimentary processes in the Canterbury Basin. (A) Middle Miocene to early Pliocene sequences S4-S8 have sigmoid internal reflection geometries and are inferred to comprise mainly transgressive and highstand systems tracts. Shelf edges are not exposed during sea-level lowstands. Sediment drifts were active, with the locus of drift deposition moved northward. As a result, downslope processes were dominant in the south, where shelf edges prograded rapidly, filling the limited accommodation space above extinct drifts D1-D6 and increasing slope gradient. Meanwhile, along-strike processes were dominant in the north and slope gradient was low because of the concentration of deposition in drifts on the slope. (B) Late Pliocene to Recent sequences S9-S19. Higher amplitudes of, possibly asymmetrical, sea-level cycles led to subaerial shelf exposure during lowstands and outer shelves were incised by channels, with canyons on upper slopes. Sequence boundaries were downlapped on the shelf and internal reflections are oblique; forced regressive systems tracts are interpreted to develop. Downslope processes were dominant after cessation of elongate drift formation at U13, but unconfined currents continued to produce sediment waves interbedded with gravity deposits. Shelf-edge progradation was particularly rapid in the north over the post-drift slope platform above D10 and D1.

downlapped on the shelf and internal reflections are oblique. Downslope processes dominate after cessation of elongate drift formation at U13 (Figure 4.4), in spite of the continuation of unconfined currents, which produced sediment waves interbedded with gravity deposits on the slope (Figure 4.9). Shelf-edge progradation was particularly rapid in the north over the post-drift slope platform above D10 and D11 (Figure 4.4), but also occured in the south, ultimately producing elongate depocenters on isochron maps (Figure 4.10: S9-S19).

4.5 CONCLUSIONS

Nineteen regional sequence-bounding unconformities (U1-U19) are identified in the middle Miocene to Recent shelf-slope sediment prism of the offshore Canterbury basin using high-resolution MCS data. Three larger seismic units are defined based on seismic architecture and facies. 1) U1-U4 mostly lack distinct clinoform breakpoints within the seismic coverage. 2) U5-U8 feature breakpoints; internal reflection geometries are predominantly sigmoid and paleoshelves are smooth and defined by onlap and truncation. Sequences comprise predominantly highstand deposits. 3) U9-U19 are downlapped on paleoshelves and truncate underlying reflections near paleoshelf edges; internal reflection geometries are oblique and U- and V-shaped channels incising paleoshelves indicate exposure during sea-level lowstands. Forced regressive systems tracts occur and may indicate asymmetric sea-level cycles.

Correlation with oxygen isotopic records suggests a eustatic origin for the sequence boundaries. The number of seismic sequences is similar to that of coeval cycles on the Miocene to Recent δ^{18}Osw record of Billups and Schrag (2002) when cycles of comparable frequency are considered (third- and fourth-order). Cycle frequency is an important issue when comparing records (e.g., isotopic and stratigraphic) that are filtered by data resolution. Late Pliocene and Pleistocene seismic sequences are less numerous than the correlative isotope cycles. Here, the stratigraphic record has been excessively filtered relative to the high-frequency isotopic record, either by the limitations of seismic resolution or because shelf erosion has removed evidence of some sequence boundaries during this period dominated by high-amplitude eustasy. Notable exceptions are the last two sequence boundaries (U18 and U19) which correlate well with the last two 100 k.y. oxygen isotopic cycles. Age control must be improved by additional drilling through the IODP (International Ocean Drilling Program) to enhance individual cycle correlations, but global processes appear to have played a significant role in sequence-boundary formation.

However, local processes have exerted fundamental control on sequence architecture. Along-strike currents and associated sediment drifts strongly influenced sequence development. Current erosion in drift moats formed diachronous unconformities, while deposition of adjacent mounded drifts controlled sequence thickness distributions. In addition, currents focused deposition on the slope, reducing the rate of basinward movement of the shelf

edge, but increasing that of the slope toe. As a result, slope inclination is minimized. Cessation of drift development and replacement of along-strike by downslope processes results in increased rates of shelf-edge progradation and slope steepening as the accommodation space over the expanded slope is filled. Slope platforms can form above extinct drifts, reducing accommodation and locally accelerating shelf-edge progradation. Along strike from some large, elongate drifts, seismic evidence for current activity is lacking and coeval strata are clinoformal, in spite of the demonstrable presence of a current. Therefore, elongate drift formation is the product of multiple controls, including current intensity, seafloor morphology and sediment input. Furthermore, along-strike transport could play a role in forming clinoform morphologies worldwide, even where geometries diagnostic of current reworking are lacking. Sea-level change can also affect drift development by causing changes in current intensity and pathways, leading to formation of complex drifts, and high sea-level amplitudes may contribute to drift termination by enhancing downslope processes when the shelf edge is exposed.

Chapter 5: Miocene-Recent tectonic controls on sediment supply and sequence stratigraphy: Canterbury basin, New Zealand

5.1 ABSTRACT

The well-constrained seismic stratigraphy of the offshore Canterbury basin provides the opportunity to investigate long-term changes in sediment supply related to the formation of a transpressive plate boundary (Alpine Fault). The relative motion of the Australian and Pacific plates is reconstructed at eleven points spaced at 50 km intervals along the Alpine Fault for six Oligocene-Recent time intervals (~33.5-26.5, 26.5-20.1, 20.1-11.5, 11.5-6, 6-2.6, 2.6-0 Ma). The reconstructions reveal divergence in the central Southern Alps prior to ~20.1 Ma (chron 6o), followed by increasing average rates of convergence, with a marked increase after ~6 Ma (late Miocene). A strike-slip component existed prior to 33.5 Ma (chron 13o) and perhaps as early as Eocene (45 Ma). However, rapid strike-slip motion (>30 mm/yr) began at ~20.1 Ma (chron 6o). Since ~20.1 Ma there has been no significant change in the strike-slip component of relative plate motion.

Sedimentation rates are calculated from individual sequence volumes that are then summed to represent sequence groups covering the same time periods as the tectonic reconstructions. Rates are relatively high (>22 mm/yr) from 15-~11.5 Ma (sequence group 1). Rates decrease to a minimum (<15 mm/yr) during the ~11.5-6 Ma interval (sequence group 2), followed by an increased rates during the

periods ~6-2.6 Ma (21 mm/yr; sequence group 3) and 2.6-0 Ma (~25 mm/yr; sequence group 4). Good agreement between sedimentation and tectonic convergence rates in sequence groups 2-4 indicates that tectonism has been the dominant control on sediment supply to the Canterbury basin since ~11.5 Ma. In particular, high sedimention rates of 21 mm/yr and ~25 mm/yr in groups 3 and 4, respectively, may reflect increased plate convergence and uplift at the Southern Alps at ~6 Ma. Mountain glaciation since late Pliocene may have contributed to the high sedimentation rate of sequence group 4. The early-middle Miocene (~15-11.5 Ma) high sedimentation rate (22 mm/yr) correlates with low convergence rates (~2 mm/yr) and is mainly a response to global climatic forcing and eustasy.

5.2 INTRODUCTION

The literature of sequence stratigraphy has emphasized the effects of eustasy (e.g., Vail et al., 1977; Van Wagoner et al., 1988), though some have argued that the primary control on sequence development at the 1-10 M.y. time scale is sediment supply (e.g., Poag and Sevon, 1989; Galloway and Williams, 1991; Thorne and Swift, 1991a,b; Liu and Galloway, 1997). Others have focused on tectonic control on the sequence development (Burger et al., 2003; Vilas et al., 2003).

The effect of tectonism on third- and higher-order regional sequences is generally limited, though it can produce high-frequency local unconformities in the immediate vicinity of uplifting anticlines (Naish and Kamp, 1997; Burger et

al., 2002). In-plane stress has been shown to be theoretically capable of producing vertical displacements of the order of 100 m (Cloetingh et al., 1985; Karner, 1986), but is, by itself, unlikely to represent an alternative mechanism to eustasy for generation of third- and higher-order sequences (Christie-Blick et al., 1990; Karner et al., 1993). However, tectonism exerts a fundamental control on sequence architecture through its influence on sediment supply. For example, high erosion rates and thick sedimentary deposits (e.g., fans) are related to active tectonics in major orogens (Browne and Field, 1988; Milliman and Syvitski, 1992; Leturmy et al., 2003; Lucazeau et al., 2003).

The offshore Canterbury basin provides an opportunity to investigate sediment supply variations related to strike-slip to transpressional relative motion at the Alpine Fault plate boundary (Figure 5.1). High rates of sediment supply since the middle Miocene, and perhaps earlier, associated with uplift along the plate boundary, have resulted in the preservation of an unusually high-frequency (~0.1–1.4 m.y. periods), seismically-resolvable record of depositional cyclicity in the basin (Abbott and Carter, 1994; Fulthorpe et al., 1996; Lu and Fulthorpe, in press). High-resolution (30 to 140 Hz; vertical resolution ~5 m within the upper 0.5 s.) MCS data collected in January 2000 (cruise EW00-01; Figure 5.1A) image the Miocene to Recent section. Sequence geometries and unconformity morphologies reflect competing influences of eustasy, contour currents, rate of sediment supply, and seafloor morphology (Fulthorpe and Carter, 1991; Lu et al., 2003; Lu and Fulthorpe, in press). Correlation with regional and global oxygen

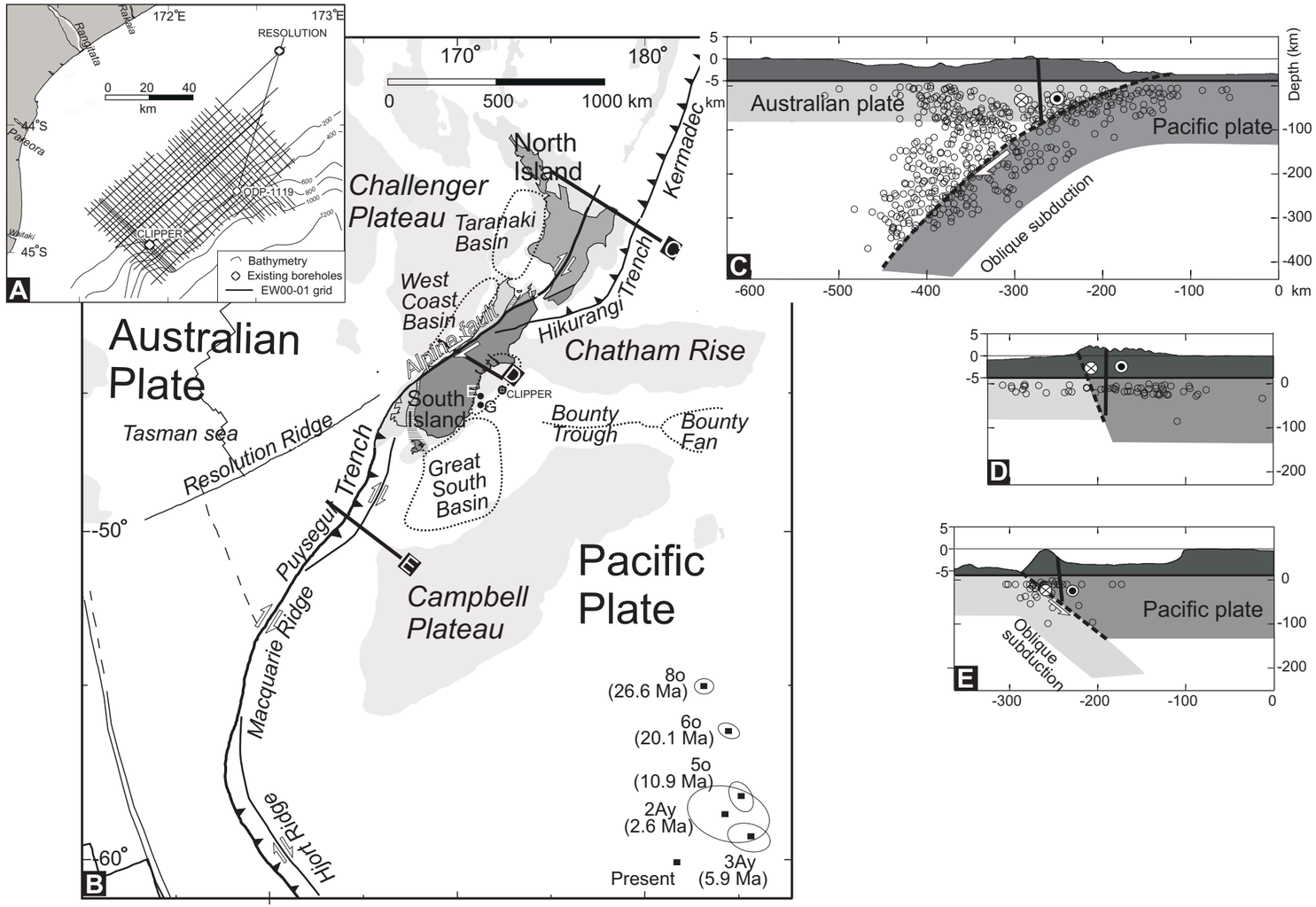

Figure 5.1. (**A**) EW00-01 high-resolution MCS data grid, petroleum exploration wells Clipper and Resolution and ODP Site 1119. (B) Tectonic setting of New Zealand (after Sutherland, 1999; Lebrun et al., 2000; Moore et al., 2000; and Koons et al., 2003) and location of Canterbury basin. The Canterbury basin underlies the present-day onshore Canterbury Plains and offshore continental shelf. It is bounded by the Miocene volcanic centers of Banks Peninsula (BP; 12-5.8 Ma) to northeast and Otago Peninsula (OP: 12.9-9.6 Ma) to southwest (Watters, 1978; Barley, 1987; Sewell and Lewis, 1988). The Alpine Fault, to the northwest, forms the Australian-Pacific plate boundary. The fault is a dextral strike-slip fault with increasing convergence since ~8-5 Ma. Finite poles (squares with error ellipses) are from Cande and Kent (1995). Exploration wells Endeavour (E) and Galleon (G) are indicated by black dots. (**C, D and E)** Three sections across the plate boundary (see Figure 1B for locations). The Pacific plate subducts beneath the Australian plate in the north (C), with dextral strike-slip motion along the Alpine Fault in central South Island (D) and subduction of the Australian plate beneath the Pacific Plate in the south (E; Tippett and Kamp, 1993a; Batt et al., 2000; Earthquake data (ISC epicenters) are from 1999 ISC CD-ROMS).

isotopic records and the Haq et al. (1987) eustatic curve suggests a strong component of eustatic control of sequence formation (Lu and Fulthorpe, in press). Comparison of sequence sedimentation rates, tectonic reconstructions, and Miocene global climate, suggests that increasing plate convergence rates since ~6 Ma resulted in uplift of the Southern Alps and correlate with increasing rates of sediment supply to the offshore basin. In contrast, high rates of sediment supply from ~15-11.5 Ma are a response to a global climatic cooling following a mid-Miocene temperature optimum.

5.3 RESULTS

5.3.1 Tectonic Reconstruction of the Australian-Pacific Plate Boundary

5.3.1.1. Methodology

Reconstructions of the Australian-Pacific plate boundary have evolved as new data have become available. I use the finite pole parameters (Table 5.1) from Cande and Kent (1995) and Cande and Stock (in press) because: 1) relatively high-resolution of chrons (3Ay-2Ay) allows us to calculate the relative motion between the Australian and Pacific plates without the need for interpolation; 2) the pole parameters are well constrained from a range of data, including magnetic, satellite-derived gravity, and seafloor spreading data; 3) Meckel et al. (2003) and Meckel et al. (2003) applied the same pole parameters to the Australian-Pacific

Table 5.1. Finite rotation poles used in this study from Cande and Stock (in press)

Plate Pair	Chron or anomaly (age) (Cande and Kent, 1995)	Latitude °S	Longitude °E	Rotation (°)
Australian-Pacific	13o (33.54 Ma)	-52.14	181.01	37.11
Australian-Pacific	8o (26.5 Ma)	-55.03	183.11	29.23
Australian-Pacific	6o (20.13 Ma)	-56.39	184.44	22.22
Australian-Pacific	5o (11.53 Ma)	-58.24	-58.24	11.93
Australian-Pacific	3Ay (6.04 Ma)	-59.35	185.67	6.38
Australian-Pacific	2Ay (2.58 Ma)	-58.76	184.33	2.77
Australian-Pacific	Present Day (0 Ma)*	-60.08	181.74	1.07

* NUVEL- 1A pole of DeMets et al., 1994.

plate boundary reconstruction at the Hjort Trench. Their results are consistent with interpretations based on new marine geophysical data (swath bathymetry/ reflectivity, seismic reflection, gravity, magnetic), and teleseismic data.

Plate boundary tectonic reconstructions are generated at intervals of 2 Ma for the last ~26 Ma (chon 8o) using UTIG PLATES software and magnetic data from the PLATES database (Lawver et al., 2001). Figure 5.2 illustrates six snap-shots of these reconstructions, corresponding to chrons 8o, 6o, 5o, 3Ay, 2Ay, plus the present configuration.

I also apply stage rotations to define the relative motion of the Australian-Pacific (AUS-PAC) plate system during six time intervals (~33.5-26.5, 26.5-20.1, 20.1-11.5, 11.5-6, 6-2.6, 2.6-0 Ma, corresponding to chrons 13o-8o, 8o-6o, 6o-5o, 5o-3Ay, 3Ay-2Ay, 2Ay-0 Ma, respectively) at eleven locations, 50 km apart, along the plate boundary (Figure 5.3). For each time interval, the components of relative motion both normal and parallel to the plate boundary, together with the angle between the plate motion vector and plate-boundary orientation, are calculated for each of the eleven locations using the method of Le Pichon (1968).

5.3.1.2 Observations

Both the Pacific and Australian plates have moved northward since the late Oligocene, but their relative motion in the vicinity of New Zealand is complex (Figure 5.2). High convergence rates in the north, at the Hikurangi Trench, have resulted in subduction of the Pacific plate beneath the Australian

plate. In contrast, the Australian plate subducts beneath Pacific plate at the Puysegeur Trench, south of New Zealand. Between these convergent segments, the Alpine Fault represents a transition fault, where the relative motion has changed from pure strike slip to transpressive, with increasing convergence particularly since ~6 Ma (Figures 5.2 and 5.3).

In the central part of the Southern Alps, relative plate motion varies both spatially and temporally and is calculated and compared at the eleven locations (Figures 5.3 and 5.4). Spatially, plate convergence angles and perpendicular components of relative motion (convergence) are lowest in center of this zone (locations 5-9) and larger to both north and south (Figure 5.3B-D). However, the spatial variation in convergence angles among all locations is <10º. Convergence angles increase particularly rapidly southward from locations 9-11 (Figure 5.3B; negative angles represent divergence).

Temporally, average convergence rate has increased since ~20.1 Ma (chron 6o; Figure 5.4). Before chron 6o, the average plate relative motion was divergent (Figure 5.4, also see central South Island in Figure 5.2A-B). There was essentially no convergence prior to 11.5 Ma (chron 5o) at location 7 (44° S), while to both north and south, there was already a significant amount of convergence prior to ~20.1 Ma (chron 6o; Figure 5.3B-C). The highest rates of convergence (>7 mm/yr) occur after ~6 Ma. Convergence rates increase through time at all locations until the interval between ~6-2.6 Ma (chrons 3Ay-2Ay). Convergence rates have remained relatively stable since that time (Figures 5.3B,

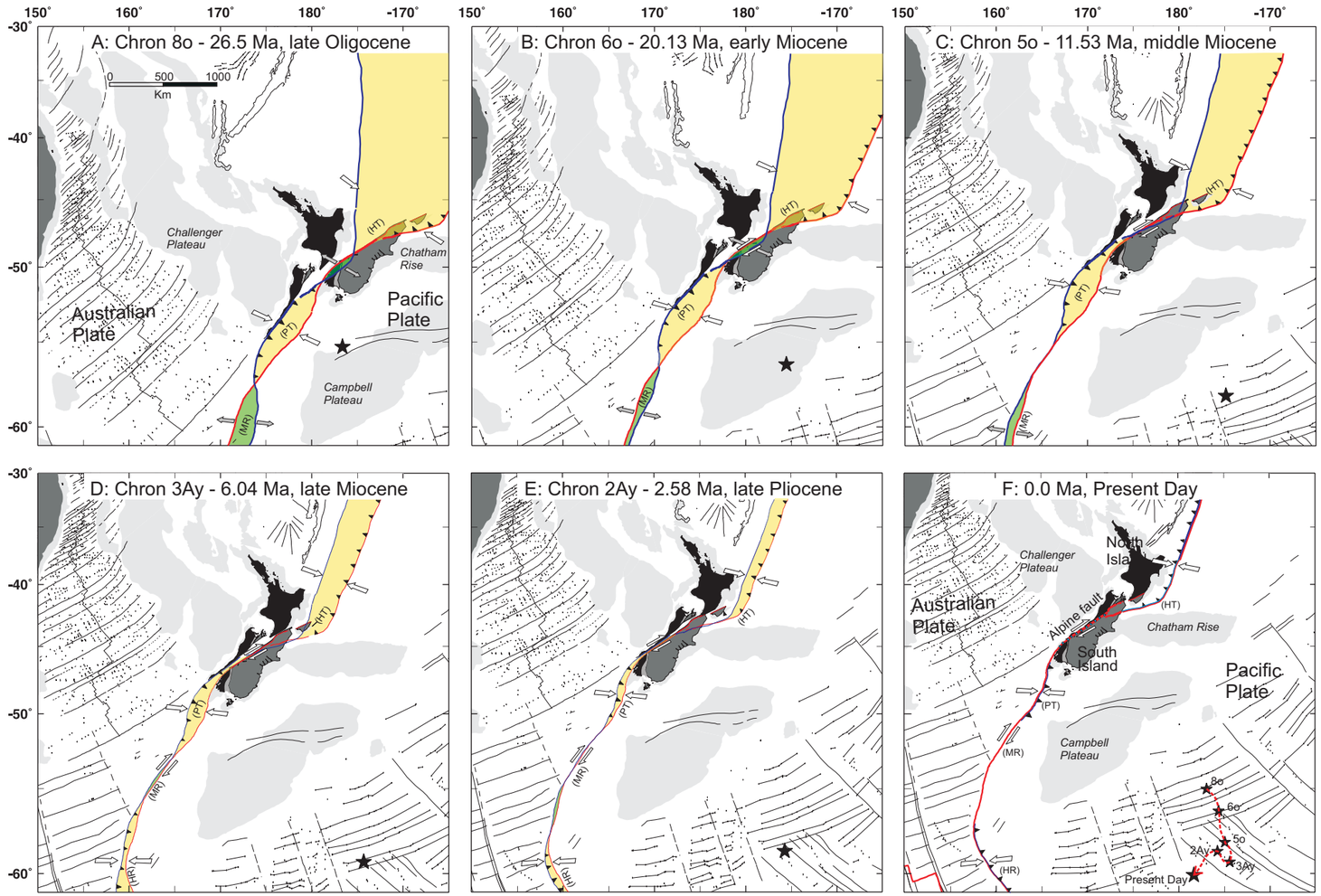

Figure 5.2. Kinematic reconstructions of the Australian-Pacific plate boundary from chron 8o (~26.5 Ma) to Present. Reconstructions use the finite poles of rotation of Cande and Kent (1995), and Cande and Stock (in press; Figure 1B). Colored regions represent overlaps (yellow) or gaps (green) between plates along the plate boundary. Overlaps are sites of crustal (plate) shortening or subduction leading to topographic uplift and/or subduction. Gaps are sites of crustal extension and topographic depression (Heubeck and Mann, 1991). Constructed using UTIG's PLATES software with magnetic data from the PLATES database (Lawver et al., 2001).

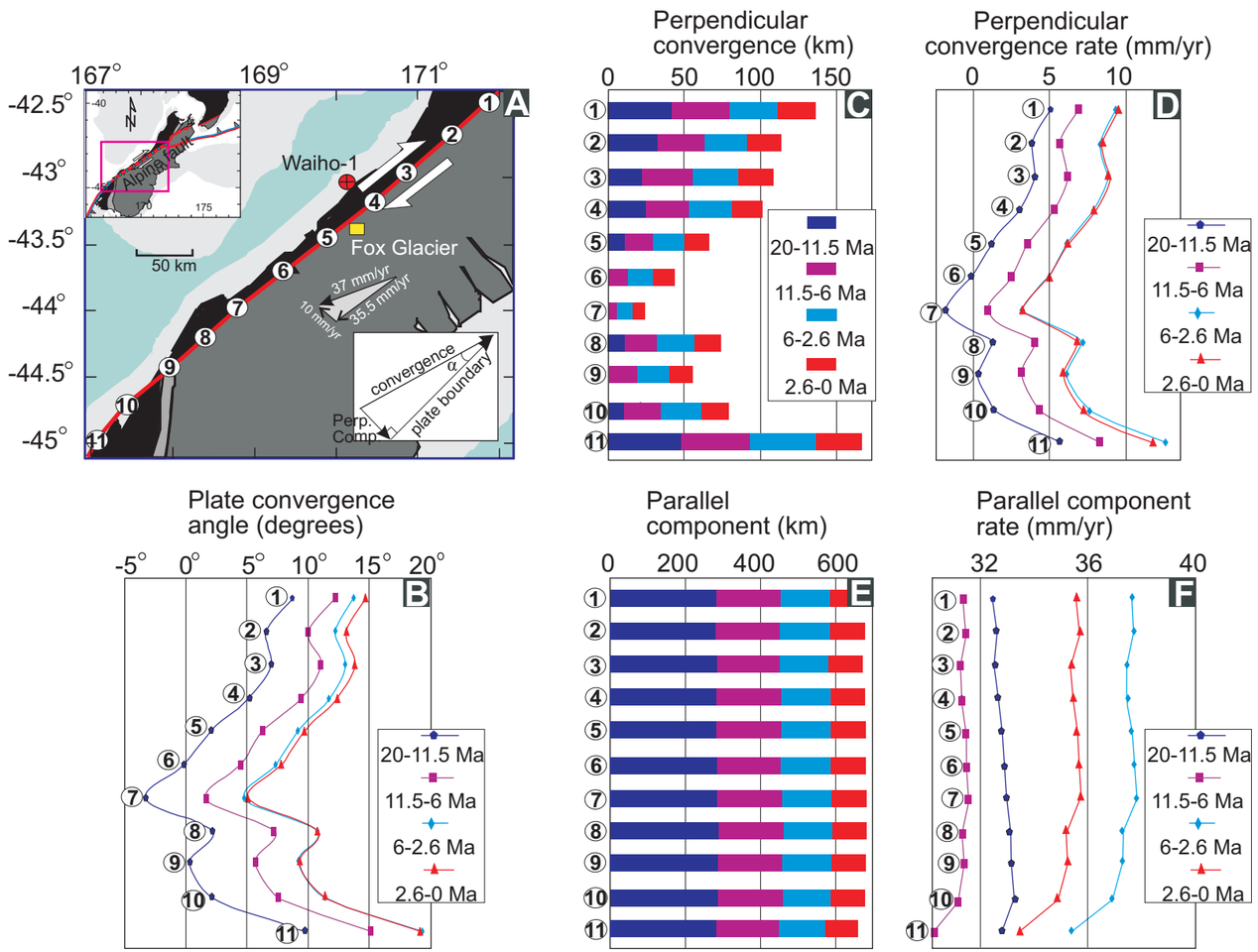

Figure 5.3. Angles and rates of convergence with respect to plate boundary orientation predicted by stage rotations for eleven locations along the Alpine Fault since ~20 Ma (chron 6o). (A) Locations at which relative motions are calculated. Also shown are the locations Fox Glacier and exploration well Waiho-1 and the present-day relative motions at the Alpine Fault (Norris and Cooper, 2000). (B) Angles between the relative plate motion vector and plate boundary orientation (see bottom-right inset in Figure 6A). Negative angles imply divergence (e.g., location 7 from chrons 6o-5o) and positive angles imply convergence. (C-D) Normal components of relative motion (convergence). Convergence rates increases at all locations through time. (E-F) Parallel components of relative motion (convergence). Parallel component displacements at most locations are similar, with a slightly decrease to southward locations 9-11 (E). However, parallel component rates are change come and forth ranging from 30 to 38 mm/yr (F).

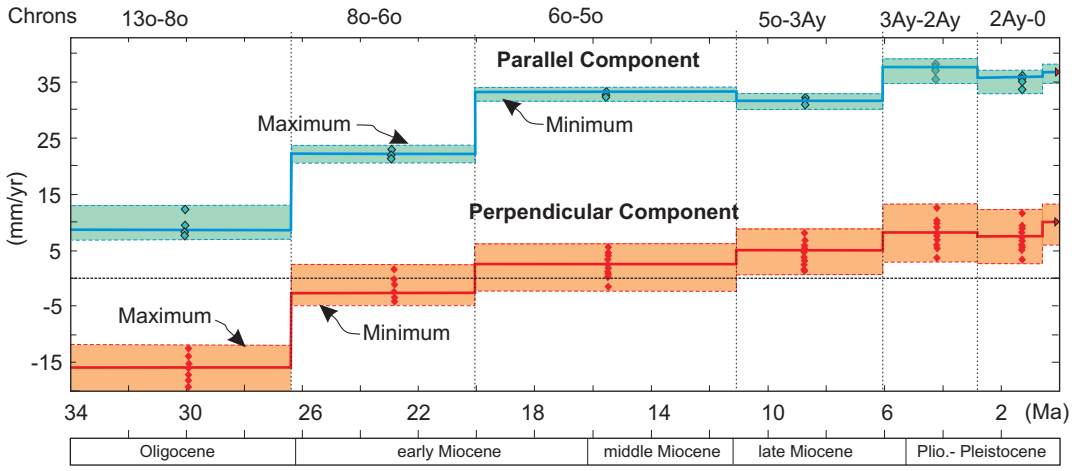

Figure 5.4. Comparison between plate-boundary-parallel and normal components of relative motion since ~33.5 Ma (early Oligocene, chron 13o). Within each time interval, rates at each of the eleven locations are shown at the midpoint of the time interval. Maximum, minimum and average values are delineated. Present-day rates are from Norris and Cooper (2000) based on GPS measurements.

D and 5.4). The small decrease in convergence rates at locations 8-11 in the south, and small increase at locations 1-5 in the north, from the 6-2.6 Ma (chron 3Ay-2Ay) interval to the 2.6-0 Ma (2Ay-Recent) interval, result in the average convergence decreasing slightly (Figure 5.4). However, data for the Present (10±2 mm/yr, based on GPS measurements; Norris and Cooper, 2000) and last 1.3±0.3 Ma (~7-10 mm/yr in the Fox Glacier region, Figure 5.3A, based on fission track analysis; Tippett and Kamp, 1993a) indicate a continuation of the trend of increasing convergence (Figure 5.4). In contrast, the average parallel component of relative plate motion has not changed greatly since ~20.1 Ma (chron 6o) relative to the significant increases before chron 6o (Figure 5.4).

5.3.2 Sequence Volumes and Sedimentation Rates

5.3.2.1 Methodology

Sequence grain volume is defined as the volume of sedimentary grains in an individual sequence (total sequence volume minus volumes of cement and porosity; Liu and Galloway, 1993, 1997). It represents the actual volume of sediment grains accumulating at a given locality (assuming no post-depositional erosion). Use of grain volume for calculating sediment accumulation or supply rates is one way to account for the effect of compaction on the volumes of buried sequences (Liu and Galloway, 1997). Sediment accumulation or supply rates derived from grain volumes have several advantages over those derived from unmodified sequence thickness or even decompacted thickness (Liu and

Galloway, 1997). For example, assumptions about original sediment porosity distribution, needed for decompaction calculations, are unnecessary. Instead, measured porosity-depth relationships are used to calculate grain volumes. Furthermore, comparison of sediment accumulation rates for sequences with differing burial depths can be made without being affected by lithology-dependent variations in compaction behavior.

High-resolution MCS profiles (EW00-01 survey, Figure 5.1A), tied to exploration wells and ODP Site 1119 (Figure 5.1A-B), provide a high-frequency sequence stratigraphic framework for the offshore Canterbury basin (Figures 4.3, 4.4, and 5.5). Nineteen regional sequence-bounding unconformities (U1-19) are identified in the middle Miocene to Recent shelf-slope sediment prism (Figure 5.5, Lu and Fulthorpe, in press). Uncorrected sequence volumes (Figure 5.6A-B, red bars) are calculated using stacking velocities (Figure 2.7) and isochron maps (Lu and Fulthorpe, in press). Sequence grain volumes and sedimentation rates (Figure 5.6A-B, yellow bars) are then calculated using borehole porosity data (Figure 5.5D and F) and sequence ages (Figures 5.5E; Lu and Fulthorpe, in press).

A number of limitations and sources of error must be borne in mind when evaluating results of sediment volume calculations. In particular, the EW00-01 survey covers a limited area and sediment volume calculations do not include sediment deposited outside the limits of the survey, e.g., in the Bounty Trough and Fan (Figure 5.1B). In addition, this work ignores that portion of the sediment eroded from the Southern Alps that is deposited on the west coast of New

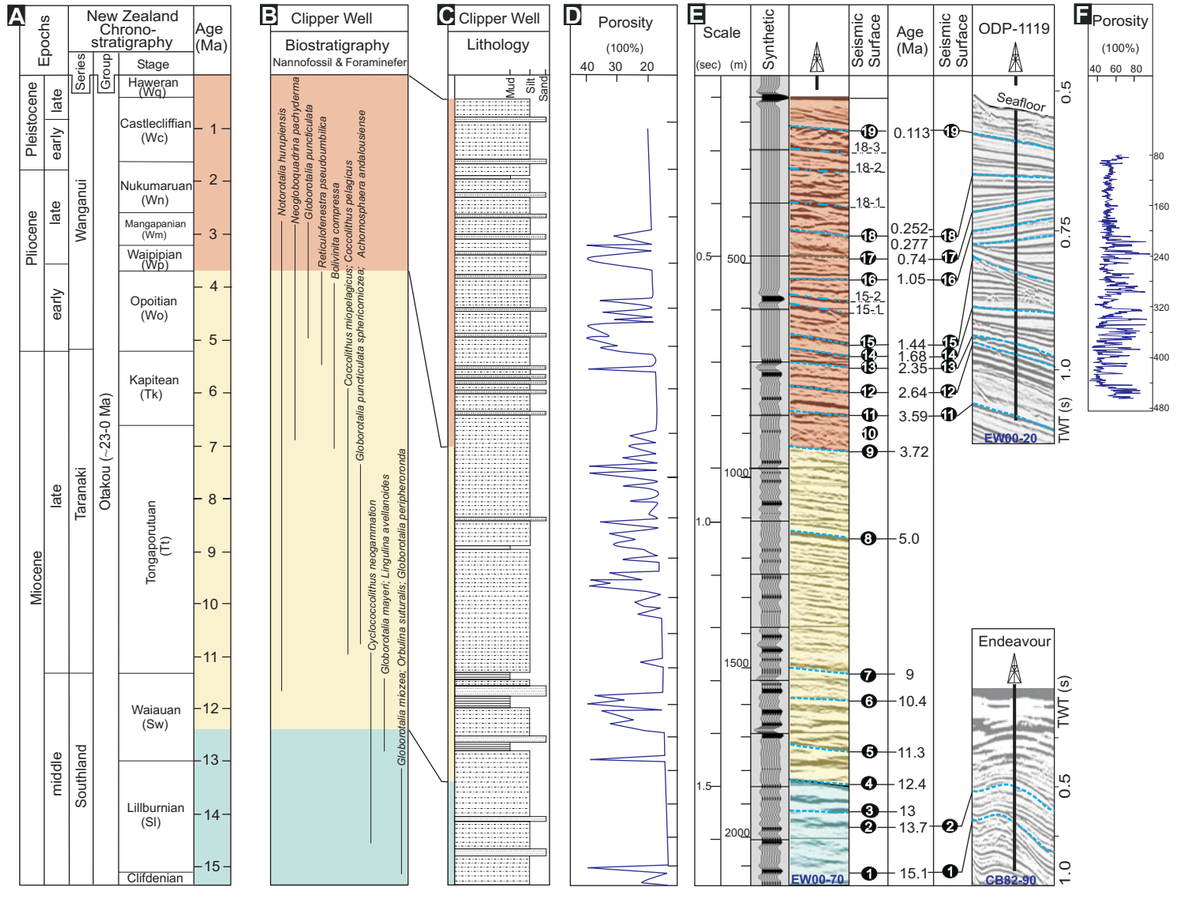

Figure 5.5. (A). New Zealand chronostratigraphy (Homibrook, 1992; Shipboard Scientific Party, 1999). (B-D) Biostratigraphy, lithology, and porosity at Clipper exploration well (Hawkes and Mound, 1984). (E) Ages of sequence-bounding unconformities based on ties to Clipper (Hawkes and Mound, 1984) and Endeavour (Wilding and Sweetman, 1971) exploration wells and to ODP Site 1119 (Shipboard Scientific Party, 1999; R.M. Carter, personal communication, 2002). See Figure 5.1A-B for locations. (F). Porosity at Site 1119 (Shipboard Scientific Party, 1999).

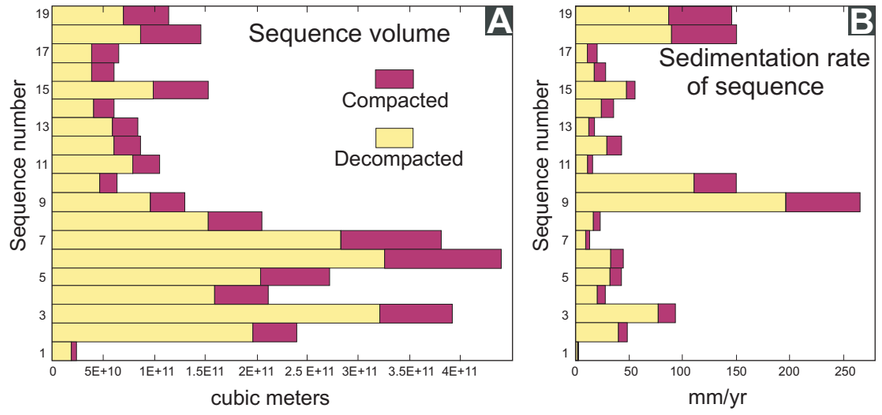

Figure 5.6. Sequence volumes and sedimentation rates and comparison with convergence rates. (A-B) Volumes and sedimentation rates for individual sequences. The red bars are values of sequence volumes (A) and sedimentation rates (B) without compaction correction and yellow bars represent sequence grain volumes, and associated rates, and therefore represent compaction-corrected values. (C) Sedimentation rates grouped into the same time intervals as those of the tectonic reconstructions in Figures 5.3 and 5.5 for comparison with convergence rates. (D) Convergence rates at Alpine fault since 18 Ma (identical to Figure 5.4) (E) Sedimentation and convergence rates for sequence groups 2-4 are strongly correlated (R^2=0.9), whereas there is no correlation for group 1.

Zealand. Therefore, the sediment volumes represent a relative measure of sediment accumulation through time and not an absolute measure of total sediment eroded from the Southern Alps.

Sequence boundary ages are the most important source of error for sedimentation rate calculations. Age control relies on two exploration wells (Clipper and Endeavour) and ODP Site 1119 (Figure 5.5; Lu and Fulthorpe, in press). Ages of late Pliocene to Recent unconformities U11-U19 are most reliable since they derive from Site 1119, which continuously cored a near-complete section of late Pliocene and Pleistocene sediments; only one downlap unconformity (U18 at 87 mbsf) has a significant hiatus (~25 k.y.). U19 (48 mbsf) corresponds to the stage 5/6 boundary (~113 ka) and the age of the deepest sediment recovered is ~3.6 Ma (Shipboard Scientific Party, 1999; Carter et al., 2004). Furthermore, ages within the upper ~100 m below sea floor at Site 1119 have been refined using radiocarbon dates and by matching the Site 1119 gamma-ray log with the Vostok ice core record (Carter et al., 2004). Ages of Miocene unconformities are less well constrained, with the possible exceptions of U3 (13 Ma), U5 (11.3 Ma), and U8 (5 Ma), which are coincident with New Zealand chronostratigraphic stage or series boundaries.

The high sedimentation rates in sequences 9 and 10 (overlying U9 and U10, respectively; Figure 5.6B) arise from the short durations of these sequences (Figure 5.5E). These sedimentation rates could be greatly reduced if the sequence boundary ages are only slightly in error. To reduce the impact of such

anomalously high rates, sequences are collected into groups (labeled 1-4 on Figure 5.6C). This mutes the effect of dating errors by averaging sedimentation rates over longer periods (duration of each sequence group is at least 2 M.y.). Furthermore, seismic sequences groups 1-4 cover the same four intervals as the tectonic reconstructions (20.1-11.5, 11.5-6, 6-2.6, 2.6-0 Ma; compare Figure 5.6C-D), facilitating comparison of sedimentation rates with tectonic reconstructions.

Cementation by material derived from outside individual sequences may lead to overestimation of sediment volumes. Whereas compaction is particularly important in clayey sediments, cementation is more pronounced in sandstone (Larsen and Chilingar, 1979; Baldwin and Butler, 1985). In the Canterbury basin, middle Miocene-Recent sediment is dominated by terriginous silts and silty muds (Figure 5.5C), and burial depths relatively shallow (<2 km below sea floor, Figure 4.3). Therefore I assume that cementation is negligible and total sequence grain volume is here assumed to equal total sequence volume minus porosity volume.

In contrast, post-depositional erosion can lead to underestimation of depositional sediment volumes. Sequences groups 3 and 4 (S8-11 and S12-19), contain erosional unconformities (U9-U19, Figure 4.3), which must have led to loss of sediment. The increasing amplitudes of late Neogene glacioeustatic sea-level cycles may also have contributed to underestimation of sedimentation rates in these sequence groups by causing an increased proportion of sediment to bypass to deep-basin systems where it is outside the EW00-01 grid and, therefore,

not reflected in sediment-volume calculations (Galloway, 2001). However, this would not change the overall trend of increasing sedimentation rates in sequence groups 2-4 (Figure 5.6C). Submarine currents also form erosional surfaces in the Canterbury basin, but most of the eroded sediments are redeposited basinward of erosional moats and along the slope toe after only limited along-strike transport (Lu et al., 2003). Currents may have transported some sediment outside of the basin northeastward, or introduced sediment from the southwest, but our data do not allow us to document the amounts. However, the co-existence of sediment drifts and downslope processes suggest that the influence of along-strike transport is local and that most current-eroded sediment is redeposited within the basin (Lu et al., 2003; Lu and Fulthorpe, in press).

5.3.2.2 Observations

Early sequences (S2-S8) have the largest volumes, ranging from 1.52x10 ^{11} (S8) to 3.34x10 ^{11} m^3 (S6; Figure 5.6A; the depocenter of S1 is not fully covered by the EW00-01 survey, so its volume is uncertain). Volumes of later sequences (S9-S19) are relatively small, ranging from 0.4x10 ^{11} (S10) to about 1x10 ^{11} m^3 (S15; Figure 5.6A). Differences in absolute volumes mainly reflect sequence durations (Figure 5.5): the longer, third-order sequences (S2-S8) have large volumes, whereas the shorter, fourth- to sixth-order sequences (S9-S19) have smaller volumes (Figure 5.6A). When sedimentation rates are considered, three peaks occur, at S3, S9-S10, and S18-S19 (Figure 5.6B). S9-S10 are of short

duration and dating errors may have magnified sedimentation rates. Comparison of sequence groups provides a more robust measure of sedimentation rate variations and reveals that rates are relatively high (> 22 mm/yr) in group 1, lowest in group 2 (< 15 mm/yr), and subsequently increase in groups 3 (21 mm/yr) and 4 (~25 mm/yr; Figure 5.6C).

5.4 DISCUSSION

5.4.1 Evolution of the Alpine Fault

The modern Alpine fault has been intensively studied for its seismic potential (Moore et al., 2000; Pearson et al., 2000; Leitner et al., 2001; Beavan and Haines, 2001) and kinematics (Pearson et al., 2000; Beavan and Haines, 2001). At present, the Australian plate is moving east-northeast relative to the Pacific plate with oblique convergence at ~37 mm/yr, calculated using the Nuvel 1A rotation pole (DeMets et al., 1994; Leitner et al., 2001). This motion translates to 35.5 mm/year parallel to, and 10 mm/year perpendicular to, the Alpine Fault (Norris and Cooper, 2000). Convergence has resulted in uplift of the Southern Alps and exhumation of deep-seated crustal rocks immediately east of the fault during the last few million years (Norris et al., 1990). Recent uplift resulting from glacio-isostatic rebound is limited (<10 %; Matthews, 1967). Exhumation rates based on reset zircon ages have accelerated with time to reach a maximum, calculated over the last 1.3±0.3 Ma, of ~7-10 mm/year close to the Alpine fault in

the Fox Glacier-Mount Cook region (Figure 5.3A; Tippett and Kamp, 1993a). Norris et al. (1990) reported that the Southern Alps uplift rate approaches 10 mm/yr in central Westland, coincident with the present perpendicular component of Alpine Fault convergence (Norris and Cooper, 2000). Uplift (= exhumation) rates is roughly balanced by erosion at the central part of Southern Alps near Fox Glacier (Figure 5.3A; Wellman, 1979; Adams, 1980; Walcott, 1998). The positive relationship between plate convergence and Southern Alps uplift implies that convergence rates control sediment supply to adjacent basins.

Sutherland (1999) noted that the history of the Alpine Fault and the timing and amount of bending of New Zealand basement terranes, have been two of the most widely debated subjects in the literature on New Zealand geology (e.g., Little and Roberts 1997; Sutherland 1999; King, 2000; Lebrun et al., 2000, 2003). Much of this debate is concerned with the relative importance of Cretaceous versus Cenozoic crustal deformation, and the relative contributions and timing of faulting, distributed shear, and local rotations (see Table 5.2). Most variability in Neogene tectonic reconstructions of the Alpine Fault results from use of different finite pole locations and ages and from performing reconstructions with different time steps (see Table 5.3).

The Alpine Fault connects subduction and reverse fault zones to the north (Hikurangi Trough; Berryman et al., 1992; Anderson and Webb, 1994) and south (Puysegeur Trench; Davey and Smith, 1983), which have opposite convergence directions (compare Figures 5.1C and 5.1E). The intervening Alpine Fault is a

Table 5.2. Evolution of Alpine Fault

Tectonic style		Displacement	Tectonic significance
Present-day: active transpression		Present-day rate of relative motion is 37±2 mm/yr with parallel component of 35.5 mm/yr and perpendicular component of 10 mm/yr (Leitner et al., 2001; Norris and Cooper, 2000).	Oblique relative motion at Australian-Pacific plate boundayr resulted in the uplift of the Southern Alps and exhumation of deep-seated crustal rocks immediately east of the fault (Norris et al., 1990).
Initiation of convergence-related uplift	5 Ma: Chamberlain et al. (1995) 6.2-6.4 Ma: Lewis et al. (1986); Walcott (1998); 6-7 Ma: Molnar et al. (1999); 8-5 Ma: Tippett and Kamp (1993b); Batt et al. (2000); Batt et al. (in review) 10-8 Ma: Molnar et al. (1975); Carter and Norris (1976); Norris et al. (1978); Adams (1979); ~15 Ma: Fulthorpe and Carter (1991).	Fault-normal displacement is mainly accommodated by underthrusting of the Australian plate offshore west of New Zealand, due to a change in the nature of the crust from continental to oceanic (Norris and Cooper, 2000). Accommodation of excess continental crust is by crustal thickening and erosion. Rock uplift at a rate of 11 mm/yr is balanced by erosion with some is accommodated as a root to the Southern Alps (Walcott, 1998). Shortening: 70- 110 km (since 6.4 Ma): Walcott (1978, 1998); Molnar et al. (1999).	
Initiation of strike-slip motion	Late Oligocene-early Miocene (23-25 Ma): Adams and Cooper (1996); Cooper at al. (1987); Kamp (1987a,b); Lebrun et al. (2003). Middle Oligocene (30 Ma): Carter and Norris, 1976; Eocene (45 Ma): Sutherland, (1999) Cretaceous (100 Ma): Wellman and Cooper (1971)	Dextral offset, 460-500 km (since ~ 23 Ma): Wellman (1953); Kamp (1987a,b).; 800 km: Sutherland (1999). 25-30 mm/yr during Pliocene-Pleistocene; Berryman et al. (1992), Southerland and Norris (1995); 25-35 mm/yr: Walcott (1998); Alpine fault accommodates half to three quarters of the relative plate motion (Norris and Cooper, 1995; Sircombe and Kamp, 1998; Beavan et al., 1999).	Transform plate boundary, connects subduction zones to the north (Hikurangi Trench) and south (Puysegur Trench) with opposite-facing convergence directions.

Table 5.3. Comparison of Neogene tectonic reconstructions of the Australian-Pacific plate boundary, Alpine Fault

Authors	Origin of finite rotation parameters	Evaluation of methods
Walcott (1998)	Finite rotation parameters from Cande et al. (1995); anomaly numbers and ages based on Cande and Kent (1995); Some data (chrons 5r, 6r) are from Royer and Sandwell (1989)	There are no intermediate rotation poles for the period around 6 Ma. Therefore, the conclusion that, prior to 6.4 Ma, Australian-Pacific relative plate motion was strike slip with only a small compressive component was obtained by interpolating a 6 Ma rotation for Australian-Antarctic motion between the Royer and Sandwell (1989) rotation and the NUVEL1A (DeMets et al., 1994) rotation. Royer and Sandwell (1989) used gravity constraints from satellite altimetry measurements to refine the rotation, but still at roughly 20 Ma intervals.
Cande and Stock (in press)	Uses archival magnetic anomaly data and fracture zones constrained from the satellite-derived gravity field of Sandwell and Smith (1997) Ages are based on the timescale of Cande and Kent (1995).	With new rotations for chrons 3Ay and 2Ay, a detailed late Miocene history can be calculated directly, without interpolation between a 5o rotation and NUVEL1A pole. Error ellipses for each finite pole have been calculated.
Sutherland (1995, 1999)	Geosat-derived digital gravity grid (GEOS-3P resolution), computed by Marks et al. (1993)	Rotations at ~5 M.y. intervals, and can be used to reconstruct short stages, such as from chron 3Ay-2Ay and 2Ay-Present.

continent/continent collision zone between Challenger Plateau to the west and the Chatham Rise/Campbell Plateau to the east (Figures 5.1 and up left inset of 5.3A). Minima in convergence angle and rate occur at locations 6-9 (Figures 5.3B-D). These minima occur because the nature of motion at a plate boundary depends on the orientation of the boundary relative to small circles centered on the pole.

The tectonic reconstructions of the central Southern Alps reveal the following. 1) Australian-Pacific relative motion was divergent prior to ~20.1 Ma (chron 6o; .5.2 and 5.4). 2) Convergence, averaged for all locations, began as early as chron 6o (Figure 5.4) and increased through time. Convergence rate was ~4.5 mm/yr by ~11.5 Ma (close to chron 5o) and became especially high after ~6 Ma (>7 mm/yr). This is in agreement with the suggestion that there was a significant change in relative plate motion at chron 3Ay (6-6.5 Ma; see Table 5.2; Walcott, 1998). Convergence decreased slightly after 2.6 Ma (chron 2Ay; Figure 5.4), but present-day rates show an increase to ~10 mm/yr (Norris and Cooper, 2000). 3) Previous studies indicate that uplift rates in the central part of the Southern Alps (near Fox-Glacier region; locations 4-6; Figure 5.3A) decrease to the north, south and east (Wellman, 1979; Tippett and Kamp, 1993a,b). However, our reconstructions show that convergence rates increase to the north (locations 3-4) and decrease to the south (location 5-7), before increasing again (Locations 9-11). The maximum convergence rate occurs north of the Fox Glacier area at location 1 (Figure 5.3A and D). Furthermore, high rates (>7 mm/yr) of convergence were initiated earlier (~6 Ma) than suggested by Tippett and Kamp

(1993a; 1.3±0.3 Ma). 4) Estimates of the age of commencement of a strike-slip component of relative motion along the Alpine Fault have varied widely and include ages as old as early Cretaceous (Table 5.2). More recent estimates have converged on an initiation of strike-slip motion at ~23-25 Ma (e.g., Kamp, 1987b, Lebrun et al., 2003; Table 5.2). Our reconstructions show that relatively rapid (~23 mm/yr) strike-slip motion already existed between 26.5-20.1 Ma (chrons 8o-6o; Figure 5.4). Strike-slip motion at slower rates (<8mm/yr) was occurring from 33.54-26.5 Ma (chrons 13o-8o; Figure 5.4) and may, therefore, have begun as early as Eocene (45 Ma), as suggested by Sutherland (1999; Table 5.2). However, there is a ~400% increase in strike-slip rate (from 8 mm/yr to 33mm/yr) between the chron 13o-8o and 6o-5o intervals (Figure 5.4). This result is consistent with the existing view that strike-slip motion began at about 23-25 Ma (Table 5.2). There has been little variation in rates of fault-parallel relative motion since ~20.1 Ma (chron 6o; Figure 5.4). However, the average rates calculated for the last ~20.1 Ma (30-37 mm/yr) are higher than those of Walcott (1998) and Sutherland and Norris (1995; Table 5.2).

5.4.2 Global and Local Controls on Sediment Supply

5.4.2.1 Local tectonism

Tectonic uplift in the hinterland has been proposed to explain the increasing sediment flux seen at continental margins during the Tertiary, and

particularly since the Miocene. For example, Tertiary uplift of Africa can account for an increase in clastic sedimentary supply on its margins (Bond 1978; Lavier et al., 2000, 2001) and uplift of the Adirondack dome in the Appalachians (Hack, 1982; Gardner, 1989; Poag and Sevon, 1989) has been proposed as the sediment source for the progradational middle Atlantic passive margin, with isostasy providing a feedback between denudation and deposition (Pazzaglia and Gardner, 1994).

Adams (1980), Tippett and Kamp (1993a,b), and Walcott (1998) noted that the Southern Alps make up about half of the land area of the South Island, but almost all of the rapidly eroding part. Most of the material (>70-80%) eroded during the Pliocene-Quaternary has been transported to basins on the west side of the Alpine Fault; the remaining 20-30% was transported to the east side of the fault, including the Canterbury basin, Great South basin, Bounty Fan, and Hikurangi and Kermadec Trenches (Figure 5.1B; Adams, 1980; Carter and McCave, 1994; Sutherland, 1996; Walcott, 1998). Walcott (1998) argues that major increases in sedimentation rate recorded by Waiho-1 borehole on the west coast (for location see Figure 5.3A) at ~12 and 6.4 Ma are linked to rapid changes in Australian-Pacific relative plate motion. Others (e.g., Sutherland, 1995) also state that large volumes of sediment derived from southeast of the Alpine Fault reflect widespread uplift of the Southern Alps during this period. Sircombe and Kamp (1998) attributed a rapid increase in subsidence at 5-6 Ma to loading within

the collision zone onshore, based on their study of Miocene-Recent South Westland basin (or West Coast basin, Figure 5.1B)

The EW00-01 survey covers the principal Miocene-Recent depocenter of the Canterbury basin (Figure 5.1A). Therefore, the sedimentation rates there represent a relative measure of the sediment supply resulting from uplift of the Southern Alps. Correlation of sedimentation rates within sequence groups with convergence rates (Figure 5.6C-D) is good for the most recent three groups (Figure 5.6E; R^2=0.9 for sedimention rates after compaction correction), suggesting that plate boundary tectonism has controlled sediment supply since ~11.5 Ma. In particular, high rates of sediment supply in groups 3 and 4 may reflect the increase in convergence rate since ~6 Ma (Figure 5.6C-D). The high rate of subsidence since 8-6 Ma (Figure 2.2) may have been caused by plate flexure accompanying this increase in convergence at ~6 Ma (Figure 5.6D). However, the high sedimentation rate in sequence group 1 correlates with a period of low convergence rates.

5.4.2.2 Climatic influence

The Cenozoic was a time of great tectonic, eustatic and climatic transformation (Head and Nelson, 1994; Clark et al., 1999; Zachos et al., 2001, Steckler and Lavier, submitted). Latitudinal temperature gradients increased, polar icecaps formed and high-amplitude glacioeustatic fluctuations developed. Cooling at the poles altered ocean circulation and temperatures and biota evolved

to adapt to the changing conditions (Figure 5.7D-F; Gill, 1968; Hornibrook 1992). Steckler et al. (1999) and Lavier et al. (2001) concluded that high sediment supply on the New Jersey and West Africa margins (Figure 5.7B-C) during ~16-11.5 Ma was linked to global cooling coupled with a 45-70 m sea-level fall (Figure 5.7G; Miller et al., 1991; Lear et al., 2000). The $\delta^{18}O$ curve (Figure 5.7F; deduced from benthic taxa, Zachos et al., 2001) indicates a long-term trend to colder Neogene and Quaternary temperatures, culminating in Pleistocene high frequency glaciations. Formation of continental ice sheets has a direct impact on sea level (Figure 5.7F-G), and the associated climatic deterioration can also contribute to increase in erosion rates on the continents and, consequently, clastic sediment supply to continental margins (Molnar, 2001; Atkins, 2001). Both warmer land temperatures and higher precipitation have been linked to warmer sea-surface temperature anomalies around New Zealand (Folland and Salinger, 1995; Mullan, 1998; White and Cherry, 1999). Therefore, I expect colder Neogene and Quaternary temperatures to result in lower temperatures and less precipitation on the South Island. The transition from Greenhouse to Icehouse conditions is accompanied by important increases in seasonal and latitudinal temperature gradients, as well as a strong continent/ocean temperature contrast that implies more arid conditions (Seranne, 1999). All these effects combine to increase erosion on the continents (Molnar, 2001), and consequently clastic sediment supply to continental margins (Leckie, 2001; Steckler and Lavier, submitted). In

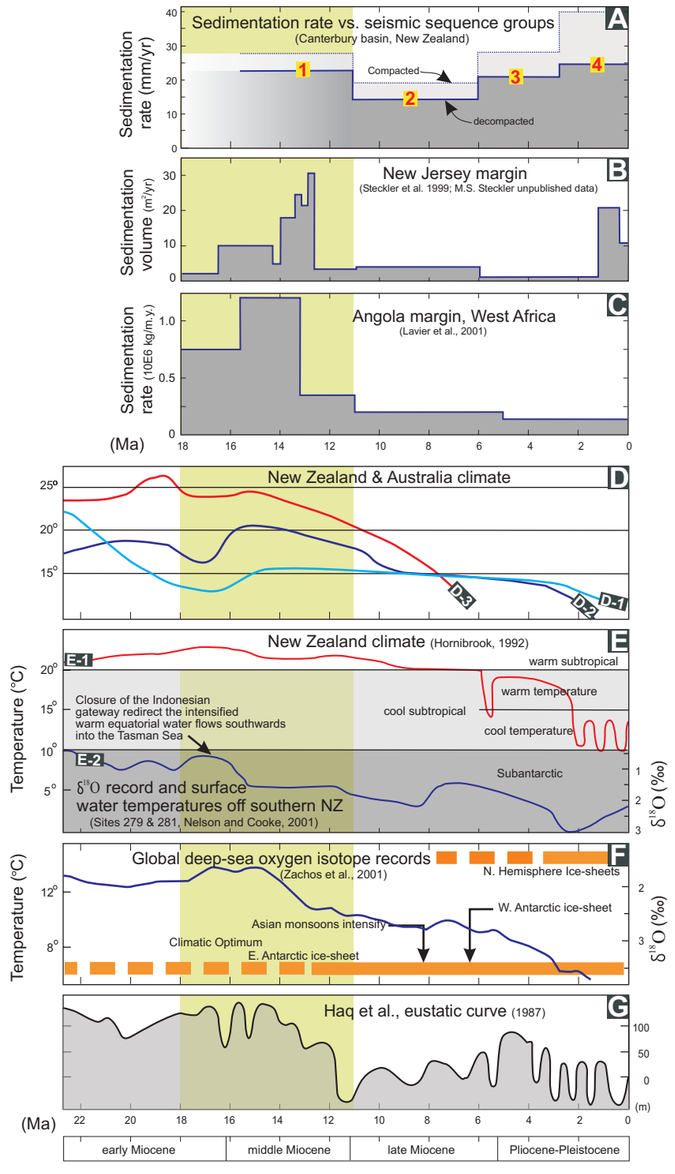

Figure 5.7. Comparisons among sedimentations rates in the Canterbury Basin (A), New Jersey (B) and West Africa (C), paleoclimate of the New Zealand/Australia region (D), New Zealand marine paleoclimate (E), global deep-sea oxygen isotopic record (F), and eustatic curve of Haq et al. (1987; G). The green shaded area represents the duration of sequence group 1 (> 15.1-11.5 Ma). (B-C) Show high sedimentation rates from ~16.5-12.5 Ma, interpreted to be the result of global climate change (Steckler et al., 1999; Lavier et al., 2001; Steckler, unpublished data). (D) Shows the Neogene climatic optimum near the early/middle Miocene boundary (~16 Ma). D-1 is an oxygen isotope paleotemperature curve from two series of Tertiary mollusk shells from Victoria, Australia (Gill, 1968). D-2 is an oxygen isotope paleotemperature curve based on planktonic foraminifera and macrofossils from shallow water deposits of New Zealand (Devereux, 1968). D-3 is a temperature curve deduced for the New Zealand Cenozoic based on the distribution and temperature tolerances of fossil fauna such as scleractinian corals (Keyes, 1968). (E) E-1 is a New Zealand shallow-water marine paleoclimate curve compiled by Hornibrook (1992) from southernmost records of fossil occurrences of warm shallow-water stenothermal benthic marine organisms (e.g., molluscan, *Lingula*, *Amphistegina,* mangroves, and *cocos*). E-2 is a record of planktonic foraminiferal oxygen isotopic and inferred near-surface water temperatures off southern New Zealand (ODP sites 279 and 281; Nelson and Cooke, 2001). Both curves show the climatic optimum at ~16 Ma. (F) Global deep-sea oxygen isotopic record (Zachos et al., 2001); the decrease in temperature from early middle Miocene to late Miocene (~16-5 Ma) was associated with formation of a permanent ice sheet on East Antarctic. (G) Eustatic curve of Haq et al. (1987). Note the positive correlation between long-term eustasy (G) and the global oxygen isotopic record (F).

any event, lowered sea level linked to the build up of Antarctic ice led to rivers discharging near paleoshelf edges, increasing rates of deposition on the outer shelf and slope.

Figure 5.7D-E shows evidence for a Neogene climatic optimum near the early/middle Miocene boundary (~16 Ma) derived from a range of data types (Gill, 1968; Devereux, 1968; Keyes, 1968; Hornibrook 1992; Zachos et al., 2001; Nelson and Cooke 2001). Nelson and Cooke (2001) suggested that this climatic optimum is due to the closure of the Indonesian gateway, which redirected warm equatorial water southwards into the Tasman Sea, leading to high sea-surface temperatures in the New Zealand area. However, this temperature optimum also occurs on global temperature records (Figure 5.7F). The high sediment supply in sequence group 1 corresponds to this climatic optimum and the subsequent rapid decrease in temperature from ~15 Ma to ~11.5 Ma (Figure 5.7). Sequence group 1 also falls during a period of relatively high frequency sea-level cycles followed by a long-term fall (Figure 5.7G).

In Australia and New Zealand, only one montane glaciation believed to be early Pleistocene in age that has been recognized before the late Pleistocene, even though upper Miocene and Pliocene marine sediments in New Zealand record several occasions when the climate was colder than it is today and some of these events were of glacial-age severity (Mercer, 1983; Ward 1988; Nelson et al., 2000). Therefore, mountain glaciation did not influence high rates of sediment supply to the Canterbury basin from ~15 Ma to ~11.5 Ma (sequence group 1).

Instead, high sedimentation rates in sequence group 1 probably resulted from global climatic and eustatic changes related to the formation of east Antarctic ice-sheet (Figure 5.7F-G, Haq et al., 1987; Zachos et al., 2001). Plate boundary tectonism has become the dominant control for sediment supply since ~11.5 Ma. However, sediment supply within sequence groups 3 and 4 (~6 Ma-Recent) may have been significantly influenced by glacial processes, especially during the late Quaternary (Leckie, 2001; Browne and Naish, 2002). Iinfer that high rate of sediment supply within sequence group 4 (late Pliocene-Pleistocene) was controlled by a combination of local plate boundary tectonism and mountain glaciation, the latter a product of tectonic uplift and deteriorating global climatic conditions (Mercer, 1983; Gellatly et al., 1988; Ward 1988; Chinn, 1989; Denton and Hendy, 1994; Singer et al., 1998).

Distinguishing between tectonic uplift and climate change as causes of increased continental erosion, and deciphering the feedbacks between the two, is difficult (Molnar and England, 1990; Raymo and Ruddiman, 1992; Vitor et al., 2000). Milliman and Syvitski (1992) argue that uplift (topographic relief) exerts the greatest influence on sediment supply by an order of magnitude over other factors (e.g., climate, runoff). However, the erosional dissection of the Rocky Mountains, which provides much of the sediment to the Gulf of Mexico, has been reinterpreted to be due to climatic change, rather than the result of Pliocene epeirogeny, because the mean elevation of the Rocky Mountains has remained unchanged since the Eocene (Gregory and Chase, 1992, 1994). Likewise, an

increase in sediment supply to the Greenland margin in the mid-Oligocene may have resulted from increased erosion rates of a preexisting uplift due to Oligocene high latitude cooling (Larsen et al., 1994). Lavier et al. (2001) proposed that the increase in sediment supply to the Angola margin during ~16-13 Ma (Figure 5.7C) correlated with southern hemisphere cooling and ice accumulation in Antarctica (Barron et al., 1991; Wise et al., 1992). However, on the southwestern African margin (Walvis Ridge, north of Angola margin), sediment accumulation decreased by half at the Eocene/Oligocene transition, which involved a similar change from warmer to cooler climates (Rust and Summerfield, 1990). Furthermore, the high Tertiary sediment discharge to the Guinea passive margin, north of the Angola margin, since South Atlantic breakup (including the pulse at ~16-12 Ma) has also been interpreted to be mainly controlled by reorganization of drainage in connection with vertical movements, rather than global climatic changes (Leturmy et al., 2003). Also, sedimentation rates in North Sea (Liu and Galloway, 1997) and Gulf of Mexico (Fillon and Lawless, 2000; Galloway, 2001) do not show a middle Miocene pulse. Climate, expressed as continental and montane glaciation, has clearly been as influential as tectonism in controlling rates of sediment supply in the Pleistocene. Debate continues about the relative roles of climate versus tectonism in the middle Miocene-Pleistocene (Galloway, in press). The high sedimentation rate in sequence group 1, therefore, may yet prove to have a local origin.

5.5 CONCLUSIONS

Reconstruction of relative motion at the Australian-Pacific plate boundary reveals divergence at the Alpine Fault in the central Southern Alps prior to ~20.1 Ma (chron 6o), followed by increasing average rates of convergence, with a marked increase after ~6 Ma. A strike-slip component existed prior to >33.5 Ma (chron 13o, Figure 5.4) and could have existed, at low rates, as early as Eocene (45 Ma; Sutherland, 1999). However, rapid strike-slip motion (>30 mm/yr) began ~20.1 Ma (chron 6o) and there has been little change in the strike-slip component since then.

Nineteen regional sequence-bounding unconformities, identified in the middle Miocene to Recent shelf-slope sediment prism using high-resolution MCS profiles, are divided into four sequence groups in order to compare sedimentation rates with tectonic reconstructions. Sedimentation rate is relatively high (>22 mm/yr) in sequence group 1, then decreases to a minimum (<15 mm/yr) in group 2, followed by a continuous increase through groups 3 (21 mm/yr) and 4 (~25 mm/yr). Good agreement between sedimentation and convergence rates in sequence groups 2-4 indicates that tectonism has been the dominant control on sediment supply since ~11.5 Ma. In particular, high sedimentation rates in groups 3 and 4 may reflect increased plate convergence and uplift at the Southern Alps at ~6 Ma (e.g., Sircombe and Kamp, 1998; Walcott, 1998). The high rate of sediment supply of group 4 may also reflect the increasing importance of mountain glaciation during the Pleistocene. Early-middle Miocene (~15-11.5 Ma)

high sedimentation rates correlate with low convergence rates and may be a response to global climatic and eustatic forcing.

Chapter 6: Conclusions

6.1 SUMMARY

The goal of this research is to understand the interplay of global (eustastic) and local controls (tectonics, sediment supply rate, and current activity) responsible for continental margin depositional cyclicity and sequence architecture based on multichannel seismic (MCS) reflection images of the offshore Canterbury basin. Along-strike currents exert significant control on sequence development and, therefore, a second goal is to define the 3-D architecture of mid-water sediment drifts, and reconstruct along-strike transport and depositional processes. The target strata are middle Miocene to Recent. Ages of seismic horizons interpreted using the high-resolution, EW00-01, MCS data and lower resolution, CB82, commercial data, are constrained by three exploration wells and one ODP Site. These boreholes also provide porosity and lithologic information, used for sedimentation rate calculations. Plate boundary tectonic reconstructions were generated using UTIG PLATES software and magnetic data from the PLATES database (Lawver et al., 2001). Stage rotations were applied to define the relative motion of the Australian-Pacific plate system during six time intervals using the method of Le Pichon (1968). A summary of conclusions based on seismic interpretation and tectonic reconstruction follows.

6.1.1 Chapter 3: Three-Dimensional Architecture of Mid-Water Sediment Drifts

6.1.1.1 Sediment drift distribution and geometry

The Neogene shelf/slope prism in the Canterbury basin was formed by a combination of conventional clinoform progradation and the accretion of large, elongate sediment drifts. The drifts are inferred to have been formed by a northward flowing current analogous to the present Southland Current. Eleven drifts (D1-11) have been recognized and mapped within the early Miocene to Recent shelf sediment prism. Drift deposition was initiated in the southwestern part of the EW00-01 seismic grid and the locus of drift activity migrated northeastward. Most drifts are classified as simple drifts, with a well-defined moat, sub-parallel to paleoshelves, and a large drift mound basinward of the moat. The youngest and largest of these simple drifts occurs in the northwestern part of the EW00-01 survey area. Their internal seismic facies (base, core and crest) reflect increasing confinement and intensification of the current, initially by Coriolis deflection and later by physical confinement within the moat as the adjacent drift aggrades.

Shelf relief, and the water depths in which drifts initiated (~300 to~750 m), increased through time while the drifts progressed from simple (D1-D6) to complex (D7-D9) and back to simple (D10-D11). For all types, drift thickness differs from shelf relief. Instantaneous shelf relief and water depth are smaller

than final drift thicknesses (up to 1000 m, without decompaction for D10 and D11) because each drift develops over an extended period of time, accompanied by increasing accommodation.

6.1.1.2 Diachroneity of current eroded unconformities

The EW00-01 data provide the first evidence that unconformities created by paleoslope erosion at the landward edges of moats can be strongly diachronous. Seismic correlation around the grid confirms that some sediment beneath the unconformities is younger than the oldest sediments overlying the unconformities and that current-related unconformities intersect sequence boundaries (Figures 3.5-3.7).

6.1.1.3 Controls on drift development

Drifts developed in response to a northward flowing current. Their subsequent evolution is influenced by sediment supply, relative sea-level change, seafloor morphology and other elements.

The identification of multi-crested drift, together with the observation that more than one drift was commonly active simultaneously, show that flow pathways were more complex than previously recognized. Progradational and retrogradational stacking patterns of multi-staged drifts may result from variations in the rate of sediment supply. The presence of canyons, both independent of, and associated with drifts, indicates that downslope sediment transport accompanied

drift development, but its significance is obscured by that of along-strike current deposition and erosion. Moats can act as canyons when current strength decreases as the moat fills.

6.1.2 Chapter 4: Seismic Stratigraphic Interpretation and Controls on Sequence Stratigraphy of a Current-Swept Passive Margin

6.1.2.1 Seismic stratigraphic framework

The offshore Canterbury basin exemplifies sequence development on a prograding passive margin strongly influenced by submarine currents. Nineteen regional sequence-bounding unconformities (U1-19) are identified in the middle Miocene to Recent shelf-slope sediment prism. Three larger seismic units are defined based on seismic architecture and facies, which reflect different combinations of controls on sequence architecture. 1) U1-U4 mostly lack distinct clinoform breakpoints within the seismic coverage. 2) U5-U8 feature breakpoints; internal reflection geometries are predominantly sigmoid and paleoshelves are smooth and defined by onlap and truncation. Sequences comprise predominantly highstand deposits. 3) U9-U19 are downlapped on paleoshelves and truncate underlying reflections near paleoshelf edges; internal reflection geometries are oblique and U- and V-shaped channels incising paleoshelves indicate exposure during sea-level lowstands. Forced regressive systems tracts occur and may indicate asymmetric sea-level cycles. Ages of these sequences are constrained by

biostratigraphies from Clipper exploration well and ODP Site 1119: sequences range from third- to sixth-order.

6.1.2.2 Role of global forcing

Correlation with oxygen isotopic records suggests a eustatic origin for the sequence boundaries. The number of seismic sequences is similar to that of coeval cycles on the Miocene to Recent δ^{18}Osw record Billups and Schrag (2002) when cycles of comparable frequency are considered (third- and fourth-order). Cycle frequency is an important issue when comparing records (e.g., isotopic and stratigraphic) that are filtered by data resolution. Late Pliocene and Pleistocene seismic sequences are less numerous than the correlative isotope cycles. Here, the stratigraphic record has been excessively filtered relative to the high-frequency isotopic record, either by the limitations of seismic resolution or because shelf erosion has removed evidence of some sequence boundaries during this period dominated by high-amplitude eustasy. Available age control precludes cycle-by-cycle correlation. However, the match between numbers of sequences and oxygen isotope cycles, in the Miocene and Pliocene (Figure 4.11) and also in the latest Pleistocene (Figure 4.12), together with trends in sequence stacking patterns, favors a strong component of eustatic control on the formation of U1-U19. However, age control must be improved by additional IODP drilling to enhance individual cycle correlations.

6.1.2.3 Influence of current activity on sequence stratigraphy

Global processes appear to have played a significant role in sequence-boundary formation, but local processes have exerted fundamental control on sequence architecture. Along-strike currents and associated sediment drifts strongly influence sequence development. Current erosion in drift moats forms diachrononous unconformities, while deposition of adjacent mounded drifts controls sequence thickness distributions. In addition, currents focus deposition on the slope, reducing the rate of basinward movement of the shelf edge, but increasing that of the slope toe. As a result, slope inclination is minimized. Cessation of drift development and replacement of along-strike by downslope processes results in increased rates of shelf-edge progradation and slope steepening as the accommodation space over the expanded slope is filled. Slope platforms can form above extinct drifts, reducing accommodation and locally accelerating shelf-edge progradation. Along strike from some large, elongate drifts, seismic evidence for current activity is lacking and coeval strata are clinoformal, in spite of the demonstrable presence of a current. Therefore, along-strike transport could play a role in forming clinoform morphologies worldwide, even where geometries diagnostic of current reworking are lacking.

6.1.2.4 Controls on drift development and evolution

The largest Canterbury basin drifts span multiple sequences, so that they do not respond to individual eustatic cycles (Figure 4.6). However, they may

develop preferentially during longer-term periods of lowered sea level. For example, most of the drifts (D1-D9) were active during middle-late Miocene, southwest Pacific cooling episodes of Kennett and von der Borch (1986; Figure 4.6; Table 4.1). The two remaining drifts (D10-D11) continued to be active during warming periods (9-6.5 Ma), perhaps because of the high rate of sediment supply associated with uplift at the Alpine Fault beginning at ~8-5 Ma (Tippett and Kamp, 1993b; Batt et al., 2000) and also their large size. Shelf edge relief had increased from several hundred meters to ~1000 m by this time (Lu et al., 2003), allowing the drifts to reach a comparable thickness. In filling the available accommodation, they were active for longer periods than earlier drifts (Figure 4.6). Their size may have contributed to their independence of sea-level change and resulting stability. Changes of sea level are small relative to drift height and less likely to influence the position of the moat of such large drifts. However, simple drifts D1-D4 formed when shelf relief was low. A relatively small change in sediment supply or relative sea level may result in abandonment and filling of the main moat and termination of the drift. The period of complex drift deposition occurred when shelf relief was intermediate. Intermediate shelf relief may favor formation of complex drifts by being sufficient for the drifts to sustain changes in sea level and sediment supply without the drift being terminated, but low enough so that such changes were able to cause moat bifurcation (D8) or moat migration (D9) without terminating the drift (Figures 4.1 and 4.8).

Termination of elongate drift development by U13 (~ 2.4 Ma) may have been caused by significant changes in the frequency and amplitude of sea level change represented by $\delta^{18}O$ records for the last 1.8 Ma (Shackleton and Opdyke, 1976; Prell, 1982). High-amplitude sea-level changes, which favor shelf-edge exposure and formation of slope canyons, resulting in the dominance of downslope processes on the slope, may be the most important element that terminates the drift development. Therefore, stable geostrophic circulation, enhanced during glacial periods, is an essential requirement for elongate drift formation. However, sediment supply, sea-level amplitudes and seafloor morphology, e.g., slope gradient and eastward deflection of the current by Chatham Rise (Figure 2.1), are contributing factors and interact to create drifts of a range of scales and architectural complexity.

6.1.2.5 Reconstruction of shelf-slope stratigraphic systems

Middle Miocene to early Pliocene sequences S4-S8 have sigmoid internal reflection geometries and are inferred to comprise mainly transgressive and highstand systems tracts (Figure 4-14 A). Shelf edges are not exposed during sea-level lowstands. Sediment drifts are active, with the locus of drift deposition moving northward. As a result, downslope processes dominate in the south, where shelf edges prograde rapidly, filling the limited accommodation space above extinct drifts D1-D6 and increasing slope gradient. Meanwhile, along-strike

processes dominate in the north and slope gradient is low because of the concentration of deposition in drifts on the slope.

Formation of late Pliocene to Recent sequences S9-S19 (Figure 4.14 B) involves higher-amplitudes, possibly asymmetrical, sea-level cycles, which lead to subaerial shelf exposure during lowstands and outer shelves are incised by channels, with canyons on upper slopes. Sequence boundaries are downlapped on the shelf and internal reflections are oblique; forced regressive systems tracts are interpreted to develop. Downslope processes dominate after cessation of elongate drift formation at U13, but unconfined currents continue to produce sediment waves interbedded with gravity deposits. Shelf-edge progradation is particularly rapid in the north over the post-drift slope platform above D10 and D11.

6.1.3 Chapter 5: Tectonic Controls on Sediment Supply and Sequence Stratigraphy

6.1.3.1 Reconstruction of relative motion at the Australian-Pacific plate boundary

The well-constrained seismic stratigraphy of the offshore Canterbury basin provides the opportunity to investigate long-term changes in sediment supply related to the formation of a transpressive plate boundary (Alpine Fault). The relative motion of the Australian and Pacific plates is reconstructed at eleven points spaced at 50 km intervals along the Alpine Fault for six Oligocene-Recent

time intervals (~33.5-26.5, 26.5-20.1, 20.1-11.5, 11.5-6, 6-2.6, 2.6-0 Ma). The reconstructions reveal divergence in the central Southern Alps prior to ~20.1 Ma (chron 6o), followed by increasing average rates of convergence, with a marked increase after ~6 Ma (late Miocene). A strike-slip component existed prior to 33.5 Ma (chron 13o) and perhaps as early as Eocene (45 Ma). However, rapid strike-slip motion (>30 mm/yr) began at ~20.1 Ma (chron 6o). Since ~20.1 Ma there has been no significant change in the strike-slip component of relative plate motion.

6.1.3.2 Calculations of sequence grain volumes and sedimentation rates

High-resolution MCS profiles (EW00-01 survey, Figure 5.1A), tied to exploration wells and ODP Site 1119 (Figure 5.1A-B), provide a high-frequency sequence stratigraphic framework for the offshore Canterbury basin (Figures 4.3, 4.4, and 5.5). Uncorrected sequence volumes (Figure 5.6A-B, red bars) are calculated using stacking velocities (Figure 2.7) and isochron maps (Chapter 4; Lu and Fulthorpe, in press). Sequence grain volumes and sedimentation rates (Figure 5.6A-B, yellow bars) are then calculated using borehole porosity data (Figure 5.5D and F) and sequence ages (Figure 5.5E; Lu and Fulthorpe, in press) following method of Liu and Galloway (1997).

Sedimentation rates are calculated from individual sequence volumes that are then summed to represent sequence groups covering the same time periods as the tectonic reconstructions (Figure 5.6). Rates are relatively high (>22 mm/yr) from 15-~11.5 Ma (sequence group 1). Rates decrease to a minimum (<15 mm/yr)

during the ~11.5-6 Ma interval (sequence group 2), followed by an increased rates during the periods ~6-2.6 Ma (21 mm/yr; sequence group 3) and 2.6 Ma-Recent (~25 mm/yr; sequence group 4).

6.1.3.3 Global and local controls on sediment supply

Good agreement between sedimentation and tectonic convergence rates in sequence groups 2-4 (Figure 5.6C-E) indicates that tectonism has been the dominant control on sediment supply to the Canterbury basin since ~11.5 Ma. In particular, high-sediment supply with rates of 21 mm/yr and ~25 mm/yr in groups 3 and 4, respectively, may reflect increased plate convergence and uplift at the Southern Alps at ~6 Ma. Early-middle Miocene (~15-11.5 Ma) high sedimentation rate (22 mm/yr) correlate with low convergence rates (~2 mm.yr) and are mainly a response to global climatic forcing and eustasy. However, distinguishing between tectonic uplift and climate change as causes of increased continental erosion, and deciphering the feedbacks between the two, is difficult (Molnar and England, 1990; Raymo and Ruddiman, 1992). The high sedimentation rate in sequence group 1, therefore, may yet prove to have a local origin.

6.2. IMPLICATIONS FOR FUTURE WORK

6.2.1 Age Control and Eustatic Amplitudes: Future IODP Drilling

Age control is fundamental to the construction of the sequence stratigraphic framework and estimation of the role of global verses local controls on sequence formation (see Chapter 4). Also, age control is vital for calculations of sedimentation rates and for correlating them with plate-boundary tectonism (see Chapter 5). Current age control is imperfect, especially that derived from the exploration wells. This is not simply a result of limited biostratigraphic resolution, but of the location of the wells relative to the seismic geometries to be calibrated. An Integrated Ocean Drilling Program (IODP) proposal to drill the Canterbury basin sequences and drifts has been submitted (Proposal 600-full). Five drill sites are proposed within the EW00-01 grid (Figure 6.1). Drilling will contrast upper Miocene-lower Pliocene sequences, with smooth, onlapped paleoshelves and rounded breakpoints (below U9), and upper Pliocene-Pleistocene sequences with eroded and incised, downlapped paleoshelves and more pronounced breakpoints (above U9; Figure 6.1). This will test the hypothesis that paleoshelves below U9 were not subaerially exposed at sequence boundaries, whereas those above U9 were exposed (see chapter 4). In addition to gathering information for estimating eustatic amplitudes, the objective is to understand differences in shelf/slope sediment transport processes operating 1) when shelves are flooded even at lowstand, and 2) when shelves are exposed at lowstand. Progradation occurs

Figure 6.1 (A) Proposed drill sites CB-01A to -05A, together with EW00-01 MCS grid (red straight lines), low-resolution CB82 commercial MCS grid (black straight lines), exploration wells Clipper and Resolution, and ODP Site 1119. Location of Figure 6.1 B is shown by red bold line and the three transects for proposed reconstruction using 2D backstripping are represented by thick red dotted lines. Bathymetric contours are in meters. (B) Uninterpreted MCS dip profile EW00-01 -66 from the southern part of the survey grid showing locations of proposed drill sites CB-01A, -02A, and -03A. (C) Interpretation showing sequence boundaries and selected locations of onlap, truncation and downlap (arrows). Clinoform breaks, are marked by circles. CB-01A and -02A sample sequence boundaries from U4 -U19 landward of their breakpoints. CB-02A also samples the paleoslope of U6 and CB-03A samples paleoslopes of U4-U7.Two other drill sites are also proposed. CB-04A is located on the slope and CB-05A penetrates drift D11 (Figure 4.4).

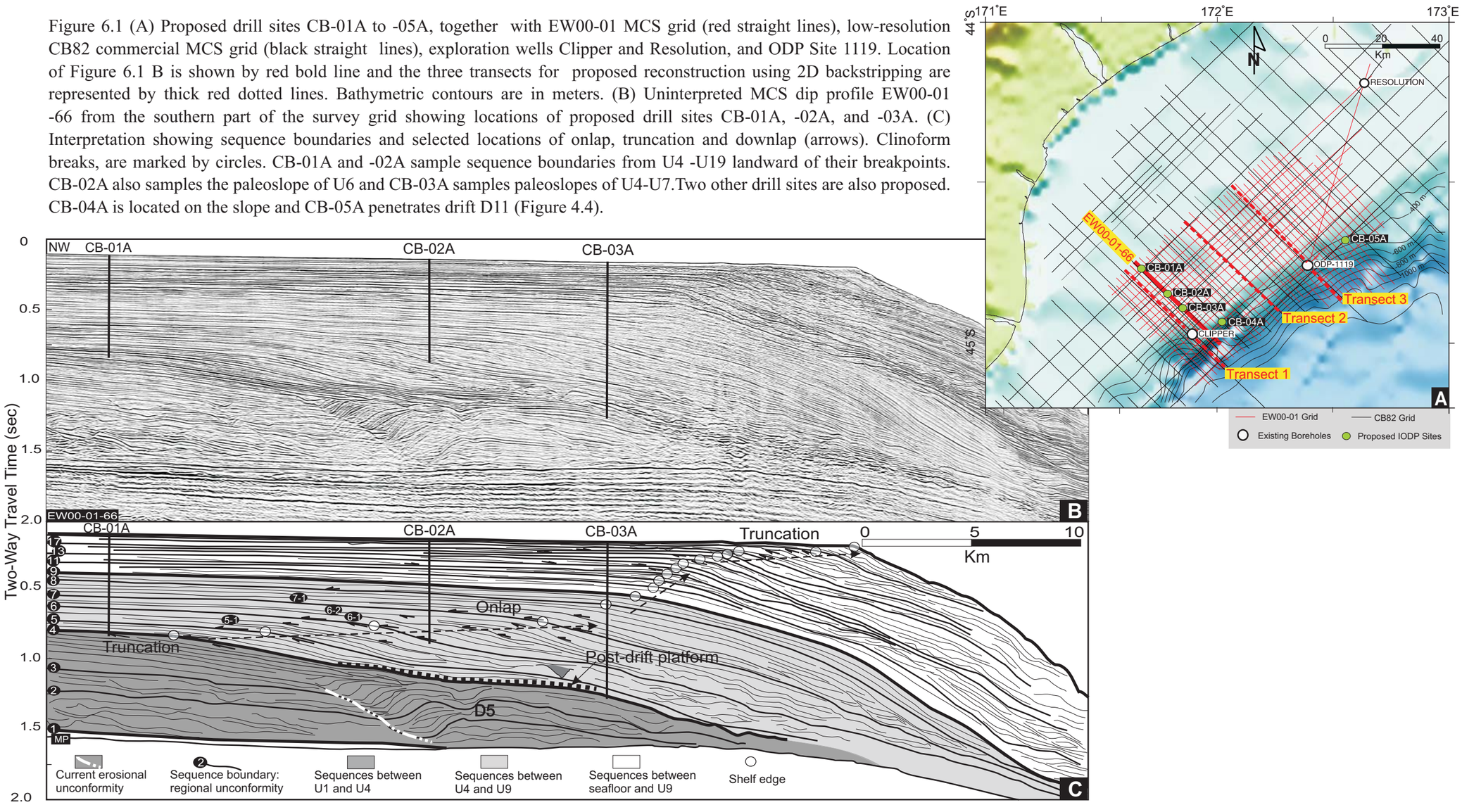

under both conditions, but the processes involved must differ.

The limitations of the available age control influence sedimentation rate estimates for individual sequences, since such rates are strongly influenced by sequence duration (see chapter 5). Therefore, sedimentation rates averaged over groups of sequences are presented instead. IODP drilling will verify ages of the progradational units, for integration with sediment volume results to provide an enhanced, sequence-by-sequence record of sedimentation rates for correlation with tectonic and climatic events.

6.2.2 Roles of Downslope and Along-Slope Processes

Along-strike current deposition and erosion is dominant in the Canterbury basin but the effects of downslope processes are also apparent, especially after U13 which marks the termination of elongate drift development. Two results indicate that downslope processes are associated with reduced drift development: 1) canyons incise the tops of some drifts (Figures 3.5B, 3.7A, C, and 3.8C); 2) The late stages of moat fill can comprise symmetrical or horizontal reflections in contrast to the more typical landward migrating or chaotic fill (Figure 3.5), suggesting that some moats acted as conduits for downslope sediment transport, particularly when individual drifts approach maturity and the current within the moat is waning. However, the relationship between downslope (canyon) and along slope (drift) processes is not necessarily entirely negative. For example, episodes of cooling at 12.5-11.5 Ma and 11-9 Ma produce both eustatic

lowstands, often associated with canyon incision, as well as enhanced current velocities, which favor drift development. One factor favoring a complex relationship between downslope and along-slope processes is that the drifts span multiple sequences, so that they do not respond to individual eustatic cycles (Figure 4.6).

There are two potential sources of sediment for the drifts: 1) sediment carried by the current along strike, and 2) sediment supplied downslope through the shelf channels and slope canyons that are imaged seismically, particularly at the younger sequence boundaries. However, it is not possible to quantify relative volumes from each source with existing data. Petrophysical analysis following future IODP drilling may yield insights into this issue by enabling sediments to be traced to source terranes.

6.2.3 Origins of Continental-Margin Sequence Architecture: Integrated 2D Backstripping Reconstruction and Forward Stratigraphic Modeling

Seismic interpretation alone cannot uniquely constrain depositional processes, in part because seismic stratal patterns are influenced by post-depositional processes, e.g., subsidence, compaction and structural deformation, and therefore differ from the morphologies at the time of deposition. In addition, seismic sequence geometries and facies are not reliable indicators of paleobathymetry and depositional facies. For example, the extent to which Neogene sea-level falls cause subaerial exposure of paleoshelves remains

uncertain (Fulthorpe and Austin, 1998; Driscoll and Karner, 1999; Fulthorpe, et al., 1999; Steckler et al., 1999; Cathro and Austin, 2001).

Alternative methods of testing hypotheses based on seismic interpretations include: (1) reconstruction of paleobathymetry and paleomorphology of the margin through time using 2D backstripping; (2) use of 2D forward stratigraphic modeling, modified to account for along-strike sediment transport, to isolate and quantify the signals recorded by the stratigraphy and determine the relative influences of global and local controls on the geological record of the margin. A proposal to conduct such work is in review.

6.2.3.1 Reconstruction of paleobathymetry and paleomorphology

Defining paleowater depths at sequence boundaries is vital in order to estimate eustatic amplitudes (e.g., Greenlee and Moore, 1988; Kominz et al., 1998; Kominz and Pekar, 2001). In the Canterbury Basin, upper Miocene-lower Pliocene sequences, with smooth, onlapped paleoshelves and rounded breakpoints (below U9) contrast with upper Pliocene-Pleistocene sequences with eroded and incised, downlapped (above U9; Figure 6.1B-C). I hypothesize that paleoshelves below U9 were not subaerially exposed at sequence boundaries during lowstands, whereas those above U9 were exposed (Lu and Fulthorpe, in press). This hypothesis must be tested quantitatively.

Improved paleobathymetric estimates will also enhance our understanding of drift development and termination. Drift activity in the southern part of the

EW00-01 grid decreases after U4 (~12.5 Ma; Figures 4.3 and 4.6) and the locus of drift activity migrates northeastward through time, finally ceasing by U13 (~2.5 Figure 4.4). I propose that drift development is inhibited by downslope processes that are enhanced when sea level falls to the shelf edge (Lu and Fulthorpe, in press). However, there is no evidence, within the EW00-01 grid, of subaerial exposure at U4 and overlying sequence boundaries up to and including U8, though paleoshelf exposure during high-amplitude Plio-Pleistocene sea-level cycles may be responsible for overall cessation of drift development at U13 (Figure 4.6).

Improved paleobathymetry will improve estimates of water depths in which drifts formed, grew and terminated and depth ranges of the paleocurrents responsible. Our existing estimate of the paleowater depth in which drifts began to form (300-750 mbsf) is based on shelf edge relief shown on isopach maps. However, these do not take into account post-depositional alteration of sequence architecture. Therefore, reconstruction by removal of distortion resulting from compaction and subsidence due to sediment loading and restoration of true slope inclinations and relief, will allow us to accurately assess geomorphological and paleobathymetric controls on: 1) current flow pathways, which can be complex when multiple drifts are active simultaneously, or during development of "complex" drifts (D8-D9; Figure 4.1), 2) transitions between along-strike and downslope processes and causes of the termination of the southern drifts at U4

(12.5 Ma; Figures 4.3 and 4.6) and final termination of all elongate drift deposition at U13 (Figure 4.6).

The paleotopography of the Miocene-Recent sequences can be reconstructed using 2D backstripping (Steckler et al., 1999; Lavier et al., 2001). 2D backstripping sequentially removes sediment layer by layer, accounts for the physical and geologic processes that caused deformation of the section and mathematically undoes their effects (Figure 6.2). This approach will reveal the bathymetric evolution of paleoshelf edges, as well as paleoshelf-edge relief and paleoslope gradients at the time of deposition. This technique has already been used to reconstruct paleobathymetries of two passive margins with different tectonic histories: New Jersey and West Africa (Steckler et al., 1999; Lavier et al., 2000; 2001). Resulting paleobathymetric estimates are consistent with depth estimates from paleontology and biofacies studies, indicating the reliability of this method. In preparation for 2D backstripping, seismic sections in traveltime will be converted to depth sections using seismic stacking velocities. At least three, depth-converted transects are proposed (Figure 6.3).

6.2.3.2 Forward stratigraphic modeling

Sea level, sediment supply, subsidence rates, and the balance of downslope and along-strike processes have all changed during the middle Miocene to Recent. 2D forward stratigraphic modeling (Frohlich and Matthews,

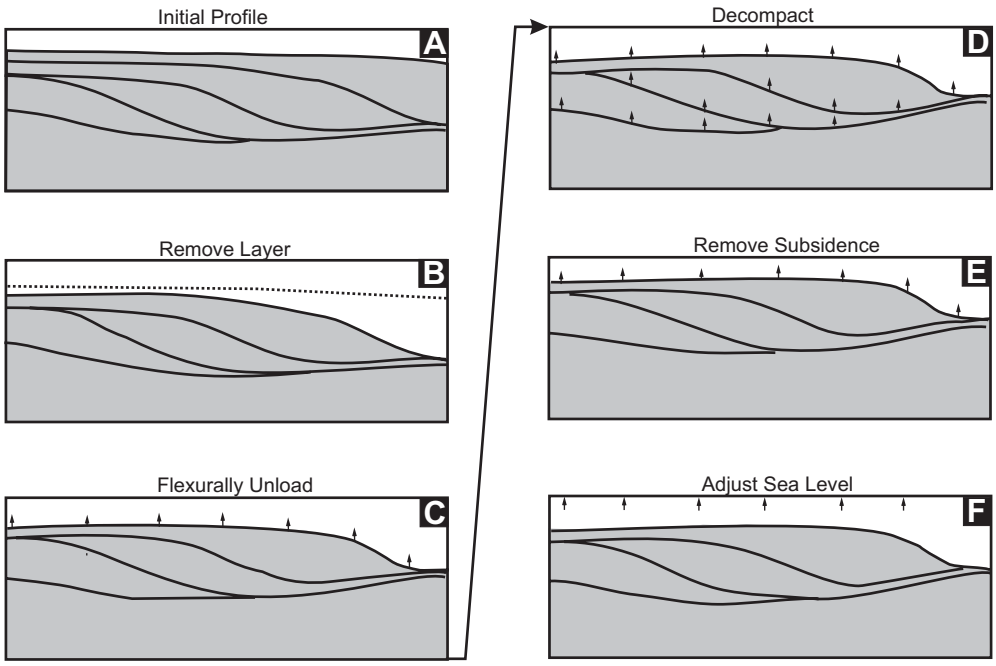

Figure 6.2. The process of reconstructing continental margin development by 2D backstripping involves several steps to account for the physical and geologic processes that cause deformation and mathematically undo them. First remove all sediment above the surface of interest (B), then calculate the weight of sediment removed and flexurally unload the remaining layers (C). The next step is to correct the sediment layers below the horizon of interest for the compaction caused by the sediment removed (D). Decompaction calculations will use porosity laws obtained from analysis of well logs (Bond and Kominz, 1984). An alternative approach is to apply lithology-dependent, exponentially decreasing porosity curves (Sclater and Christie, 1980). Underlying layers are decompacted to porosities appropriate to their new burial conditions and their depths adjusted. The thermal subsidence occurring during the period represented by the missing layer is then removed (E). Finally, the profile is adjusted for sea-level change (F). This involves both changing the reference level for the profile, and accounting for water loading /unloading. The water loading is removed using the same flexural routines as for removal of the sediment load. (After Steckler et al., 1999).

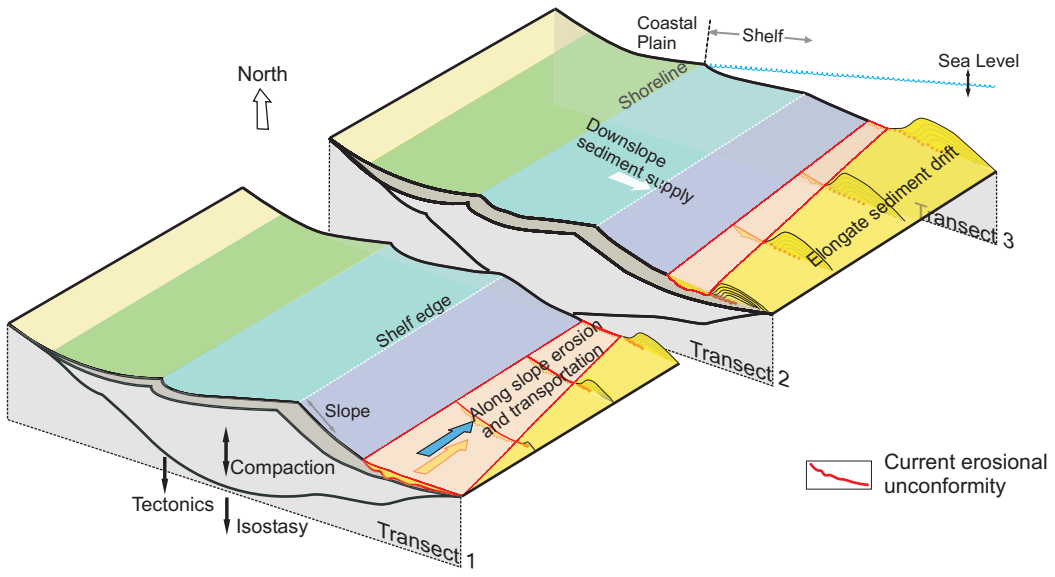

Figure 6.3. Strategy for accounting for along-strike sediment erosion, transport and deposition during forward modeling. SEQUENCE4 assumes that the direction of sediment supply is from landward to basinward. However, in the southern part of the Canterbury Basin, along-strike current erosion can be an important process (Transect 1). Eroded sediment is transported northeastward along the slope to be deposited in sediment drifts (Transects 2 and 3). Slope gradient decreases northeast ward because deposition is concentrated in drifts on the slope. We will simulate the process of drift development by locally removing (Transect 1) or adding (Transects 2 and 3) sediment to the slope during SEQUENCE4 model runs to account for current erosion and drift deposition. Erosion by currents will also affect the results of 2D backstripping. For example, there may have been more sediment present in the past on Transect 1 than seismic profiles currently indicate. We will use results of SEQUENCE4 modeling as inputs to 2D backstripping. The amount of current-related erosion and deposition cannot be known with certainty because the drift in Transects 2 and 3 is made up of material transported directly downslope and by sediment transported into the basin from far to the south, as well as from sediment eroded from the southern part of the basin (e.g., Transect 1). We will therefore test different assumptions about the amount of slope erosion and redeposition to test the sensitivity of backstripping and forward modeling results to along-strike processes. (See Figure 6.1 for roughly locations of transects).

1991; Reynolds et al., 1991; Steckler et al., 1999) will allow us to test the relative importance of these parameters and quantify their effects.

A forward model is based on a specified set of input parameters and assumptions that attempt to describe the physical laws controlling geological processes (Frohlich and Matthews, 1991; Lawrence et al., 1990; Matthews and Frohlich, 1998; Weltje, et al., 1998; Prather, 2000). Parameters derived from 2D backstripping (paleobathmetry of shelf and slope, shelf and slope gradients, flexural rigidity, initial basin geometry), together with results from seismic interpretation, such as sedimentation rates derived from sequence volumes, would be used as inputs to the forward model SEQUENCE4 (Steckler et al., 1999, Figure 6.4). SEQUENCE4 has been used for long-term modeling of the New Jersey margin and has successfully captured the major features of the imaged sequences (Reynolds et al., 1991; Steckler et al., 1993, 1999).

The drifts must be modeled both to understand how they were deposited and to assess how much uncertainty they add to backstripping calculations. SEQUENCE4 assumes that the direction of sediment supply is from landward to basinward. The process of drift development can be simulated by locally removing or adding sediment to the slope during SEQUENCE4 model runs to account for current erosion and deposition (Figure 6.3). This source term can be estimated using the seismic interpretations. 2D backstripping would then be repeated, making use of the outcome of the forward model.

6.3 CONCLUDING REMARKS

The stratal geometries defining sequences result from the interplay of processes, acting in three dimensions, including global sea-level (eustatic) change, climatic and paleoceanographic variations, tectonics, rate of sediment supply, and submarine currents. These local and global processes act in combination and at overlapping time-scales, so determining their relative importance to the generation and preservation of stratigraphy is difficult. The research described here provides new insights into these relationships and proposed future work in the Canterbury basin will further advance and refine our understanding of the origins of the sequence stratigraphic record. The effort is worthwhile because such understanding is fundamental to deciphering the long history of geological, climatic, and oceanographic processes imprinted on continental margin stratigraphic records. The research described here provides new insights into, together with planned future work.

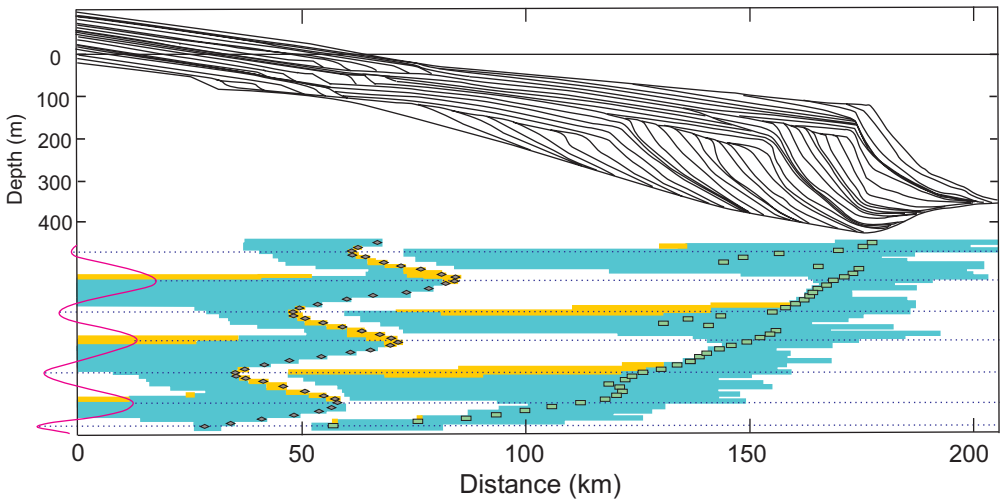

Figure 6.4. SEQUENCE4 simulation of continental-margin stratigraphy showing an example of progradation of several sequences across a pre-existing ramp. The model is driven by a long-term falling sea-level on which is superimposed a 30-m-amplitude sinusoidal variation (the sea-level curve is shown at the lower left in red). Timelines are drawn every 100,000 years. The shoreline positions are located between 30-80 km. The lower part of the figure shows a time stratigraphic diagram showing preserved sediments (blue), sediments that were deposited and subsequently eroded (yellow), and non-depositional hiatuses (white). Diamonds and rectangles indicate positions of shoreline and clinoform breakpoint, respectively. (After Steckler et al., 1999.)

References

Abbott, S. T., 1997, Foraminiferal paleobathymetry and mid-cycle architecture of mid-Pleistocene depositional sequences, Wanganui Basin, New Zealand: Palaios, v. 12, p. 267-281.

Abbott, S.T. and Carter, R.M., 1994, The sequence architecture of mid-Pleistocene (c. 1.1-0.4 Ma) cyclothems from New Zealand: Facies development during a period of orbital control on sea-level cyclicity: Special Publication of the International Association of Sedimentologists, v. 19, p. 367-394.

Adams, C.J.D., 1979, Age and origin of the South Alps, i*n* Walcott, R.I. and Cresswell, M.M., eds., The Origin of the Southern Alps: Royal Society of New Zealand Bulletin, v. 18, p. 73-78.

Adams, C.J.D., 1980, Contemporary uplift and erosion of the Southern Alps, New Zealand: GSA Bulletin, v. 91, p. 1-114.

Adams, C.J.D., and Cooper, A.F., 1996, K-Ar age of a lamprophyre dike swarm near lake Wanaka, west Otago, South Island, New Zealand: New Zealand Journal of Geology and Geophysics, v. 39, p. 17-23.

Adrian, A.B., 1997, Sea caves, relict shore and rock platforms; evidence for the tectonic stability of the Banks Peninsula, New Zealand: New Zealand Journal of Geology and Geophysics, v. 40, p. 299-305.

Anderson, H., and Webb, T., 1994, New Zealand seismicity, patterns revealed by the upgraded National Seismograph Network: New Zealand Journal of Geology and Geophysics, v. 37, p. 477-493.

Anderson, J.B., Abdulah, K., Sarzalego, S., Sirigan, F., Thomas, M.A., 1996, Later Quaternary sedimentation and high-resolution sequence stratigraphy of the east Texas shelf, *in* De Batist, M. and Jacobs, P., eds., Geology of Siliciclastic Shelf Seas: Geology Society Special Publication, v. 117, p. 95-124.

Armishaw, J.E., Holmes, R.W., and Stow, D.A.V., 2000, The Barra Fan: A bottom-current reworked, glacially-fed submarine fan system: Marine and Petroleum Geology, v. 17, p. 219-238.

Atkins, C.B., 2001, Glacial influence from clast features in Oligocene and Miocene strata cored in CRP-2/2A and CRP-3, Victoria Land Basin, Antarctica: Terra Antartica, v. 8, p. 263-274.

Aubry, M.P., 1991, Sequence stratigraphy: eustasy or tectonic imprint: Journal of Geophysics Research, v. 96, p.6641-6679.

Austin, J.A., Jr., Christie-Blick, N., Malone, M.J., et al., 1998, *Proc. ODP, Init. Repts.*, 174A: College Station, TX (Ocean Drilling Program), p. 20-27.

Baldwin, B., and Butler, C.O., 1985, Compaction curves: American Association of Petroleum Geologists Bulletin, v. 69, p. 622-626.

Barley, M.E., 1987, Origin and evolution of mid-Cretaceous, garnet-bearing, intermediate and silicic volcanics from Canterbury, New Zealand, *in* Weaver, S. D. and Johnson, R. W., J., eds., Volcanology and Geothermal Research, v. 32, p. 247-267.

Barnes, P.M., 1992, Mid-bathyal current scours and sediment drifts adjacent to the Hikurangi deep-sea turbidite channel, eastern New Zealand: evidence from echo character mapping: Marine Geology, v. 106, p. 169–187.

Barnes, P.M., 1995, High-frequency sequences deposited during Quaternary sea-level cycles on a deforming continental shelf, north Canterbury, New Zealand: Sedimentary Geology, v. 97, p. 131-156.

Barron, J., Larsen, B., and Baldauf, J.G., 1991, Evidence for late Eocene to early Oligocene Antarctic glaciation and observations on late Neogene glacial history of Antarctic: Results from Leg 119, Pro. Ocean Drill. Program Sci. Results. v. 119, p. 869-891.

Bartek, L.R., Vail, P.R., Anderson, J.B., Emmet, P.A., and Wu, S., 1991, Effect of Cenozoic ices sheet fluctuations in Antarctica on the stratigraphic signature of the Neogene: Journal of Geophysical Research, v. 96 (B4), p. 6753-6778.

Bartek, L.R., Henrys, S.A., Anderson, J.B., and Barrett, P.J., 1996, Seismic stratigraphy of McMurdo Sound, Antarctica: implications for glacially influenced early Cenozoic eustatic change?: Marine Geology, v. 130, p. 79-98.

Bartek, L.R., Anderson, J.B., and Oneacre, T.A., 1997, Substrate control on distribution of subglacial and glaciomarine seismic facies based on stochastic models of glacial seismic facies deposition on the Ross Sea continental margin, Antarctica: Marine Geology, v. 143, p. 223-262.

Batt, G. E., Braun, J., Kohn, B.P., and McDougall, I., 2000, Thermochronological analysis of the dynamics of the Southern Alps, New Zealand: Geological Society of American Bulletin, v. 112, p. 250-266.

Batt, G.E, Suzanne, L.B., Cottam, M., in review, Cenozoic plate boundary evolution in the South Island of New Zealand: New Zealand Thermochronological constrains: Tectonics.

Beavan, J., Moore, M., and Pearson, C., 1999, Crustal deformation during 1994-1998 due to oblique continental collision in the central Southern Alps, New Zealand, and implications for seismic potential of the Alpine fault, Journal of Geophysical Research, v. 104, p. 25233-25255.

Beavan, J., and Haines, J., 2001, Contemporary horizontal velocity and strain rate fields of the Pacific-Australian plate boundary zone through New Zealand: Journal of Geophysical Research, v. 106, p. 741-770.

Berger, W.H., and Labeyrie, L.D., eds., 1986, The Book of Abstracts and Reports from the Conference on Abrupt Climatic Change: Scripps Institute of Oceanography, Reference 85-8, La Jolla, California, p. 274.

Berggren, W.A., Kent, D.V., Swisher, C.C. III, and Aubry, M.P., 1995, A revised Cenozoic geochronology and chronostratigraphy, *in* Berggern, W.A., Kent, D.V., and Hardenbol, L., eds., Geochronology, Time Scales, and Global Stratigraphic Correlations: a Unified Temporal Framework for a Historical Geology: Tulsa, Society of Economic Paleontologists and Mineralogists Special Publication, No. 54, p. 138-144.

Berryman, K.R., Beanland, S., Cooper, A.F., Cutten, H.N., Norris, R.J., and Wood, P.R., 1992, The Alpine fault, New Zealand: variation in Quaternary structural style and geomorphic expression, *in* Buckman, R.C., and Hancock, P.L., eds., Major Active Faults of the World; Results of IGCP Project 206: Editrice I1 Sedicesimo, Frorence, Italy, p. 126-163.

Billups, K., and Schrag, D.P., 2002, Paleotemperatures and ice volume of the past 27 Myr revisited with paired Mg/Ca and $^{18}O/^{16}O$ measurements on benthic foraminifera: Nature, v. 17(1), p. 10.1029.

Bond, G.C., 1978, Speculations on real sea-level changes and vertical motions of continents at selected times in the Cretaceous and Tertiary Periods: Geology, v. 6, p. 247-250.

Bond, G.C., and Kominz, M.A., 1984, Construction of tectonic subsidence curve for the early Paleozoic miogeocline, southern Canadian Rocky Mountains:

implications for subsidence mechanisms, age of breakup, and crustal thinning: Geological Society of America Bulletin, v. 95, p. 155-173.

Bourne, S.J., England, P.C., and Parsons, B., 1998, The motion of crustal blocks and driven by flow of the lower lithosphere and implications for slip rates of continental strike-slip faults: Nature, v. 391, p. 655-659.

Broecker, W.S., and van Donk, J., 1970, Insolation changes, ice volumes, and the $\delta^{18}O$ record in deep sea cores: Review of Geophysics and Space physics, v. 8, p. 169-198.

Browne, G.H., and Field, B.D., 1988, A review of Cretaceous-Cenozoic sedimentation and tectonic, east coast, South Island New Zealand, *in* James, D.P. and Leckie, D.A., eds., Sequences, Stratigraphy, Sedimentology: Surface and Subsurface: Canadian Society of Petroleum Geologists Memoir 15, p. 37-48.

Browne, G.H., and Naish, T.R., 2003, Facies development and sequence architecture of a late Quaternary fluvial marine transition, Canterbury Plains and shelf, New Zealand: implications for forced regressive deposits: Sedimentary Geology, v. 158, p. 57-86.

Bryden, H., and Heath, R.A., 1985, Energetic eddies at the northern edge of the Antarctic Circumpolar Current in the southwest Pacific: Progress in Oceanography, v. 14, p. 65–87.

Burger, R.L., Fulthorpe, C.S., and Austin, J.A., Jr., 2001, Late Pleistocne channel incisions in the southern Eel River Basin, north California: implications for tectonic vs. eustatic influences on shelf sedimentation patterns: Marine Geology, v. 177, p. 317-330.

Burger, R.L., Fulthorpe, C.S., Austin, J.A., Jr., and Gulick, S.P.S., 2002, Lower Pleistocene to present structural deformation and sequence stratigraphy of the continental shelf, offshore Eel River Basin, Northern California. Marine Geology: v. 185 (3-4), p. 249-281.

Burger, R., Fulthorpe, C.S., and Austin, J.A., Jr., 2003, Effects of triple junction migration and glacioeustatic cyclicity on evolution of upper slope morphologies, offshore Eel River basin, Northern California: Marine Geology, v. 199, p. 307-336.

Burling, R., 1961, Hydrology of circumpolar water south of New Zealand: Bulletin of the New Zealand Department of Scientific and Industrial Research, v. 143, p. 66-72.

Cande, S.C., and Kent, D.V., 1995, Revised calibration of the geomagnetic polarity timescale for the Late Cretaceous and Cenozoic: J. Geophys. Res., v. 100, p. 6093-6095.

Cande, S.C., Raymond, C.A., Stock, J., and Haxby, W.F., 1995, Geophysics of the Pitman Fracture Zone and Pacific-Antarctic plate motions during the Cenozoic: Science, v. 270, p. 947-953.

Cande, S.C, and Stock, J.M., in press, Pacific-Antarctic-Australia Motion and the Formation of the Macquarie Plate: Geophysical Journal International.

Carter, L., and Herzer, R.H., 1979, The hydraulic regime and its potential to transport sediment on the Canterbury continental shelf: New Zealand Oceanographic Institute Memoir, No. 83, p. 2-30.

Carter, L., Carter R.M., Nelson C.S., Fulthorpe C.S., and Neil, H.L., 1990, Evolution of Pliocene to Recent abyssal sediment waves on Bounty Channel levees: New Zealand: Marine Geology, v. 95, p. 97-109.

Carter, L., and McCave, I.N., 1994, Development of sediment drifts approaching and active plate margin under the SW Pacific deep western boundary current: Paleoceanography, v. 9, p. 1061-1085.

Carter, L., and Wilkin, J., 1999, Abyssal circulation around New Zealand - a comparison between observations and a global circulation model: Marine Geology, v. 159, p. 221–239.

Carter, R.M., 1985, The Mid-Oligocene Mashall Paraconformity, New Zealand: coincidence with global eustatic se-level fall or rise?: Geology, v. 39, p. 359-371.

Carter, R.M., 1988a, Post-breakup stratigraphy of the Kaikoura Synthem (Cretaceous-Cenozoic), continental margin, southeastern New Zealand: New Zealand Journal of Geology and Geophysics, v. 31, p. 405-429.

Carter, R.M., 1988b, Plate boundary tectonic, global sea-level changes and the development of the eastern South Island continental margin, New Zealand, Southwest Pacific: Marine and Petroleum Geology, v. 5, p. 90-107.

Carter, R.M., and Norris, R.J., 1976, Cainozoic history of southern New Zealand: an accord between geological observations and plate-tectonic predictions: Earth and Planetary Science Letters, v. 31, p. 85-94.

Carter, R.M., and Carter, L., 1982, The Motunau Fault and other structures at the southern edge of the Australian-Pacific plate boundary, offshore Marlborough: New Zealand Tectonophysics, v. 8, p. 133-159.

Carter, R.M., and Carter, L., 1987, The Bounty channel system: A 55-million-year-old sediment conduit to the deep sea, Southwest Pacific Ocean: Geo. Mar. Lett., v. 7, p. 183-190.

Carter, R.M., Abbott, S.T., Fulthorpe, C.S., Haywick, D.W., and Henderson, R.A., 1991, Application of global sea-level and sequence-stratigraphic models in southern hemisphere Neogene strata from New Zealand: Special Publication of the International Association of Sedimentologists, v. 2, p. 41-65.

Carter, R.M., Carter, L., and MacCave, I.N., and Gamble, J., 1996, Regional sediment recycling in the abyssal Southwest Pacific Ocean: Geology, v. 24, p. 735-738.

Carter, R.M., Fulthorpe, C.S., and Naish, T.R., 1998, Sequence concepts at seismic and outcrop scale: the distinction physical and conceptual stratigraphic surfaces: Sedimentary Geology, v. 122, p. 165-179.

Carter, R.M., Gammon, P.R., and Millwood, L., 2004, Glacial-interglacial (MIS 1-10) migrations of the Subtropical Front across ODP Site 1119, Canterbury Bight, Southwest Pacific Ocean: Marine Geology, v. 205, p. 29-58.

Cathro, D.L., 2002, Three-demensional stratal development of a carbonate-siliciclastic sediment regime, Northern Carnarvon basin, Northwest Australia: Ph.D Dissertation, The University of Texas at Austin, p. 60.

Cathro, D.L., and Austin, J.A., Jr., 2001, An early mid-Miocene, strike-parallel shelfal trough and possible karstification in the North Carnarvon Basin, northwest Australia: Marine Geology, v. 178, p. 157-169.

Chamberlain, C.P., Zeitler, P.K., and Cooper, A.F., 1995, Geochronologic of the uplift and metarmorphism along the Alpine Fault, South Island, New Zealand: New Zealand Journal of Geology and Geophysics, v. 38, p. 515-523.

Chappell, J., and Shackleton, N.J., 1986, Oxygen isotopes and sea level: Nature, v. 324, p. 137-140.

Chinn, T.J.H., 1989, Glaciers of New Zealand: United States Geological Survey Professional Paper, No. 1386, p. H25-H48.

Chiocci, F.L., 2000, Depostional response to Quaternary fourth-order sea-level fluctuation on the Latium margin, *in* Hunt, D., and Gawthorpe, R.L., eds., Sediment Responses to Forced Regressions: Geological Society Special Publication, No. 172, p. 271-289.

Chiocci, F.L., Ercilla, G., and Terres, J., 1997, Stratal architecture of western Mediterranean margins as the result of the stacking of quaternary lowstand deposits below 'glacio-eustatic flunctuation base-level': Sedimentary Geology, v. 112, p. 195-217.

Chiswell, S., 1996, Variability in the Southland Current, New Zealand: New Zealand Journal of Marine and Freshwater Research, v. 30, p. 1-17.

Christie-Blick, N., 1991, Onlap, offlap, and origin of unconformity-bounded depositional sequences: Marine Geology, v. 97, p. 35-56.

Christie-Blick, N., Mountain, G.S., and Miller, K.G., 1990, Seismic stratigraphy record of sea-level change, *in* Revelle, R., Barnett, T.P., Barron, E.J., Bloom, A.L., Christie-Blick, N., Harrison, C.G.A., Hay, W.W., Matthews, R.K., Meier, M.F., Munk,W.H., Peltier, W.R., Roemmich, D., Sturges, W., Sundquist, E.T., Thompson, K.R., and Thompson, S.L., eds., Sea-level Change: Wahington, D. C., National Academy of Science Studies in Geophysics, p. 116-140.

Clark, P.U., Alley, R.B., and Pollard, D., 1999, Northern Hemisphere ice-sheet influences on global climate change: Science, v. 286, p. 1104-1111.

Cloetingh, S., McQueen, H., and Lambeck, K., 1985, On a tectonic mechanism for regional sealevel variations: Earth and Planetary Science Letters, v. 75, p. 157-166.

Coombs, D.S., Cas, R.A., Kawachi, Y., Landis, C.A., McDonough, W.F., and Reay, A., 1986, Cenozoic volcanism in north, east and central Otago, *in* Smith, I.E.M., ed., Late Cenozoic Volcanism in New Zealand: Royal Society of New Zealand Bulletin, v. 23, p. 278-312.

Cooper, A.F., Barreiro, B.A., Kimbrough, D.L., and Mattinson, J.M., 1987, Lamprophyer dike intrusion and the age of the Alpine fault, New Zealand: Geology, v. 15, p. 941-944.

COSOD I, 1981, *Report of the Conference on Scientific Ocean Drilling*: Joint Oceanographic Institutions, Inc. Washington, D.C., p. 112.

COSOD II, 1987, *Report of the Second Conference on Scientific Ocean Drilling*: Joint Oceanographic Institutions, Inc. Washington, D.C., p. 142.

Crux, J.A., Eaton, G.L., and Sturrock, S.J., 1984, Biostratigraphy of the Clipper well offshore NZ PPL 38202: Ministry of Commerce New Zealand Unoublished Petroleum Report Series PR1044, Wellington, p. 1-12.

Davey, F.J., and Smith, E.G.C., 1983, The tectonic setting of the Fiordland region, south-west New Zealand: Geophys. J.R., Astron. Soc., v. 72, p. 23-38.

Davey, F.J., Henyey, T., Holbrook, W.S., Okaya, D., Stern, T.A., Melhuish, A., Henrys, S., Anderson, H., Eberhart-Phillips, D., McEvilly, T., Uhrhammer, R., Wu, F., Jiracek, G.R., Wannamaker, P.E., Caldwell, G., and Christensen, N., 1998, Preliminary results from a geophysical study across a modern, continent-continent collisional plate boundary–the Southern Alps, New Zealand: Tectonophysics, v. 288, p. 221-235.

Davis, G.H., 1984, Structural geology of rocks and regions: New York, John Wiley & Sons, p. 242-244.

Davis, R., 1998, Preliminary results from directly measuring mid-depth circulation in the tropical and South Pacific: Journal of Geophysical Research, v. 103, p. 24619-24639.

DeMets, C., Gordon, R.G., Argus, D.F., and Stein, S., 1990, Current plate motions: Geophysical Journal International, v. 101, p. 425-478.

DeMets, C., Gordon, R.G., Argus, D.F., and Stein, S., 1994, Effect of recent revisions to the geomagnetic reveral time scale on estimates of current plate motions: Geophysical Research Letters, v. 21, p. 2191-2194.

Denton, G.H., and Hendy, C.H., 1994, Younger Dryas age advance of Franz Josef glacier in the Southern Alps of New Zealand: Science, v. 264, p. 1434-1437.

Devereux, I., 1968, Oxygen isotope paleotemperatures from the Tertiary of New Zealand: Journal of the Biological Society Victoria University of Wellington, New Zealand, v. 16, p. 41-45.

Dickinson, W. R., 1993, The EXXON global cycle chart: an event for every occasion? Discussion: Geology, v. 21, p. 282-283.

Dowling, L.M., and McCave, I.N., 1993, Sedimentation on the Feni Drift and late Glacial bottom water production in the north Rockall Trough: Sedimentary Geology, v. 82, p. 79-87.

Driscoll, N.W., and Karner, G.D., 1999, Three-dimensional quantitative modeling of clinoform development: Marine Geology, v. 154, p. 383-398.

Duncan, C.S., Goff, J.A., Austin, J.A., Jr., Fulthorpe, C.S., 2000, Tracking the last sea-level cycle: seafloor morphology and shallow stratigraphy of the latest Quaternary New Jersey middle continental shelf: Marine Geology, v. 170, p. 395-421.

Duplessy, J.C., Shachleton, N.J., Fairbanks, R.G., Labeyrie, L., Oppo, D., and Kannel, N., 1988, Deep-water source variation during the last climate variation: Palaeoceanography, v. 3, p. 343-360.

Duval, B.C., Cramez, C., and Vail, P.R., 1998, Stratigraphic cycles and major marine source rocks, *in* de Graciansky, P.C., Hardenbol, J., Jacquin, T., and Vail, P.R., eds., Mesozoic and Cenozoic Sequence Stratigraphy of European Basins: Tulsa, Society of Economic Paleontologists and Mineralogists Special Publication, No. 60, p. 44-51.

Eberli, G. et al, 1996, Leg 166 Preliminary Reports: Ocean Drilling Program: College Station, TX, p. 77.

Falvey, D.A. and Deighton, I., 1982, Recent advances in burial and thermal geohistory analysis: Australian Petrol. Explo. Ass. J., v. 22, p. 65-81.

Faugeres, J.C., and Stow, D.A.V., 1993, Bottom-current-controlled sedimentation: a synthesis of the contourite problem: Sedimentary Geology, v. 82, p. 287-297.

Faugeres, J.C., Stow, D.A.V., Imbert, P., and Viana, A., 1999, Seismic features diagnostic of contourite drifts: Marine Geology, v. 162, p. 1-38.

Field, B.D., and Browne, G.H., 1993, A subsiding platform adjacent to a plate boundary transpression zone: Neogene of Canterbury, New Zealand, *in* Balance, P.F., ed., South Pasific Sedimentary Basins: Sedimentary Basins of the World: Netherlands, Elsvier Science Publishers, p. 271-278.

Fillon, R.H., and Lawless, P.N., 2000, Lower Miocene-early Pliocene deposystems in the Gulf of Mexico: regional sequence relationships: Gulf Coast Association of Geological Societies Transactions, v. L (2000), p. 411-428.

Folland, C.K., and Salinger, M.J., 1995, Surface temperature trends and variations in New Zealand and the surrounding ocean, 1871-1993: International Journal of Climatology, v. 15(11), p. 1195-1218.

Franz, Sven-Oliver, and Tiedemann, R., 2002, Depositional changes along the Blake-Bahama Outer Ridge deep water transect during marine isotope stages

8 to 10; links to the Deep Western Boundary Current: Marine Geology, v. 189 (1-2), p. 107-122.

Frohlich, C., and Matthrews, R.K., 1991, STRATA-VARIOUS: A flexible Fortran program for dynamic forward modeling of stratigraphy: Sedimentary Modeling, *in* Franseen, E.K., ed., Computer Simulations and Methods for Improved Parameter Definition: Kansas Geological Survey Bulletin, v. 233, p. 449-461.

Fulthorpe, C.S., 1991, Geological controls on seismic sequence resolution: Geology, v. 19, p. 61-65.

Fulthorpe, C.S., and Carter, R.M., 1989, Test of seismic sequence methodology on a Southern Hemisphere passive margin The Canterbury Basin, New Zealand: Marine and Petroleum Geology, v. 6, p. 348-359.

Fulthorpe, C.S., and Carter, R.M., 1991, Continental-shelf progradation by sediment-drift accretion: Geological Society of America Bulletin, v. 103, p. 300-309.

Fulthorpe, C.S., Carter, R.M., and Wilson, J., 1996, Marshall Paraconformity: a mid-Oligocene record of inception of the Antarctic Circumpolar current and coeval glacio-eustatic lowstand?: New Zealand Journal of Marine and Petroleum Geology, v. 13, p. 61-77.

Fulthorpe, C.S., and Austin, J.A., Jr., 1998, Anatomy of rapid margin progradation: three-dimensional geometries of Miocene clinoforms, New Jersey margin: American Association of Petroleum Geologists Bulletin, v. 82 (2), p. 251-273.

Fulthorpe, C.S., Austin, J.A., Jr., and Mountain, G.S., 1999, Buried fluvial channels off New Jersey: did sea-level lowstands expose the entire shelf during the Miocene?: Geology, v. 27, p. 203-206.

Galloway, W.E., 1989a, Genetic stratigraphic sequence in basin analysis, I. Architecture and genesis of flooding-surface bounded depositional units: AAPG, v. 73, p.125-142.

Galloway, W.E., 1989b, Genetic stratigraphic sequence in basin analysis, II. Application to northwest Gulf of Mexico Cenozoic Basin: AAPG, v. 73, p.143-154.

Galloway, W.E., 1998, Siliciclastic slope and base-of-slope depositional systems: component facies, stratigraphic architecture, and classification: AAPG Bull., v. 82, p. 569-595.

Galloway, W.E., 2001, Cenozoic evolution of sediment accumulation in deltaic and shore-zone depositional systems, North Gulf of Mexico Basin: Marine and Petroleum Geology, v. 18, p. 1031-1040.

Galloway, W.E., in press, Gulf of Mexico basin depositional record of Cainozoic north American drainage basin evolution, *in* Blum, M., Marriott, S., and Leclair, S., eds., Fluvial Sedimentology VII: IAS Special Publication 35.

Galloway, W.E., and Williams, T.A., 1991, Sediment accumulation rates in time and space: Paleogene genetic stratigraphic sequences of the northwestern Gulf of Mexico: Geology, v. 19, p. 986-989.

Galloway, W.E. and Hobday, D.K., 1996, Terrigenous Clastic Depositional Systems: Springer, New York, p. 200-205.

Gao, Z., Kenneth, A.E., and He, Y., 1998, Deep-Water Traction Current Deposits: Beijing, Science Press, p. 57-99.

Gardner, T.W., 1989, Neotectonism along the Atlantic passive continental margin: a review: Geomorph., v. 2, p. 71-97.

Gellatly, A.F., Chinn, T.J.H., Rothlisberger, F., 1988, Holocene glacier variations in New Zealand: A review: Quaternary Science Reviews, v. 7, p. 227-242.

Gill, E.D., 1968, Oxygen isotope paleotemperature determinations from Victoria, Australia: Journal of the Biological Society Victoria University of Wellington, New Zealand, v. 16, p. 56-61.

Godfrey, N.J., Davey, F., Stern, T.A., and Okaya, D., 2001, Crustal structure and thermal anomalies of the Dunedin region, South Island, New Zealand: Journal of Geophysical Research, v. 106, p. 30835-30848.

Greenlee S.M., and Moore, T.C., 1988, Recognition and interpretation of depositional sequences and calculation of sea-level changes from stratigraphic data–offshore New Jersey and Alabama Tertiary, *in* Wilgus, C.K., Hastings, B.S., Kendall, C.G., Posamentier, H.W., Ross, C.A., and Van Wagoner, J.C., eds., Soc. Econ. Paleo. Min. Spec. Publ., No. 42, p. 329-353.

Gregory, K.M., and Chase, C.G., 1992, Tectonic significance of paleobotanically estimated climate and altitude of the late Eocene erosion surface, Colorado: Geology, v. 20, p. 581-585.

Gregory, K.M., and Chase, C.G., 1994, Tectonic and climatic significance of a late Eocene low-relief, high-level geomorphic surface, Colorado: Journal of Geophysical Research, v. 99, p. 20141-20160.

Hack, J.T., 1982, Physiographic divisions and differential uplift in the Piedmont and Blue Ridge: U.S. Geol. Sur. Prof. Pap., No. 1265, p. 49.

Haq, B.U., Hardenbol, J., and Vail, P.R., 1987, Chronology of fluctuating sea levels since the Triassic (250 millian years ago to present): Science, v. 235, p. 1156-1167.

Haq, B.U., Hardenbol, J., and Vail, P.R., 1988, Mesozoic and Cenozoic chronostratigraphy and cycles of sea-level change, *in* Wilgus, C. K., Hastings, B. S. et al., eds., Sea-level Changes: An Integrated Approach: Soc. Econ. Paleo. Min. Spe. Publ., No. 42, p. 71-108.

Harland, W.B., Armstrong, R.L., Cox, A.V., Craig, L.E., Smith, A.G. Smith, D.G., 1990, A geologic time scale, 1989: Cambridge Earth Science Series, Cambridge University Press, Cambridge, p. 263.

Hawkes, P.W., and Mound, D,D., 1984, Clipper-1 Geological Completion Report, for BP, Shell, Todd (Canterbury) Services Limited New Zealand Institute of Geological and Nuclear Sciences Unpublished Open-file Petroleum Report, Wellington, No. 1036, p. 10-28.

Head, P.S., and Nelson, C.S., 1994, A high-resolution oxygen isotope record for the past 6.4 million years at DSDP Site 593, Challenger Plateau, southern Tasman Sea, *in* van der Lingen et al., eds., Evolution of the Tasman Sea Basin (Tasman Sea Conference, Christchurch, New Zealnd, Nov. 27-30, 1992): A.A. Balkema: Rotterdam, Netherlands, p. 20-27.

Heezen, B.C., and Rawson, M., 1977, Visual observations of contemporary current erosion and tectonic deformation on the Cocos Ridge crust: Marine Geology, v. 23, p. 173-196.

Hernandez-Molina, F.J, Somoza, L., and Lobo, F., 2000, Seismic stratigraphy of the Culf of Cadiz continental shelf: a model for late Quaternary very high-resolution sequence stratigraphy and response to sea-level fall, *in* Hunt, D., and Gawthorpe, R.L., eds., Sediment Responses to Forced Regressions: London, Geological Society Special Publication, No. 172, p. 329-362.

Hernandez-Molina, F.J., Llave, E., Somoza, L., 2003, Looking for clues to paleoceanographic imprints; a diagnosis of the Gulf of Cadiz contourite depositional systems: Geology, v. 31, p. 19-22.

Herzer, R.H., 1981, Late Quaternary stratigraphy and sedimentation of the Canterbury continental shelf, New Zealand: New Zealand Oceanographic Institute Memoir 89, p. 4-60.

Heubeck, C., and Mann, P., 1991, Geologic evaluation of plate kinematic models for the North American-Caribean plate boundary zone: Tectonophysics, v. 191, p. 1-26.

Hollister, C.D., 1993, The concept of deep-sea contourites: Sedimentary Geology, v. 82, p. 5-11.

Hornibrook, N.B., 1992, New Zealand Cenozoic marine paleoclimates: a review based on the distribution of some shallow water and terrestrial biota, *in* Ryuichi, T., ed., Pacific Neogene, Environment Evolution, and Events: University of Tokyo Press, p. 83-106.

International Seismological Centre, Bulletin Disks 10 [CD-ROM], 1999, Internatl. Seis. Cent., Thatcham, United Kingdom.

Jones, C. E. et al, 1994a, Strontium isotope variations in Jurassic and Cretaceous seawater: Geochim Cosmochim. Acta., v. 58, p. 3061-3074.

Jones, C. E. et al, 1994b, Strontium isotope in early Jurassic seawater: Geochim Cosmochim. Acta., v. 58, p. 1285-1301.

Joyce, J.E., Tjalsma, L.R.C., and Prutzman, J.M., 1990, High-resolution planktonic stable isotope record and spectral analysis for the last 5.35 m.y. Ocean Drilling Project site 625 Northeast Gulf of Mexico: Paleoceanography, v. 5, p. 507-529.

Kamp, P.J.J., 1987a, Geological constraints on the Cenozoic Antarctica-Australia-Pacific relative plate motion circuit: Geology, v. 15, p. 649-697.

Kamp, P.J.J., 1987b, Age and origin of the New Zealand Orocline in relative to Alpine Fault movement: J. Geol. Soc., London, v. 144, p. 641-652.

Karner, G.D., 1986, Effects of lithospheric in-plane stress on sedimentary basin stratigraphy: Tectonics, v. 5, p. 573-588.

Karner, G.D., Driscoll, N.W., and Weissel, J.K., 1993, Response of the lithosphere to in-plane force variations: Earth and Planetary Science Letters, v. 114, p. 397-416.

Kennett, J.P., and von der Borch, C.C., 1986, Southwest Pacific Cenozoic paleoceanography, *in* Blakeslee, J.H., ed., Initial Report of the Deep Sea Drilling Project. Volume XC Part 2, Leg 90, Sites 587-594, p. 1493-1517.

Keyes, I.W., 1968, Cenozoic marine temperatures indicated by the Scleractinian coral fauna of New Zealand: Journal of the Biological Society Victoria University of Wellington, New Zealand, v. 16, p. 21-25.

Kidd, R.B., and Hailwood, E.A., 1993, High-resolution stratigraphy in modern and ancient marine sequences: ocean sediment cores to Paleozoic outcrop, *in* Hailwood, E. A., and Kidd, R. B., eds., High Resolution Stratigraphy: London, Geological Society Special Publication, No. 70, p. 1-8.

Killops, S.D., Cook, R.A., and Sykes, R., 1997, Petroleum potential and oil-source correlation in the Great South and Canterbury basins: New Zealand Journal of Geology and Geophysics, v. 40, p. 405-423.

King, P.R., 2000, Tectonic reconstruction of New Zealand: 40 Ma to the Present: Nea Zealand Journal of Geology and Geophysics, v. 43, p. 611-638.

Kirk, R.M., and Tierney, B.M., 1978, Nearshore sediment movement around the Port of Timaru: Proceedings of the 7th Biennial Conference, New Zealand Harbour Engineers Association, Dunedin, p. 80-140.

Kolla, V., Biondi, P., Long, B., and Fillon, R., 2000, Sequence stratigraphy and architecture of the late Pleistocene Lagniappe delta complex, northeast Gulf of Mexico, *in* Hunt, D., and Gawthorpe, R.L., eds., Sediment Responses to Forced Regressions: London, Geological Society Special Publication, No. 172, p. 291-327.

Kominz, M.A., Miller, K.G., and Browning, J.V., 1998, Long-term and short-term global Cenozoic sea-level estimates: Geology, v. 26, p. 311-314.

Kominz, M.A., and Pekar, S.F., 2001, Oligocene eustasy from two-dimensional sequence stratigraphic backstripping: Geological Society of America Bulletin, v. 113, p. 291-304.

Koons, P.O., 1994, Three-dimensional critical wedges: tectonics and topography in oblique collisional orogens: J. Geophys. Res., v. 99, p. 12301-12315.

Koons, P.O., and Henderson, C.M., 1995, Geodetic analysis of model oblique collision and comparison to the Southern Alps of New Zealand: New Zealand Journal of Geology and Geophysics, v. 38, p. 545-552.

Koons, P.O. Craw, D., Cox, S.C., Upton, P., Templeton, A.S., and Chamberlain, C.P., 1998, Fluid flow during active oblique convergence: a Southern Alps model from mechanical and geochemical observations: Geology, v. 26, p. 159-162.

Koons, P.O., Norris, R.J., Craw, D., and Cooper, A.F., 2003, Influence of exhumation on the structural evolution of transpressional plate boundaries: an example from the Southern Alps, New Zealand: Geology, v. 31, p. 3-6.

Laberg, J.S., Dahlgren, T., Vorren, T.O., Haflidi, H., and Bryn, P., 2001, Seismic analyses of Cenozoic contourite drift development in the Northern Norwegian Sea: Marine Geophysical Researchs, v. 22, p. 401-416.

Laine, E.P., Gardner, W.D., Rcihardson, M.J., and Kominz, M., 1994, Abyssal currents and advection of resuspended sediment along the northeastern Bermuda Rise: Marine Geology, v. 119, p. 159-171.

Larsen, G., and Chilingar, G.V., 1979, Introduction-diagenesis of sediments and rocks, *in* Larsen, G., and Chilingar, G.V. eds., Diagenesis in sediments and sedimentary rocks: Amsterdam Elsvier Scientific, p. 1-30.

Larsen, H.C., Saunder, A.D., Clift, P.D., 1994, Proc. ODP, Init. Reps. 152: Colleage Station, TX, (Ocean Drilling Program), p. 977.

Lavier, L.L., Steckler, M.S., and Brigaud, F., 2000, An improved method for reconstructing the stratigraphy and bathymetry of continental margin: application to the Cenozoic tectonic and sedimentary history of Congo margin: American Association of Petroleum Geologists Bulletin, v. 78, p. 923-939.

Lavier, L.L., Steckler, M.S., and Brigaud, F., 2001, Climatic and tectonic control on the Cenozoic evolution of the West African margin: Marine Geology, v. 178, p. 63-80.

Lawrence, D.T., Doyle, M., and Aigner, T., 1990, Stratigraphic simulation of sedimentary basins: concepts and calibration: American Association of Petroleum Geologists Bulletin, v. 74, p. 273-295.

Lawver, L.A., Gahagan, L.M., 1994, Constraints on timing of extension in the Ross Sea: tectonic evolution of the Southwest Pacific from 110 Ma to Present: Terra Antarctica, v. 1, p. 545-552.

Lawver, L.A., Coffin, M.F., Dalziel, I.W., Gahagan, L.M., and Campbell, D.A., 2001, The Plates 2001 atlas of plate reconstructions (750 Ma to present day), Plates Progress Report No. 260-0801, UTIG Technical Report, No. 189, p. 83.

Le Pichon, X., 1968, Sea-floor spreading and continental drift: Journal of Geophysical Research v. 73, p. 3661-3697.

Lear, C.H., Elderfield, H., and Wilson, P.A., 2000, Cenozoic deep-sea temperatures and global ice volumes from Mg/Ca in benthic foraminiferal calcite: Science, v. 287, p. 269-272.

Lebrun, J.F., Lamarche, G., Collot, J., and Delteil, J., 2000, Abrupt strike-slip fault to subduction transition: the Alpine fault-Puysegur Trench connection, New Zealand: Tectonics, v. 19, p. 688-706.

Lebrun, J.F., Lamarche, G., and Collot, J., 2003, Subduction initiation at a strike-slip plate boundary: the Cenozoic Pacific-Australian plate boundary, south of New Zealand: Journal of Geophysical Research, v. 108, B9, p. 2453-2469.

Leckie, D.A., 2001, Climatic controls on nonmarine sedimentation-maximum aggradation during lowstand, incision during transgression and highstand: AAPG 2001 annual meeting, Denver, US, v. 2001, p. 114.

Leitner, B., Eberhart-Phillips, D., Anderson, H., and Nabelek, J. L., 2001, A focused look at the Alpine Fault, New Zealand: seismicity, focal mechanisms, and stress observations: Journal of Geophysical Research, v. 106, B2, p. 2193-2220.

Leturmy, P., Lucazeau, F., and Brigaud, F., 2003, Dynamic interactions between the gulf of Guinea passive margin and the Congo River drainage basin: 1. Morphology and mass balance: Journal of Geophysical Research, v.108 (B8), 2383.

Lewis, D.W., 1992, Anatony of an unconformity on mid-Oligocene Amuri Limestone, Canterbury, New Zealand: New Zealand Journal of Geology and Geophysics, v. 35, p. 463-475.

Lewis, K.B., Bennett, D.J, Herzer, R.H., and von der Borch, C.C., 1986, Seismic stratigraphy and structure adjacent to an evolving plate boundary, western

Chatham Rise, New Zealand, *in* Blakeslee, J.H., ed., Initial Report of the Deep Sea Drilling Project, Vol. 90, Part 2, Leg 90, Sites 587–594, p. 1325–1338.

Little, T.A., and Roberts, A.P., 1997, Distribution and mechanisms of Neogene to Present-day vertical axis rotations, Pacific-Australian plate boundary zone, South Island, New Zealand: Journal of Geophysical Research, v. 102, p. 20447-20468.

Liu, X., and Galloway, W.E., 1993, Sediment accumulation rate: problems and new approach, in Armentrout, J.M., Bloch, R., Olson, H.C., and Perkins, B.F., eds., Rates of Geological processes-tectonics, sedimentation: Proceedings of the Fourteenth Annual Research Conference, Gulf Coast Section SEPM, p. 101-107.

Liu, X., and Galloway, W.E., 1997, Quantitative determination of Tertiary sediment supply to the North Sea Basin: AAPG Bulletin, v. 81, p. 1482-1509.

Llave, E., Hernandez-Molina, F.J, Somoza, L., Diaz-del-Rio, V., Stow, D.A.V., Maestro, A., and Alveirinho-Dias, J.M., 2001, Seismic stacking pattern of the Fro-Albufeira contourite system (Gulf of Cadiz): a Quaternary record of paleoceanographic and tectonic influences: Marine Geophysical Researches, v. 22, p. 487-508.

Locker, S.D, and Laine, E. P., 1992, Paleogene-Neogene depositional history of the middle U.S. Atlantic continental rise: mixed turbidite and contourite depositional systems: Marine Geology, v. 103, p. 137-164.

Loutit, T.S., and Kennett, J.P., 1981, New Zealand and Australian Cenozoic sedimentary cycles and global se-level changes: American Association of Petroleum Geologists of Petroleum Geologists Bulletin, v. 65, p. 1586-1600.

Lu, H., Fulthorpe, C., and Mann, P., 2003, Three-dimensional architecture of shelf-building sediment drifts in the offshore Canterbury Basin, New Zealand: Marine Geology, v. 193, p. 19 – 47.

Lu, H., and Fulthorpe, C.S., in press, Controls on sequence stratigraphy of a middle-Miocene to Recent, current-swept, passive margin: offshore Canterbury Basin, New Zealand: Geological Society of America Bulletin.

Lucazeau, F., Brigaud, F., and Leturmy, P., 2003, Dynamic interaction between the Gulf of Guinea passive margin and the Congo River drainage basin: 2 isostasy and uplift: Journal of Geophysical Research, v. 108 (B8), p. 2384.

Lucchi, R.G., Rebesco, M., Camerlenghi, Angelo, Busetti, M., Tomadin, L., Villa, G., Persico, D., Morigi, C., Bonci, M.C., Giorgetti, G., 2002, Mid-late Pleistocene glacimarine sedimentary processes of a high-latitude, deep-sea sediment drift (Antarctic Peninsula Pacific margin): Marine Geology, v. 189, p. 343-370.

Marani, M., Argnani, A., Roveri, M., and Trincardi, F., 1993, Sediment drifts and erosional surfaces in the central Mediterranean: Seismic evidence of bottom-current activity: Sedimentary Geology, v. 82, p. 207-220.

Marks, K.M., McAdoo, D.C., and Smith, W.H.F., 1993, Geosat gravity anomaly grid south of 30 °S, *in* National Geophysical Data Grids; Gamma-Ray, Gravity, Magnetic, and Topographic Data for the Conterminous United States, compiled by Philips, J.D, Duval, J.S., and Ambroziak, R.A., eds., CD-ROM, Digital Data Series, U.S. Geoloical Survey, Washington, D.C., p. 33-38.

Masson, D.G., Howe, J.A., Stoker, M.S., 2002, Bottom-current sediment waves, sediment drifts and contourites in the northern Rockall Trough: Marine Geology, v. 192, p. 215-237.

Mathews, W.H., 1967, Profiles of late Pleistocene glaciers in New Zealand: New Zealand Journal of Geology and Geophysics, v. 10, p. 146-163.

Matthews, R.K., and Frohlich, C., 1998, Forward modeling of sequence stratigraphy and diagenesis: Application to rapid, cost-effective carbonate reservoir characterization: GeoAbrabia, v. 3, p. 359-382.

McCave, I.N., and Tucholke, B.E., 1986, Deep current-controlled sedimentation in the western North Atlantic, *in* Vogt, P.R., and Tucholke, B.E., eds., The Geology of North American, Volume M, The western North Atlantic region: GSA, p. 451-468.

McGinnis, J.P., Hayes, D.E., and Driscoll, N.W., 1997, Sedimentary processes across the continental rise of the southern Antarctic Peninsula: Marine Geology, v. 141, p. 91-109.

Meckel, T.A. 2003, Tectonics of the Hjort region of the Macquarie Ridge Complex, southernmost Australian-Pacific plate boundary, southwest Pacific Ocean: Ph.D dissertation, The University of Texas at Austin, p. 91-122.

Meckel, T.A., Coffin, M.F., Mosher, S., Symonds, P., Bernardel, G., and Mann, P., 2003, Underthrusting at the Hjort Trench, Australian-Pacific plate boundary: incipient subduction?: Geochemistry Geophysics Geosystems G3, v. 4, number 12.

Mederios, B.P., Karner, D.B., Muller, R.A., and Levine, J., 2000, The global ice volume record as viewed through a benthic $\delta^{18}O$ stack: EOS trans. American Geophysics Union 81 (Suppl.), F597.

Mercer, J.H., 1983, Cenozoic glaciation in the southern hemisphere: Annual Review of Earth and Planetary Science, v. 11, p. 99-132.

Miall, A.D., and Miall, C.E., 2001, Sequence stratigraphy as a scientific enterprise: the evolution and persistence of conflicting paradigms: Earth Science Reviews, v. 54, p. 321-348.

Michels, K.H., Rogenhagen, J., and Kuhn, G., 2001, Recognition of contour-current influence in mixed contourite-turbidite sequences of the western Weddell Sea, Antarctia: Marine Geophysical Researchs, v. 22, n. 5/6, p. 465-485.

Miller, K.G., 1990, Recent advances in Cenozoic marine stratigraphic resolution: Palaios., v. 5, p. 301-302.

Miller, K.G., Wright, J.D., and Fairbanks, K.G., 1991, Unlocking the icehouse: Oligocene-Miocene oxygen isotope, eustasy and margin erosion: Journal of Geophysical Research, v. 96, p. 6829-6848.

Miller, K.G., Mountain, G.S., 1996, Drilling and dating New Jersey Oligocene-Miocene sequence: ice volume, global sea-level, and Exxon records: Science, v. 271, p. 1092-1095.

Milliman, J.D., and Syvitski, J.P.M., 1992, Geomorphic/tectonic control of sediment discharge to the ocean: the importance of small mountainuous rivers: Journal of Geology, v. 100, p. 525-544.

Milne, A.D., 1975, Well completion report Resolution, for BP, Shell, Todd Canterbury Service Limited New Zealand Institute of Geological and Nuclear Scientific Unpublished Open-file Petroleum Report, Wellington, No. 648, p. 5-26.

Molnar, P., 2001, Climate change, flooding in arid environments, and erosion rates: Geology, v. 29, p. 1071-1074.

Molnar, P., Atwater, T., Mammerycx, J., and Smith, S.M., 1975, Magnetic anomalies, bathymetry and the tectonic evolution of the South Pacific since Later Cretaceous: Geophysical Journal of the Royal Astronomical Society, v. 40, p. 383-420.

Molnar, P., and England, P., 1990, The late Cenozoic uplift of mountain ranges and global climate changes: Chicken or egg?: Nature, v. 346, p. 29-34.

Molnar, P., Anderson, H.J., Audoine, E., 1999, Continuous deformation versus faulting through the continental lithosphere of New Zealand: Sciences, v. 286, p. 516-519.

Moore, M.A., Anderson, H.J., and Pearson, C., 2000, Seismic and geodetic constraints on plate boundary deformation across the northern Macquarie Ridge and southern South Island of New Zealand: Geophy. J. Int. v. 143, p. 847-880.

Morris, M., Stanton, B., and Neil, H., 2001, Subantarctic oceanography and New Zealand: preliminary results from an ongoing survey: New Zealand Journal of Marine and Freshwater Research, v. 35, p. 499-519.

Mullan, A.B., 1998, Southern Hemisphere sea-surface temperatures and their contemporary and lag association with New Zealand temperature and precipitation: International Journal of Climatology, v. 18(8), p. 817-840.

Naish, T.R., and Kamp, P.J.J., 1997, Sequence stratigraphy of 6^{th}- order (41 k.y.) Pliocene-Pleistocene cyclothems, Wanganui basin, New Zealand: a case for the regressive systems tract: Geological Society of America Bulletin, v. 109, p. 978-999.

Nelson, C.S., Hendy, C.H., Cuthbertson, A.M., and Jarrett, G.R, 1986, Late Quaternary carbonate and isotope stratigraphy, subantarctic Site 594, Southwest Pacific, *in* Blakeslee, J.H., eds., Initial Report of the Deep Sea Drilling Project. Volume XC Part 2, Leg 90, Sites 587-594, p. 1425-1436.

Nelson, C.S., and Cooke, P.J., 2001, History of oceanic front development in the New Zealand sector of the Southern Ocean during the Cenozoic-a synthesis: New Zealand Journal of Geology and Geophysics, v. 2001, p. 535-553.

Nittrouer, C.A., 1999, STRATAFORM: overview of its design and synthesis of its results: Marine Geology, v. 154, p. 3-12.

Nittrouer, C.A., and Kravitz, J.H., 1996, Strataform: A program to study the creation and interpretation of sedimentary strata on continental margin: Oceanography, v. 9, p. 146-152.

Norris, R.J., Carter, R.M., and Turnbull, I.M., 1978, Cenozoic sedimentation in basins adjacent to a major continental transform boundary in southern New Zealand: Journal of Geological Society, Landon, v. 135, p. 319-335.

Norris, R.J., Koons, P.O., and Cooper, A.F., 1990, The obliquely-convergent plate boundary in the South Island of New Zealand: implications for ancient collision zones: Journal of Structure Geology, v. 12, p. 715-725.

Norris, R.J., and Cooper, A.F., 1995, Origin of small-scale segmentation and transpressional thrusting along the Alpine Fault, New Zealand: Geological Society of American Bulletin, v. 107, p. 231-240.

Norris, R.J., and Cooper, A.F., 2000, Late Quaternary slip rates and slip partitioning on the Alpine fault, New Zealand: Journal of Structure Geology, v. 23, p. 507-520.

Orsi, A.H., Whitworth, T., and Nowlin, W.D., Jr., 1995, On the meridional extent and fronts of the Antarctic Circumpolar Current: Deep Sea Research, v. 42, p. 641–673.

Pazzaglia, F.J., and Gardner, T.W., 1994, Late Cenozoic flexural deformation of the middle U.S. Atlantic passive margin: Journal of Geophysical Research, v. 99, p. 12143-12157.

Pearson, C.F., Beavan, J., Darby, D.J., Blick, G.H., and Walcott, R.I., 1995, Strain distribution across the Australian-Pacific plate boundary in the central South Island, New Zealand, from 1992 GPS and earlier terrestrial observations: Journal of Geophysical Research, v. 100, p. 22071-22081.

Pearson, C.F, Denys, P., and Hodgkinson, K., 2000, Geodetic constraints on the kinematics of the Alpine fault in the southern South Island of New Zealand, using results from the Hawea-Haast GPS transect: Geophysical Research Letters, v. 27, p. 1319-1322.

Pinet, P.R., and Normark, W.R., 1985, A scenario of Mesozoic-Cenozoic ocean circulation over the Blake Plateau and its environs: GSA Bull., v. 96, p. 618-626.

Plint, A.G., and Nummedal, D., 2000, The falling stage system tract: recognition and importance in sequence stratigraphic analysis, *in* Hunt, D., and Gawthorpe, R.L., eds., Sediment Responses to Forced Regressions: Landon, Geological Society Special Publication, No. 172, p. 1-17.

Poag, C.W., and Sevon, W.D., 1989, A record of Appalachian denudation in postrift Mesozoic and Cenozoic sedimentary deposits of the U.S. middle Atlantic continental margin: Geomorph., v. 2, p. 119-157.

Posamentier, H.W. and Vail, P.R., 1988, Eustatic control on clastic deposition II-sequence and systems tracts models, *in* Wilgus, C.K., Hastings, B.S., Kendell, C.G.St.C., Posamentier, H.W., eds., Sea-level Changes: An Integrated Approach: Society of Economic Paleontologists and Mineralogists, Spec. Publ. No. 42, p. 124-154.

Posamentier, H.W., and Morris, W.R., 2000, Aspects of the stratal architecture of force regressive deposits, *in* Hunt, D., and Gawthorpe, R.L., eds., Sediment Responses to Forced Regressions: Landon, Geological Society Special Publication, No. 172, p. 20-46.

Prather, B.E., 2000, Calibration and visualization of depositional process models for above-grade slopes: a case study from the Gulf of Mexico: Marine and Petroleum Geology, v. 17, p. 619-638.

Pratson, L.F., and Laine, E.P., 1989, The relative importance of gravity-induced versus current-controlled sedimentation during the Quaternary along the mideast U.S. outer continental margin revealed by 3.5 kHz echo character: Marine Geology, v. 89, p. 87-126.

Prell, W.L., 1982, Oxygen and carbon isotope stratigraphy for the Quaternary of Hole 502B: evidence for two modes of isotopic variability, *in* Prell, W.L., and Gardner, J.V., eds., Initial Report of the Deep Sea Drilling Project, v. 68, p. 455-464.

Raymo, E.M. and Ruddiman, W.F., 1992, Tectonic forcing of late Cenozoic climate: Nature, v. 359, p. 117-122.

Rebesco, M., and Stow, D., 2001, Seismic expression of contourites and related deposits: a preface: Marine Geophysical Researches, v. 22, p. 303-308.

Reynolds, D.J., Steckler., M.S., and Coakley, B.J., 1991, The role of sediment load in sequence stratigraphy: the influence of flexural isostasy and compaction: Journal of Geophysical Research, v. 96, p. 6931-6949.

Rodero, J., Pallares, L., and Maldonado, A., 1999, Late Quaternary seimic facies of the Gulf of Cadiz Spanish margin depositional processes influences by sea-level change and tectonic controls: Marine Geology, v. 155, p. 131-156.

Rona, P.A., and Clay, C.S., 1967, Stratigraphy and structure along a continuous seismic reflection profile from cape Hatteras, north Carolina, to the Bermuda Rise: Journal of Geophysical Research, v. 72, p. 2170-2130.

Rona, P.A., 1969, Middle Atlantic continental slope of United States: deposition and erosion: AAPG Bull., v. 53, p. 1453-1465.

Rona, P.A., 1970, Submarine canyon origin on upper continental slope off Cape Hatteras: Geology, v. 78, p. 141-152.

Royer, J.Y., and Sandwell, D.T., 1989, Evolution of the Indian Ocean since the late Cretaceous: constraints from Geosat altimetry: Journal of Geophysical Research, v. 94, p. 13755-13782.

Rust, D.J., and Summerfield, M.A., 1990, Isopach and borehole data as indicators of rifted margin evolution in southwestern Africa: Marine and Petroleum Geology, v. 7, p. 277-287.

Saito, Y., Katayama, H., Ikehara, K., Kato, Y., Matsumoto, E., Oguri, K., Oda, M., and Yumoto, M., 1998, Transgressive and highstand systems tracts and post-glacial transgression, the East China Sea: Sedimentary Geology, v. 122, p. 217-232.

Sandwell, J.G., and Smith, W., 1997, Marine gravity-anomaly from Geosat and ERS-1 satellite altimetry: Journal of Geophysical Research, v. 102, p. 10039-10054.

Sclater, J.G., and Christie, P.A.F., 1980, Continental stretching: an explanation of the most mid-Cretaceous subsidence of the central North Sea Basin: Journal of Geophysical Research, v. 85, p. 3711-3739.

Serranne, M., 1999, Early Oligocene stratigraphic turnover on the west Africa continental margin: a signature of the Tertiary greenhouse-to-Icehouse conditions: Terra Nova, v. 11, p. 135-140.

Seranne, M., and Abeigne, C.N., 1999, Oligocene to Holocene sediment drifts and bottom currents on the slope of Gabon continental Margin (west Africa)–consequences for sedimentation and southeast Atlantic upwelling: Sedimentary Geology, v. 128, p. 179-199.

Sewell, R.J., and Lewis, D.W., 1988, Petrology and geochemistry of Tertiary volcanic rocks from central inland and south Canterbury, South Island, New Zealand, New Zealand: Journal of Geology and Geophysics, v. 31, p. 250-261.

Shackleton, N.J., and Opdyke, N.D., 1973, Oxygen isotope and palaeomagnetic stratigraphy of equatorial Pacific core V28-238: Oxygen isotope temperatures

and ice volumes on a 10^5 year and 10^6 year scale: Quaternary Research, v. 3, p. 39-55.

Shackleton, N.J., and Opdyke, N.D., 1976, Oxygen isotope and paleomagnetic stratigraphy of Pacific core V28-239: Late Pliocene to latest Pliocene, *in* Cline, R.M., and Hays, J.D., eds., Investigations of Late Quaternary Paleoceanography and Paleoclimatology: Geological Society of America Memoir 145, p. 449-464.

Shipboard Scientific Party, 1999, Leg 181 Summary: Southwest Pacific Paleoceanography, *in* Carter, R.M., McCave, I.N., Richter, C., Carter, L., eds., Proc. ODP, Init. Repts., 181: College Station, TX (Ocean Drilling Program), p. 1-80.

Singer, C., Shulmeister, J., and Mclea, B., 1998, Evidence against a significant Younger Dryas cooling event in New Zealand: Science, v. 281, p. 812-814.

Sircombe, K.N., and Kamp, P.J.J., 1998, The South Westland Basin: seismic stratigraphy, basin geometry and evolution of a foreland basin within the Southern Alps collision zone, New Zealand: Tectonophysics, v. 300, p. 359-387.

Sorensen, J.C., Gregersen, U., Breiner, M., and Michelsen, O., 1997, High-frequency sequence stratigraphy of upper Cenozoic deposits in the central and southeastern North Sea area: Marine and Petroleum Geology, v. 14 (2), p. 99-123.

Steckler, M.S., Reynolds, D.J., Coakley, B.J., Swift, B.J., and Jarrard, R.D., 1993, Modeling passive margin sequence stratigraphy, *in* Posamentier, H.W., Summerhayes, C.P., Haq, B.U., and Allen, G.P., eds., Sequence Stratigraphy and Facies Associations: International Association of Sedimentologists, No. 18, p. 19-41.

Steckler, M.S., Mountain, G.S., Miller, K.G., and Christie-Blick, N., 1999, Reconstruction of Tertiary progradation and clinoform development on the New Jersey passive margin by 2-D backstripping: Marine Geology, v. 154, p. 399-420.

Steckler, M.S., and Lavier, L.L., submitted, Morphology and stratigraphy of continental margins during Tertiary global change: From carbonate ramps to clastic progradation: Science: Marine Geology.

Stern, T., Kleffmann, S., Okaya, D., Scherwath, M., and Bannister, S., 2001, Low seismic-wave speeds and enhanced fluid pressure beneath the Southern Alps of New Zealand: Geology, v. 29, p. 679-682.

Stewart, R.B., and Neall, V.E., 1984, Chronology of palaeoclimatic change at the end of the last glaciation: Nature, v. 311, p. 47–48.

Stoker, M.S., Akhurst, M.C., Howe, J.A, and Stow, D.A.V., 1998, Sediment drifts and contourites on the continental margin off northwest Britain: Sediment. Geol., v. 15, p. 33-51.

Stow, D.A.V., Faugeres, J.C., Viana, A., and Gonthier, E., 1998, Fossil contourites: a critical review: Sedimentary Geology, v. 115, p. 3-13.

Stow, D.A.V., and Mayall, M., 2000, Deep-water sedimentary systems: new models for the 21st centry: Marine and petroleum Geology, v. 17, p. 125-135.

Sutherland, P., 1995, The Australia-Pacific boundary and Cenozoic plate motions in the southwest Pacific: some constrains from Geosat data: Tectonic, v. 14, p. 819-831.

Sutherland, P., 1996, Transpressional development of the Australia-Pacific boundary through southern South Island, New Zealand: constraints from Miocene-Pliocene sediments, Waiho-1, South Westland: New Zealand Journal of Geology and Geophysics, v. 39, p. 251-264.

Sutherland, P., 1999, Cenozoic bending of New Zealand basement terranes and Alpine fault displacement: a brief review: New Zealand Journal of Geology and Geophysics, v. 42, p. 5-301.

Sutherland, P., and Norris, R.J., 1995, Late Quaternary displacement rate, paleoseismicity and geomorphic evolution of the Alpine fault: evidence from near Hokuri Creek, south Westland, New Zealand: New Zealand Journal of Geology and Geophysics, v. 38, p. 419-430.

Sutherland, R., and Browne, G., 2003, Canterbury basin offers potential on South Island: New Zealand: Oil & Gas Journal, Feb. 3, p, 45-49.

Telford, W.M., Geldart, L.P., Sheriff, R.E., and Keys, D.A.Y., 1976, Applied Geophysics: Cambridge, Great Britain, Cambridge University Press, p. 860.

Thiede, J., 1979, Wind regimes over the late Quaternary Southwest Pacific Ocean: Geology, v. 7, p. 259–262.

Thorne, J.A., and Swift, D.J.P., 1991a, Sedimentation on continental margins, II: application of the regime concept, *in* Swift, D.J.P., Oertel, G.F., Tillman, R.W., and Thorne, J.A., eds., Shelf sand and sandstone bodies, geometry, facies, and sequence stratigraphy: International Association of Sedimentologists Special Publication 14, p. 33-58.

Thorne, J.A., and Swift, D.J.P., 1991b, Sedimentation on continental margins, VI: a regime model for depositional sequences, their component systems tracts, and bounding surfaces, *in* Swift, D.J.P., Oertel, G.F., Tillman, R.W., and Thorne, J.A., eds., Shelf sand and sandstone bodies, geometry, facies, and sequence stratigraphy: International Association of Sedimentologists Special Publication 14, p. 189-255.

Tippett, J.M., and Kamp, P.J.J., 1993a, Fission Track analysis of the late Cenozoic vertical kinematics of continental Pacific crust, South Island, New Zealand: Journal of Geophysical Research, v. 98, p. 16119-16148.

Tippett, J.M., and Kamp, P.J.J., 1993b, The role of faulting in rock uplift in the Southern Alps. New Zealand: New Zealand Journal of Geology and Geophysics, v. 36, p. 497-504.

Tippett, J.M., and Kamp, P.J.J., 1995. Quantitative relationships between uplift and relief parameters for the Southern Alps, New Zealand, as determined by fission track analysis: Earth Surfaces and Landforms, No. 20, p. 153-175.

Trincardi, F., and Correggiari, A., 2000, Quaternary regression deposits in the Adriatic basin and the record of composite sea-level cycles, *in* Hunt, D. and Gawthorpe, R.L., eds., Sediment Responses to Forced Regressions: Landon, Geological Society Special Publication, No. 172, p. 245-269.

Tucholke, B.E., and Mountain, G.S., 1979, Seismic stratigraphy, lithostratigraphy and paleosedimentation patterns in the North American Basin, *in* Talwani, M., Hay, W., and Ryan, W.B.F., eds., Deep Drilling Results in the Atlantic Ocean: Continental Margins and Paleoenvironment: American Geophysical Union, Maurice Ewing Series, 3, p. 58-86.

Vail, P.R., 1987, Seismic stratigraphy interpretation using sequence stratigraphy, Part 1: Seismic stratigraphy interpretation procedure, *in* Bally, A.W., ed., Atlas of Seimic Stratigraphy: AAPG Studies in Geol., 27(1), p. 1-10.

Vail, P.R., Mitchum, R.M., and Thompson III, S., 1977, Seismic stratigraphy and global changes of sea-level, Part 5, Chronostratigraphic Significance of Seismic Reflections, *in* Payton, C. E. ed., Seismic Stratigraphy- Application to Hydrocarbon Exploration: AAPG, Memoir 26, p. 99-116.

Vail P.R., Hardenbol, J., and Todd, R.G., 1984, Jurassic unconformities, chronostratigraphy and, sea-level change from seismic stratigraphy and biostratigraphy, *in* Schlee, J.S., ed., Interregional Unconformities and Hydrocarbon Accumulation: AAPG Memoir 36, p. 129-144.

Vail, P.R., Audemard, F., Bowman, S.A., Eisner, P.N., and PerezCruz, C., 1991, The stratigraphic Signatures of tectonic, eustasy and sedimentology-anoverview, *in* Einsele, G., Ricken, W., and Seilacher, A. eds., Cycle and Events in Stratigraphy: Springer-Verlag, Berlin, p. 167-659.

Van Vagoner, J.C., Posamentier, H.W., Mitchum, R.M., Jr., Vail, P.R., Sarg, J.F., Loutit, T.S., and Hardenbol, J., 1988, An overview of the fundamentals of sequence stratigraphy and key definitions, *in* Wilgus, C.K., Gastings, B.S., Kendall., C.G.St. C., Posamentier, H.W., Ross. C.A., and Van Wagoner, J.C., eds., Sea-level Changes: an Integrated Approach: Tulsa, Society of Economic Paleontologists and Mineralogists Special Publications, No. 42, p. 39-46.

Viana, A.R., Faugeres, J.C., and Stow, D.A.V., 1998, Bottom-current-controlled sand deposits-a review of modern shallow- to deep-water environments: Sedimentary Geology, v. 115, p. 53-80.

Vilas, L., Martin-Chivelet, J., and Arias, C., 2003, Integration of subsidence and sequence stratigraphic analyses in the Cretaceous carbonate platforms of the Prebetic (Jumilla-Yecla region), Spain: Palaeogeography, Palaeoclimatology, Palaeoecology, v. 200 (1-4), p. 107-129.

Visser, K., Thunell, R., and Stott, L., 2003, Magnitude and timing of temperature change in the Indo-Pacific warm pool during deglaciation: Nature, v. 421, p. 152-155.

Vitor, A., Covington, G., Elliott, T., Droxler, A., Belopolsky, A.V., Mutch, A., 2000, Miocene stacking patterns and climatic records: are the sequences global?: AAPG Bulletin, v. 84, p. 1395-1518.

Walcott, R.I., 1978, Present tectonics and late Cenozoic evolution of New Zealand: Royal Astronomical Society Geophysical Journal, v. 52, p. 137-164.

Walcott, R.I., 1979, Plate motion and shear strain rates in the vicinity of the Southern Alps, *in* Walcott, R.I., and Cresswell, M.M., eds., The Origin of the Southern Alps: Royal Society of New Zealand Bulletin, v. 18, p. 5-12.

Walcott, R. I., 1998, Modes of oblique compression: late Cenozoic tectonics of the South Island of New Zealand: Review of Geophysics, v. 36, p. 1-26.

Ward, C.M., 1988, Marine terraces of the Waitutu District and their relation to the late Cenozoic tectonics of the southern Fiordland region, New Zealand: Journal of the Royal Society of New Zealand, v. 18, p. 1-28.

Watkins, J.S., and Mountain, G.S., eds., 1990, Role of ODP Drilling in the Investigation of Global Changes in Sea Level, Report of JOI/USSAC Workshop, El Paso, Texas, October 24-26, 1988, p. 70.

Watters, W.A., 1978, Tertiary volcanism–Miocene, *in* Suggate, P.R., Stevens, G.R., eds., The Geology of New Zealand: Wellington, New Zealand. Government Printer 2, p. 637-644.

Weaver, S.D., Storey, B.C., Pankhurst, R.J., Mukasa, S.B., DiVenere, V.J., and Bradshaw, J.D., 1994, Antarctica-New Zealand rifting and Marie Byrd Land lithospheric magnetism linked to ridge subduction and mantle plume activity: Geology, v. 22, p. 81-814.

Weissel, J.K., Hayes, D.E., and Herron, E.M., 1977, Plate tectonic synthesis: the displacements between Australia, New Zealand and Antarctica since the Later Cretaceous: Marine Geology, v. 25, p. 231-227.

Wellman, H.W., 1953, Data from the study of recent and late Pleistocene faulting in the South Island of New Zealand: N. Z. J. Sci. Technol., Sect. B, 34, p. 270-288.

Wellman, H.W., 1979, An uplift map for the South Island New Zealand, and a model for uplift of the Southern Alps, *in* Walcott, R.I., Cresswell, M.M., eds., The Origin of the Southern Alps: Bulletin of the Royal Society of New Zealand, v. 18, p. 282-306.

Wellman, P., and Cooper, A.F., 1971, Potassium-argon ages of some New Zealand lamprophyre dikes near the Alpine fault: New Zealand Journal of Geology and Geophysics, v. 14, p. 341-350.

Weltje, G.J., Meijer, X.D., and de Boer, P.L., 1998, Stratigraphic inversion of siliciclastic basin fills: a note on the distinction between supply signals resulting from tectonic and climatic forcing: Basin Research, v. 10, p. 129-152.

White, W.B., and Cherry, N.J., 1999, Influence of the Antarctic Circumpolar Wave upon New Zealand temperature and precipitation during autumn-winter: Journal of Climate, v. 12 (4), p. 960-976.

Wilding, A., and Sweetman, I.D., 1971, Endeavour-1, for BP, Aquitaine and Todd Petroleum Development Limited New Zealand Institute of Geological and Nuclear Scientific Unpublished Open-file Petroleum Report, Wellington, No. 303, p. 22-34.

Williams, D.F., 1988, Evidence for and against sea-level changes from the stable isotopic record of Cenozoic, *in* Wilgus, C.K., et al., eds., Sea-level Changes: an Integrated Approach: Tulsa, Society of Economic Paleontologists and Mineralogists Special Publications, No. 42, p. 30-36.

Williams, D.F., Thunell, R.C., Tappa, E., Rio, D., and Raffi, I., 1988, Chronology of the Pleistocene oxygen isotope record: 0-1.88 m.y. B.P.: Palaeogeography, Palaeoclimatology, Palaeoecology, v. 64, p. 221-240.

Wilson, I.R., 1985, Galleon-1 geological completion report, for BP, Shell, Todd (Canterbury) Services Limited. New Zealand Geological Survey Open-file Petroleum Report, Wellington, No.1146, p. 2-18.

Wise, S.W., Breza, J.R., Harwood, D.M., Wei, W., and Zachos, J.C., 1992, Paleogene glacial history of Antarctica in light of leg 120 drilling results, Proc. Ocean Drill. Program Sci. Results, v. 120, p. 1001-1030.

Zachos, J., Pagani, M., Sloan, L., Thomas, E., and Katharina, B., 2001, Trends, rhythms, and aberrations in global climate 65 Ma to present: Science, v. 292, p. 686-693.

Vita

Hongbo Lu was born on September 13, 1970, in Changning county, Yunnan province, People's Republic of China. Both of his parents are primary school teachers and provided Hongbo with a favorable environment for study. Hongbo's interest in a career in the Earth Sciences was fundamentally influenced by his middle school mentor, Mr. Shixi Cun. Mr. Cun was rigorous, energetic, honest, and especially knowledgeable in geography. Hongbo was president of the student union for three years at Changning First High School and was awarded the Province Outstanding Student Leader in 1989 by Yunnan province. In 1989, Hongbo passed the University Entrance Examination (the percentage passing this exam was <5% at that time) and was admitted by the University of Petroleum, China (UPC), majoring in Petroleum Geology. Hongbo was the class monitor at UPC for four years from 1989-1993. After receiving his B.S. in 1993, he enrolled in the sedimentology graduate program at Petroleum Exploration Department of UPC under the direction of professor Zaixing Jiang. Hongbo's master's research, *Sequence stratigraphy and paleontology study of Ili Basin, west China*, was published as a book (Fong, Jiang, and Lu, 2000). In addition, four papers related to this work were published in Chinese journals and an oral presentation was given at the 30th International Geological Congress. From 1993-1998, he participated four other cooperative projects supported by Chinese oil companies. These projects allowed him to work with petroleum geologists and geophysicists on-site as part of an exploration group to gain experience of the Chinese oil industry. While at UPC, Hongbo was asked to become an assistant professor. He

taught undergraduate courses in sedimentology and sedimentary facies, comprehensive geological fieldwork, modern sedimentary investigations, and a sedimentology laboratory. He was also a mentor for about 240 freshmen in the Petroleum Geology Department. Supported by UPC, he was a registered Ph.D student at the Institute for Geology (Beijing), Chinese Natural Science Academy, majoring in reservoir sedimentology and supervised by Dr. Rengwei Li, from 1997 to 1999. He enrolled in the Ph.D program at The University of Texas at Austin Department of Geological Sciences in Fall 1999. He has since been working at the University of Texas Institute for Geophysics, investigating the seismic stratigraphy of the offshore Canterbury basin, eastern South Island, New Zealand. To date, his dissertation research has resulted in two publications (Lu et al., 2003; Lu and Fulthorpe, in press). A third paper is in preparation.

Permanent address: Dabing Primary School, Changning, Yunnan 678101, China
This dissertation was typed by the Author.